ON ADAPTIVE FILTERING IN OVERSAMPLED SUBBANDS

A DISSERTATION
SUBMITTED TO THE SIGNAL PROCESSING DIVISION,
DEPARTMENT OF ELECTRONIC AND ELECTRICAL ENGINEERING
AND THE COMMITTEE FOR POSTGRADUATE STUDIES
OF THE UNIVERSITY OF STRATHCLYDE
IN PARTIAL FULFILLMENT OF THE REQUIREMENTS
FOR THE DEGREE OF
DOCTOR OF PHILOSOPHY

By
Stephan Weiß
May 1998

Declaration

I declare that this Thesis embodies my own research work and that it is composed by myself. Where appropriate, I have made acknowledgement to the work of others.

Stephan Weiß

Meinen lieben Eltern, Werner und Ursula Weiß

Abstract

For a number of applications like acoustic echo cancellation, adaptive filters are required to identify very long impulse responses. To reduce the computational cost in implementations, adaptive filtering in subband is known to be beneficial. Based on a review of popular fullband adaptive filtering algorithms and various subband approaches, this thesis investigates the implementation, design, and limitations of oversampled subband adaptive filter systems based on modulated complex and real valued filter banks.

The main aim is to achieve a computationally efficient implementation for adaptive filter systems, for which fast methods of performing both the subband decomposition and the subband processing are researched. Therefore, a highly efficient polyphase implementation of a complex valued modulated generalized DFT (GDFT) filter bank with a judicious selection of properties for non-integer oversampling ratios is introduced. By modification, a real valued single sideband modulated filter bank is derived. Non-integer oversampling ratios are particularly important when addressing the efficiency of the subband processing. Analysis is presented to decide in which cases it is more advantageous to perform real or complex valued subband processing.
Additionally, methods to adaptively adjust the filter lengths in subband adaptive filter (SAF) systems are discussed.

Convergence limits for SAFs and the accuracy of the achievable equivalent fullband model based on aliasing and other distortions introduced by the employed filter banks are explicitly derived. Both an approximation of the minimum mean square error and the model accuracy can be directly linked to criteria in the design of the prototype filter for the filter bank. Together with an iterative

least-squares design algorithm, it is therefore possible to construct filter banks for SAF applications with pre-defined performance limits.

Simulation results are presented which demonstrate the validity and properties of the discussed SAF methods and their advantage over fullband and critically sampled SAF systems.

Acknowledgements

I wish to express my deepest gratitude to Dr Robert W. Stewart for his enthusiasm, encouragement, dedication, and support, which he has shown over the past years for the work which I have performed under his supervision and of which a part is compiled in this thesis. Particularly, I would like to thank Dr Stewart for arranging to spend part of my PhD time at the Signal and Image Processing Institute, University of Southern California. I would further like to thank Prof Richard Leahy of SIPI for his hospitality and the great experience of both staying at SIPI and working with his functional brain imaging group.

Thanks are also due to my colleague and friend Moritz Harteneck for inspiring discussions and all the fun we had while working together. I am also greatly endebted to Dipl.-Ing. Alexander Stenger and Priv.-Doz. Dr.-Ing. habil Rudolf Rabenstein from Telecommunications Institute I, University of Erlangen-Nürnberg, Germany, for many helpful discussions and collaboration. Part of the work presented here was performed in undergraduate projects, and I would particularly like to mention Lutz Lampe and Dipl.-Ing. Uwe Sörgel for their valuable input.

This work would have been impossible without the generous support by a studentship from William Garven Research Bequest, which I gratefully acknowledge. I am also indebted to the Signal Processing Division and its members for providing both the facilities and social background that enabled joyful working. Particular thanks to Dr Asoke Nandi for some valuable discussions, and exciting Badminton games.

I would like to thank Dipl.-Phys. Dr. Ing. Ulrich Hoppe and Prof Richard Leahy, whos literary interest offered a great number of suggestions, which I have

devoured with appetite.

Finally, I owe many thanks to my family at home, and my friends here and abroad for their support and encouragement. I could not have done without it.

Stephan Weiß
Glasgow, April 1998

Contents

List of Figures

List of Tables

Mathematical Notations

General Notations

h	scalar quantity
$\mathbf{h}$	vector quantity
$\mathbf{H}$	matrix quantity
$h(t)$	function of a continuous variable t
$h[n]$	function of a discrete variable n
h_n	short hand form for $h[n]$ for dense notation
$H(e^{j\Omega})$	periodic Fourier spectrum of a discrete function $h[n]$
$H(z)$	z-transform of a discrete function $h[n]$

Relations and Operators

$\stackrel{!}{=}$	must equal
$\circ\!\!-\!\!\bullet$	transform pair, e.g. $h[n] \circ\!\!-\!\!\bullet H(e^{j\Omega})$ or $h[n] \circ\!\!-\!\!\bullet H(z)$
$(\cdot)^*$	complex conjugate
$(\cdot)^H$	Hermitian (conjugate transpose)
$\tilde{\mathbf{H}}(z)$	parahermitian, $\tilde{\mathbf{H}}(z) = \mathbf{H}^H(z^{-1})$
$(\cdot)^T$	transpose
$*$	convolution operator
$\mathcal{E}\{\cdot\}$	expectation operator
∇	gradient operator (vector valued)
$\mathrm{lmc}(\cdot,\cdot)$	least common multiple
$a\mathrm{mod}_b$	modulo operator: remainder of a/b
$\mathcal{P}(\cdot)$	probability of

$\lceil \cdot \rceil$	ceiling operator (round up)
$\lfloor \cdot \rfloor$	floor operator (round off)

Sets and Spaces

$\mathbb{C}$	set of complex numbers
$\mathbb{C}^{M \times N}$	set of $M \times N$ matrices with complex entries
$\mathbb{C}_{(z)}^{M \times N}$	set of $M \times N$ matrices with complex polynomial entries in z
$l^2(\mathbb{Z})$	space of square integrable (i.e. finite energy) discrete time signals
$\mathbb{N}$	set of integer numbers ≥ 0
$\mathbb{R}$	set of real numbers
$\mathbb{R}^{M \times N}$	set of $M \times N$ matrices with real entries
$\mathbb{R}_{(z)}^{M \times N}$	set of $M \times N$ matrices with real polynomial entries in z
$\mathbb{Z}$	set of integer numbers

Symbols and Variables

α	energy bias
β	RLS forgetting factor
γ	weighting in iterative LS filter design
$\delta[n]$	Kronecker function, $\delta[n] = 1$ for $n = 0$, $\delta[n] = 0$ for $n \neq 0$
η	relaxation factor for APA
μ	LMS adaptive algorithm step size
$\tilde{\mu}$	NLMS normalized step size
$\phi[n]$, $\psi[n]$	basis functions
ϕ, θ	angles
ξ_{LS}	least squares cost function
ξ_{MSE}	mean square error cost function
ξ_{MMSE}	minimum mean square error
ω	(angular) frequency
Ω	normalized (angular) frequency $\Omega = \omega T_s$, with sampling period T_s
A	gain

A_p, A_s	passband and stopband gain
B	bandwidth
$d[n]$	desired signal
$d_k[n]$	desired signal in kth subband
$\mathbf{D}_1, \mathbf{D}_2$	factorial (diagonal) matrices of the GDFT transform matrix
$F_x(e^{j\Omega})$	transfer path, with decimated white noise input and output signal $x[n]$
$F_x^{(A)}(e^{j\Omega})$	transfer path $F_x(e^{j\Omega})$ for aliased signal components only
$F_x^{(S)}(e^{j\Omega})$	transfer path $F_x(e^{j\Omega})$ for signal of interest only
$F_x(e^{j\Omega})$	transfer path, with decimated white noise input and output signal $x[n]$
$g_k[n]$	kth filter of the synthesis filter bank
$G_{n\|k}(z)$	n of N polyphase components of the kth synthesis filter
$G_k(e^{j\Omega})$	frequency response of kth filter of synthesis filter
$\underline{G}(z)$	vector of synthesis filters
$\mathbf{G}(z)$	polyphase matrix of the synthesis filter bank
$\mathbf{G}_m(z)$	modulation description of the synthesis filter bank
$h_k[n]$	kth filter of the analysis filter bank
$H_{k\|n}(z)$	n of N polyphase components of the kth analysis filter
$H_k(e^{j\Omega})$	frequency response of kth analysis filter
$\mathbf{H}(z)$	polyphase matrix of the analysis filter bank
$\mathbf{H}_r(z)$	reduced polyphase matrix of the analysis filter bank
$\mathbf{H}_m(z)$	modulation description of the analysis filter bank
$\mathbf{I}_K$	$K \times K$ identity matrix
$\mathbf{J}_K$	$K \times K$ reverse identity matrix
K	(channel number) — $K/2$ subbands covering the frequency interval $\Omega = [0; \pi]$ for both real and complex filter banks (see page 64)
L_a	filter length of adaptive FIR filter
L_f	filter length of FIR filter
L_p	filter length of prototype filter
L_s	length of impulse response of unknown system in system identification

N	decimation factor; for modulated filter banks, N is defined based on the bandwidth (including transition bands) of the prototype filter
$\mathcal{O}$	complexity order
p	APA projection order; norm for adaptive tap-assignment criterion
$p[n]$	prototype filter
$P_k^{(2K)}(z)$	kth of $2K$ polyphase components of $P(z)$
$\mathbf{p}$	cross-correlation vector
$\mathbf{P}(z)$	polyphase matrix of prototype filter
$\mathbf{P}_n$	solution hyperplane in affine projection algorithm
$q_T(t-t_0)$	rectangular window with $q_T(t-t_0)=1$ for $t \in [t_0; t_0+T]$
Q	update period for adaptive tap-profile algorithms
$\mathbf{Q}$	modal matrix containing eigenvectors of auto-correlation matrix $\mathbf{R}$
$r_{xx}(\tau)$	auto-correlation function of a stochastic process x
$r_{xy}(\tau)$	cross-correlation function between two stochastic processes x and y
R	window length for estimation of tap-assignment criterion
$\mathbf{R}$	auto-correlation matrix
$s[n]$	impulse response of unknown system (plant)in system identification
$\mathbf{S}_m(z)$	modulation description of the unknown system projected into subbands
$\mathbf{S}_1, \mathbf{S}_2$	permutation matrices
$S_{xx}(e^{j\Omega})$	power spectral density of the discrete time random process x
$S_{xy}(e^{j\Omega})$	cross power spectral density between discrete time random processes x and y
$t[n]$	impulse response of distortion function, $t[n] \circ\!\!-\!\!\bullet\, T(z)$
$t_{k,n}$	transform coefficients
$T(z)$	distortion function of filter bank
$\mathbf{T}$	transform matrix
$\mathbf{T}_{\mathrm{DCT}}$	discrete cosine transform matrix
$\mathbf{T}_{\mathrm{DFT}}$	discrete Fourier transform matrix
$\mathbf{T}_{\mathrm{GDFT}}$	generalized discrete Fourier transform matrix

$u[n]$	white noise excitation signal of source model $L(e^{j\Omega}$
$\mathbf{w}$	coefficient vector of a filter
$\mathbf{w}_{\text{opt}}$	optimum coefficient vector (Wiener filter)
$\mathbf{W}_m(z^K)$	adaptive filter matrix
$x[n]$	input signal to adaptive filter / filter bank
$\underline{X}(z)$	polyphase vector of input signal
$\underline{X}_m(z)$	modulation description of the decimated input signal
$x_k[n]$	decimated input signal in kth subband
$x'_k[n]$	decimated and expanded input signal in kth subband
$\hat{x}_k[n]$	kth subband signal after passing through synthesis filter
$\hat{x}[n]$	reconstructed fullband signal, summed over all $\hat{x}_k[n]$
$\mathbf{x}_n$	input vector to adaptive filter
$\mathbf{X}_n$	collection of current and past input vectors to adaptive filter
$y[n]$	output signal of adaptive filter
z	z-transform variable
$z[n]$	observation noise
$z_k[n]$	observation noise in kth subband

Acronyms

AEC	acoustic echo cancellation
APA	affine projection algorithm
DCT	discrete cosine transform
DFT	discrete Fourier transform
DSP	digital signal processor
DWT	discrete wavelet transform
FDAF	frequency domain adaptive filter
FIR	finite impulse response
FFT	fast Fourier transform
GDFT	generalized discrete Fourier transform
IIR	infinite impulse response
LMS	least mean squares (algorithm)
LPTV	linear periodically time-varying
LTI	linear time-invariant
LS	least squares
MMSE	minimum mean squared error
MSE	mean squared error
NLMS	normalized least mean square (algorithm)
OSR	oversampling ratio
PC	power complementary
PR	perfect reconstruction
PSD	power spectral density
QMF	quadrature mirror filter
RE	reconstruction error

RLS	recursive least squares (algorithm)
SAF	subband adaptive filter
SAR	signal-to-aliasing ratio
SNR	signal-to-noise ratio
SSB	single sideband (modulation)
TDAF	transform domain adaptive filter

Contents

List of Tables

List of Figures

Chapter 1

Introduction

1.1 Context of Work

Despite the constant growth in processing power, many digital signal processing algorithms are still too complex to be implemented in real time. In the field of adaptive filtering the technological advances have recently enabled long-concepted applications such as active noise control to be realized [37]. However almost continually new application ideas emerge that are yet more demanding in complexity. Thus, in parallel with the increasing hardware optimization to realize faster and more powerful DSPs, a second track of optimization is dedicated to reduce the computational complexity of implemented DSP algorithms.

A key example is acoustic echo cancellation (AEC) for hands-free telephony and teleconferencing as shown in Fig. 1.1, which is often claimed to be one of the currently most computationally complex DSP applications [61, 62, 63]. In a hands-free telephone environment, the signal $x[n]$ of the far end speaker is output to a loudspeaker. Over a free standing microphone, the near end speaker communicates back to the far end. Unfortunately, the microphone signal $d[n]$ not only consists of the near end speaker's speech, but has superimposed on it the feedback of the far end speaker signal $x[n]$ filtered by the impulse response of a system composed of loudspeaker, acoustic room transfer function, and the microphone (LEMS — loudspeaker–enclosure–microphone system). This feedback is perceived by the far end speaker as an echo of his/her own voice, which can

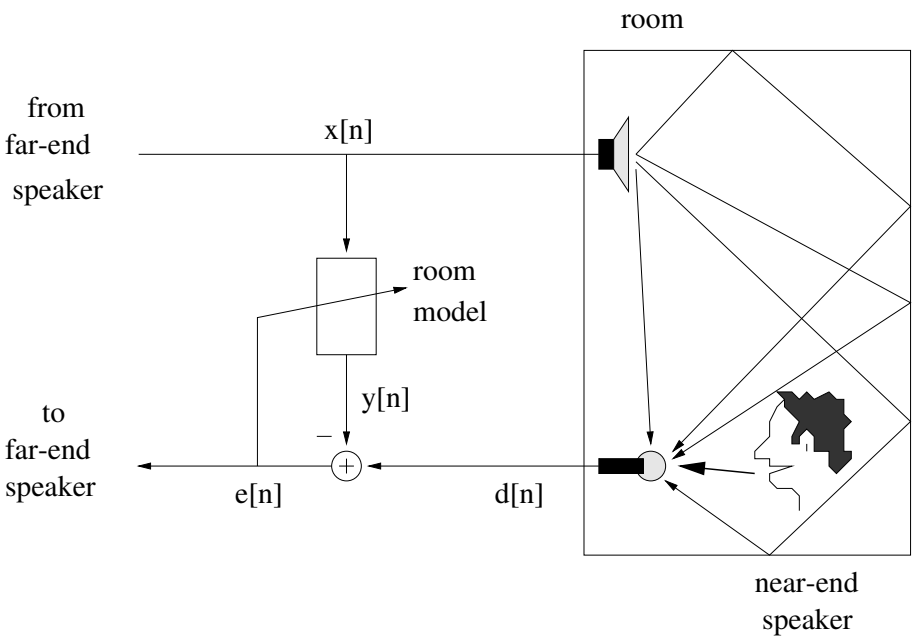

Figure 1.1: Acoustic echo cancellation using an adaptive filter to identify a replica of the room impulse response.

create considerable disturbance and, at worst, make communication impossible.

The acoustic echo cancellation approach is to incorporate a model of the LEMS into the communication system, which filters the far end speaker signal $x[n]$ to produce a close replica $y[n]$ of the echo contained in the near end signal $d[n]$. Thus, the echo can be subtracted out to yield a signal $e[n]$ containing the near end speaker only. Since the room acoustics are likely to be time-varying due to the changing presence, absence and mobility of conferees, the room model has to be adjusted on-line to track changes; hence adaptive solutions are required. Acoustic echo cancellation by adaptive means may be interpreted as the hybrid form of two fundamental adaptive filtering set-ups, adaptive noise cancellation and system identification.

Adaptive System Identification. For the adaptive identification of some unknown system, a digital filter with variable coefficients is set up in parallel to the system to be identified, as seen in Fig. 1.2. The adaptive filter will then try to produce an output signal $y[n]$ such that when subtracted from the desired signal

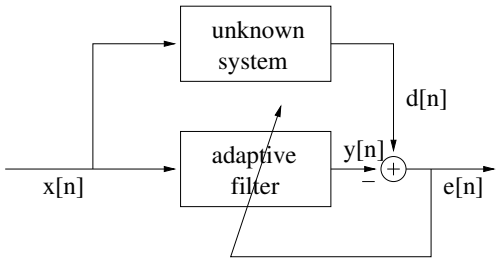

Figure 1.2: Adaptive filter in system identification set-up.

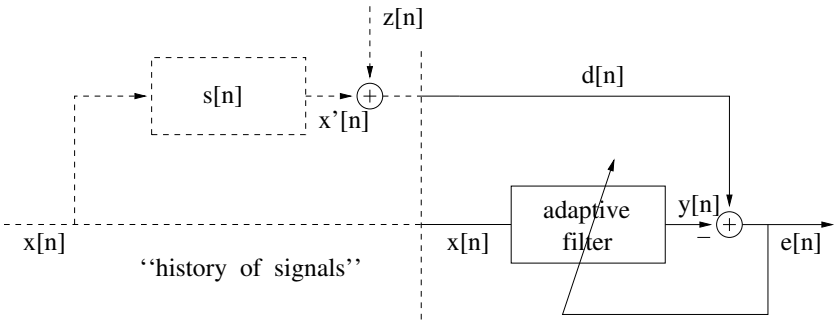

Figure 1.3: Adaptive filter in adaptive noise cancellation set-up.

$d[n]$, the resulting error signal $e[n]$ will be minimized in an appropriate sense. If the error tends towards zero, the unknown system and the adaptive filter have the same input/output behaviour. Thus, if the exciting signal $x[n]$ has been broadband, a complete parameterization of the unknown system is achieved.

Adaptive Noise Cancellation. The application of adaptive filtering to noise cancellation [174] is shown in Fig. 1.3. The desired signal $d[n]$ consists of a signal of interest $z[n]$, which is corrupted by some unwanted noise (in case of AEC the echo). If a noise probe $x[n]$ is available, which is correlated with the corrupting noise $x'[n]$, an adaptive filter can be employed to suppress the corrupting noise as best as possible, such that the error signal $e[n]$ contains the signal of interest only. Considering the history of the signals $x[n]$ and $d[n]$, the similarity to a system identification set-up as given in Fig. 1.2 becomes apparent: the correlation between the noise probe $x[n]$ and the signal $d[n]$ can be described by a filter $s[n]$, which the adaptive filter will try to identify, if the input signal $x[n]$ is broadband.

In case of system identification, the signal $z[n]$ is termed observation noise.

The LEMS is to be identified over the spectral range of the human voice, and has therefore some flavour of both system identification and active noise cancellation. While the coloured speech input is a problem on its own since it will considerably slow the convergence speed of many adaptive algorithms, the main problem stems from the algorithmic complexity required for AEC, as the length of the room impulse response in the LEMS usually spans several hundred milliseconds. If the sampling rate is set to 16kHz, adaptive finite impulse response filters of several thousand coefficients length would be required. Similar problems arise when the classical system identification set-up is attempted to determine room impulse responses and parameterize acoustics [46, 124].

One method for reducing the complexity of adaptive systems is given by the subband approach, whereby the signals involved are split into a number of frequency bands, which can be operated at a lower sampling rate. As shown for the system identification set-up in Fig. 1.4, adaptive filtering is then performed in the subbands at the decimated sampling rate and with shorter filter lengths, which can yield a considerable reduction in computational complexity. Although the original idea introduced by Kellermann [84, 85] and Gilloire [52] is now more than a decade old, the research effort in this particular area has been probably higher than ever in the last years, driven by the promise of the high commercial relevance of acoustic echo cancellers.

To perform subband adaptive filtering (SAF) as shown in Fig. 1.4 a wide variety of approaches exist, including critically decimated and oversampled systems, and ranging from perfectly reconstructing systems to some that introduce spectral loss or even distortion. However, the case of critical decimation, where the decimation ratio equals the number of uniform subbands, requires either cross-terms at least between adjacent frequency bands [54], which compensates the information loss due to aliasing distortion, or gap filter banks [176, 148], which introduces spectral loss that may not be acceptable. Oversampled filter banks can resolve this problem by introducing spectral redundancy, whereby oversampling in this context means that the subband signals are decimated by a factor smaller than the critical one. While complex analytic subband signals can be

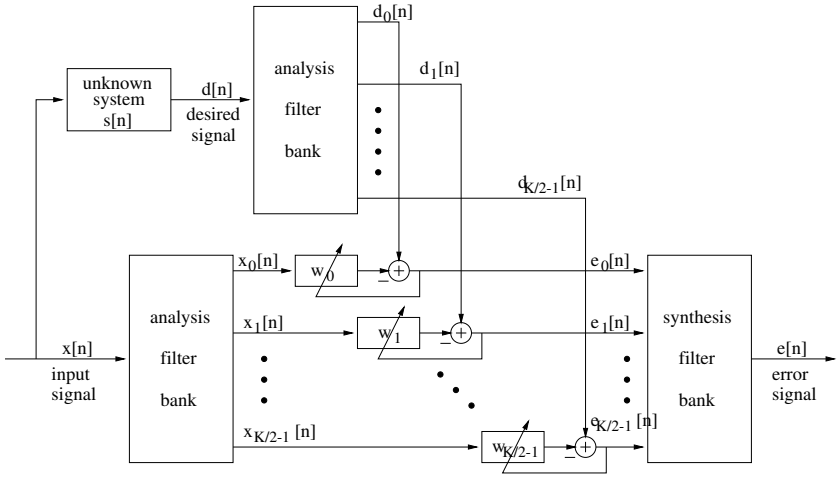

Figure 1.4: Adaptive filtering in subbands.

decimated at any integer factor above the critical one, for the real valued case bandpass signals are problematic to decimate, and oversampling requires either non-uniform filter banks [71, 69] or single side band (SSB) modulation [27, 167].

1.2 Original Contribution

The research presented in this thesis has been mostly dedicated to a particular type of oversampled complex valued filter bank, where the filters are derived by a generalized DFT (GDFT) transform from a real valued prototype filter. The efficiency when incorporated in an SAF system is given by two facts.

Firstly, despite the requirement of complex arithmetic, the complex subband approach will be shown to be surprisingly efficient compared to the processing in real valued oversampled subbands. This is particularly true if the computational order of the algorithm to be implemented in subbands is greater than linear in the length of the adaptive filter. It will also outperform critically sampled systems, if the oversampling ratio is close to one.

Secondly, we will introduce a highly efficient way of implementing our GDFT modulated filter bank based on a polyphase factorization for non-integer oversampling ratios, such that the filter bank can be operated close at the critical rate. This will prove a common "subband" misconception wrong, which has led

many researchers to use either less efficient integer oversampling ratios for SAF systems, or to use other, less efficient implementations for the filter banks.

Another key point in this thesis is the analysis of final convergence limits for subband adaptive filters based on aliasing and other distortions introduced by the employed filter banks. We will derive explicit limits, and approximations thereof, which can be directly linked to the prototype filter on which the modulated filter banks are based. Together with an iterative least-squares design algorithm, it will be possible to construct filter banks for SAF systems with pre-defined performance limits.

The following ideas, derivations, and experiments summarise original contributions of this work:

- a highly efficient implementation of GDFT banks based on a polyphase representation, for K channel banks with arbitrary integer decimation ratio (i.e. including non-integer oversampling);
- a real-valued single sideband modulated filter bank based on a modified GDFT filter bank in polyphase implementation;
- a discussion of the computational complexity for complex and real valued subband adaptive filter (or general subband processing) implementations;
- a description of aliasing in the subbands and its inhibition of adaptation; a description of this phenomenon as information leakage in the time domain;
- the derivation of limits for the minimum error PSD, and the minimum mean square error (MMSE) of an SAF system based on aliasing in the subbands;
- a derivation of the limit for the accuracy of the fullband equivalent model identified by the SAF system;
- approximations linking the performance limitations to design specifications of the prototype filter of a modulated filter bank;
- a fast prototype filter design using an iterated least squares algorithm;

- a discussion of adaptive tap-assignment in the light of global error minimization;
- a simplified robust adaptation scheme for variable tap-profiles.

1.3 Overview

The following chapters of this thesis are organized as follows.

Chapter 2 introduces adaptive filters, with particular respect to their computational complexity. Where necessary and relevant for the subband approach, other properties are discussed.

Chapter 3 introduces background theory for subband adaptive filtering. Starting from basic operations and components of multirate systems, the justifications for a sampling alteration are discussed. This leads to filter banks, for which analysis methods are presented. Using these methods, both efficient implementations of the filter banks and the further analysis of subband adaptive systems are enabled. Based on the latter, different strategies for subband adaptive structures are reviewed and evaluated. This includes critically sampled systems, which either require additional cross-terms between bands in the structure shown in Fig. 1.4, or spectrally lossy filter banks, and oversampled approaches using either complex or real valued filter banks.

Chapter 4 concentrates on the description, analysis, and design of complex valued oversampled GDFT modulated filter banks. Based on the prototype and the parameters of the GDFT transform, properties of the filter bank such as band-position and linear phase are discussed. By introducing a polyphase representation of the filter bank, conditions for perfect reconstruction can be drawn. Also, interesting properties can be derived from the connection of complex modulated filter banks to Gabor frames. Further, the polyphase representation is factorized into a filter network consisting only of real valued polyphase components of the prototype filter, and a rotation by a GDFT transform. The latter can

be further factorized such that the transform matrix can be mainly implemented using a standard FFT. This fast efficient implementation can also be used for real valued subband processing by modification of the subband signals such that effectively a single sideband modulated filter bank is performed.

This motivates to investigate which — real or complex valued subband processing — can be considered more efficient when implementing a specific subband adaptive filter; this can be answered by separately evaluating the costs for the filter bank operations and for the algorithms operating in the subbands.

Finally, two design methods for GDFT and SSB modified GDFT filter banks are introduced. The first is an iterated halfband method producing power-of-two channel filter banks from tabled halfband filters; the second yields a prototype filter using a least squares design to achieve both near perfect reconstruction and high stopband attenuation.

Chapter 5 evaluates the performance of subband adaptive filters. This includes a review of general aspects of performance, such as convergence speed and final error behaviour. First, we identify aliasing in the subbands as an inhibition to adaptation. Based on a source model of the subband signals, it is possible to calculate the power spectral density of the final error signal due to aliasing. An approximation for the MMSE is derived, which is solely based on the stopband properties of the prototype filter. Second, we show how the fullband model can be reconstructed from the final adapted weights of the SAFs. This then allows us to establish a lower model accuracy of the equivalent fullband system as given by the distortion function of the employed filter banks.

The experimentational part of this chapter demonstrates the influence of the oversampling ratio and the number of subbands on the convergence speed of an SAF system using the NLMS algorithm, for both white and coloured input noise, and compares a number of different SAF structures, amongst themselves and to a fullband implementation. Another part of experiments presents simulation examples to validate our prediction of final error PSD, final MMSE and the model accuracy of the reconstructed fullband equivalent model of the SAF system.

Chapter 6 discusses and reviews the idea of a variable tap-profile for the SAF system, whereby each subband may have a different number of filter coefficients in its adaptive filter. We motivate this approach by evaluating the potential benefits due to either decreased system complexity, or increased length of the equivalent reconstructed fullband model of the SAF system. This also yields comparisons for the computational efficiency of different subband structures, namely the over-sampled complex and real valued subband approaches compared to a critically decimated SAF structure with cross-terms.

Finally, based on an adaptive algorithm controlling the distribution of computational power over different subbands, two different performance criteria are derived using a global error minimization approach. Simulations are presented to give an idea of the benefits offered by variable tap-profile algorithms, and some insight into their convergence behaviour.

Chapter 7 summarizes the main results of this thesis, and puts forward ideas for continued and future investigation.

Chapter 2

Adaptive Filtering Algorithms

The filter problem, characterized in Sec. 2.1, is under stationary conditions optimally addressed in the linear least squares sense by the open loop Wiener filter solution described in Sec. 2.2. Closed loop adaptive filters which converge towards this optimal solution become attractive due to their reduced complexity and tracking performance where non-stationary situations arise. Two different types of adaptive filters, based on mean squared and least squares error minimization, are discussed in Secs. 2.3 and 2.4, respectively. Sec. 2.5 establishes links and similarities between both algorithmic approaches. Finally, Sec. 2.6 reviews methods to implement adaptive filters with reduced computational cost, of which subband implementations of adaptive filters will be further researched in Chap. 3. For generality, all algorithms will be presented in complex notation.

2.1 General Filtering Problem

The general application of filters within this thesis can be described as modelling the relation (or more precisely correlation) between two signals: an input signal $x[n]$ to the filter, and a desired signal $d[n]$ to which the filter output is compared. This situation is illustrated in Fig. 2.1. The task is to minimize the error signal $e[n]$ in some sense by selecting appropriate filter parameters. A number of methods will be discussed in the following sections.

In terms of possible filters, the scope within this thesis is restricted to linear

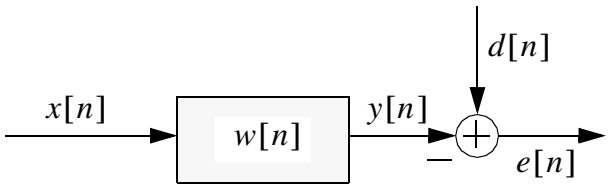

Figure 2.1: General filter problem with input $x[n]$, filter impulse response $w[n]$, output signal $y[n]$, desired signal $d[n]$, and residual error signal $e[n]$.

filters with finite impulse response (FIR). Particularly in the context of AEC, acoustics are perfectly linear; non-linear distortions usually only arise from low-cost audio equipment [74], and often can be compensated by some non-linear structures in series with the linear processing [138]. The restriction to FIR filters has two reasons. Firstly, infinite impulse response (IIR) filters include a feedback which can cause some stability problems when adaptive solutions are sought. Secondly, many researchers suggest that the nature of acoustic impulse responses favours FIR filter over IIR [59, 60, 118, 64]. More generally, if the system being modelled is not recursive then there is no advantage in using IIR.

For the derivations, we are interested in the filter output, calculated by a discrete convolution denoted as '$*$',

$$y[n] = w[n] * x[n] = \sum_{\nu=0}^{L_a-1} w[\nu] \cdot x[n-\nu] = \mathbf{w}^H \mathbf{x}_n \tag{2.1}$$

between the coefficients or weights $w[n]$ of a filter of length L_a and the input signal $x[n]$. This convolution can be conveniently expressed in vector notation, whereby we define a coefficient vector $\mathbf{w}$ and a state vector $\mathbf{x}_n$,

$$\mathbf{w} = \left[w_0^*,\ w_1^*,\ \ldots\ w_{L_a-1}^*\right]^T \tag{2.2}$$

$$\mathbf{x}_n = \left[x[n],\ x[n-1],\ \ldots\ x[n-L_a-1]\right]^T . \tag{2.3}$$

Note, that for later convenience the coefficient vector $\mathbf{w}$ contains *complex conjugate* coefficients w_i^*. Finally, the error is given by

$$e[n] = d[n] - y[n] = d[n] - \mathbf{w}^H \mathbf{x}_n \quad . \tag{2.4}$$

2.2 Optimum Wiener Filter

This section presents a mean squared optimum filter, given by the Wiener-Hopf solution, for the general filtering problem introduced in Sec. 2.1. The derivation is performed by optimization of a quadratic error cost function derived in Sec. 2.2.1.

2.2.1 Mean Squared Error Formulation

Minimization of the mean squared error (MSE) is common practice and widely used for optimization problems due to the relative mathematical ease with which the derivation can be performed. However, the MSE may be unsuitable for stochastic signals with heavy-tail distributions [108] where norms other than l_2 are more applicable. Also, perceptual error criteria may differ for some audio [15] or video applications [55] from the MSE. However, for most applications Gaussianity of the signals may generally be assumed.

The mean squared error (MSE) criterion ξ_{MSE} is given by the statistical expectation of the squared error signal,

$$\begin{aligned}
\xi_{\text{MSE}} &= \mathcal{E}\{e[n]e^*[n]\} = \mathcal{E}\left\{(d_n - \mathbf{w}^H\mathbf{x}_n)(d_n^* - \mathbf{x}_n^H\mathbf{w})\right\} && (2.5)\\
&= \mathcal{E}\{d_n d_n^*\} - \mathcal{E}\left\{\mathbf{w}^H\mathbf{x}_n d_n^*\right\} - \mathcal{E}\left\{d_n\mathbf{x}_n^H\mathbf{w}\right\} + \mathcal{E}\left\{\mathbf{w}^H\mathbf{x}_n\mathbf{x}_n^H\mathbf{w}\right\} && (2.6)\\
&= \sigma_{dd} - \mathbf{w}^H\mathcal{E}\{\mathbf{x}_n d_n^*\} - \mathbf{w}^T\mathcal{E}\{d_n\mathbf{x}_n^*\} + \mathbf{w}^H\mathcal{E}\left\{\mathbf{x}_n\mathbf{x}_n^H\right\}\mathbf{w} && (2.7)\\
&= \sigma_{dd} - \mathbf{w}^H\mathbf{p} - \mathbf{w}^T\mathbf{p}^* + \mathbf{w}^H\mathbf{R}\mathbf{w}, && (2.8)
\end{aligned}$$

where substitutions with the cross-correlation vector $\mathbf{p}$ and the auto-correlation matrix (covariance matrix for zero-mean processes) $\mathbf{R}$ have taken place. The cross-correlation vector $\mathbf{p}$ is thus defined by

$$\begin{aligned}
\mathbf{p} &= \mathcal{E}\{\mathbf{x}_n d_n^*\} = \left[\mathcal{E}\{x_n d_n^*\},\ \mathcal{E}\{x_{n-1} d_n^*\},\ \ldots\ \mathcal{E}\{x_{n-L_a+1} d_n^*\}\right]^T && (2.9)\\
&= \left[r_{xd}[0],\ r_{xd}[-1],\ \ldots\ r_{xd}[-L_a+1]\right]^T && (2.10)
\end{aligned}$$

where $r_{xd}[\tau]$ is the cross-correlation function between $x[n]$ and $d[n]$ [57, 149],

$$r_{xd}[\tau] := \mathcal{E}\{x[n+\tau]d^*[n]\} = r_{dx}^*[-\tau], \qquad (2.11)$$

where both $x[n]$ and $d[n]$ are assumed wide-sense stationary (wss) and independent. The "classic" assumption of statistical independence of $\mathbf{w}$ and $\mathbf{x}_n$ was also

assumed. The entries of the auto-correlation matrix $\mathbf{R} \in \mathbb{C}^{L_a \times L_a}$

$$\begin{aligned}\mathbf{R} &= \mathcal{E}\left\{\mathbf{x}_n \mathbf{x}_n^H\right\} = \mathcal{E}\left\{\begin{bmatrix} x_n x_n^* & x_n x_{n-1}^* & \dots & x_n x_{n-L_a+1}^* \\ x_{n-1} x_n^* & x_{n-1} x_{n-1}^* & \dots & x_{n-1} x_{n-L_a+1}^* \\ \vdots & \vdots & \ddots & \vdots \\ x_{n-L_a+1} x_n^* & x_{n-L_a+1} x_{n-1}^* & \dots & x_{n-L_a+1} x_{n-L_a+1}^* \end{bmatrix}\right\} \\ &= \begin{bmatrix} r_{xx}[0] & r_{xx}[-1] & \dots & r_{xx}[-L_a+1] \\ r_{xx}^*[-1] & r_{xx}[0] & \dots & r_{xx}[-L_a+2] \\ \vdots & \vdots & \ddots & \vdots \\ r_{xx}^*[-L_a+1] & r_{xx}^*[-L_a+2] & \dots & r_{xx}[0] \end{bmatrix} \end{aligned} \tag{2.12}$$

are samples of the auto-correlation function $r_{xx}[\tau]$ defined analogously to (2.11). $\mathbf{R}$ is Töplitz, i.e. has a band structure with identical elements on all diagonals and is Hermitian, i.e. $\mathbf{R}^H = \mathbf{R}$. Furthermore, $\mathbf{R}$ is positive semi-definite and has real valued eigenvalues, by sole virtue of these structural properties [72, 58].

The cost function ξ_{MSE} is apparently quadratic in the filter coefficients, and due to the positive semi-definiteness of $\mathbf{R}$, (2.8) has a minimum, which is unique for a positive definite (full rank) auto-correlation matrix $\mathbf{R}$. The cost function therefore forms an upright hyperparabola over the L_a-dimensional hyperplane defining all possible coefficient sets $\mathbf{w}_n$.

2.2.2 Minimization and Wiener-Hopf Solution

For the form of (2.8) and the properties of $\mathbf{R}$ mentioned in the last section, optimization of the cost function can be yielded by determining a coefficient vector, for which the first derivative of ξ_{MSE} with respect to the coefficients is zero.

Wirtinger Calculus. For a general function $f(w)$ of the complex valued variable $w = w_r + j w_i \in \mathbb{C}$, where w_r is the real part and w_i the imaginary part of w with the complex number $j = \sqrt{-1}$, Wirtinger calculus [43] gives derivatives

$$\frac{\partial f(w)}{\partial w} = \frac{1}{2}\left(\frac{\partial f(w)}{\partial w_r} - \frac{\partial f(w)}{\partial w_i}\right) \tag{2.13}$$

$$\frac{\partial f(w)}{\partial w^*} = \frac{1}{2}\left(\frac{\partial f(w)}{\partial w_r} + \frac{\partial f(w)}{\partial w_i}\right). \tag{2.14}$$

Using these equations, the two statements

$$\frac{\partial w}{\partial w} = 1 \quad , \qquad \frac{\partial w^*}{\partial w} = 0 \tag{2.15}$$

can easily be verified. To optimize for multiple parameters in the filter coefficient vector $\mathbf{w}$, a gradient operator ∇^*

$$\nabla^* = \frac{\partial}{\partial \mathbf{w}} = \begin{bmatrix} \frac{\partial}{\partial w_0} \\ \frac{\partial}{\partial w_1} \\ \vdots \\ \frac{\partial}{\partial w_{L_a-1}} \end{bmatrix}^* \tag{2.16}$$

is required. The asterix * indicates complex conjugation in accordance with the definition of the weight vector in (2.3). By applying (2.15), the important derivatives

$$\frac{\partial \mathbf{w}^T}{\partial \mathbf{w}} = \begin{bmatrix} \frac{\partial w_0}{\partial w_0} & \frac{\partial w_1}{\partial w_0} & \cdots & \frac{\partial w_{L_a-1}}{\partial w_0} \\ \frac{\partial w_0}{\partial w_1} & \frac{\partial w_1}{\partial w_1} & \cdots & \frac{\partial w_{L_a-1}}{\partial w_1} \\ \vdots & \vdots & \ddots & \vdots \\ \frac{\partial w_0}{\partial w_{L_a-1}} & \frac{\partial w_1}{\partial w_{L_a-1}} & \cdots & \frac{\partial w_{L_a-1}}{\partial w_{L_a-1}} \end{bmatrix}^* = \mathbf{I} \in \mathbb{R}^{L_a \times L_a} \tag{2.17}$$

and

$$\frac{\partial \mathbf{w}^H}{\partial \mathbf{w}} = \mathbf{0} \in \mathbb{R}^{L_a \times L_a} \tag{2.18}$$

can be denoted.

For optimization of a convex functional of complex parameters, according to (2.14) the functional has to be derived with respect to its *complex conjugate* coefficients

$$\xi_{\mathrm{MSE}}(\mathbf{w}) \stackrel{!}{=} \min \quad \longleftrightarrow \quad \nabla \xi_{\mathrm{MSE}} = \frac{\partial \xi_{\mathrm{MSE}}}{\partial \mathbf{w}^*} \stackrel{!}{=} \mathbf{0}, \tag{2.19}$$

to obtain the correct gradient. Therefore, to minimize the MSE performance function with respect to the coefficients requires

$$\frac{\partial \xi_{\mathrm{MSE}}}{\partial \mathbf{w}^*} = -\mathbf{p} + \frac{\partial}{\partial \mathbf{w}^*} \mathbf{w}^H \mathbf{R} \mathbf{w} \stackrel{!}{=} \mathbf{0}. \tag{2.20}$$

With transposing the scalar quantity $(\mathbf{w}^H\mathbf{R}\mathbf{w})^T = \mathbf{w}^T\mathbf{R}^T\mathbf{w}^*$, the product rule can be applied to solve the derivative for the second summand in (2.20),

$$\frac{\partial}{\partial \mathbf{w}^*}\mathbf{w}^H\mathbf{R}\mathbf{w} = \left(\frac{\partial}{\partial \mathbf{w}^*}\mathbf{w}^H\right)\mathbf{R}\mathbf{w} + \left(\frac{\partial}{\partial \mathbf{w}^*}\mathbf{w}^T\mathbf{R}^T\right)\mathbf{w}^*. \tag{2.21}$$

Thus, with (2.17) and (2.18), (2.20) yields with $\mathbf{R}^T = \mathbf{R}^*$

$$\frac{\partial \xi_{\mathrm{MSE}}}{\partial \mathbf{w}^*} = -\mathbf{p} + \mathbf{R}\mathbf{w} \stackrel{!}{=} \mathbf{0}. \tag{2.22}$$

If the auto-correlation matrix $\mathbf{R}$ is regular, by inversion of $\mathbf{R}$ (2.22) can be solved for the optimum coefficient set

$$\mathbf{w}_{\mathrm{opt}} = \mathbf{R}^{-1}\mathbf{p}, \tag{2.23}$$

which is well-known as Wiener-Hopf solution.

If $\mathbf{R}$ has not full rank, (2.23) cannot be computed. Due to the non-uniqueness of the minimum, an infinite number of optimal solutions exists. If $\mathbf{R}$ has reduced rank r, the solution for $\mathbf{w}$ with the smallest l_2-norm is given by the pseudo-inverse of a matrix consisting of r linearly independent rows of $\mathbf{R}$ and the according entries in the cross-correlation vector $\mathbf{p}$.

2.2.3 Minimum Mean Squared Error

If the desired signal $d[n]$ is assumed to be a superposition of a signal correlated with the input signal $x[n]$, and uncorrelated noise $z[n]$,

$$d_n = \mathbf{w}_{\mathrm{opt}}^H\mathbf{x}_n + z_n, \tag{2.24}$$

where $\mathbf{w}_{\mathrm{opt}}$ is responsible for the correlation between $x[n]$ and $d[n]$, the residual error signal e_n will possess non-zero variance. The actual residual MSE at the optimum solution, i.e. $\mathbf{w} = \mathbf{w}_{\mathrm{opt}}$, is called Minimum MSE (MMSE) and can be calculated by inserting the expansion (2.24) for $d[n]$ into (2.5),

$$\xi_{\mathrm{MMSE}} = \mathcal{E}\{e_n e_n^*\}\Big|_{\mathbf{w}=\mathbf{w}_{\mathrm{opt}}} = \mathcal{E}\{z_n z_n^*\} = \sigma_{zz}^2 \tag{2.25}$$

which is the variance of the observation noise, $z[n]$. Any mismatches in the model $\mathbf{w}$, e.g. as a result of impulse response truncation due to a too short model, can be included into the observation noise and will represent an offset from zero for the MSE cost function.

2.3 Least Mean Square Algorithms

2.3.1 Preliminaries — Gradient Descent Techniques

The quadratic form of the cost function ξ_{MSE} derived in Sec. 2.2.2 allows for iterative solutions to find the minimum. For minimization of convex functionals the general rule is to step-by-step follow the negative gradient of the cost function, which will eventually lead to the unique global minimum. Mathematically, this can be phrased as

$$\mathbf{w}[n+1] = \mathbf{w}[n] - \mu \nabla \xi_{\mathrm{MSE}}[n], \tag{2.26}$$

where $\mathbf{w}[n]$ marks the current weight vector at time n, from where a step is taken in direction of the negative gradient $\nabla\xi[n]$ of the cost function to yield a new improved coefficient vector $\mathbf{w}[n+1]$. The notation $\nabla\xi_{\mathrm{MSE}}[n]$ is to indicate that the gradient is applied to the MSE cost function yielded by the coefficient vector $\mathbf{w}_n$ at time n. The parameter μ is referred to as step-size, loosely defining the length of a step by relaxation of the modulus of the gradient.

The explicit term for the gradient has been derived with (2.22),

$$\nabla \xi_{\mathrm{MSE}}[n] = \frac{\partial \xi_{\mathrm{MSE}}}{\partial \mathbf{w}_n^*} = -\mathbf{p} + \mathbf{R}\mathbf{w}_n \quad , \tag{2.27}$$

and insertion into (2.26) leads to the update equation known as the steepest descent algorithm [174, 72]. Apparently, no more inversion of the auto-correlation matrix is required, but both auto-correlation matrix $\mathbf{R}$ and cross-correlation vector $\mathbf{p}$ have to be reliably estimated. This can involve very long data windows, however recursive estimates can be performed as discussed later in Sec. 2.4.2. Furthermore, the multiplication with $\mathbf{R}$ creates a computational cost of order $\mathcal{O}(L_a^2)$.

2.3.2 One Sample Gradient Estimates

To lower the computational complexity and statistical record of the involved signals, in a next step the true gradient is replaced by an estimate based only on

LMS Algorithm	
1:	$y_n = \mathbf{w}_n^H \mathbf{x}_n$
2:	$e_n = d_n - y_n$
3:	$\mathbf{w}_{n+1} = \mathbf{w}_n + \mu \mathbf{x}_n e_n^*$

Table 2.1: Equations for filter update by LMS adaptive algorithm.

the previous samples of $x[n]$ and $d[n]$,

$$\hat{\mathbf{p}} = \mathbf{x}_n d_n^* \tag{2.28}$$

$$\hat{\mathbf{R}} = \mathbf{x}_n \mathbf{x}_n^H \tag{2.29}$$

which is equivalent to minimizing the instantaneous squared error, $e_n e_n^*$, rather than the MSE. Inserting these estimates into (2.27)

$$\hat{\nabla}\xi_n = -\hat{\mathbf{p}} + \hat{\mathbf{R}}\mathbf{w}_n = -\mathbf{x}_n(d_n^* - \mathbf{x}_n^H \mathbf{w}_n) = -\mathbf{x}_n e_n^* \tag{2.30}$$

gives a gradient estimate, which together with (2.26) forms the basis for the least mean squares (LMS) algorithm [173, 174, 72]

$$\mathbf{w}_{n+1} = \mathbf{w}_n + \mu \mathbf{x}_n e_n^* \quad . \tag{2.31}$$

The complete LMS equations are listed in Tab. 2.1, and are compared to previous adaptive algorithms only of order $\mathcal{O}(L_a)$. Some of the LMS' properties are discussed below.

2.3.3 Convergence Characteristics

For a full proof of convergence, the reader is referred to standard text books [174, 72, 73, 132, 93]. To prove that the LMS algorithm converges to the Wiener-Hopf solution, two steps are required: (i) convergence in the mean to show that the LMS solution is bias-free, (ii) convergence in the mean square to prove consistency. Although (ii) presents a much stronger proof of convergence, (i) is easier to derive and motivates some insight into the behaviour of the LMS algorithm. Therefore, in the following, the presentation is restricted to (i).

2.3.3.1 Convergence Limits

To prove convergence in the mean, the LMS update equation — the one sample gradient estimate (2.30) inserted into (2.26) — is modified by taking expectations:

$$\mathcal{E}\{\mathbf{w}_{n+1}\} = \mathcal{E}\{\mathbf{w}_n\} + \mu \cdot \mathcal{E}\{\mathbf{x}_n e_n^*\} \,. \tag{2.32}$$

We insert $d_n = \mathbf{w}_{\text{opt}}^H \mathbf{x}_n + z_n$, i.e. the output of the unknown system at time n, superposed by observation noise, into the error equation

$$e_n^* = d_n^* - \mathbf{x}_n^H \mathbf{w}_n = \mathbf{x}_n^H (\mathbf{w}_{\text{opt}} - \mathbf{w}_n) + z_n \tag{2.33}$$

and substitute this error term into (2.32) to yield

$$\mathcal{E}\{\mathbf{w}_{n+1}\} = \mathcal{E}\{\mathbf{w}_n\} + \mu \cdot \mathcal{E}\left\{\mathbf{x}_n \mathbf{x}_n^H (\mathbf{w}_{\text{opt}} - \mathbf{w}_n) + \mathbf{x}_n z_n\right\} . \tag{2.34}$$

Assuming that the observation noise z_n is uncorrelated with the input signal x_n, i.e. $\mathcal{E}\{\mathbf{x}_n z_n\} = 0$ leads to

$$\mathcal{E}\{\mathbf{w}_{n+1}\} = \mathcal{E}\{\mathbf{w}_n\} + \mu \cdot \mathcal{E}\left\{\mathbf{x}_n \mathbf{x}_n^H\right\} \cdot (\mathbf{w}_{\text{opt}} - \mathcal{E}\{\mathbf{w}_n\}) \tag{2.35}$$

By expanding with a summand $-\mathbf{w}_{\text{opt}}$ on either side, a substitution with

$$\mathbf{v}_n = \mathcal{E}\{\mathbf{w}_n\} - \mathbf{w}_{\text{opt}} \tag{2.36}$$

translates the average weight vector $\mathcal{E}\{\mathbf{w}_n\}$ such that the resulting coefficient vector $\mathbf{v}_n$ fulfills

$$\mathbf{v}_n \longrightarrow \mathbf{0} \qquad \text{for} \qquad n \longrightarrow \infty \tag{2.37}$$

if the algorithm converges. The expected update equation in terms of $\mathbf{v}_n$ now can be written as

$$\mathbf{v}_{n+1} = \mathbf{v}_n - \mu \mathbf{R} \cdot \mathbf{v}_n = (\mathbf{I} - \mu \mathbf{R}) \mathbf{v}_n \quad . \tag{2.38}$$

Now conider the eigenvalue decomposition of the auto-correlation matrix $\mathbf{R}$,

$$\mathbf{R} = \mathbf{Q} \Lambda \mathbf{Q}^H \tag{2.39}$$

where $\Lambda = \text{diag}\{\lambda_0, \lambda_1, \cdots \lambda_{L_a-1}\}$ holds the eigenvalues $\lambda_i \geq 0$ and $\mathbf{Q}$ the eigenvectors of $\mathbf{R}$. In particular, the modal matrix $\mathbf{Q}$ is unitary, i.e. possessing the property $\mathbf{Q}^{-1} = \mathbf{Q}^H$, and therefore $\mathbf{Q}\mathbf{Q}^H = \mathbf{I} \in \mathbb{R}^{L_a \times L_a}$. Using the modal matrix $\mathbf{Q}$, a rotation

$$\mathbf{u}_n = \mathbf{Q}\mathbf{v}_n, \tag{2.40}$$

is introduced to substitute $\mathbf{v}_n = \mathbf{Q}^H\mathbf{u}_n$ for $\mathbf{u}_n$,

$$\mathbf{u}_{n+1} = \mathbf{Q}(\mathbf{I} - \mu\mathbf{R})\mathbf{Q}^H\mathbf{u}_n = (\mathbf{I} - \mu\Lambda)\mathbf{u}_n. \tag{2.41}$$

Therefore, by taking expectations in (2.32), translation (2.36), and rotation (2.40), the LMS weight update arrives at a form which exhibits coefficients in a decoupled representation. Eqn. (2.41) also allows to trace adaptation back to the initial coefficient vector $\mathbf{u}_0$,

$$\mathbf{u}_n = (\mathbf{I} - \mu\Lambda)^n\mathbf{u}_0 \quad , \qquad \mathbf{u}_0 \text{ arbitrary.} \tag{2.42}$$

The evolution of each decoupled weight is described by a geometric series

$$u_{i,n} = (1 - \mu\lambda_i)^n u_{i,0} \qquad \text{for } i = 0(1)L_a - 1 \tag{2.43}$$

for arbitrary start values $u_{i,0}$, which converges iff

$$|1 - \mu\lambda_i| < 1 \quad \Longleftrightarrow \quad 0 < \mu < \frac{2}{\lambda_i} \qquad \text{for } i = 0(1)L_a - 1 \tag{2.44}$$

holds for each of the L_a modes. Therefore, the general requirement on μ demands limits

$$0 < \mu < \frac{2}{\lambda_{\max}}. \tag{2.45}$$

In practice, the upper convergence limit on μ can be safely approximated by

$$\lambda_{\max} \leq \sum_{i=0}^{L_a-1} \lambda_i = \text{tr}\{\mathbf{R}\} = L_a \cdot \sigma_{xx}^2, \tag{2.46}$$

where the positive semi-definiteness of $\mathbf{R}$ insures the approximation by the trace $\text{tr}\{\cdot\}$ of the auto-correlation matrix $\mathbf{R}$, which according to (2.12) can be expressed by the power or variance $\sigma_{xx}^2 = r_{xx}[0]$ of the input signal $x[n]$ and the filter length L_a, yielding

$$0 < \mu < \frac{2}{L_a\sigma_{xx}^2} \tag{2.47}$$

as practically calculable convergence limits for μ.

2.3.3.2 Convergence Speed

In the mean, the LMS exhibits an exponential convergence, which can be seen from the decoupled evolution of the algorithm in (2.43). A measure for the convergence speed in form of a time constant T can be derived by fitting an exponential $e^{-n/T}$ to the geometric series in (2.43),

$$(1-\mu\lambda_i)^n = e^{n\cdot\ln(1-\mu\lambda_i)} \qquad \Longrightarrow T_i = -\frac{1}{\ln(1-\mu\lambda_i)} \quad \text{for } i = 0(1)L_a-1. \tag{2.48}$$

A simplification for the T_i is possible by exploiting the series expansion [18]

$$\ln(1-\alpha) = -\alpha - \frac{\alpha^2}{2} - \frac{\alpha^3}{3}\cdots - \frac{\alpha^n}{n}\cdots \qquad \forall \quad -1 \leq \alpha < 1 \tag{2.49}$$

$$\approx -\alpha \qquad \forall \quad |\alpha| \ll 1 \quad . \tag{2.50}$$

Thus for $\alpha = \mu\lambda_i$, (2.48) yields

$$T_i \approx \frac{1}{\mu\lambda_i} \qquad \forall|\mu\lambda_i| \ll 1. \tag{2.51}$$

Although the validity of this approximation is based on restrictions on λ, two statements can be made:

- the overall convergence is governed by the slowest converging mode belonging to the smallest eigenvalue $\lambda_{\min}$ of $\mathbf{R}$;
- the maximum speed of convergence has to be set according to (2.45) to accommodate for the largest eigenvalue $\lambda_{\max}$ of $\mathbf{R}$.

Therefore, if the eigenvalues of $\mathbf{R}$ differ greatly, the convergence of the adaptive system is slowed down. This influence of the auto-correlation sequence of the input signal on the convergence speed of the adaptive system can be expressed by the condition number of $\mathbf{R}$ [141, 58], also often referred to as *eigenvalue spread* [72]

$$\rho = \frac{\lambda_{\min}}{\lambda_{\max}} \leq \frac{\min_\Omega S_{xx}(e^{j\Omega})}{\max_\Omega S_{xx}(e^{j\Omega})}. \tag{2.52}$$

This ratio between the minimum and maximum eigenvalue can be shown to relate to the extrema of the power spectral density (PSD) of the input signal $x[n]$, $S_{xx}(e^{j\Omega})$ [72] as indicated on the right hand side of (2.52).

2.3.3.3 Bias and Consistency

The analysis of convergence of the LMS algorithm in the mean in Sec. 2.3.3.1 has shown that the coefficients approach the optimum if the step-size μ of the LMS algorithm is kept within its convergence bounds. Therefore, the adaptation is free of bias terms [72]. This holds as long as the system to be identified is stationary. If changes over time occur, or in the extreme case a dynamic system has to be tracked, a bias is produced by lagging behind the optimum solution by an amount proportional to the step size [93, 73, 165].

Analysis of LMS convergence in the mean squared reveals that the final error variance will differ from the MMSE value by an excess MSE, $\xi_{\mathrm{EX}} = \xi_{\mathrm{MSE}}[n] - \xi_{\mathrm{MMSE}}$ with $n \to \infty$, which can be derived as [72]

$$\xi_{\mathrm{EX}} = \xi_{\mathrm{MMSE}} \cdot \frac{a}{1-a}, \qquad \text{with } a = \sum_{i=0}^{L_a-1} \frac{\mu\lambda_i}{2-\mu\lambda_i}. \tag{2.53}$$

The influence of μ is such that a trade-off is created between convergence speed (large for large μ) and the size of the final MSE, $\xi_{\mathrm{MSE}}[n]$ for $n \to \infty$, which is kept small if a small parameter μ is selected.

2.4 Least Squares Methods

Instead of trying to minimize the expectation of the squared error as done in the gradient descent and LMS techniques in Sec. 2.3, least squares (LS) algorithms directly optimize the coefficient set in terms of a sum of squared errors. Although taking a different approach, in the limit this method will tend towards the Wiener-Hopf solution. Here, first the general LS methodology is introduced. A recursive estimation of required quantities then leads to the well-known recursive LS (RLS) algorithm. The last part of this section will then discuss complexity issues of the RLS.

2.4.1 Least Squares Formulation

The performance criterion to be minimized in the least squares approach is a sum of squared errors over all previous samples up to the current time, n

$$\xi_{\mathrm{LS},n} = \sum_{\nu=0}^{n} \beta^{\nu} e[n-\nu] e^{*}[n-\nu], \tag{2.54}$$

where $0 < \beta \leq 1$ — often referred to as forgetting factor — is introduced to de-emphasize past error contributions by an exponential time window. Analogue to (2.19), the minimization of this error criterion requires

$$\nabla \xi_{\mathrm{LS},n} = \frac{\partial \xi_{\mathrm{LS},n}}{\partial \mathbf{w}_n^{*}} \stackrel{!}{=} \mathbf{0}. \tag{2.55}$$

The optimization procedure runs similar to the derivations in Sec. 2.2.2 [149, 72] and yields

$$\mathbf{R}_n \mathbf{w}_n = \mathbf{p}_n \tag{2.56}$$

with close similarity to the original Wiener-Hopf equation (2.23), whereby the quantities $\mathbf{R}_n$ and $\mathbf{p}_n$ are defined as

$$\mathbf{R}_n = \sum_{\nu=0}^{n} \beta^{\nu} \mathbf{x}[n-\nu] \mathbf{x}^{H}[n-\nu] \tag{2.57}$$

and

$$\mathbf{p}_n = \sum_{\kappa=0}^{n} \beta^{\nu} d^{*}[n-\nu] \mathbf{x}[n-\nu], \tag{2.58}$$

thus implementing estimates of the auto-correlation matrix $\mathbf{R}$ and the cross-correlation vector $\mathbf{p}$ in the original derivation of the Wiener-Hopf solution. In particular with $\beta = 1$ and for $x[n]$ and $d[n]$ being wide sense stationary (WSS) signals, in the limit case the estimates (2.57) and (2.58) tend towards the true statistical quantities, e.g. $\lim_{n\to\infty} \mathbf{R}_n = \mathbf{R}$, apart from a normalization factor.

2.4.2 Recursive Least Squares Algorithm

The aim of RLS is to allow an updated vektor $\mathbf{w}_{n+1}$ to be produced from a knowledge of $\mathbf{w}_n$, $\mathbf{R}_{n-1}$, and $\mathbf{p}_{n-1}$, i.e. without explicitly solving $\mathbf{w}_{n+1} = \mathbf{R}_n^{-1} \mathbf{p}_n$.

This is based on recursively updating the estimates (2.57) and (2.58) by

$$\mathbf{R}_n = \beta \mathbf{R}_{n-1} + \mathbf{x}_n \mathbf{x}_n^H \tag{2.59}$$

and

$$\mathbf{p}_n = \beta \mathbf{p}_{n-1} + d_n^* \mathbf{x}_n, \tag{2.60}$$

and solving (2.56) for each time index n. This equation involves an inversion of $\mathbf{R}_n$, which can also be performed iteratively by applying the Matrix Inversion Lemma [174, 72]

$$(\mathbf{A} + \mathbf{BCD})^{-1} = \mathbf{A}^{-1} - \mathbf{A}^{-1}\mathbf{B}(\mathbf{C}^{-1} + \mathbf{D}\mathbf{A}^{-1}\mathbf{B})^{-1}\mathbf{D}\mathbf{A}^{-1} \tag{2.61}$$

to (2.59) and identifying $\mathbf{A} = \lambda \mathbf{R}_{n-1}$, $\mathbf{B} = \mathbf{x}_n$, $\mathbf{C} = 1$, and $\mathbf{D} = \mathbf{x}_n^H$. By denoting the recursive inverse of the estimated auto-correlation matrix by $\mathbf{S}_n = \mathbf{R}_n^{-1}$, this yields

$$\mathbf{S}_n = \frac{1}{\beta}\left(\mathbf{S}_{n-1} - \frac{\mathbf{S}_{n-1}\mathbf{x}_n\mathbf{x}_n^H\mathbf{S}_{n-1}}{\beta + \mathbf{x}_n^H\mathbf{S}_{n-1}\mathbf{x}_n}\right) \quad . \tag{2.62}$$

Note that the initial $\mathbf{S}_0$ is required to be regular; it is usually set equal to some small diagonal matrix. Defining a gain vector

$$\mathbf{g}_n = \frac{\mathbf{S}_{n-1}\mathbf{x}_n}{\beta + \mathbf{x}_n^H\mathbf{S}_{n-1}\mathbf{x}_n} \tag{2.63}$$

and inserting (2.59) and (2.62) into $\mathbf{w}_{n+1} = \mathbf{S}_n\mathbf{p}_n$, one finally arrives with some re-arrangements in the resulting equation [149] at the RLS weight update

$$\mathbf{w}_{n+1} = \mathbf{w}_n + \mathbf{g}_n e_n^*. \tag{2.64}$$

Together with the filter equations, the update procedure is listed in Tab. 2.2 in a numerically efficient fashion.

The initial setting $\mathbf{S}_0 = \delta\mathbf{I}$ introduces a bias into the estimate of the inverse auto-correlation matrix. When analyzing the convergence [72], it can be shown that the bias tends to zero and the MSE converges — different from the LMS — toward the MMSE without any excess MSE for $n \to \infty$ under the assumption of wss signals, a small observation noise level, and for a infinite memory with a

RLS Algorithm	
1:	$y_n = \mathbf{w}_n^H \mathbf{x}_n$
2:	$e_n = d_n - y_n$
3:	$\mathbf{r} = \mathbf{x}_n^H \mathbf{S}_{n-1}$
4:	$\kappa = \beta + \mathbf{r}\mathbf{x}_n$
5:	$\mathbf{g}_n = \mathbf{S}_{n-1}\mathbf{x}_n / \kappa$
6:	$\mathbf{w}_{n+1} = \mathbf{w}_n + \mathbf{g}_n e_n^*$
7:	$\mathbf{S}_n = \frac{1}{\beta}(\mathbf{S}_{n-1} - \mathbf{g}_n \mathbf{r})$

Table 2.2: Equations for filter update by RLS adaptive algorithm.

forgetting factor $\beta = 1$. Generally, in stationary environments, the behaviour of the RLS is therefore far superior to the LMS, both in terms of convergence speed and final misadjustment.

Problems arise in non-stationary situations. There, a forgetting factor $\beta < 1$ has to be chosen to ensure that the algorithm "focuses" on the current statistics and is not biased by its old memory. This has a serious influence on the tracking of dynamic systems which sometimes may arise in identification problems [165, 140], for which the LMS can actually in certain situations attain better performances [9, 92, 10, 94].

2.4.3 Algorithm Complexity

The computational complexity of the RLS algorithm as listed in the summary of Tab. 2.2 results in

$$C_{\mathrm{RLS}} = 3L_a + 3L_a^2 \tag{2.65}$$

multiplications, where L_a is the filter length. Note that a total of L_a divisions per sampling period are required. Clearly, the RLS has a complexity which is an order higher than the LMS with its $\mathcal{O}(L_a)$ complexity $C_{\mathrm{LMS}} = 1 + 2L_a$. Therefore in the past much effort has been dedicated to achieve fast versions of the RLS with reduced complexity.

2.5 Links Between LMS and RLS Algorithms

2.5.1 Normalized LMS Algorithm

A couple of different approaches to derive the update equations of what is commonly known as the normalized LMS (NLMS) algorithm will give some insight into the links between LMS and RLS. Furthermore, this will lead over to affine projection algorithms which are very popular for applications like acoustic echo cancellation [111, 50, 51, 95] due to there fast convergence even for coloured input signals with high eigenvalue spread such as speech.

2.5.1.1 Approaching from the LMS: Normalization of the Step Size

A simple description of the step size bounds for the LMS has been derived in Sec. 2.3.3.1, with a dependence on the signal energy and the filter length. A fixed choice of μ generally has the drawback that in a non-stationary environment, where the variance of the input signal is changing, the convergence speed at times of low variance may be insufficient, as the algorithm still has to be stable at times of high signal power. Therefore, a step size normalization to exclude the influence of the signal power appears desirable.

If the variance of the input signal $x[n]$ is estimated over a rectangular window of length L_a, i.e.

$$\sigma_{xx}^2 \approx \frac{1}{L_a} \sum_{\nu=0}^{L_a-1} |x[n-\nu]|^2 = \frac{1}{L_a} \mathbf{x}_n^H \mathbf{x}_n, \tag{2.66}$$

the step size parameter μ can be substituted by

$$\mu = \frac{\tilde{\mu}}{\mathbf{x}_n^H \mathbf{x}_n}, \tag{2.67}$$

resulting in the update equation for the NLMS algorithm in Tab. 2.3. The substitution introduced with (2.67) performs a normalization of the step size parameter by imposing new convergence limits

$$0 < \tilde{\mu} < 2. \tag{2.68}$$

The selection of $\tilde{\mu}$ sets a relative convergence speed independent of the variance of the filter input signal $x[n]$.

NLMS Algorithm	
1:	$y_n = \mathbf{w}_n^H \mathbf{x}_n$
2:	$e_n = d_n - y_n$
3:	$\mathbf{w}_{n+1} = \mathbf{w}_n + \tilde{\mu} \frac{\mathbf{x}_n e_n^*}{\mathbf{x}_n^H \mathbf{x}_n}$

Table 2.3: Equations for filter update by NLMS adaptive algorithm.

The complexity of the NLMS has two additional multiplications over the LMS to compute the power estimate $\mathbf{x}^H\mathbf{x}$, if a moving average (MA) is considered whereby the change over the previous power estimate is the inclusion of the new value $x_n^* x_n$ and the exclusion of $x_{n-L_a}^* x_{n-L_a}$, values which have to be kept in the tap-delay line anyway. The required division can be circumvented by a fast look-up table or an approximation with a shift and add procedure.

2.5.1.2 Least-Squares Approach to NLMS: Projection Algorithm

Different from the normalization approach, the NLMS can also be seen as the solution of the following optimization problem:
Given the present weight vector $\mathbf{w}_n$*, the state vector* $\mathbf{x}_n$*, and present value of the desired signal* d_n*, calculate a new coefficient set* $\mathbf{w}_{n+1}$ *such that*

$$\|\mathbf{w}_{n+1} - \mathbf{w}_n\|_2 \stackrel{!}{=} \min, \tag{2.69}$$

subject to the condition

$$\mathbf{w}_{n+1}^H \mathbf{x}_n \stackrel{!}{=} d[n]. \tag{2.70}$$

Haykin [72] explicitly shows how solving this problem analytically will yield the NLMS with $\tilde{\mu} = 1$. Instead, here a geometrical interpretation will be given to derive the NLMS solution from (2.69) and (2.70).

The interpretation starts from the scalar product (2.70) between the vectors $\mathbf{x}_n$ and $\mathbf{w}_{n+1}$, both of dimension L_a, by introducing a normalization with $1/\|\mathbf{x}_n\|_2$ on either side,

$$\mathbf{w}_{n+1}^H \frac{\mathbf{x}_n}{\|\mathbf{x}_n\|_2} \stackrel{!}{=} \frac{d_n}{\|\mathbf{x}_n\|_2} \quad . \tag{2.71}$$

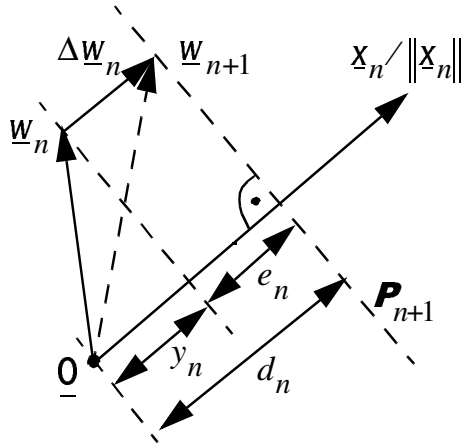

Figure 2.2: Geometrical interpretation of the NLMS.

It follows from Fig. 2.2, that possible solutions for $\mathbf{w}_{n+1}$ orthogonally project onto the unit length vector $\mathbf{x}_n/\|\mathbf{x}_n\|_2$ such that the resulting projection has length $d_n/\|\mathbf{x}_n\|_2$. The solution space for $\mathbf{w}_{n+1}$ has dimension L_a-1 and forms a hyperplane $\mathbf{P}_{n+1}$ defined by its normal $\mathbf{x}_n/\|\mathbf{x}_n\|_2$.

Eqn. (2.70) demands that from the hyperplane $\mathbf{P}_{n+1}$ we select the solution with minimum distance from the previous solution $\mathbf{w}_n$. Again, minimum distance in the l_2 sense means the orthogonal projection from $\mathbf{w}_n$ onto $\mathbf{P}_{n+1}$, which is marked as the innovation $\Delta\mathbf{w}_n$ in Fig. 2.2. For this innovation vector, the direction and length can be obtained by inspection:

- as the projection is orthogonal, the direction is given by the normal of $\mathbf{P}_{n+1}$, the normalized state vector $\mathbf{x}_n/\|\mathbf{x}_n\|_2$;
- the length of the projection $\Delta\mathbf{w}_n$ can be stated as $e_n/\|\mathbf{x}_2\|_2$.

Together, this yields for the innovation

$$\mathbf{w}_{n+1} = \mathbf{w}_n + \Delta\mathbf{w}_n = \mathbf{w}_n + \underbrace{\frac{e_n^*}{\|\mathbf{x}_n\|_2}}_{\text{length}} \cdot \underbrace{\frac{\mathbf{x}_n}{\|\mathbf{x}_n\|_2}}_{\text{direction}} \quad . \tag{2.72}$$

By introducing a relaxation $\tilde{\mu}$ into the update, i.e. at each iteration the innovation gets scaled by $\tilde{\mu}$,

$$\mathbf{w}_{n+1} = \mathbf{w}_n + \tilde{\mu}\frac{\mathbf{x}_n \cdot e_n^*}{\mathbf{x}_n^H\mathbf{x}_n}, \tag{2.73}$$

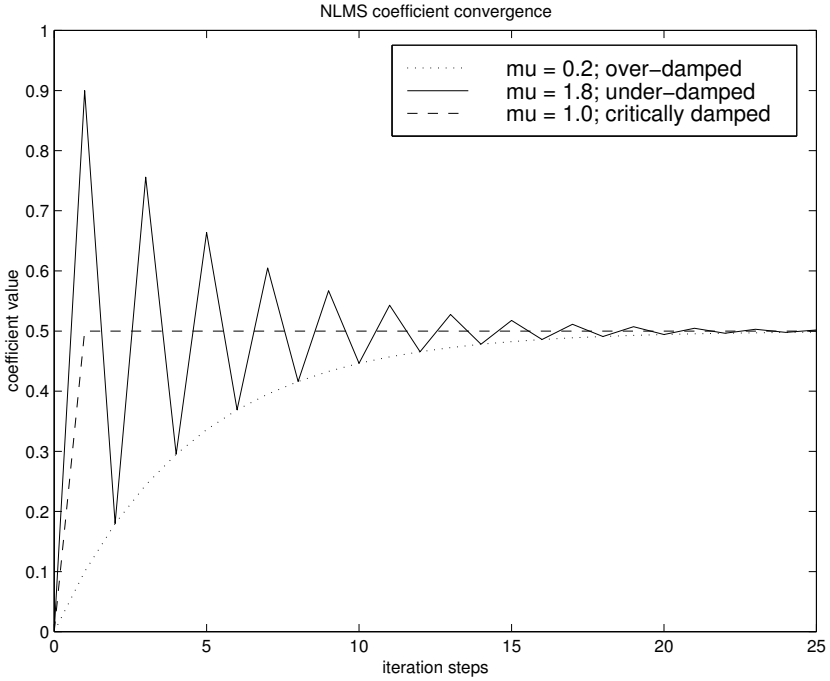

Figure 2.3: NLMS with different convergence parameters, resulting in different forms of adaptation.

finally the NLMS update equation is reached.

It can be noted that for the fastest convergence parameter, the NLMS can be viewed as a best fit solution in the least squares sense of the filter output to the desired signal regardless of correlations [130]. However different from the RLS method discussed in Sec. 2.4.1 minimizing sums of squared errors, this least-squares fit only refers to one single time step. This clearly forms a disadvantage in the presence of noise, as the filter will try to suppress any desired signal regardless of underlying statistics [140].

For the noise-free case, depending on the size of the relaxation factor, convergence may be classified into three cases as shown in Fig. 2.3 for a single-coefficient filter. Apart from fastest convergence for $\tilde{\mu} = 1$, slower convergence can either mean sliding down the performance surface ($\tilde{\mu} < 1$) or jumping from side to side resulting in an alternating asymptotic behaviour ($\tilde{\mu} > 1$).

2.5.2 Affine Projection Algorithms

Affine projection algorithms (APA) are a class of popular algorithms within the acoustic echo cancellation community [111, 50, 51, 95], and are therefore believed to be important in this context. Furthermore, the APA forms a cohesive link between NLMS and RLS, as will be shown in the following.

2.5.2.1 Formulation

Similar to the NLMS, the APA demands a change in the coefficients

$$\|\mathbf{w}_{n+1} - \mathbf{w}_n\|_2 \stackrel{!}{=} \min, \tag{2.74}$$

which is minimum in the sense of the l_2 norm. However, besides the fit to the present data, the new coefficient set $\mathbf{w}_{n+1}$ also has to best fit $p-1$ past input vectors to the according desired signals

$$\mathbf{x}_n^H \mathbf{w}_{n+1} \stackrel{!}{=} d_n^* \tag{2.75}$$

$$\mathbf{x}_{n-1}^H \mathbf{w}_{n+1} \stackrel{!}{=} d_{n-1}^* \tag{2.76}$$

$$\vdots \tag{2.77}$$

$$\mathbf{x}_{n-P+1}^H \mathbf{w}_{n+1} \stackrel{!}{=} d_{n-P+1}^*, \tag{2.78}$$

where p defines the order of the APA. The above system of equations can be conveniently expressed in matrix notation

$$\mathbf{X}_n^H \mathbf{w}_{n+1} \stackrel{!}{=} \mathbf{d}_n^*. \tag{2.79}$$

Defining the coefficient innovation in (2.74) as $\Delta\mathbf{w}_{n+1} = \mathbf{w}_{n+1} - \mathbf{w}_n$, we have

$$\mathbf{X}_n^H \Delta\mathbf{w}_{n+1} \stackrel{!}{=} \mathbf{e}_n^* \quad , \tag{2.80}$$

where $\mathbf{e}_n^* = \mathbf{d}_n^* - \mathbf{X}_n^H \mathbf{w}_n$. The minimum norm solution for $\Delta\mathbf{w}_{n+1}$ as demanded in (2.74) is given by the pseudo-inverse of $\mathbf{X}_n^H$ [22, 58]. Depending on whether the system of equations (2.80) is underdetermined ($P < L_a$) or overdetermined ($P \geq L_a$), either the left or right pseudo-inverse has to be used. Here, we only consider the underdetermined case $P < L_a$ which involves the left pseudo-inverse $(\mathbf{X}_n^H)^\dagger = \mathbf{X}_n(\mathbf{X}_n^H\mathbf{X}_n)^{-1}$, yielding the APA update [111, 89]

$$\mathbf{w}_{n+1} = \mathbf{w}_n + \mathbf{X}_n(\mathbf{X}_n^H\mathbf{X}_n)^{-1}\mathbf{e}_n^* \quad . \tag{2.81}$$

pth order APA Algorithm	
1:	update $\mathbf{X}_n$ and $\mathbf{d}_n$
2:	$\mathbf{e}_n = \mathbf{d}_n - \mathbf{X}_n^T \mathbf{w}_n^*$
3:	$\mathbf{R}_n^{-1} = (\mathbf{X}_n^H \mathbf{X}_n + \alpha \mathbf{I})^{-1}$
4:	$\mathbf{w}_{n+1} = \mathbf{w}_n + \eta \mathbf{X}_n \mathbf{R}_n^{-1} \mathbf{e}_n^*$

Table 2.4: Equations for filter update by APA adaptive algorithm.

Introducing a relaxation factor η into (2.81), one yields the update equation for the pth order affine projection algorithm:

$$\mathbf{w}_{n+1} = \mathbf{w}_n + \eta \mathbf{X}_n (\mathbf{X}_n^H \mathbf{X}_n)^{-1} \mathbf{e}_n^* \quad . \tag{2.82}$$

A numerically efficient implementation of this algorithm is listed in Tab. 2.4, where a weighted identity matrix is included in the matrix inversion of step (3) for regularization purposes.

The convergence of APA is surveyed in e.g. [111, 100], and its speed is for rising projection order p less dependent on the eigenvalue spread, i.e. the colouredness of the input signal. A noise-free simulation for different projection orders is shown in Fig. 2.4, where a system identification is attempted using a coloured input signal. Also shown are the learning curves of NLMS and RLS, which represent both extremes of the projection order. The APA for $p = 1$ yields an NLMS, while for $p = n$, the function to be minimized is equal to an RLS with $\beta = 1$. For $p = L_a$, the APA can be linked to a block version of the RLS [100].

Following the implementation steps in Tab. 2.4, the computational complexity of the APA can be recorded as

$$C_{\mathrm{APA}} = (p^2 + \mathcal{O}(p^3)) + 2pL_a \quad , \tag{2.83}$$

where L_a is the length of the adaptive filter and p the projection order. The term $\mathcal{O}(p^3)$ indicates the complexity of the matrix inverse calculated in step (3:) of Tab. 2.4. Fast implementations of APA (FAPA) claim to reduce this cost to $C_{\mathrm{FAPA}} = 2L_a + 20p$ [51, 145].

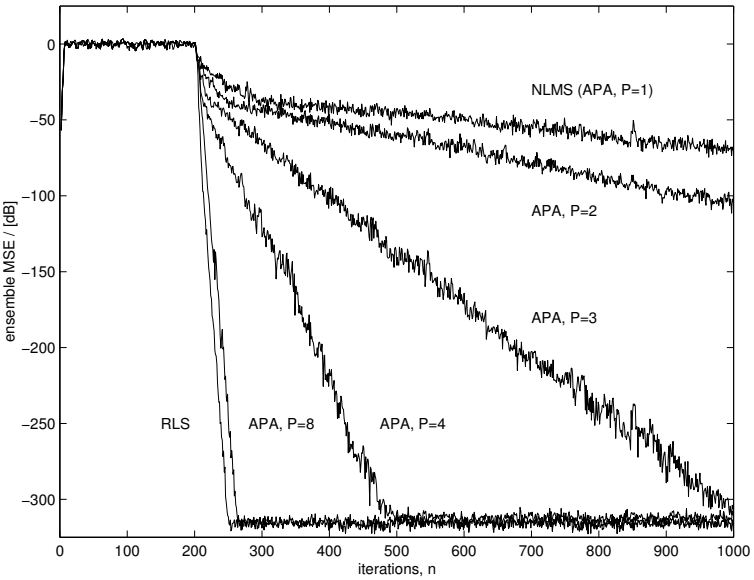

Figure 2.4: Comparison of convergence speed for different algorithms with coloured input signal; the curves represent the ensemble MSE averaged over 40 runs with NLMS (identical to first order APA), APAs of orders 2,3,4, and 8, and an RLS adaptive filter.

2.5.2.2 Geometrical Interpretation

Similar to the geometrical consideration arising from the NLMS update, the APA can be interpreted as a generalization of Fig. 2.2. If the hyperplane $\mathbf{P}_{n-i+1}$ defines the solution space of the ith equation of the system of equations (2.75) – (2.78), successive projections from the current coefficient vector $\mathbf{w}_n$ onto the hyperplanes $\mathbf{P}_{n-p+2}$, $\mathbf{P}_{n-p+3}$, $\cdots \mathbf{P}_{n+1}$ will solve (2.79) if it is consistent, i.e. all hyperplanes $\mathbf{P}_{n-i+1}$ cross at least in one point [50], which is equivalent to demand $\mathbf{X}_n$ to have full column rank. Through observation noise in the measurements d_n or model mismatch (e.g. insufficient filter length L_a) this system can become inconsistent [50] causing a noisy coefficient vector being projected around the optimum solution, and thus an excess mean squared error is procduced.

Various versions of this algorithm have been introduced in different technical areas. Depending on the application, they are known as e.g. row action projection (RAP) algorithms [78, 50] based on its geometrical interpretation, algebraic reconstruction technique (ART) in tomographic applications [78], or simply “new

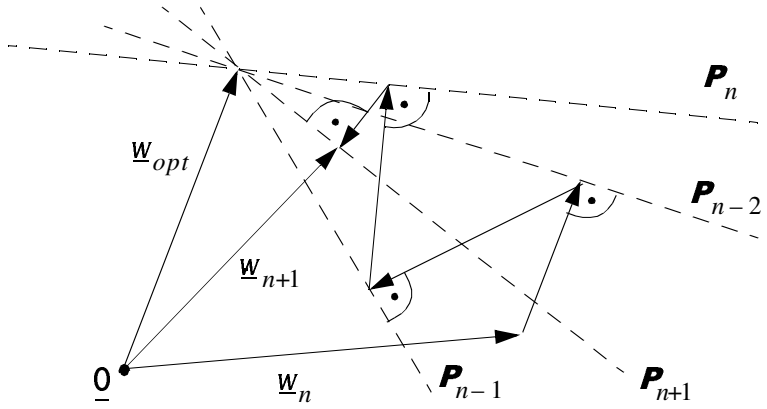

Figure 2.5: Geometrical interpretation of affine projection algorithms; the example shown uses a 4th order APA with 4 successive orthogonal projections onto different solution hyperplanes marked by the system of equations (2.75) – (2.78).

algorithm" [100].

2.6 Implementations and Complexity Issues

A number of approaches exist to lower the computational complexity of adaptive algorithms, like for RLS or APA. Often these are based on exploiting redundancies in the processing, or on approximations. One technique to reduce the computational complexity of the general adaptive filtering problem is the application of frequency domain methods, where convolutions can be simply expressed as products. Similarly, subband implementation, whereby the appeal lies in processing filtering tasks more efficiently at a reduced sampling rate, can also be used to efficiently implement adaptive filters.

2.6.1 Frequency Domain Implementation

The implementation of filters in the frequency domain is essentially based on performing adaptive filtering in the time domain on blocks of data, rather than for every sample of incoming data [23]. This requires that the input $x[n]$ and the error signal $e[n]$ are buffered over a block length L_b. Once the data is collected,

in case of the LMS a convolution is performed between input and coefficients, and a correlation for the weight update is calculated over the block of data. Both correlation and convolution operations can be reduced to simple multiplications of signals when transformed into the frequency domain [24, 42, 128]. However drawbacks arise, as convergence speed and tracking ability of the algorithm are likely to be reduced, since the maximum allowable step size is scaled down by the block length L_b. Furthermore, block processing introduces an overall delay into the system which is equivalent to the block length [128].

The transformation of the blocked time domain data into the frequency domain is performed by DFT algorithms, which can be efficiently implemented using the FFT for appropriate block lengths [20]. Problems arise, as the DFT/FFT implements a circular convolution, i.e. introduces a periodization of the time domain data block. In the implementation, this will lead to inaccuracies and distortions [8, 114]. To obtain linear convolution / correlation, modifications are necessary, which can be implemented using either overlap-add or overlap-save strategies [27, 24, 128].

Of the two methods for insuring a linear convolution, overlap-save performs a DFT of twice the block length on the new data block, appended at the previous data block. After transformation, multiplication with the DFT of the filter coefficients, and inverse transform, the correct block of data is selected, the rest discarded. Overlap-add [24] works similarly, but adds the old, shifted data in the frequency domain to the transformation of the current, zero-padded block. In both cases, DFTs/FFTs of twice the block length are required to satisfy the linearity of the convolution. Usually, the DFT/FFT length will match the length of the filter, L_a [128].

The computational complexity of this approach results in 2 FFTs for transforming input and error signal, an inverse FFT for the output signal $y[n]$, $2L_a$ complex multiplications for both computing convolution and correlation in the frequency domain. Additionally, the weight vector usually has to be constraint in the time domain requiring another forward and inverse FFT of length $2L_a$, resulting in

$$C_{\mathrm{FDAF}} = \frac{1}{L_a}\left(40L_a \log_2(2L_a) + 16L_a\right) = 40\log_2(2L_a) + 16 \tag{2.84}$$

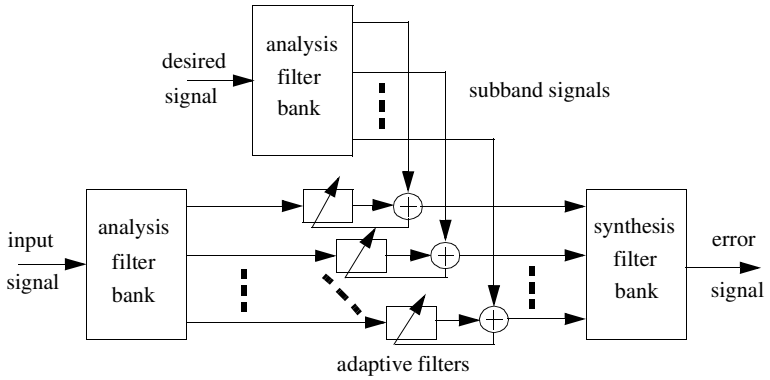

Figure 2.6: Generic diagram of adaptive filtering in subbands.

real multiplications per sampling period for a frequency domain adaptive filter (FDAF) implementation of the LMS [128]. The division by L_a is justified, as the complete procedure is only performed once per block, i.e. every L_a samples. Thus, savings can become substantial for large block sizes, although restrictions may apply due to the also growing system delay.

If long filters are required to be implemented as found in e.g. acoustic applications like AEC, the overall system delay can be cut shorter by partitioning into smaller blocks and applying shorter transforms [35, 39]. This however will also drastically reduce the possible saving in computational complexity, such that relative complexities vary in the range of 20-30% [110] of the original time domain method for typical AEC.

Although mainly applied to LMS-type FIR filters, frequency domain methods can also potentially be used for other algorithms like APA where the scalar products (2.75) – (2.78) become a filtering operation in a block implementation [49, 100], and thus motivate a possible frequency domain approach.

2.6.2 Subband Implementation

The idea behind subband implementations is to decompose a fullband signal into a number of channels — usually with restricted bandwidth — which are allowed to be sampled at a lower rate. Such a system is depicted in Fig. 2.6, whereby both input and desired signals are split into subbands by analysis filter banks.

Adaptive filtering can then be performed on the subband signals, and the error or output signal, depending on the application, be reconstructed by a synthesis filter bank. The components of the system in Fig. 2.6 will be subject of Chap. 3 and discussed in greater detail therein.

The advantages generally associated with subband structures include [52, 86, 53, 54]:

complexity reduction due to the reduced sampling rate, filters require fewer taps to cover the same time interval as in the fullband, and are updated at a lower rate;

parallelization the parallel structure of the subbands can be exploited to distribute tasks over different DSPs for systems of high computational complexity;

spectral whitening occurs for the decomposition of coloured input signals, as the filter banks divide the original fullband spectrum in smaller intervals with reduced magnitude range and a greater likelihood of inband whiteness.

The motivational force here is the use of subband structures to reduce the computational complexity of implemented adaptive filter systems. While parallelization is an obvious feature, spectral whitening has its pitfalls. The appeal of spectral whitening lies in the dependency of algorithms like the LMS onto the eigenvalue spread, linking the spectral characteristics by (2.52) to the convergence speed of the algorithm, which then could be increased. However, as will be seen in the following chapters, the filters in the filter banks themselves colour the subband signals significantly and reduce or even compensate the advantage of separation into spectral intervals.

Depending on the length of the filters used in the filter banks, a delay is imposed on the overall system. The length of the filters depends on a number of factors, like the number of subbands, the rate at which subband signals are sampled, and the quality requirements of the filter bank, which can be linked to the performance of the subband adaptive system [172]. Given a certain critical delay which must not be surpassed, trade-offs can be applied to keep the filter length within limits.

Different from frequency domain methods, this approach is modular not only in its parallelization of processing tasks, but also independent of the specific algorithm used in the subband structure. Once the filter banks are set up, almost any kind of adaptive filter can be placed there. This contrasts the inflexibility of the frequency domain implementation, where individual solutions for different algorithmic approaches have to be sought.

2.7 Concluding Remarks

This chapter has introduced adaptive filtering algorithms. Based on the optimal Wiener filter for stationary problems, two classes of algorithms, least-mean squares (LMS) and recursive least squares (RLS), have been derived along with some important properties. As adaptive filtering in this thesis is targetted towards the identification of systems with very long impulse responses, the computational complexity of the adaptive algorithm is of high importance, and implementational schemes to lower this complexity are in demand. Here, we have basically looked at frequency domain and subband approaches to lower complexity. From these, the subband approach is particularly valuable due its convenient modularization of the processing task, the generality to apply just any algorithm to the subbands, and its low computational complexity, which has not been demonstrated but will be the main aspects of the following chapters.

In terms of adaptive algorithm performance, the LMS algorithm has been shown to be dependent on the eigenvalue spread of the auto-correlation matrix of the input signal, while this does not affect convergence of the RLS. Affine projection algorithms (APA) as a generalization of the normalized LMS have been introduced, which, depending on the projection order, show a convergence behaviour linking LMS and RLS type algorithms. This aspect is important, as for coloured input signals, as e.g. found with speech in the AEC environment, the convergence rate of an algorithm can be seriously affected under this dependency. The sensitivity to the eigenvalue spread will also be important, as the filter banks to be constructed in Chap. 4 will impose a colouring on the input signal.

Chapter 3

Filter Banks and Subband Structures for Adaptive Subband Processing

This chapter discusses all components required for building and analysing subband structures for subband adaptive filtering. We start by introducing basic multirate operations in Sec. 3.1. These constitute the elements of filter banks, as seen in Fig. 3.1, which perform signal decompositions to be addressed in Sec. 3.2. The following Sec. 3.3 is dedicated to analysis methods for filter banks, which will help to review prevalent subband structures for adaptive filtering discussed in Sec. 3.4, as well as lay the foundations for fast filter bank implementations that will be derived in Chap. 4.

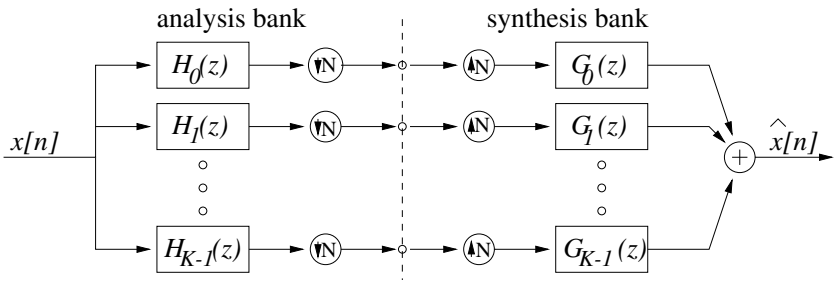

Figure 3.1: Analysis and synthesis branch of a K-channel filter bank with subbands decimated by N.

Figure 3.2: Basic multirate operations for sampling rate alteration: (a) decimation; (b) expansion of signal $x[n]$ by a factor of N.

3.1 Preliminaries on Multirate Systems

A multirate system comprises of components running at different sampling frequencies. A typical example is the filter bank in Fig. 3.1, where each of the K subband signals between analysis and synthesis bank is sampled slower by a factor of N compared to the input or output fullband signal. This section will introduce the basic operations and building blocks of a multirate system, and give definitions and insight into the alteration of sampling rates for subband signals. Before discussing another approach in Sec. 3.2 based on signal expansions, the legitimation for sampling rate reductions will first be drawn from a review of the sampling theorem.

3.1.1 Basic Multirate Operations

The sampling rate alterations motivating the term *multirate* system are performed by two main operations, decimation and expansion, which are shown in Fig. 3.2.

Decimation. If a signal is fed through a decimator in Fig. 3.2(a), only every Nth sample is retained in the output signal $y[n]$,

$$y[n] = x[Nn], \tag{3.1}$$

where $N \in \mathbb{N}$ is assumed [1]. An example is given in Fig. 3.3(b). Fractional values N are possible and lead to non-uniform sampling [26], which is not considered here, although it has been employed in the context of adaptive filtering [129]. In

[1] Throughout this thesis, this action is termed *decimation* or *downsampling*, performed by *decimators* or *downsamplers*. Note that no prior anti-alias filtering is involved.

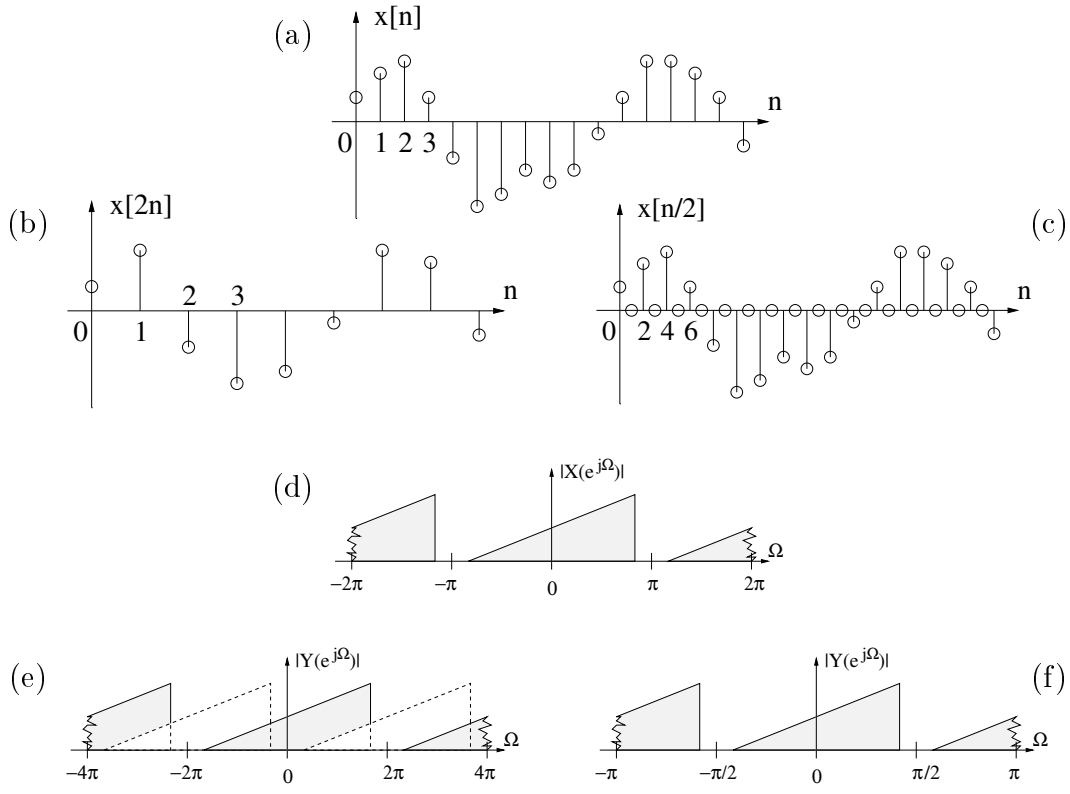

Figure 3.3: Example for decimation and expansion by 2: (a) original time domain signal; (b) decimated signal; (c) expanded signal; (d) frequency domain of a complex signal; (e) frequency domain of decimated signal; (f) frequency domain of expanded signal.

the frequency domain, relation (3.1) can be expressed by [151]

$$Y(z) = \frac{1}{N} \sum_{n=0}^{N-1} X(z^{1/N} W_N^n) \quad , \tag{3.2}$$

where $W_N = e^{-j2\pi/N}$. Thus, the spectrum $Y(e^{j\Omega})$ is assembled by superimposing $X(e^{j\Omega})$ stretched by a factor of N with $N-1$ versions shifted by multiples of 2π, as illustrated by an example in Fig. 3.3(e). This superposition leads to spectral overlap ("aliasing"), if $x[n]$ is not a suitably band-limited signal. Problems associated with aliasing in a subband adaptive filter system will be discussed in Sec. 3.4.1.

Expansion. The expander in Fig. 3.2(b) is described by

$$y[n] = \begin{cases} x[\frac{n}{N}] & n = \lambda N \\ 0 & n \neq \lambda N \end{cases} \quad , \lambda \in \mathbb{Z}, \tag{3.3}$$

inserting $N-1$ zeros between every original sample [2]. An example for $N = 2$ is depicted in Fig. 3.3(c). In the frequency domain, expansion can be expressed by

$$Y(z) = X(z^N), \tag{3.4}$$

which for the spectrum $Y(e^{j\Omega})$ means a rescaling of the frequency axis with respect to $X(e^{j\Omega})$ by a factor of N. An illustration is given in Fig. 3.3(f).

3.1.2 Signal Bandwidth and Sampling

For an analogue signal $x(t)$ which is band-limited in the frequency domain to the baseband interval $[-\omega_g; \omega_g]$, Shannon's sampling theorem [126, 127] states that

Theorem 1 (Sampling Theorem) *if $x(t)$ is sampled at an angular frequency $\omega_s > 2\omega_g$, the analogue signal $x(t)$ can be perfectly recovered by an ideal lowpass filter with an angular cutoff frequency $\omega_s/2$ (cited from [83]).*

[2] This operation will be termed *expansion* or *upsampling*, and the according device named *upsampler* or *expander*, which does not include interpolation filtering.

Therefore, if a discrete baseband signal has signal components such that the bandwidth is $[-\omega_b;\omega_b]$, where $\omega_b < \omega_s/2$, its sampling rate may be lowered in adherence with the above theorem.

However for bandpass signals, the sampling theorem has to be amended. First, the term *bandwidth* has to be defined by the following

Definition 1 (Bandwidth) *The bandwidth B is the total length of frequency intervals, on which the discrete time function $x[n]$ has non-zero contributions within the normalized angular frequency interval $[-\pi;\pi]$.*

Using this definition, we look into the validity of the sampling theorem for both analytic and real valued functions, both of which are key elements within this thesis.

3.1.2.1 Analytic Signals

An analytic signal is a complex valued signal $x^{(a)}[n]$,

$$x^{(a)}[n] = \mathrm{Re}\{x^{(a)}[n]\} + j\mathrm{Im}\{x^{(a)}[n]\}\,, \tag{3.5}$$

where real and imaginary part are related by the Hilbert transform, $\mathrm{Im}\{x^{(a)}[n]\} = \mathcal{H}\{\mathrm{Re}\{x^{(a)}[n]\}\}$. The Fourier domain of an analytic bandpass signal $X^{(a)}(e^{j\Omega})$ is characterized by the absence of a negative frequency spectrum,

$$X^{(a)}(e^{j\Omega}) = \begin{cases} X(e^{j\Omega}) & \Omega \in]0;\pi] \\ \frac{1}{2}X(1) & \Omega = 0 \\ 0 & \Omega \in]-\pi;0[\end{cases}\,, \tag{3.6}$$

with an example shown in Fig. 3.4. Although $X^{(a)}(e^{j\Omega})$ has only been defined on the interval $]-\pi;\pi]$, it is in fact periodic with 2π. Therefore, an analytic bandpass signal of bandwidth B can be decimated by a factor

$$N = \left\lfloor \frac{2\pi}{B} \right\rfloor \tag{3.7}$$

without causing spectral overlaps due to the aliasing present in (3.2).

It can be easily verified that the decimation according to (3.7) is also applicable to general complex signals not fulfilling (3.6), as long as their bandwidth B consists of one coherent interval.

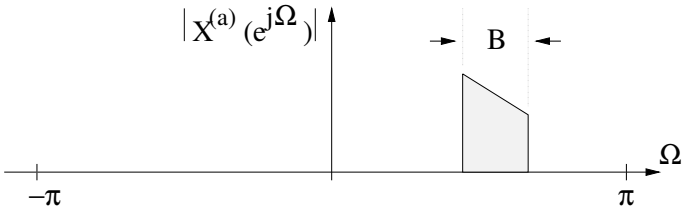

Figure 3.4: Spectrum of an analytic signal $x^{(a)}[n]$ with bandwidth B.

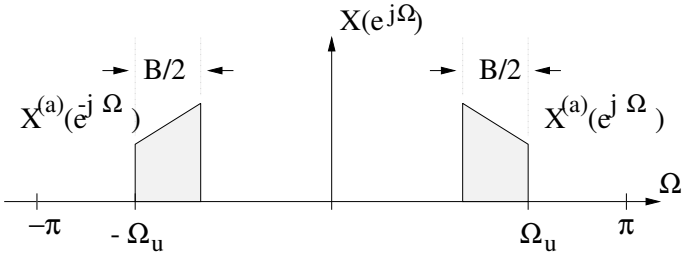

Figure 3.5: Symmetric spectrum with respect to $\Omega = 0$ of a real valued signal $x[n]$ with bandwidth B.

3.1.2.2 Real Valued Signals

A real valued signal $x[n]$ possesses an axial symmetry to the frequency origin in the frequency domain, and relates to an analytic signal $x^{(a)}[n]$ by

$$x[n] = \mathrm{Re}\{x^{(a)}[n]\} \tag{3.8}$$

$$X(e^{j\Omega}) = X^{(a)}(e^{j\Omega}) + X^{(a)}(e^{-j\Omega}), \tag{3.9}$$

which is illustrated as an example in Fig. 3.5. The identity of $X(e^{j\Omega})$ to the linear superposition of its analytic spectrum and the frequency reversed version leads to a straightforward explanation of the effects of decimation. As decimation is a linear operation, it can be applied separately to each of the summands on the right hand side of (3.9) with a superposition of the results. It is obvious, that critical decimation is again limited by (3.7), but that the band-position (i.e. defined by the upper cut-off frequency Ω_u in Fig. 3.5) has critical importance, as otherwise spectral overlaps between the terms in (3.2) due to $X^{(a)}(e^{j\Omega})$ and $X^{(a)}(e^{-j\Omega})$ occur.

The restriction imposed by the band-position in addition to (3.7) for the

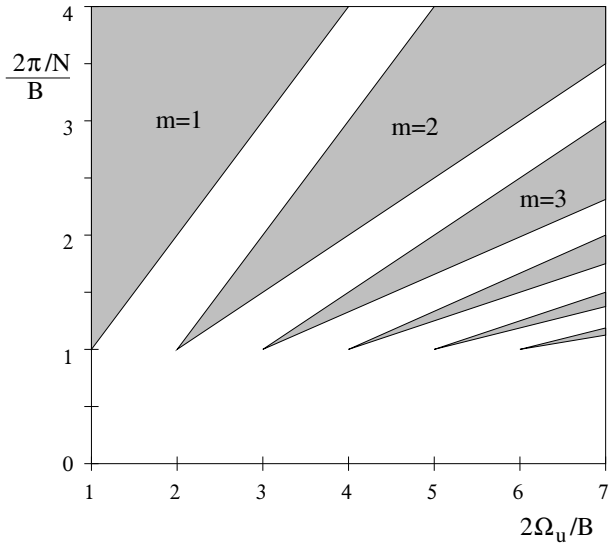

Figure 3.6: Valid decimation rates N for real valued bandpass signals in dependency on the bandwidth B and the upper bound of the passband Ω_u; allowed combinations lie within the shaded areas.

selection of a valid decimation ratio N is given by [153, 19]

$$\frac{k}{m} \leq \frac{2\pi}{N \cdot B} \leq \frac{k-1}{m-1}, \qquad k = \frac{2\Omega_u}{B \cdot m}, \quad m \in \mathbb{N}, \tag{3.10}$$

where the sampling frequency is normalized to 2π, Ω_u is the upper bound of the passband and B the bandwidth as in Fig. 3.5, and N the decimation factor by which the sampling frequency may be lowered. Eqn. (3.10) has to be satisfied for any integer m. Possible choices are illustrated in Fig. 3.6 [153, 26, 81].

3.2 Signal Decompositions

The band-limited nature of a signal as a motivation to reduce its sampling rate is based on stringent frequency domain considerations. In the following, a time domain approach by orthogonal signal decompositions is reviewed, which justifies a lowering of the sampling rate by other means. Finally, this is generalized to non-orthogonal, redundant signal expansions.

3.2.1 Orthogonal Decompositions

Consider a signal expansion, which develops a discrete time input signal $x[n]$ after a set of functions $h_k[n]$, $k \in \{0; K-1\}$

$$y_k[n] \;=\; \sum_{\nu} h_k^*[nK-\nu] \cdot x[\nu] \tag{3.11}$$

where the $y_k[n]$ are the coefficients of the expansion. Interpreted in terms of the analysis filter bank in Fig. 3.1, the kernel functions $h_k[n]$ can be associated with the bandpass filters producing the K frequency bands. Note that the convolution in (3.11) already performs an implicit decimation by K. Using the vector notation definitions

$$\mathbf{h}_k \;=\; [h_k[0]\; h_k[1]\; \cdots\; h_k[L_h-1]]^T; \tag{3.12}$$

$$\mathbf{x}_\nu \;=\; [x[\nu]\; x[\nu-1]\; \cdots\; x[\nu-L_h+1]]^T \quad , \tag{3.13}$$

where L_h is the length of the functions $h_k[n]$, the convolution in (3.11) can now be written as an iterated evaluation of scalar products

$$y_k[n] \;=\; \mathbf{h}_k^H \cdot \mathbf{x}_{nK} \quad . \tag{3.14}$$

For each new calculation of the scalar product, the function $h_k[n]$ is shifted K samples along the time axis n.

If additionally $\|\mathbf{h}_k\|_2 = 1$ is fulfilled, then (3.11) performs an orthonormal projection, which can be geometrically interpreted as in Fig. 3.7. Therefore, the scalar product performs a best approximation of $\mathbf{x}_{nN}$ by $y[n]\cdot\mathbf{h}_k$ in a least squares sense. Note that the scalar product in the convolution 3.11 is only evaluated for shifts of K, implicitly performing a critical decimation.

Orthonormal basis for $l^2(\mathbb{Z})$. If a set of functions $h_k[n]$ form an orthonormal basis for the space $l^2(\mathbb{Z})$ of square integrable discrete signals, (3.11) performs a rotation of the coordinate system of the vector space. While the original basis of $x[n]$ is a comb of Kronecker functions $< \delta[n] >$, the coefficients $y_k[n]$ express this signal in terms of the new basis $< h_k[n] >$. For the $h_k[n]$ to form an orthonormal basis of the signal space $l^2(\mathbb{Z})$, two conditions have to be satisfied:

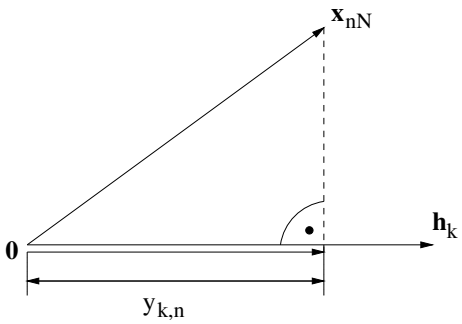

Figure 3.7: Orthonormal projection as geometrical interpretation of the scalar product for $\|\mathbf{h}_k\|_2 = 1$.

(C1) Mutual orthonormality of the basis functions and versions shifted by K:

$$\sum_{\nu=0}^{L_h-1} h_i^*[\nu] \cdot h_j[\nu - nK] = \delta[i-j] \cdot \delta[n]; \tag{3.15}$$

(C2) Dense representation: the set of basis functions $< h_k[\nu - nK] >$ is dense in $l^2(\mathbb{Z})$.

Parseval's Theorem and Inverse Transform. From the orthonormal basis representation of $< h_k[n] >$, two useful properties follow. First, (3.11) represents an orthonormal transformation, under which the l_2-norm is invariant [58]. This is also known as Parseval's Theorem [149, 151]

$$\sum_n |x[n]|^2 = \sum_{k=0}^{K-1} \sum_n |y_k[n]|^2, \tag{3.16}$$

i.e. energy is preserved. Second, the existence of a unique inverse transform

$$x[n] = \sum_{k=0}^{K-1} \sum_\nu y_k[\nu] \cdot h_k^*[n - K\nu]. \tag{3.17}$$

is guaranteed.

Example. Fig. 3.8 shows a low- and highpass filter pair $h_0[n]$ and $h_1[n]$ fulfilling the above conditions (C1) and (C2) for $K = 2$. The filter $h_0[n]$ is also known as Haar wavelet filter [31].

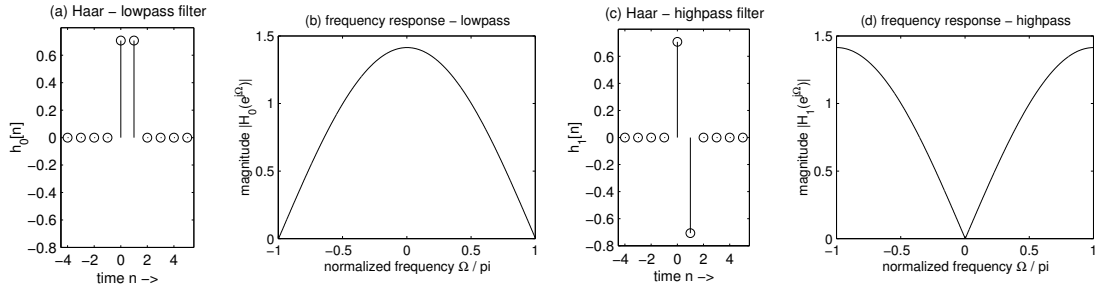

Figure 3.8: Example for filters performing an orthonormal decomposition: (a) lowpass filter $h_0[n]$; (b) frequency response $H_0(e^{j\Omega})$; (c) highpass filter $h_1[n]$; (d) frequency response $H_1(e^{j\Omega})$.

Note that the decomposition in (3.11) implicitly performs a decimation by K between $x[n]$ and $y_k[n]$. The transform is therefore free of redundancy and there is an equal number of samples in the coefficient sets $\{x[n]\}$ and $\{y_k[n]\}$. Returning to the decimation problem, the coefficients $y_k[n]$ form the samples of K subband signals decimated by K, *without* reference to the bandwidth or spectral characteristic of the filters $h_k[n]$ and solely based on the properties of an orthonormal decomposition.

3.2.2 Redundant Decompositions

If the decomposition of a signal $x[n]$ into K subbands is described by

$$y_k[n] = \sum_{\nu} h_k^*[nN - \nu] \cdot x[\nu], \qquad k \in [0, K-1], \quad N \leq K \tag{3.18}$$

(3.15) is no longer valid since the implicit decimation is performed by some factor $N < K$. The set of functions $< h_k[n] >$ now is linearly dependent, and constitutes a *frame* when dense in $l^2(\mathbb{Z})$ [142, 113]. For frames there exists an energy relation between the samples of the original signal and the transform coefficients in the subbands similar to Parseval's theorem,

$$A \cdot \sum_n |x[n]|^2 \leq \sum_{k=0}^{K-1} \sum_n |y_k[n]|^2 \leq B \cdot \sum_n |x[n]|^2, \tag{3.19}$$

valid for every $x[n] \in l^2(\mathbb{Z})$. The constants A and B are called frame bounds, and have the interesting property $A \leq K/N \leq B$. If $A = B$, i.e. there is a fixed energy

relation, the frame $< h_k[n] >$ is called tight. Through its linear dependency, expanding a signal $x[n]$ in a frame obviously is a redundant representation.

3.3 Filter Bank Analysis

The signal decompositions discussed in Sec. 3.2 are usually performed by filter banks as shown in Fig. 3.1, i.e. a tree of filters of different spectral characteristics. In the following, filter banks are analysed in the z-domain using the notation by Vaidyanathan [151] with an extension to arbitrary integer decimation [88].

3.3.1 Modulation Description

As described in Fig. 3.1, an input signal $x[n]$ is split into K subband signals decimated by factors $N \leq K$. For $N = K$, the filter bank is called critically sampled, and oversampled for $N < K$. If the K decimated subband signals are referred to as $V_0(z), V_1(Z), \cdots V_{K-1}(z)$ in the z-domain, we can write according to (3.2)

$$\underline{V}(z) = [V_0(z)\ V_1(z)\ \cdots V_{K-1}(z)]^T = \frac{1}{N}\mathbf{H}_m(z^{1/N})\underline{X}_m(z^{1/N}) \tag{3.20}$$

where the subscript $(\cdot)_m$ refers to the use of the modulation representation[3] [155, 131, 119] also known as alias component (AC) notation [151] of vectors and matrices

$$\mathbf{H}_m(z) = \begin{bmatrix} H_0(z) & H_0(zW_N) & \dots & H_0(zW_N^{N-1}) \\ H_1(z) & H_1(zW_N) & \dots & H_1(zW_N^{N-1}) \\ \vdots & \vdots & \ddots & \vdots \\ H_{K-1}(z) & H_{K-1}(zW_N) & \dots & H_{K-1}(zW_N^{N-1}) \end{bmatrix} \tag{3.21}$$

$$\underline{X}_m(z) = \left[X(z)\ X(zW_N)\ \cdots X(zW_N^{N-1})\right]^T \quad , \tag{3.22}$$

where $H_k(z) \bullet\!\!-\!\!\circ\ h_k[n]$ is the z-transform of the kth filter of the analysis bank, and $X(z) \bullet\!\!-\!\!\circ\ x[n]$ the input signal. The matrix $\mathbf{H}_m(z)$ is termed modulation matrix of the synthesis filter bank.

[3]The modulation description expresses the aliasing introduced by decimation as a sum of scaled and modulated terms, as defined in (3.2).

Let the output of the expanders be denoted by $U_0(z), U_1(z), \cdots U_{K-1}(z)$, which are given by

$$\underline{U}(z) = \underline{V}(z^N) = \frac{1}{N}\mathbf{H}_m(z)\underline{X}_m(z). \tag{3.23}$$

With the synthesis filters

$$\underline{G}(z) = \left[G_0(z)\; G_1(z) \cdots G_{K-1}(z)\right]^T, \tag{3.24}$$

the filter bank output on the synthesis side can be written as

$$\hat{X}(z) = \underline{G}^T(z)\underline{U}(z) = \frac{1}{N}\underline{G}^T(z)\mathbf{H}_m(z)\underline{X}_m(z). \tag{3.25}$$

Therefore, (3.25) describes the input-output relationship of the filter bank in Fig. 3.1. Conditions for perfect reconstruction, i.e. $\hat{X}(z) = cz^{-\Delta}X(z)$, $c \in \mathbb{C}/\{0\}$, will be discussed in Sec. 3.3.3 based on a polyphase representation to be introduced next.

3.3.2 Polyphase Representation

The polyphase representation [152, 7, 150, 151, 119] is an alternative form to analyse multirate systems and has the advantage of leading to computationally efficient implementations of filter banks. The term polyphase refers to the decimation of a signal — if it is appropriately bandlimited and can be decimated by a factor N, N possibilities exist which set of samples to keep; in fact, one is as good as any, as in the Fourier domain they only differ by their phase, but not by their magnitude.

Transfer functions $H_k(z)$ and $G_k(z)$ can be expressed in the forms

$$H_k(z) = \sum_{n=0}^{N-1} z^{-n} H_{k|n}(z^N) \quad \text{(Type 1 polyphase)} \tag{3.26}$$

and

$$G_k(z) = \sum_{n=0}^{N-1} z^{-(N-1-n)} G_{n|k}(z^N) \quad \text{(Type 2 polyphase)} \tag{3.27}$$

respectively, where

$$H_{k|n}(z) = \sum_{k=-\infty}^{\infty} h_k(Nk+n)z^{-k} \tag{3.28}$$

$$G_{n|k}(z) = \sum_{k=-\infty}^{\infty} g_k(Nk+N-1-n)z^{-k} \quad . \tag{3.29}$$

The terms $H_{k|n}(z)$, $n = 0(1)N-1$, are the N Type 1 polyphase components of $H_k(z)$, which arise from decimation of differently phase shifted analysis filters $h_k[n]$ and subsequent z-transformation. Correspondingly, $G_{n|k}(z)$, $n = 0(1)N-1$, represent the N Type 2 polyphase components of $G_k(z)$. Note that the special case $G_k(z) = H_k(z)$ gives $G_{n|k}(z) = H_{k|N-1-n}(z)$.

Application of (3.26) yields

$$\underline{H}(z) = \mathbf{H}(z^N) \cdot [1 \; z^{-1} \; \ldots \; z^{-(N-1)}]^T, \tag{3.30}$$

where

$$\mathbf{H}(z) = \begin{bmatrix} H_{0|0}(z) & H_{0|1}(z) & \ldots & H_{0|N-1}(z) \\ H_{1|0}(z) & H_{1|1}(z) & \ldots & H_{1|N-1}(z) \\ \vdots & \vdots & \ddots & \vdots \\ H_{K-1|0}(z) & H_{K-1|1}(z) & \ldots & H_{K-1|N-1}(z) \end{bmatrix}. \tag{3.31}$$

Correspondingly, (3.27) leads to

$$\underline{G}^T(z) = [z^{-(N-1)} \; z^{-(N-2)} \; \ldots \; 1] \cdot \mathbf{G}(z^N), \tag{3.32}$$

where

$$\mathbf{G}(z) = \begin{bmatrix} G_{0|0}(z) & G_{0|1}(z) & \ldots & G_{0|K-1}(z) \\ G_{1|0}(z) & G_{1|1}(z) & \ldots & G_{1|K-1}(z) \\ \vdots & \vdots & \ddots & \vdots \\ G_{N-1|0}(z) & G_{N-1|1}(z) & \ldots & G_{N-1|K-1}(z) \end{bmatrix}. \tag{3.33}$$

The matrices $\mathbf{H}(z)$ and $\mathbf{G}(z)$ are called the polyphase matrices of the filter bank. Using (3.30) and (3.32) in the filter bank in Fig. 3.1 yields an equivalent representation shown in Fig. 3.9(a). With respect to subsampling and upsampling,

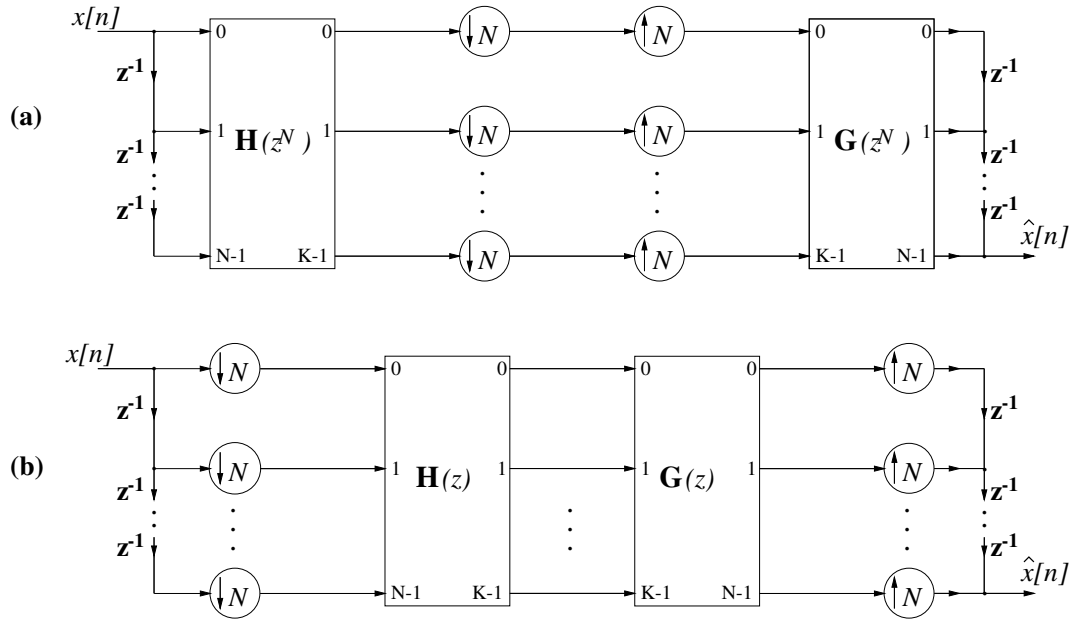

Figure 3.9: (a) Polyphase representation of a K-channel filter bank decimated by a factor N; (b) re-arrangement using noble identities.

the following identities hold [151, 142]

$$H(z)(\downarrow N) = (\downarrow N)H(z^N) \quad \text{First Noble Identity} \tag{3.34}$$

$$(\uparrow N)G(z) = G(z^N)(\uparrow N) \quad \text{Second Noble Identity,} \tag{3.35}$$

where $(\downarrow N)$ denotes N-fold decimation, and $(\uparrow N)$ N-fold expansion. By using noble identities, the filter bank can be modified and the equivalent form shown in Fig. 3.9(b) obtained. This structure has the advantage that the filtering is performed at the subsampled rate.

In terms of analysis, the flow chart in Fig. 3.9(b) has separated the filter bank into two system types. Time multiplexers, which perform the separation into or interleaving of K channels decimated by N, are linear periodically time-varying (LPTV) systems with period N. In contrast, the polyphase matrices $\mathbf{H}(z)$ and $\mathbf{G}(z)$ define multiple-input multiple output (MIMO) systems, which are linear time-invariant (LTI) and therefore convenient to analyze.

3.3.3 Lossless Expansions

In its most general form, the filter bank system can be shown to have perfect reconstruction property if and only if the product $\mathbf{G}(z)\mathbf{H}(z)$ fulfills [151]

$$\mathbf{G}(z)\mathbf{H}(z) = cz^{-\Delta} \begin{bmatrix} \mathbf{0} & \mathbf{I}_{N-r} \\ z^{-1}\mathbf{I}_r & \mathbf{0} \end{bmatrix}, \quad \begin{array}{l} r \in \mathbb{Z}, 0 \leq r \leq N-1, \\ \Delta \in \mathbb{N},\ c \in \mathbb{C}/\{0\}. \end{array} \tag{3.36}$$

If this condition is satisfied, the reconstructed signal is only a scaled and delayed version of the filter bank input $\hat{x}[n] = cx[n-\kappa]$, where $\kappa = \Delta K + r + K - 1$ constitutes the delay.

A sufficient even though not necessary condition to ensure (3.36) is the paraunitary property of $\mathbf{H}(z)$. A matrix $\mathbf{H}(z) \in \mathbb{C}_{(z)}^{K \times N}$ of transfer functions is called paraunitary if

$$\tilde{\mathbf{H}}(z)\mathbf{H}(z) = c\mathbf{I}_N, \quad c \in \mathbb{C}/\{0\}, \tag{3.37}$$

where the matrix $\tilde{\mathbf{H}}(z)$ is called the parahermitian of $\mathbf{H}(z)$, i.e. is transposed with its polyphase entries complex conjugated and time reversed [151, 29]. With $\mathbf{H}(z)$ being paraunitary it is easy to recognize that simply choosing

$$\mathbf{G}(z) = cz^{-l}\tilde{\mathbf{H}}(z), \quad c \neq 0, \tag{3.38}$$

satisfies the perfect reconstruction condition. If its polyphase matrix $\mathbf{H}(z)$ is paraunitary and N equals K, the filter bank is also denoted orthogonal [142].

As a consequence of (3.38) the synthesis filters can be easily found from the analysis filters by

$$g_k[n] = c \cdot \tilde{h}_k[n-l] = c \cdot h_k^*[l-n] \qquad \text{time domain} \tag{3.39}$$

$$G_k(z) = c \cdot z^{-l}\tilde{H}_k(z) \qquad \text{z-domain,} \tag{3.40}$$

where $k = 0(1)K-1$, $l = N-1+N\Delta$. For critical decimation by a factor K, this is the only choice for the synthesis filters by assumption of a paraunitary $\mathbf{H}(z)$ to achieve perfect reconstruction (PR).

Note that the derived results in the z-domain correspond to time domain expressions in Sec. 3.2. Later, the property of paraunitarity for polyphase matrices will be explicitly linked to both orthogonal and redundant frame decompositions, which are implemented by such PR filter banks [156, 14].

3.4 Different Approaches to Subband Adaptive Filtering

Based on the subband decompositions introduced in the above section in the context of filter bank theory, the application of subband schemes to adaptive filtering is reviewed. The idea to perform adaptive filtering in frequency bands goes back to a number of researchers in the 1980s like Kellermann [84, 85, 86, 134], Furukawa and Yasukawa [48, 181], and Gilloire *et al.* [52, 53, 54], who mainly targeted the echo problem in telecommunication lines caused by hybrids [134], or the acoustic feedback problem in hands-free telephony [48, 84, 85].

The main obstacle in subband adaptive filtering is the fact that although filter banks may be perfectly reconstructing (i.e. aliasing is cancelled at the output of a synthesis bank), aliasing present in the subband signals constitutes a rather serious problem for adaptive filters. The origin of the problem and suggested solutions around it are the subject of this section.

3.4.1 Aliasing in the Decimation Stage

Sec. 3.1 has introduced two concepts that motivate the decimation of subband signals: the band-limited nature of signals, and an orthogonal basis or redundant frame decomposition of signals, where aliasing may be permitted in the subband domain but is subsequently cancelled in the signal reconstruction of the synthesis bank. However, a problem with perfect reconstruction does arise when decimated subbands of different fullband signals have to be compared.

Filter banks are linear, but periodically time-varying systems due to up- and downsampling. The alias terms introduced in the decimation stage in (3.2) manifests as a deviation from the linear time-invariant (LTI) system behaviour and can be interpreted as a distortion [117]. An exact analysis of this phenomenon in the z-domain will be performed in Sec. 3.4.2 following the explanations by Gilloire and Vetterli [54].

Information Leakage. An example of the effect caused by the cyclic time-varying nature of a critical decimation stage is shown in Fig. 3.10 [135, 19].

There, a near PR filter pair $< h_0, h_1 >$ has been used for a decomposition, with a halfband lowpass $h_0[n]$ tabulated as filter 32C in [27] and $h_1[n] = h_0[n] \cdot \cos(\pi n)$ the according QMF highpass filter modulated by π. If this filter pair is excited by the lowpass filter itself, the subband signals are

$$x_0[n] = h_0[n] * h_0[n] \qquad \text{lowpass subband} \tag{3.41}$$

$$x_1[n] = h_1[n] * h_0[n] \qquad \text{highpass subband,} \tag{3.42}$$

as shown in Fig. 3.10(a) and (d), respectively. Depending on whether even or odd samples are dropped in the decimation, two different patterns arise for each signal $x_0[n]$ and $x_1[n]$.

An awkward situation results when the differently decimated signals are correlated. Cross-correlation between the two highpass bands in Fig. 3.10(e) and (f) yields zero, while for the correlation between (b) and (c) signal components are missing that have leaked into the decimated highpass band in (e). In an adaptive system identification of an odd-numbered delay, where an adaptive filter would be expected to try and identify these cross-correlations, minimization of the error would completely fail at least in the highpass band, thus yielding an insufficient solution.

Note that an interesting case of non-causality can occur in this identification problem when the even-indexed $x_0[2n]$ in Fig. 3.10(c) forms the input signal to an adaptive filter, and the filter is supposed to provide a close fit solution to a desired signal consisting of the odd-indexed $x_0[2n+1]$ in (b). This non-causality will be further discussed in Sec. 3.4.2.

3.4.2 Critically Decimated Filter Banks

Adaptive system identification in critically decimated subbands, i.e. the decimation ratio matches the number of subbands, $N = K$, was first analysed by Gilloire [52] and Gilloire and Vetterli [53, 54], leading to a modified subband structure with cross-terms between adjacent bands. A review of their approach is given below.

The following definitions describe subband signals associated with adaptive

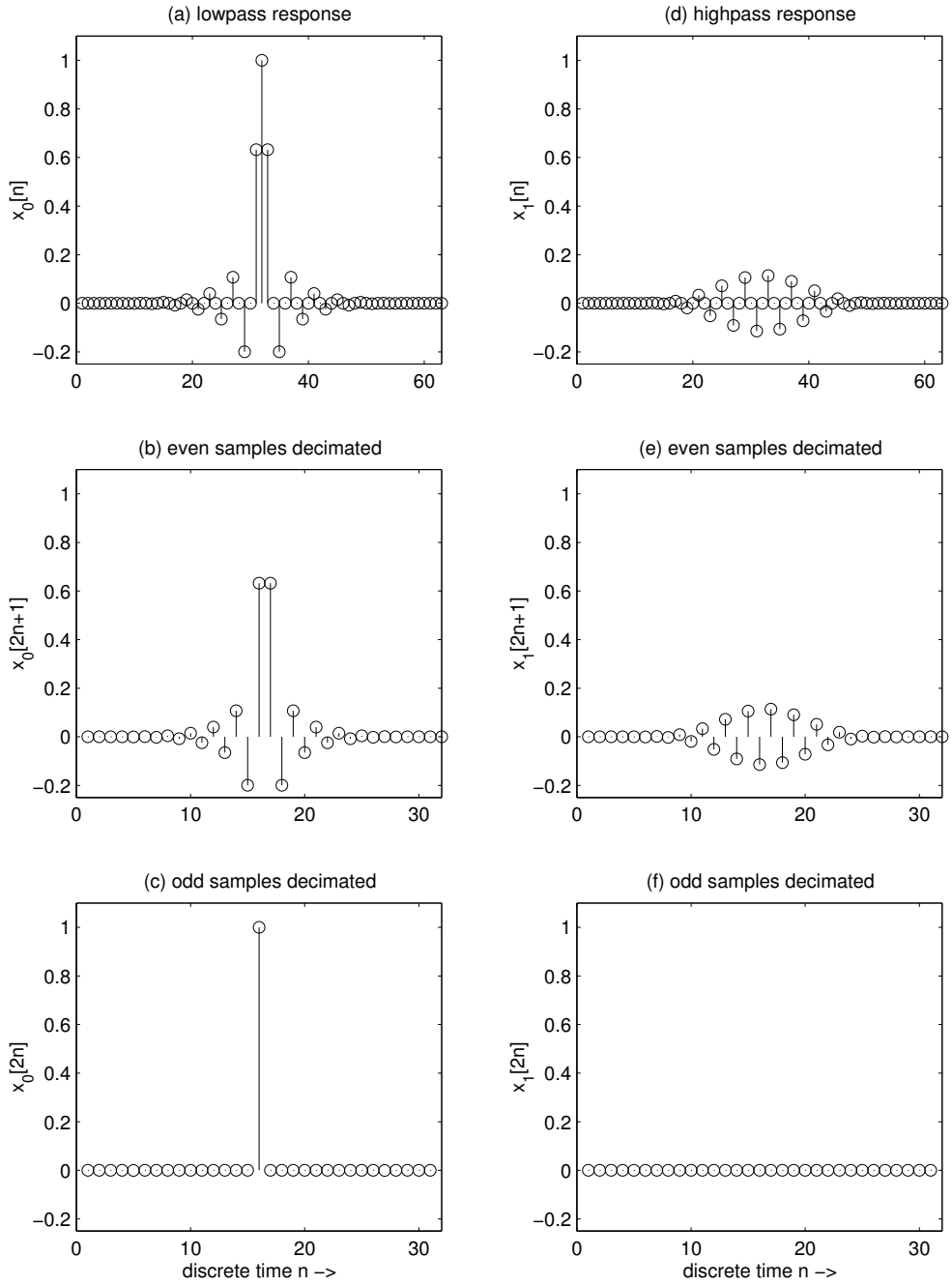

Figure 3.10: Example for "leakage" effect in the time-domain of subband signals due to the phase-variant nature of the decimation process, when excitation matches the lowpass filter 32C [27] of a 2-channel bank; (a) lowpass band $x_0[n]$ with (b) even and (c) odd decimation; (d) highpass band $x_1[n]$ with (e) even and (f) odd decimation.

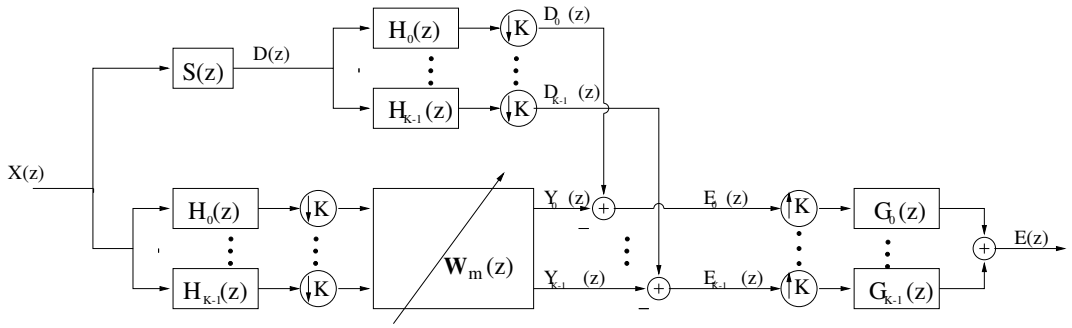

Figure 3.11: Adaptive identification in subbands.

filtering in subbands, i.e. filter input, filter output, desired and error signals associated with different subbands according to Fig. 3.11:

$$\underline{X}(z) = [X_0(z)\, X_1(z)\, \cdots\, X_{K-1}(z)]^T; \tag{3.43}$$

$$\underline{Y}(z) = [Y_0(z)\, Y_1(z)\, \cdots\, Y_{K-1}(z)]^T; \tag{3.44}$$

$$\underline{D}(z) = [D_0(z)\, D_1(z)\, \cdots\, D_{K-1}(z)]^T; \tag{3.45}$$

$$\underline{E}(z) = [E_0(z)\, E_1(z)\, \cdots\, E_{K-1}(z)]^T. \tag{3.46}$$

With these definitions, and using the modulation matrix of the analysis filter bank, $\mathbf{H}_m$, as defined in (3.21) with $N = K$ for critical sampling and a diagonal matrix

$$\mathbf{S}_m(z) = \mathrm{diag}\big\{S(z), S(zW_K), \cdots S(zW_K^{K-1})\big\} \tag{3.47}$$

which represents the modulated spectra of the system to be identified, $S(z)$, the desired subband signals yield

$$\underline{D}(z) = \frac{1}{K}\mathbf{H}_m(z^{1/K})\mathbf{S}_m(z^{1/K})\underline{X}(z^{1/K}). \tag{3.48}$$

Similarly, using a matrix $\mathbf{W}_m(z^K)$

$$\mathbf{W}_m(z^K) = \begin{bmatrix} W_{0,0}(z) & W_{0,1}(z) & \cdots & W_{0,K-1}(z) \\ W_{1,0}(z) & W_{1,1}(z) & \cdots & W_{1,K-1}(z) \\ \vdots & \vdots & \ddots & \vdots \\ W_{K-1,0}(z) & W_{K-1,1}(z) & \cdots & W_{K-1,K-1}(z) \end{bmatrix} \tag{3.49}$$

of polynomial entries for the adaptive filters, the output signals of the adaptive filters can be written as

$$\underline{Y}(z) = \frac{1}{K}\mathbf{W}_m(z)\mathbf{H}_m(z^{1/K})\underline{X}(z^{1/K}). \tag{3.50}$$

Therefore, the subband error signals are obtained from

$$\underline{E}(z) = \frac{1}{K}\ \left(\mathbf{H}_m(z^{1/K})\mathbf{S}_m(z^{1/K}) - \mathbf{W}_m(z)\mathbf{H}_m(z^{1/K})\right) \cdot \underline{X}(z^{1/K}), \tag{3.51}$$

yielding a fullband error $E(z)$ by reconstruction with the synthesis bank filters $\underline{G}(z)$ described in (3.24),

$$\begin{aligned} E(z) &= \underline{G}^T(z)\underline{E}(z^K) & (3.52)\\ &= \frac{1}{K}\,\underline{G}^T(z)\left(\mathbf{H}_m(z)\mathbf{S}_m(z) - \mathbf{W}_m(z^K)\mathbf{H}_m(z)\right) \cdot \underline{X}(z). & (3.53) \end{aligned}$$

To ensure $E(z) \to 0$, several sets of solutions exist [86]. The strictest condition to force $E(z)$ toward zero is given by

$$\mathbf{W}_m(z^K)\mathbf{H}_m(z) = \mathbf{H}_m(z)\mathbf{S}_m(z) \quad . \tag{3.54}$$

3.4.2.1 Filter Banks with Perfect Reconstruction Property

The further analysis of the critically decimated subband adaptive filter system in [54] assumes that both analysis and synthesis filter bank are derived from a common prototype filter, and that this employed filter bank has near perfect reconstruction property. Therefore,

$$\mathbf{H}_m(z) \cdot \mathbf{G}_m(z) \approx z^{-L_h+1}\mathbf{I}_k \tag{3.55}$$

holds [155], where the modulation matrix $\mathbf{G}_m(z)$ of the synthesis filters is defined analogous to $\mathbf{H}_m(z)$ in (3.21). Eqn. (3.54) then yields

$$\mathbf{W}_m(z^K) \approx z^{L_h-1}\mathbf{H}_m(z)\mathbf{S}_m(z)\mathbf{G}_m^T(z). \tag{3.56}$$

The matrix $\mathbf{W}_m(z^K)$, as defined in (3.49), is not of diagonal form, but has off-diagonal polynomial entries $W_{i,j}(z)$, which under the above mention assumptions can be derived as

$$W_{i,j}(z) \approx z^{L_h-1} \cdot \sum_{k=0}^{K-1} H_l(zW_K^k) \cdot G_j(zW_K^k) \cdot S(zW_K^k). \tag{3.57}$$

It is important to note, that this solution is potentially non-causal due to the factor z^{L_h-1}. Therefore, an appropriate delay has to be placed in the path of the desired signal. If in case of acoustic echo cancellation this delay is met by the acoustic transfer delay of the direct path between loudspeaker and microphone, no additional actions are required. Further, from (3.57) it can be easily seen, that the length L_a of the adaptive terms has to be [54, 135, 88]

$$L_a = \left\lceil \frac{2 \cdot L_h + L_s}{K} \right\rceil , \tag{3.58}$$

where L_s is the length of the impulse response of the system to be identified, in order to achieve satisfactory adaptation without truncation of the adapted model. The extreme example given in Fig. 3.10 of Sec. 3.4.1 underlines this case when trying to adaptively identify a unit delay in the lowpass band, where the input signal is even indexed (c) and the desired signal odd-indexed (b), also highlighting the non-causality inherently arising from the decimated setup and the transients of the analysis filters.

If the analysis filters are of good quality and reasonably selective, then only adjacent filters will overlap in the frequency domain, and the adaptive filter matrix $\mathbf{W}(z)$ in (3.49) can be well approximated by a tridiagonal form. In the actual implementation of the subband adaptive filter, this therefore requires adaptive cross-terms between adjacent subbands in addition to the main adaptive terms, as shown in Fig. 3.12.

The cross-terms $W_{i,j}(z), i \neq j$, can be factorized into a fixed and an adaptive part as shown in Fig. 3.14, where the fixed part is the convolution of adjacent analysis and synthesis filters decimated by a factor K [135, 53, 54]. The fixed part $W_{i,j}^{(\mathrm{fixed})}(z)$ forms a narrow bandpass covering the transition band between the synthesis filter of the source band and the analysis filter of the target band [170, 135]. Therefore, adjustment of the adaptive term $W_{i,j}^{(\mathrm{adapt})}(a)$ is restricted to this spectral interval, yielding improved convergence [54] over the unconstrained unfactorized case. With regard to the leakage interpretation of the critically decimated PR case introduced in Sec. 3.4.1, the cross-terms can be interpreted as a means to supply the subbands with information of the transition region which had leaked into adjacent frequency bands.

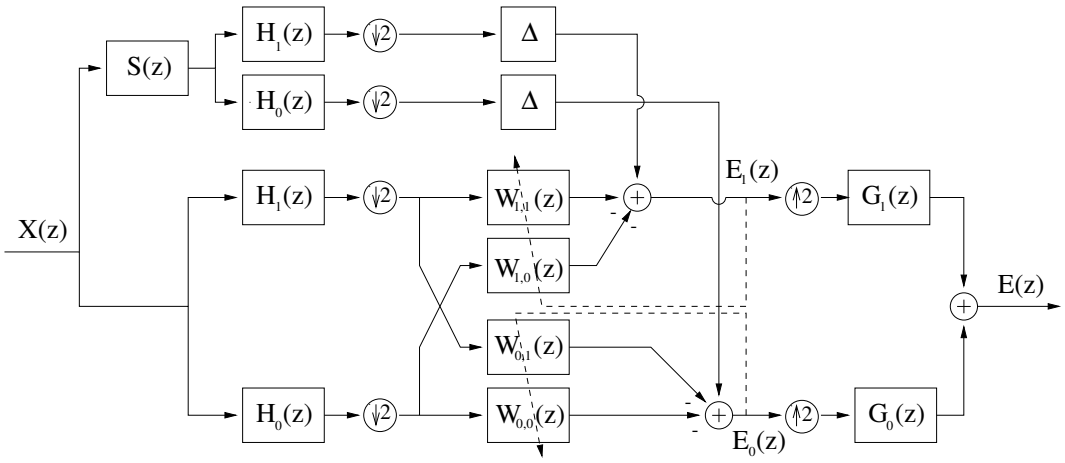

Figure 3.12: Two channel critically decimated filter bank with adaptive cross-terms between adjacent bands according to [54] and delays in the desired paths to correct for potential non-causality in (3.57) .

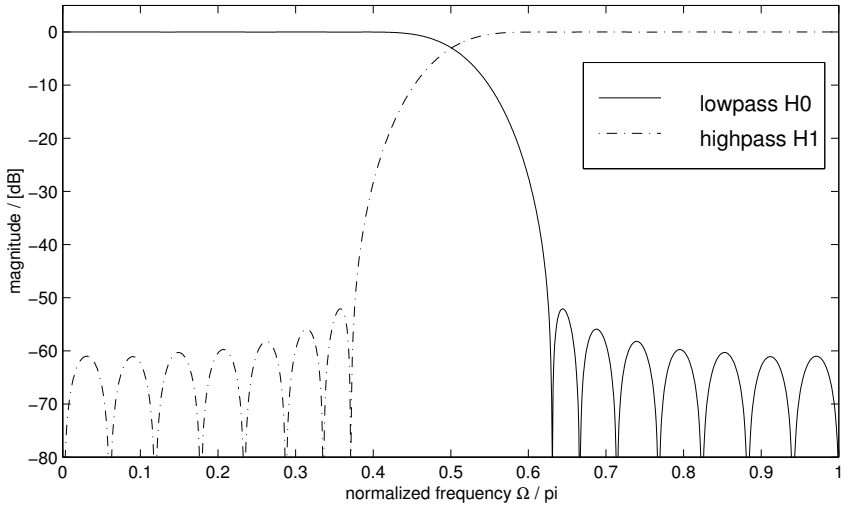

Figure 3.13: Frequency response of a near perfectly reconstructing QMF filter pair derived from the prototype 32C in [27].

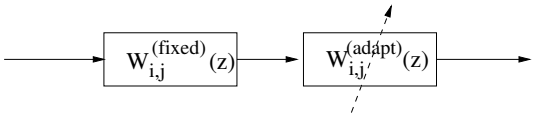

Figure 3.14: Factorization of a cross-term into a fixed part $W_{i,j}^{(\text{fixed})}(z)$ depending on the employed analysis / synthesis filters, and an adaptive system dependent part $W_{i,j}^{(\text{adapt})}(z)$.

A popular class of filter banks for this application are cosine modulated filter banks [151] which are very common in subband coding and image processing standards [56] as they produce real valued subband signals, suitable for subband adaptive filtering [54, 135, 170]. Starting from a real valued lowpass prototype, bandpass filters for analysis and synthesis bank are derived from

$$h_k[n] = 2 \cdot p[n] \cdot \cos\left(\frac{2\pi}{K}(k+\frac{1}{2})(n-\frac{L_p-1}{2}) - \frac{\pi}{4}(-1)^k\right), \quad (3.59)$$

$$g_k[n] = 2 \cdot p[n] \cdot \cos\left(\frac{2\pi}{K}(k+\frac{1}{2})(n-\frac{L_p-1}{2}) + \frac{\pi}{4}(-1)^k\right), \quad (3.60)$$

with $n = 0(1)L_p-1$ and $k = 0(1)K/2-1$ [4]. This particular choice of offsets in the argument of the cosine is referred to as DCT-IV [142]. With careful choice of the prototype $p[n]$ — some design methods will be introduced in Sec. 4.5 — the resulting filter bank forms a pseudo-QMF bank with near perfect reconstruction property. i.e. both alias and phase distortion of the filter bank are minimized and aliasing is cancelled only between adjacent subbands [151, 142]. Since a stronger overlap of not only adjacent filters would also introduce a much higher number of cross-terms in the SAF system, this inconvenient case is excluded here. Cosine modulated filter banks can be implemented very efficiently using polyphase implementations [151, 170].

[4] Different from standard notation in the literature [151, 142], here we refer to the DCT modulated filter bank as having $K/2$ (instead of K) subbands covering the frequency interval $\Omega \in [0; \pi]$. The reason will be elaborated on page 64.

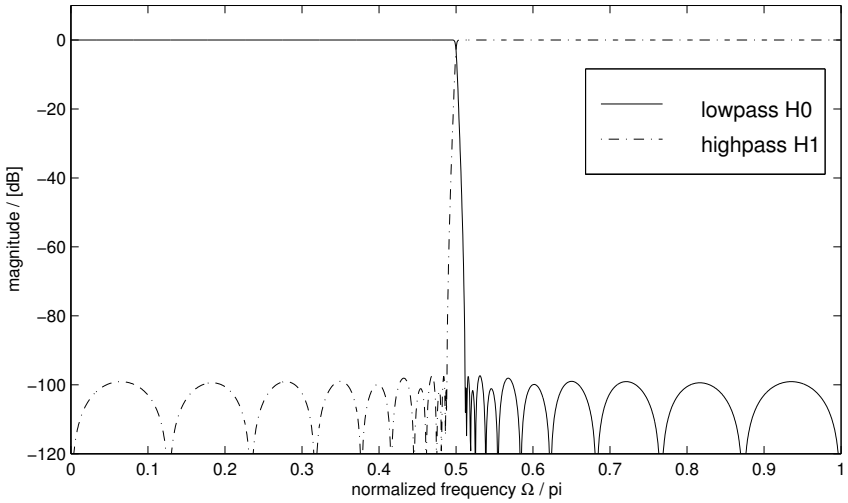

Figure 3.15: Power symmetric IIR filters with small alias level due to narrow transition region according to [148].

3.4.2.2 Critically Sampled Filter Banks with Minimized Alias Distortion

To avoid the large spectral overlap created by FIR filter banks as e.g. seen with the filter 32C from [27] in Fig. 3.13, IIR filters can be used for the filter banks, generally leading to shorter filters and a sharper cut-off. The latter property is exploited to reduce the spectral overlap to a minimum. Very narrow spectral intervals, where no identification of the unknown system or suppression of the error signal is possible, are ignored.

An elegant approach [146, 148] is to utilize coupled allpass filter sections to implement IIR filters with a flat passband and a very narrow transition band. There, the allpasses are designed such that for one halfband their behaviour is identical while for the other halfband they exhibit a phase shift of π with respect to each other. A lattice stage combines the two allpass outputs such that low- and highpass filters result. An example shown in Fig. 3.15 shows the magnitude responses of both low- and highpass filters. Polyphase implementations of this filter bank type are possible [65], but are strictly limited to critically sampled systems or systems involving integer oversampling ratios [160].

Although the low- and highpass filters arising from the allpass / lattice concatenation are power symmetric [146], the phase is considerably distorted at the band edges, which may not be too disruptive for speech signals which are relatively insensitive to phase distortions, but could not be accepted for data communications.

3.4.2.3 Filter Banks with Spectral Loss / Distortion

In [147, 148], the power symmetric IIR filter bank approach with small spectral overlap at band edges is further refined by inserting notch filters prior to performing the analysis filter bank operations. The notch filters are designed to remove the spectral intervals around the band edges which would otherwise be insufficiently adapted due to aliasing. This can significantly reduce the residual error power and positively influence the overall convergence by the thus lowered MMSE. However, clearly the resulting filter bank system is now lossy, as spectral gaps occur due to the additional notch filters.

The same result can be achieved by employing lossy filter banks with spectral gaps at the band edges in first place. Explicit descriptions of how these gap filter banks are constructed to comply with subband adaptive filtering can be found in [181, 179, 180, 178]. Subband adaptive filtering in combination with IIR filter banks is described in e.g. [176].

Two comments should be made here. Firstly, the introduction of spectral gaps, although they may be kept to a minimum by using IIR filters with sharp transition bands, may reduce the perceived quality for speech applications and can even be unacceptable for e.g. data communication system applications. Secondly, the filter design task of non-overlapping transition bands does not imply that the resulting filter banks will be completely alias free. There always is a residual alias level due to the finite stop-band attenuation of filters, which sets limits to the achievable MSE in the adaptation [172]; this will be described in more detail in Sec. 5.2.

3.4.3 Oversampled Filter Banks

Distinct from critically sampled subband structures a non-critical decimation of the subband signals can avoid the aliasing problem, which gave rise to either complicated inclusion of cross-terms or gap-filter banks with spectral loss in Sec. 3.4.2. In terms of the information leakage interpretation of the decimation stage in Sec. 3.4.1, the redundancy introduced by non-critical decimation will be located around the band-edges, such that in every band enough information is available to succeed in adaptation. In the following, we want to briefly discuss subband adaptive filter structures based on oversampled near PR filter banks. From the introduction of the sampling theorem for bandpass signals in Sec. 3.1.2, we distinguish between complex and real valued filter banks. More detail on some underlying techniques will be highlighted in Chap. 4.

3.4.3.1 Complex Valued Filter Banks

If the bandpass filters in Fig. 3.1 are analytic, and the input signal real valued, the output of the filters will also be analytic. Therefore, decimation of the subband signals can usually be applied down to any rate above the critical sampling frequency [5]. This means a decimation factor $N < K$ is employed, whereby K is the number of subbands covering the interval $\Omega \in [0; 2\pi]$. Usually some of these subbands will be complex conjugate and will not need to be processed as they carry redundant information, depending on how the bandpass filters in the analysis and synthesis filter bank are arranged. While other designs are possible, in the following we will concentrate on uniform, modulated filter banks, as they offer particularly efficient methods of implementation.

DFT Modulated Filter Banks. A simple organization of bandpass filters $h_k[n]$ is given by DFT modulation of a lowpass filter by [27, 151, 29]

$$h_k[n] = p[n] \cdot e^{j\frac{2\pi}{K}kn} \quad , \quad n = 0(1)L_p - 1 \quad \text{and} \quad k = 0(1)K - 1, \tag{3.61}$$

where L_p is the length of a prototype lowpass filter $p[n]$ with a passband width $B = 2\pi/K$. For an even number K, there result $K/2 + 1$ frequency bands to

[5] This also holds for complex valued filters and signals in the sense of Sec. 3.1.2.1.

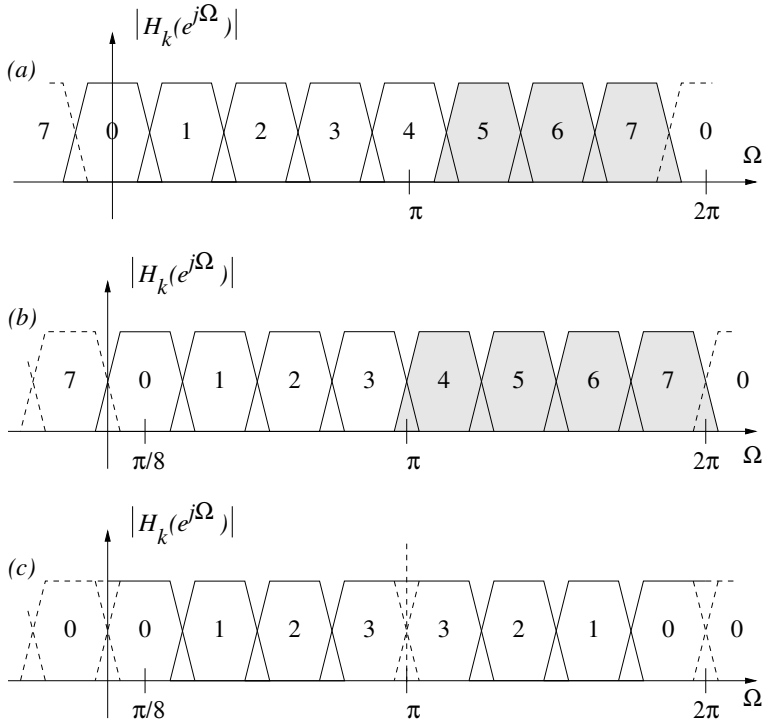

Figure 3.16: Arrangement of bandpass filters for $K = 8$ for (a) DFT modulated filter bank and (b) GDFT modulated filter bank with $k_0 = 1/2$; (c) DCT modulated filter bank; shaded spectra are redundant and are not required to process.

be processed. An example for $K = 8$ is sketched in Fig. 3.16(a). Obviously, the lowest and highest band are only real valued, and decimation can be performed for all subbands by a factor of $N \leq K$. If N is chosen sufficiently small, no spectral overlap of image spectra as stated in (3.2) will occur, and the adaptive filter matrix of the SAF system shown in Fig. 3.11 takes on a diagonal form [86, 50, 3].

GDFT Modulated Filter Banks. A generalized DFT (GDFT) transform [27] can also be employed to modulate a prototype filter $p[n]$,

$$h_k[n] = p[n] \cdot e^{j(\frac{2\pi}{K}(k+k_0)(n+n_0)+\theta_k)} \quad , \quad n = 0(1)L_p-1 \quad \text{and} \quad k = 0(1)K-1, \tag{3.62}$$

where offsets k_0 and n_0 for frequency and time indices, respectively, and a phase offset θ_k are introduced. For even K, the frequency interval $\Omega \in [0;\pi]$ will be covered by exactly $K/2$ subband signals, while the rest is complex conjugate as described by an example in Fig. 3.16(b). The case $k_0 = \frac{1}{2}$ is also sometimes referred to as "odd-stacked" DFT [12], in contrast to an "even-stacked" DFT in (3.61). Further note that insertion of a suitable parameter set $\{k_0 = \frac{1}{2}; n_0 = -\frac{L_p-1}{2}; \theta_k = \frac{\pi}{4}(-1)^k\}$ (3.62) represents the analytic expansion of a DCT-IV pseudo-QMF modulated filter bank for critical sampling as described in (3.59) [166]. Vice versa, a real valued DCT modulated filter bank can be derived from a GDFT filter bank by adding complex conjugate pairs of filters, i.e.

$$h_k[n] + h_{K-1-k}[n] \;=\; h_k[n] + h_k^*[n] \;=\; 2 \cdot \mathrm{Re}\{h_k[n]\} \quad , \tag{3.63}$$

and the result agrees with (3.59).

Here a comment on the use of the number K associated with the number of channels in a filter bank seems appropriate since its use is different from common notation. As the filter banks discussed in this thesis are modulated, we define K based on the passband width $B = \frac{2\pi}{K}$ of the prototype filter $P(e^{j\Omega})$. Similarly, N is defined as the total bandwidth of $P(e^{j\Omega})$, i.e. including the transition bands. It follows that

- for complex valued filter banks as in Fig. 3.16(a) and (b) the interval $\Omega \in [0;2\pi]$ is covered by K subbands which can be decimated by N. For real input, some bands are redundant. In case of the GDFT filter bank in Fig. 3.16(b), only $K/2$ subbands need to be processed.

- For real valued filter banks as in Fig. 3.16(c), there are $K/2$ subbands, which can be decimated by $N/2$ [6].

For the following discussions, it is easiest to realize that for any filter bank, real or complex, the number $K/2$ refers to the number of subbands completely covering the frequency interval $\Omega \in [0;\pi]$.

[6] Decimation usually cannot be directly applied as otherwise bandpass sampling will lead to spectral overlap. Intermediate steps, like modulation of the subbands into the baseband prior to decimation, may be required.

With respect to implementation, complex modulated oversampled filter banks can be efficiently calculated either by frequency domain implementation of the bandpass filters [1, 90] using the overlap-add method [27] as discussed in Sec. 2.6.1 or via a polyphase representation. A somehow common misconception is that polyphase implementations are restricted to integer oversampling ratios $\frac{K}{N} \in \mathbb{N}$ [27, 90]. Therefore, for polyphase implementations integer oversampling ratios are employed (e.g. $K/N = 2$) [3, 106, 38], which is less efficient and has poorer properties in terms of whitening the subband signals than choosing N closer to K, potentially resulting in reduced convergence rate as will be demonstrated in Chaps. 4, 5 and 6. If the main task is to efficiently process subband signals, the decimation ratio N has to chosen close to K, and preferred method in the literature are frequency domain approaches rather than polyphase implementations of the filter banks [1, 90, 38].

In a number of publications non-integer oversampling ratios are used [86, 129, 87, 32, 33], where the focus is fully concentrated on efficient subband processing or convergence speed issues and but no statements are made regarding the actual filter bank implementation.

3.4.3.2 Real Valued Filter Banks

For real valued signals, sampling of bandpass signals is restricted by the bandwidth and band position according to Fig. 3.6. It can be verified, that decimation by a factor of $1 < N < K$ will produce spectral overlap of images in at least one of the subband signals. Even for integer oversampling ratios, although sometimes applied, aliasing occurs at some of the band edges, as the sampling points in Fig. 3.6 will partly fall onto the margins of "acceptable" areas. In the following, two approaches of real valued oversampled subband structures for adaptive filtering are reviewed, the first one based on a modulation of each frequency band into the baseband prior to decimation, the second one using non-uniform filter banks, whereby band-position and bandwidth of the single filters are chosen such as to comply with Fig. 3.6.

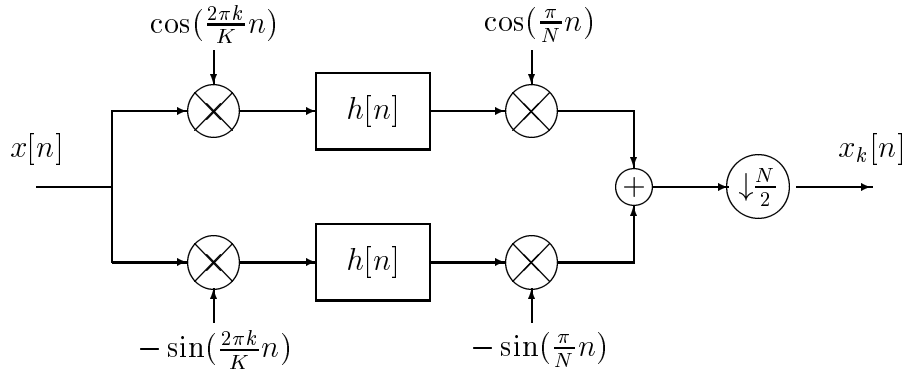

Figure 3.17: (a) Using SSB demodulation by means of quadrature modulation for the kth branch of an analysis filter bank [27, 159].

Single Sideband Modulation Single sideband modulation (SSB) by means of quadrature modulation, also know as Weaver method [88], can be employed to construct oversampled real-valued filter banks. The analysis side is performed as SSB demodulation as depicted in Fig. 3.17 by modulating different spectral intervals into the baseband, where a lowpass filter is applied to filter out higher frequency components above $\Omega = \pi/K$ for the kth subband signal prior to decimation [27, 159]. Similarly, the branches of the synthesis filter bank can be constructed from an SSB modulation shown in Fig. 3.18. If the decimation factor is chosen such that the images of the downsampled subband signals according to (3.2) do not overlap, these filter bank implementations can be used to perform subband adaptive filtering free of cross-terms [21, 95, 19, 88]. Note that in accordance with the comments on page 64, the decimation factor is here referred to as $N/2$.

A simple explanation of how the Weaver method works can be given when interpreting the normal and quadrature components (i.e. the two branches in Figs. 3.17 and 3.18) as real and imaginary part of a complex signal. Then, as shown in Fig. 3.19(a)–(c), the analysis consists of a complex modulation of the band of interest into the baseband, where it is filtered out by $H(e^{j\Omega}) \bullet\!\!-\!\!\circ\, h[n]$ from the remaining signal components. The second modulation lifts the signal up in frequency by π/N. By a real operation, the spectrum is symmetrized with

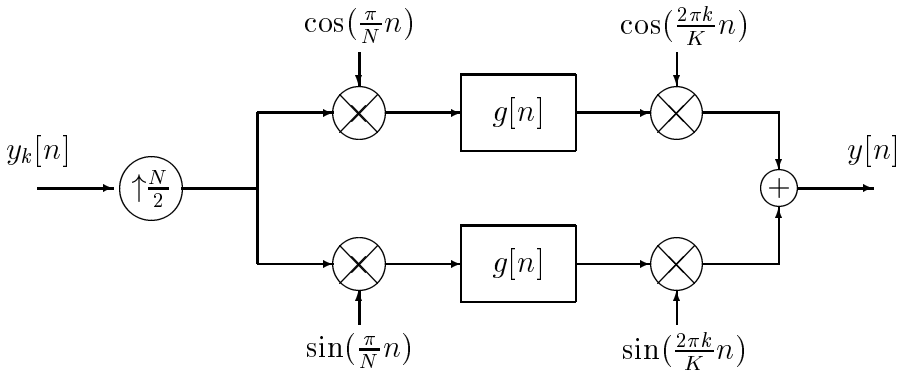

Figure 3.18: (a) Using SSB modulation by means of quadrature modulation for the kth branch of a synthesis filter bank [27, 159].

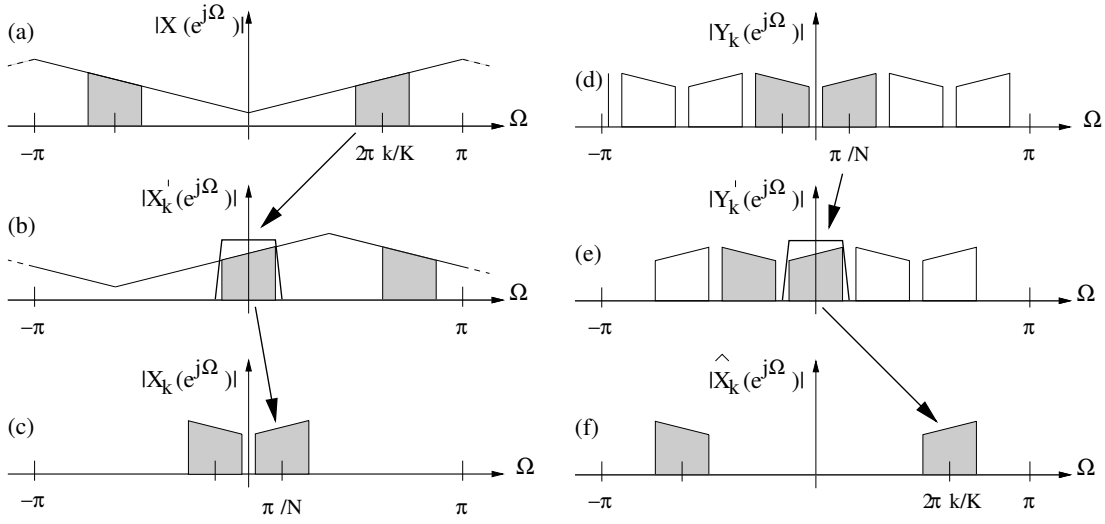

Figure 3.19: (a) –(c) SSB demodulation as analysis filter of the kth subband; (d) – (f) SSB modulation as kth synthesis filter operation in a filter bank.

respect to $\Omega = 0$, and a real valued baseband signal of bandwidth $B = 4\pi/N$ is obtained, which may now be decimated by a factor $N/2$. The SSB synthesis by Weaver can be performed by inverting the analysis process as illustrated in Fig. 3.19(d)–(f). After modulating the spectrum of interest into the baseband in Fig. 3.19(e), all image spectra introduced in the expander are removed by the lowpass filter $G(e^{j\Omega}) \bullet\!\!-\!\!\circ\, g[n]$. Finally, complex modulation by $e^{j2\pi k/K}$ and a real operation to restore a symmetric spectrum yield the original spectrum in the kth frequency band of Fig. 3.19(a).

Real valued oversampled subband signals based on an SSB modulation concept can be efficiently implemented by a modification of DFT/GDFT filter banks [27, 159, 167], which will be further discussed in the context of efficient factorizations of oversampled GDFT polyphase filter banks in Sec. 4.3.

As all filtering is either performed with or derived by modulation from a single prototype lowpass filter $p[n]$ of bandwidth $2\pi/N$, the resulting filter bank implementation is uniform.

Non-Uniform Filter Banks Dropping the restriction of uniform filter banks, band-position, bandwidth, and decimation factor of the corresponding subband can be selected independently for every bandpass filter in analysis and synthesis bank to comply with the criteria imposed by Fig. 3.6 and (3.10) [67, 71]. An example is given in Fig. 3.20, where different from Fig. 3.13, the PSD of the subband signals produced by lowpass $H_0(e^{j\Omega})$ and highpass filter $H_1(e^{j\Omega})$ do not overlap when decimated by factor 2, while the resulting gap is filled by a third band, which can be downsampled by a factor 3 with no spectral overlap occurring. A similar approach is described in [133], where the additional auxiliary band is not decimated and therefore computational efficiency of subband processing is not fully exploited. The subband approach introduced by [71] can be extended to any number of channels, whereby some implementational efficiency can be reached by constructing the filter bank from a number of modulated prototype filters [70]. However when used for subband adaptive filter applications [68, 70] on a DSP, the presence of different sampling rates and a number of prototype filters can result in inconvenient implementations, which are costlier than fully

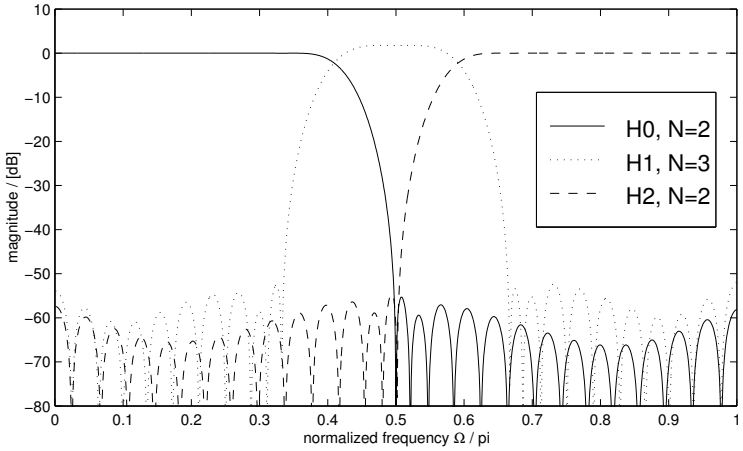

Figure 3.20: Example for a non-uniform oversampled real valued filter bank according to [67, 71]; the subband signals produced by the three filters $H_k(e^{j\Omega})$ are each decimated by different factors N.

modulated filter banks [160].

Both SSB modulated and non-uniform filter banks can be designed to be near PR. An elegant link between non-uniform filter banks as mention above and frame theory is made in [70] and allows the of design filter banks with different filters in analysis and synthesis bank. For the SSB case, we will return to the PR propery in Sec. 4.5.

3.5 Concluding Remarks

This chapter has introduced filter banks, their description and analysis methods, and reviewed their application to subband adaptive filter structures. Of all the different types of subband adaptive filter system discussed, three properties are believed to be of key importance:

Perfect Reconstruction. Generally, filter banks for subband adaptive filtering should posses PR or near PR property, as otherwise applications are limited to areas insensitive to distortion, spectral loss, or inadequate modelling.

Aliasing. Aliasing in the subband signals has to be suppressed as far as possible in order to guarantee satisfactory performance of the adaptive system.

Efficient Implementation. Subband processing is performed to save computations. Therefore, firstly subband signals should be sampled as close as possible at the critical rate, $N \to K$. Secondly, analysis and synthesis filter bank operations should be performed with as few computations as possible. This is the more important, since the computational complexity of the original processing task usually decreases with the number of subbands, while the cost involved in performing analysis and synthesis operations increases.

Although the demand for near PR property of the employed filter banks may seem harsh for some applications, it is useful to have, and as will be seen later in Chap. 5 can be relaxed and traded off against other properties of the subband adaptive system such as the overall delay imposed on signals.

In the following two chapters, we will introduce and analyse a very efficient implementation of complex oversampled GDFT filter banks based on a generalization of the polyphase concept introduced in Sec. 3.3.2, and apply them for subband adaptive filter structures. In terms of efficiency, the relation and tradeoff between critical and oversampled non-critical implementations, and filter bank and subband calculations using complex and real valued arithmetic will be of particular interest and closely researched.

Chapter 4

Oversampled GDFT Filter Banks

This chapter concentrates on the implementation and design of oversampled generalized DFT (GDFT) filter banks, beginning with a view of their general properties in Sec. 4.1. In Sec. 4.2 an extension and factorization of the polyphase description will then produce a highly efficient implementation of this type of filter bank producing complex valued subband signals. A restructuring of the Weaver method for SSB modulated real valued filter banks then leads to a modified GDFT filter bank described in Sec. 4.3. Sec. 4.4 discusses real and complex valued subband systems in terms of computational complexity of both filter banks and subband processing. Finally, Sec. 4.5 introduces design methods for complex oversampled GDFT filter banks which comply with the intended application to subband adaptive filtering.

4.1 Complex Valued GDFT Filter Banks

In Sec. 3.4.3.1 GDFT filter banks were briefly addressed. Here, a more detailed account of the modulation of a prototype filter and the properties of the resulting filter bank will be given.

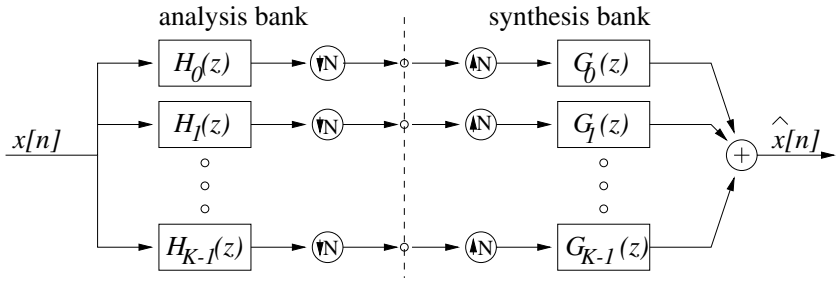

Figure 4.1: Analysis and synthesis branch of a K-channel filter bank with subbands decimated by N.

4.1.1 GDFT Modulation

The general structure of a filter bank is shown in Fig. 4.1, consisting of an analysis and a synthesis bank. The analysis bank decomposes a signal $x[n]$ into K subbands, each produced by a branch $H_k(z)$ of the analysis bank. After decimation and expansion by a factor N, the fullband signal is reconstructed from the subbands in the synthesis bank by filtering with filters $G_k(z)$ followed by summation. For modulated filter banks, both analysis and synthesis filters, $h_k[n]$ and $g_k[n]$, can be derived from a prototype filter by modulation. In the case of GDFT filter banks, the filter components of the filter bank are derived from a real valued FIR prototype lowpass filter $p[n]$ of even length L_p by modulation with a generalized discrete Fourier transform (GDFT)

$$h_k[n] = t_{k,n} \cdot p[n] \quad , \qquad t_{k,n} = e^{j\frac{2\pi}{K}(k+k_0)(n+n_0)}, \qquad k, n \in \mathbb{N}. \tag{4.1}$$

The term *generalized* DFT [27] stems from offsets k_0 and n_0 applied to frequency and time indices, which are responsible for important properties of the modulated filter bank such as the band-position of the subbands and linear phase of the modulated filters.

4.1.1.1 Bandpositions

The frequency offset k_0 is responsible for the positioning of the modulated bandpass filters $h_k[n]$ along the frequency axis. In Sec. 3.4.3.1 and Fig. 3.16 the effect of this parameter has been demonstrated, while for a full review the reader is

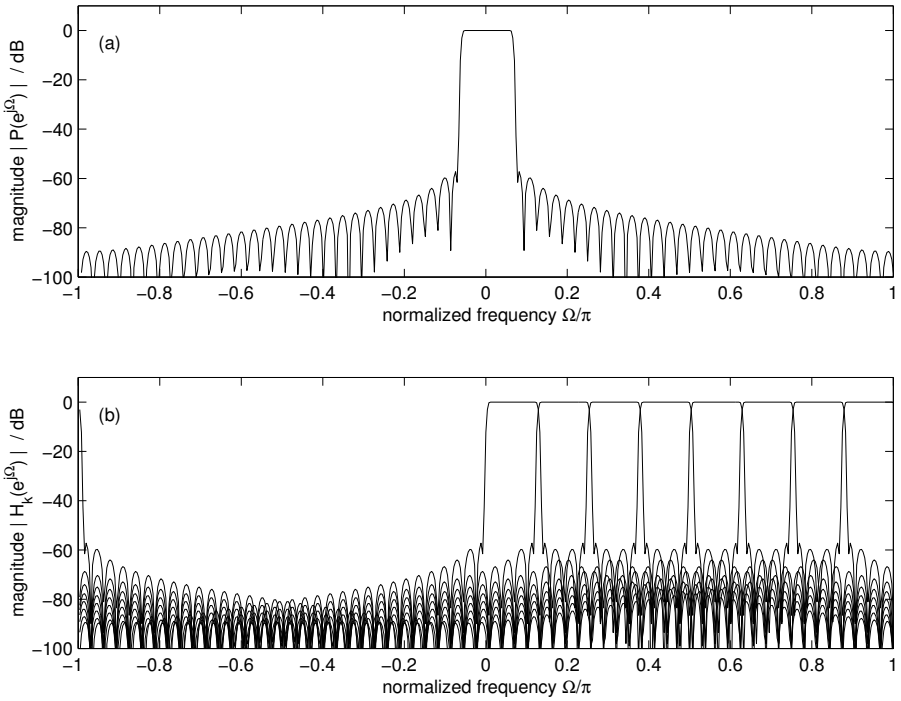

Figure 4.2: (a) Real valued prototype lowpass filter $P(e^{j\Omega})$ with bandwidth $B = 2\pi/16$; (b) reduced modulated GDFT filter bank derived from the prototype lowpass filter $P(e^{j\Omega})$ with $K/2 = 8$ filters covering the frequency range $\Omega = [0; \pi]$.

referred to [27]. With the choice of $k_0 = 1/2$ for even K, a convenient situation arises, as for real input signals $x[n]$ only $K/2$ subbands need to be processed, since the remaining subbands are complex conjugate versions of these. On the synthesis side, the $K/2$ unprocessed subbands can be restored by a real operation $\mathrm{Re}\{\cdot\}$. However, other constellations are possible and in use [50].

An example for the spectral coverage of the described reduced GDFT modulation is shown in Fig. 4.2. A lowpass filter with bandwidth $B = 2\pi/16$ depicted in Fig. 4.2(a) is modulated according to (4.1) with $k_0 = \frac{1}{2}$, $K = 16$, with the result given in Fig. 4.2(b). This *reduced* filter bank with only $K/2$ subbands has significant bearing on the computational efficiency of processing complex subbands, as will be further highlighted in Sec. 4.4.

4.1.1.2 Linear Phase

Linear phase (or constant group delay) as a property of a filter ensures that the filter output is not dispersed. Although any non-linear phase filter in the analysis bank could be compensated in the synthesis by filtering with the time reversed filter, linear phase is usually required for the filters $h_k[n]$ [31, 157].

In the time domain linear phase corresponds to a symmetry of the impulse response for real valued FIR filters. In the z-domain a linear phase filter possesses only zeros on the unit circle, $|\xi_i| = 1$, or pairs of zeros $(\xi_{j,1}, \xi_{j,2})$ with the same phase but reciprocal magnitudes, i.e. $\xi_{j,1} = 1/\xi_{j,2}$:

$$P(z) = A \cdot \prod_i (1 - \underbrace{e^{j\psi_i}}_{\xi_i} z^{-1}) \prod_j (1 - \xi_j z^{-1})(1 - \frac{1}{\xi_j} z^{-1}). \tag{4.2}$$

Clearly for real valued $p[n]$, all complex valued zeros have to be complemented by complex conjugate zeros.

A modulation with a general complex exponential $h[n] = e^{j(\phi n + \theta)} \cdot p[n]$ results in

$$H(z) = A e^{j\theta} \prod_i (1 - \xi_i e^{j\phi} z^{-1}) \prod_j (1 - \xi_j e^{j\phi} z^{-1})(1 - \frac{1}{\xi_j} e^{j\phi} z^{-1}), \tag{4.3}$$

and therefore only rotates the zero locations by an angle ϕ, but does not change the linear phase condition of the overall filter. However, with the choice

$$n_0 = -\frac{L_p - 1}{2} \tag{4.4}$$

and starting from a real valued linear phase prototype $p[n]$, both the real and imaginary part of $h_k[n]$ will separately satisfy linear phase conditions, solely through the linear phase of $p[n]$ and the symmetry of the modulation sequence $t_k[n]$ to the filter delay $(L_p - 1)/2$.

Example. Fig. 4.3 shows the impulse response and zero-plot of a real valued linear phase lowpass filter $p[n]$ with bandwidth $B = \pi$ tabulated as 32C in [27] with length $L_p = 32$. An example for a modulation by $\frac{3\pi}{2}$ and a time offset n_0 according to (4.4) results in a modulated filter $h[n]$, which is characterized in terms of its zero-plot in Fig. 4.3(b) and real and imaginary parts of its impulse, $\mathrm{Re}\{h[n]\}$ and $\mathrm{Im}\{h[n]\}$ in Fig. 4.3(d) and (e).

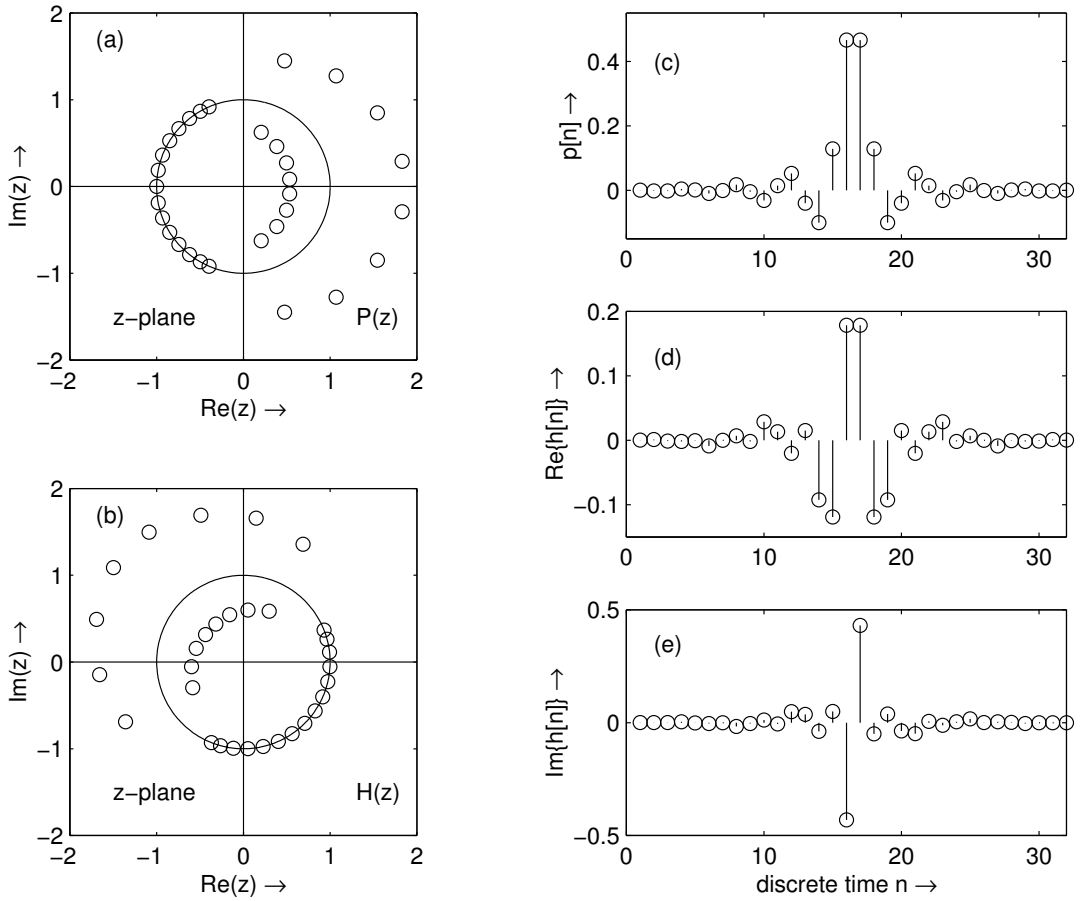

Figure 4.3: Complex GDFT modulation of a real valued linear phase filter $p[n]$ (32C from [27]) with offset n_0 according to (4.4): (a) zeros of $P(z)$; (b) zeros of $H(z)$; (c) axial symmetric impulse response of $p[n]$; (d) axial symmetric impulse response $\mathrm{Re}\{h[n]\}$; (e) point symmetric impulse response $\mathrm{Im}\{h[n]\}$.

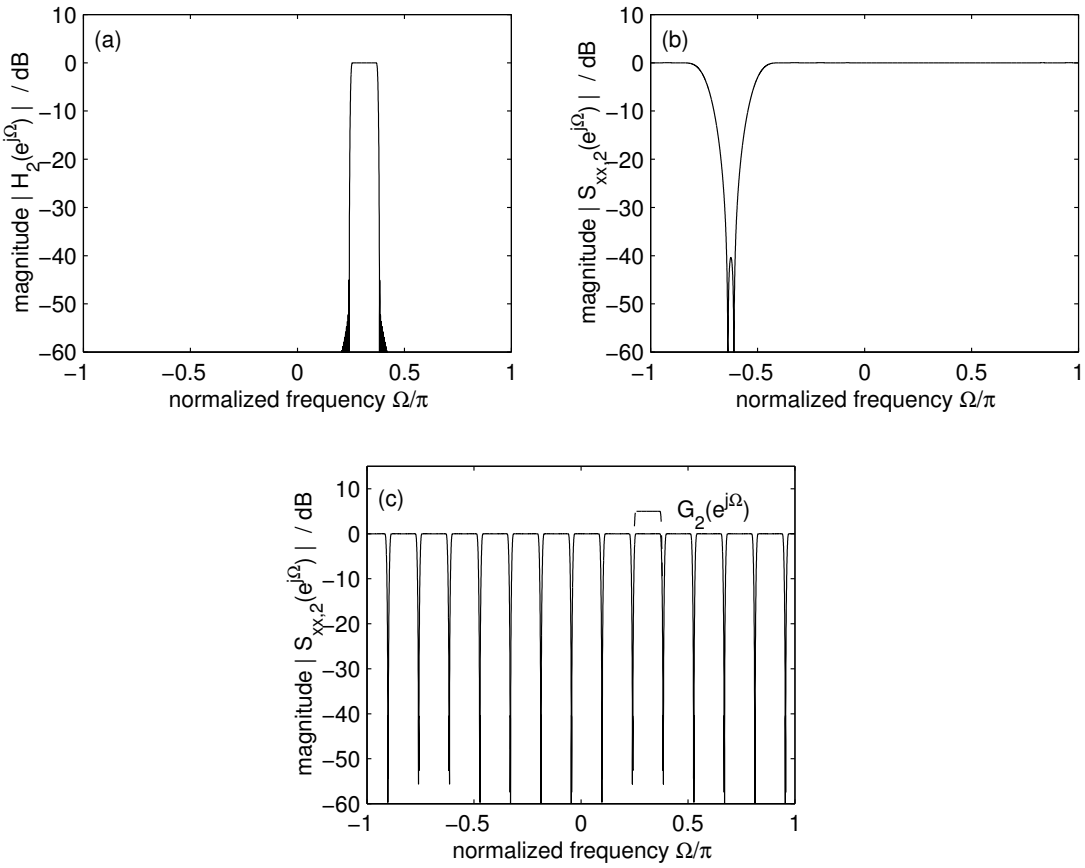

Figure 4.4: Example for spectra after decimation and expansion: (a) 3rd bandpass analysis filter $H_2(e^{j\Omega})$ from Fig. 4.2(b); (b) PSD of decimated subband signal as reaction to white noise excitation; (c) PSD of expanded subband signals with the relevant spectral part filtered out by 3rd synthesis filter $G_2(e^{j\Omega})$.

4.1.1.3 Decimation of Subband Signals

Assume that the prototype filter $P(e^{j\Omega}) \bullet\!\!-\!\!\circ\, p[n]$ has a total bandwidth including the transition bands of $2\pi/N$. The complex bandpass filters in the filter bank obtained by modulation will posses the same bandwidth. Therefore according to Sec. 3.1.2.1 the subband signals can be decimated by a factor $N \leq K$. Fig. 4.4(a) shows the third bandpass of the GDFT modulation example in Fig. 4.2(b), and the resulting power spectral density (PSD) of the subband signals for white noise input after decimation by a factor $N = 14$ in Fig. 4.4(b). Clearly, there is no spectral overlap occurring. After expansion in the synthesis bank, Fig. 4.4(c) indicates that the relevant spectral signal part can be recovered by a synthesis

filter with characteristics similar to $H_k(e^{j\Omega})$. How the synthesis filter can be chosen to allow for perfect reconstruction will be discussed in Sec. 4.1.3 based on conditions of the polyphase description of the analysis filter bank.

4.1.2 Polyphase Representation

With the kth analysis filter written in the z-domain in terms of its N polyphase components $H_{k|j}(z)$, $j = 0(1)N-1$,

$$H_k(z) = \sum_{j=0}^{N-1} z^{-j} H_{k|j}(z^N) \tag{4.5}$$

where the $H_{k,n}(z)$ refer to the type-1 polyphase components described in (3.26), a matrix $\mathbf{H}(z)$ with polynomial entries can be created for the analysis filter bank:

$$\mathbf{H}(z) = \begin{bmatrix} H_{0|0}(z) & H_{0|1}(z) & \cdots & H_{0|N-1}(z) \\ H_{1|0}(z) & H_{1|1}(z) & & H_{1|N-1}(z) \\ \vdots & & \ddots & \vdots \\ H_{K-1|0}(z) & H_{K-1|1}(z) & \cdots & H_{K-1|N-1}(z) \end{bmatrix}. \tag{4.6}$$

Together with a polyphase decomposition $X(z) = \sum_{j=0}^{N-1} z^{-j} X_j(z^N)$ of the input signal $X(z) \bullet\!\!-\!\!\circ\, x[n]$ analogue to (4.5),

$$\underline{X}(z) = \begin{bmatrix} X_0(z) \\ X_1(z) \\ \vdots \\ X_{N-1}(z) \end{bmatrix}, \qquad X_i(z) \bullet\!\!-\!\!\circ\, x_i[n] = x[nN+i], \quad i = 0(1)N-1. \tag{4.7}$$

the analysis bank operation can be expressed as

$$\underline{Y}(z) = \mathbf{H}(z) \cdot \underline{X}(z) \quad , \tag{4.8}$$

where $\underline{Y}(z) \in \mathbb{C}_{(z)}^{K\times 1}$ contains the K subband signals.

The filters in the synthesis bank can be represented by the type-2 polyphase description (3.27),

$$G_k(z) = \sum_{j=0}^{N-1} z^{-N+1+j} G_{j|k}(z^N) \tag{4.9}$$

to form a polyphase matrix

$$\mathbf{G}(z) = \begin{bmatrix} G_{0|0}(z) & G_{0|1}(z) & \cdots & G_{0|K-1}(z) \\ G_{1|0}(z) & G_{1|1}(z) & & G_{1|K-1}(z) \\ \vdots & & \ddots & \vdots \\ G_{N-1|0}(z) & G_{N-1|1}(z) & \cdots & G_{N-1|K-1}(z) \end{bmatrix}. \tag{4.10}$$

Thus, the synthesis filter bank operation can now be expressed as

$$\underline{\hat{X}} = \mathbf{G}(z)\underline{Y}(z) = \mathbf{G}(z)\mathbf{H}(z)\underline{X} \tag{4.11}$$

with

$$\underline{\hat{X}}(z) = \begin{bmatrix} \hat{X}_0(z) \\ \hat{X}_1(z) \\ \vdots \\ \hat{X}_{N-1}(z) \end{bmatrix}, \tag{4.12}$$

such that the reconstructed signal $\hat{X}(z)$ can be retrieved by interleaving its polyphase components contained in $\underline{\hat{X}}$,

$$\hat{X}(z) = \sum_{j=0}^{N-1} z^{-N+1+j} \hat{X}_j(z). \tag{4.13}$$

Conditions under which $\hat{X}(z)$ is only a delayed version of the input signal have been subject of Sec. 3.3.3 and will be further reviewed in the following section.

4.1.3 Perfect Reconstruction and Gabor Frames

For perfect reconstruction (PR) such that the reconstructed signal $\hat{X}(z)$ is identical to $X(z)$ apart from a delay, Sec. 3.3.3 introduced a general condition on the analysis and synthesis polyphase matrices $\mathbf{H}(z)$ and $\mathbf{G}(z)$. Allowing for synthesis matrices with stable but not necessarily causal entries, the existence of a matrix $\mathbf{G}(z)$ fulfilling

$$\mathbf{G}(z)\mathbf{H}(z) = c\mathbf{I} \quad , \qquad c \in \mathbb{C}, \tag{4.14}$$

ensures that the filter bank implements a frame operator [30], which is identical to the PR requirement in (3.36). Of particular interest is the special case where $\mathbf{H}(z)$ is paraunitary, i.e.

$$\tilde{\mathbf{H}}(z)\mathbf{H}(z) = c\mathbf{I} \quad , \qquad c \in \mathbb{C}, \tag{4.15}$$

as the corresponding frame expansion is tight [29, 30]. As explained in Sec. 3.2.2, a tight frame guarantees an a priori known, fixed energy translation between the fullband and its subband samples similar to Parseval's theorem for orthonormal transforms and signal decompositions. This property has importance for the derivation of performance limitations of subband adaptive filters with respect to the employed filter banks in Sec. 5.3 and tap-assignment strategies discussed in Chap. 6.

4.1.3.1 Gabor Frames and Properties

Gabor frames perform an expansion of a signal by expressing it in terms of windowed complex exponentials [13, 41], offering a uniform resolution in the time–frequency plane. In the discrete case [103] kernels of this expansion are therefore identical to the definition of the filters in the presented GDFT filter bank in (4.1).

Generally, due to their redundancy frames posses superior robustness against noise interference in the expansion domain (quantization noise, channel interference) over basis representations of signals [28, 11], which can be exploited for coding or data analysis.

Efficient schemes for computing Gabor frame expansions are reported in [47, 104, 12], however only for integer OSRs $K/N \in \mathbb{N}$. Therefore, fast schemes for computing GDFT filter banks, which will be developed below in Sec. 4.2, could also be employed for fast computational schemes to compute certain Gabor expansions.

4.1.3.2 Selection of Synthesis Filters

For oversampled filter banks, usually an infinite number of polyphase synthesis matrices $\mathbf{G}(z)$ exists fulfilling (4.14). One of these solutions is the pseudo-inverse

of $\mathbf{H}(z)$ [29]

$$\mathbf{G}(z) = \left(\tilde{\mathbf{H}}(z)\mathbf{H}(z)\right)^{-1}\tilde{\mathbf{H}}(z) \tag{4.16}$$

which is particularly interesting since the resulting synthesis filters have minimum l_2 norm. Therefore generally lowest sensitivity to noise interference in the subband domain is achieved. If the analysis prototype filter is designed such that the analysis polyphase matrix $\mathbf{H}(z)$ is paraunitary, the minimum norm solution is the synthesis polyphase matrix being identical to the parahermitian of $\mathbf{H}(z)$, $\mathbf{G}(z) = \tilde{\mathbf{H}}(z)$. Thus, the synthesis filters will be time-reversed, complex conjugate copies of the corresponding analysis filters,

$$g_k[n] = \tilde{h}_k[n] = h_k^*[L_p - 1 - n]. \tag{4.17}$$

If the GDFT transform is selected with a time off-set n_0 according to (4.4), the symmetries of the real and imaginary parts of $h_k[n]$ as discussed in Sec. 4.1.1.2 result in

$$g_k[n] \equiv h_k[n]. \tag{4.18}$$

This simple choice has two favourable advantages. First, the filter bank system represents a tight frame operator. Secondly, the implementation on a DSP becomes less memory demanding, since only one prototype filter needs to be stored, from which all filters in both analysis and synthesis bank are derived.

4.1.3.3 Reduced Filter Bank for Real Valued Input

For real input signals $x[n]$, an efficient GDFT filter bank implementation omits $K/2$ subbands. Instead, missing subbands can be substituted on the synthesis side by a real operation $\mathrm{Re}\{\cdot\}$,

$$\underline{\hat{X}}(z) = \mathrm{Re}\left\{\tilde{\mathbf{H}}_r(z) \cdot \underline{Y}_r(z)\right\} = \mathrm{Re}\left\{\tilde{\mathbf{H}}_r(z) \cdot \mathbf{H}_r(z) \cdot \underline{X}(z)\right\}. \tag{4.19}$$

The subscript r refers to a reduced matrix representation including only the upper $K/2$ rows of the analysis polyphase matrix $\mathbf{H}(z)$,

$$\mathbf{H}(z) = \begin{cases} \begin{bmatrix} \mathbf{H}_r(z) \\ -\mathbf{J}_K \mathbf{H}_r^*(z) \end{bmatrix} & , \quad \text{for } L_p \text{ even;} \\ \begin{bmatrix} \mathbf{H}_r(z) \\ \mathbf{J}_K \mathbf{H}_r^*(z) \end{bmatrix} & , \quad \text{for } L_p \text{ odd.} \end{cases} \tag{4.20}$$

where $\mathbf{J}_K$ is a reverse identity matrix flipping the rows of $\mathbf{H}_r(z)$ upside down. Since $\mathbf{J}_K \mathbf{J}_K = \mathbf{I}_K$ it is easy to confirm the validity of (4.19).

4.2 Efficient Filter Bank Implementation

To efficiently implement oversampled GDFT filter banks with real valued input signals, two steps have already been taken with the omission of $K/2$ redundant complex conjugate subbands and the polyphase representation, which avoids computing filter bank output samples that will be decimated afterwards. In this section, we will further elaborate on the polyphase matrix $\mathbf{H}(z)$ to suppress calculations common to different branches of the filter bank by factorization of $\mathbf{H}(z)$ into a real valued polyphase network containing only components of the prototype lowpass filter and a transform matrix, which can be efficiently calculated using FFT algorithms.

4.2.1 Polyphase Factorization

Since all filters in the analysis and synthesis filter bank are derived by modulation from one single prototype filter $p[n]$, the task in this section is to exploit any calculations common to different branches of the filter bank.

The way the coefficients of the analysis filters emerge by modulation from the coefficients of the prototype is illustrated in Fig. 4.5. The coefficients $h_k[n]$, $k = 0(1)K-1$, in the nth column are all derived from the same coefficient $p[n]$ by multiplication with the nth column vector $\mathbf{t}_n = [t_{0,n},\ t_{1,n},\ \cdots t_{K/2-1,n}]^T$ of a GDFT matrix. Instead of multiplying each coefficient of $p[n]$ with a transform vector $\mathbf{t}_n$, the periodicity of the GDFT transform of $2K$ can be exploited to create

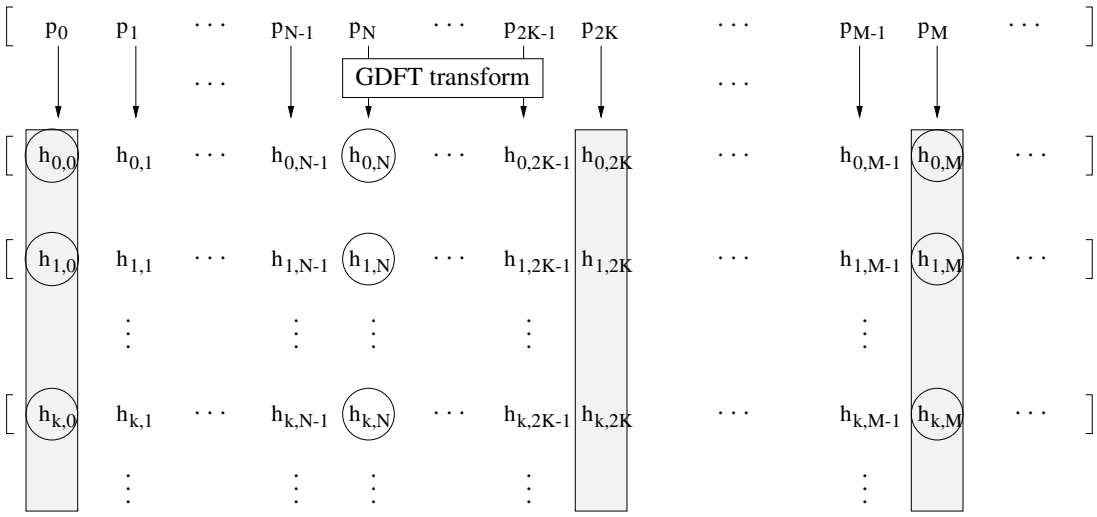

Figure 4.5: Factorization of the polyphase matrix: circles mark the coefficients belonging to the first polyphase components of the analysis filters; shaded areas indicate the periodicity of the GDFT transform, i.e. all coefficients in this area emerge from the prototype filter multiplied by the same transform coefficient vector.

sets of coefficients of $p[n]$ which will be multiplied by identical transform vectors. These coefficient sets are the $2K$ polyphase components of $p[n]$. In Fig. 4.5, the periodicity of the transform is indicated by under-laid shaded areas, where the coefficients $\{p[0],\ p[2K],\ p[4K],\ \cdots\}$ all are multiplied by the same vector $\mathbf{t}_0$ to create the first of $2K$ polyphase coefficients of the analysis filters $h_k[n]$.

However, for the polyphase representation in Sec. 4.1.2, the filters $h_k[n]$ need to be expressed in terms of their N polyphase components. In the critically sampled case $N = K$, this periodicity matches nicely with the arrangement of the polyphase components of the analysis polyphase matrix $\mathbf{H}(z)$, such that $\mathbf{H}(z)$ can be expressed as a matrix product between a polyphase network consisting of the polyphase components of the prototype filter $p[n]$ and a transform matrix performing a complex rotation on the output of the polyphase network [27, 160, 151].

For the general oversampled case $N < K$, we need to have the correct polyphase representation of the $h_k[n]$ *and* exploit the transform periodicity. It is therefore necessary to divide $p[n]$ into M polyphase components, where M is

the least common multiple (lcm) of the decimation ratio N and the transform periodicity $2K$,

$$M = \mathrm{lcm}(2K, N) \in \mathbb{N}. \tag{4.21}$$

Further, we define $M = J \cdot 2K = L \cdot N, \quad J, L \in \mathbb{Z}$. In the following, it will first be attempted to express the polyphase matrix $\mathbf{H}(z)$ from (4.5) in terms of M polyphase components, which will then enable the exploitation of the transform periodicity.

The polyphase entries of $\mathbf{H}(z)$ can be written in terms of the M polyphase components of the analysis filters $H_k(z)$, whereby the superscript indicates the number of polyphase components in the referring representation

$$H_{k|n}^{(N)}(z) = \sum_{l=0}^{L-1} z^{-l} H_{k|lN+n}^{(M)}(z^L) = \sum_{l=0}^{L-1} z^{-l} \cdot t_{k,lN+n} \cdot P_{lN+n}(z^L) \quad , \tag{4.22}$$

and the polyphase components $H_{k|lN+n}^{(M)}(z^L)$ have been written in terms of their modulation from the M polyphase components of the prototype filter $P(z)$,

$$P(z) = \sum_{m=0}^{M-1} z^{-m} P_m(z^M) \quad . \tag{4.23}$$

Using the expansion in (4.22), the kth component of the vector equation (4.8) describing the analysis filter bank can be reformulated as

$$Y_k(z) = \sum_{n=0}^{N-1} H_{k|n}^{(N)}(z) \cdot X_n(z) = \sum_{n=0}^{N-1} \sum_{l=0}^{L-1} z^{-l} H_{k|lN+n}^{(M)}(z^L) \cdot X_n(z) \tag{4.24}$$

$$= \sum_{n=0}^{N-1} \sum_{l=0}^{L-1} t_{k,lN+n} \cdot z^{-l} P_{lN+n}^{(M)}(z^L) \cdot X_n(z) \quad . \tag{4.25}$$

Now the analysis filter bank, decimated by a factor N, is fully expressed in terms of the polyphase components of the prototype filter and the transform coefficients employed for modulation. Rearranging the $M = LN$ products in (4.25) to order them in terms of the M prototype filter polyphase components yields

$$Y_k(z) = \sum_{m=0}^{M-1} t_{k,m} \cdot P_m^{(M)}(z^L) \cdot z^{\lfloor m/N \rfloor} X_{m \bmod (N)}(z) \quad , \tag{4.26}$$

which can also be verified by inspection of Fig. 4.5. Considering all $K/2$ subband signals in (4.8), (4.26) can be written in matrix notation

$$\underline{Y}(z) = \mathbf{T}'_{\mathrm{GDFT},r} \cdot \mathbf{P}'(z^L) \cdot \underline{X}'(z) \quad , \tag{4.27}$$

where $\mathbf{T}'_{\mathrm{GDFT},r} \in \mathbb{C}^{K/2\times M}$ is a GDFT transform matrix, $\mathbf{P}'(z^L)$ a diagonal matrix containing the M polyphase components of the prototype filter,

$$\mathbf{P}'(z^L) = \mathrm{diag}\big\{P_0(z^L), P_1(z^L), \ldots P_{M-1}(z^L)\big\} \quad , \tag{4.28}$$

and $\underline{X}'(z)$ is an assembly of delayed input polyphase vectors,

$$\underline{X}'(z) = \begin{bmatrix} \underline{X}(z) \\ z^{-1}\underline{X}(z) \\ \vdots \\ z^{-L+1}\underline{X}(z) \end{bmatrix} = \begin{bmatrix} \mathbf{I}_N \\ z^{-1}\mathbf{I}_N \\ \vdots \\ z^{-L+1}\mathbf{I}_N \end{bmatrix} \underline{X}(z) \quad . \tag{4.29}$$

Thus, with (4.27) a factorization into a network of prototype polyphase filters and a GDFT modulation matrix has been established.

It remains to cut any redundancy in the transform matrix $\mathbf{T}'_{\mathrm{GDFT},r}$, which contains J repetitions of the fundamental transform period, by writing

$$\mathbf{T}'_{\mathrm{GDFT},r} = \big[\mathbf{T}''_{\mathrm{GDFT},r}\ ,\ \ldots\ \mathbf{T}''_{\mathrm{GDFT},r}\big] = \mathbf{T}''_{\mathrm{GDFT},r}\,[\mathbf{I}_{2K}\ \cdots\ \mathbf{I}_{2K}] \quad , \tag{4.30}$$

where the matrix $\mathbf{T}''_{\mathrm{GDFT},r} \in \mathbb{C}^{K/2\times 2K}$ defines the upper half of a GDFT matrix,

$$\mathbf{T}''_{\mathrm{GDFT},r} = \begin{bmatrix} t_{0,0} & t_{0,1} & \ldots & t_{0,2K-1} \\ t_{1,0} & t_{1,1} & \ldots & t_{1,2K-1} \\ \vdots & \vdots & \ddots & \vdots \\ t_{K/2-1,0} & t_{K/2-1,1} & \ldots & t_{K/2-1,2K-1} \end{bmatrix} \quad , \tag{4.31}$$

containing in its rows the fundamental and harmonics of the complex exponential used in the modulation of the filter bank. The structure of the transform matrix is such that the right half of the matrix is identical to the left half apart from a sign change, and the possibility of writing

$$\mathbf{T}''_{\mathrm{GDFT},r} = \mathbf{T}_{\mathrm{GDFT},r} \cdot [\mathbf{I}_K\ -\mathbf{I}_K] \tag{4.32}$$

can easily be verified for the coefficients $t_{k,n} = e^{j\frac{2\pi}{K}(k+1/2)(n-(L_p-1)/2)}$. The condensed expression of the transform is now expressed in a matrix $\mathbf{T}_{\mathrm{GDFT},r} \in \mathbb{C}^{K/2\times K}$. With the modifications in (4.29), (4.30), and (4.32) we can define a compact notation

$$\mathbf{P}(z) = [\mathbf{I}_K \;\; -\mathbf{I}_K \ldots \mathbf{I}_K] \cdot \mathrm{diag}\big\{P_0(z^L), P_1(z^L), \ldots P_{M-1}(z^L)\big\} \cdot \begin{bmatrix} \mathbf{I}_N \\ z^{-1}\mathbf{I}_N \\ \vdots \\ z^{-L+1}\mathbf{I}_N \end{bmatrix} \tag{4.33}$$

for the prototype filter polyphase matrix. Using this generally sparse matrix $\mathbf{P}(z) \in \mathbb{C}_{(z)}^{K\times N}$ containing M non-zero entries with polyphase components of the prototype filter, it is now possible to formulate a dense matrix notation for the reduced polyphase analysis matrix

$$\mathbf{H}_r(z) = \mathbf{T}_{\mathrm{GDFT},r} \cdot \mathbf{P}(z) \quad . \tag{4.34}$$

A similar result for oversampled DFT filter banks is stated by Cvetković and Vetterli [30]. An approach omitting polyphase considerations is given by Wackersreuther [160], who, based on time domain derivations, reaches a related computational scheme which shifts N samples at a time into the prototype filter, and rearranges and rotates the output of N filter sections.

Synthesis. With the convenient choice for selection of the synthesis filters discussed in Sec. 4.1.3.2, the factorization of the polyphase synthesis matrix $\mathbf{G}(z)$ can be readily based on (4.34),

$$\mathbf{G}_r(z) = \tilde{\mathbf{H}}_r(z) = \tilde{\mathbf{P}}(z) \cdot \mathbf{T}_{\mathrm{GDFT},r}^H. \tag{4.35}$$

Therefore, using the factorizations of the polyphase analysis matrix, the analysis–synthesis operation in (4.19) can now be written as

$$\hat{\underline{X}}(z) = \tilde{\mathbf{P}}(z) \cdot \mathrm{Re}\big\{\mathbf{T}_{\mathrm{GDFT},r}^H \mathbf{T}_{\mathrm{GDFT},r} \mathbf{P}(z) \underline{X}(z)\big\} \tag{4.36}$$

where it is advantageous to perform the real operation $\mathrm{Re}\{\cdot\}$ prior to entering the real valued polyphase network on the synthesis side. The computational scheme

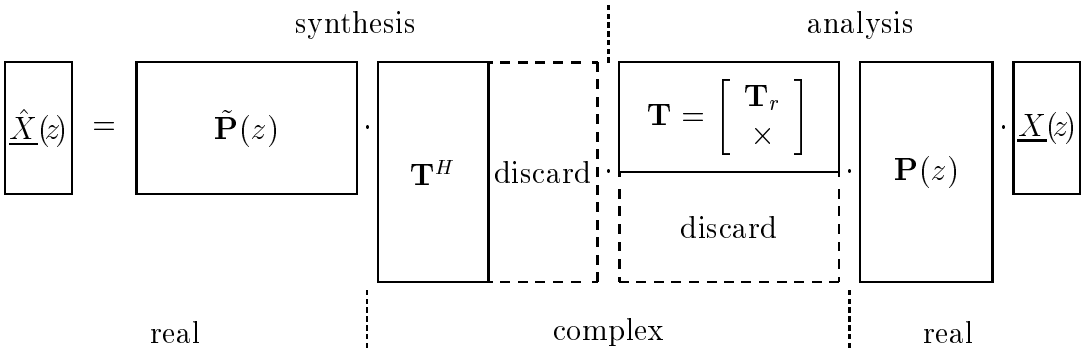

Figure 4.6: Computational scheme for analysis–synthesis operation with factorized polyphase matrices; discarded matrix parts refer to omitted subbands in accordance with Sec. 4.1.3.3.

is illustrated in Fig. 4.6. One particular appeal of the factorized representation lies in the ability to perform the filter operations in the polyphase network using entirely real valued arithmetic, while complex valued calculations are restricted to the GDFT transforms only.

Modified Prototype. Based on a decomposition of the prototype filter $P(z)$ into $2K$ polyphase components

$$P(z) = \sum_{k=0}^{2K-1} z^{-k} P_k^{(2K)}(z^{2K}) \quad , \tag{4.37}$$

whereby the superscript $\cdot^{(2K)}$ implies the number of polyphases, a modified prototype filter $\breve{p}[n] \circ\!\!-\!\!\bullet\, \breve{P}(e^{j\Omega})$ can be defined

$$\breve{P}(z) = \sum_{k=0}^{K-1} z^{-k} P_k^{(2K)}(z^{2K}) - z^{-K} \sum_{k=0}^{K-1} z^{-k} P_{k+K}^{(2K)}(z^{2K}) \quad . \tag{4.38}$$

This modification divides the impulse response of the prototype filter into blocks of K samples, and inverts the sign in every second block. The motivation for this action is that if analysis and synthesis filters, $h_k[n]$ and $g_k[n]$, are GDFT modulated versions of the modified prototype $\breve{p}[n]$, the transform periodicity has been cut to K, which can be verified by inspection of Fig. 4.5. By the virtual reduction of the transform periodicity, the least common multiple defined in (4.21)

can now be set to

$$\breve{M} = \mathrm{lcm}(K, N), \tag{4.39}$$

which may potentially be smaller than M by a factor of two, and thus may result in less indexing and book-keeping, since

$$\mathbf{P}(z) = [\mathbf{I}_K \ldots \mathbf{I}_K] \cdot \mathrm{diag}\Big\{\breve{P}_0(z^{\breve{L}}), \breve{P}_1(z^{\breve{L}}), \ldots \breve{P}_{\breve{M}-1}(z^{\breve{L}})\Big\} \cdot \begin{bmatrix} \mathbf{I}_N \\ z^{-1}\mathbf{I}_N \\ \vdots \\ z^{-\breve{L}+1}\mathbf{I}_N \end{bmatrix} \tag{4.40}$$

with $\breve{L} = \breve{M}/N$ is identical to (4.33) but carries $\breve{M}$ polyphase components of $\breve{p}[n]$ instead of $M \geq \breve{M}$ components of $p[n]$.

4.2.2 Transform Implementation

In addition to the factorization of the polyphase analysis and synthesis matrices and the resulting computational savings, this sections derives a further factorization of the GDFT transform matrix $\mathbf{T}_{\mathrm{GDFT},r}$ to make use of efficient numerical tools like the fast Fourier transform (FFT).

GDFT Matrix. For ease of presentation and later reference, first a factorization of an unreduced GDFT matrix $\mathbf{T}_{\mathrm{GDFT}} \in \mathbb{C}^{K\times 2K}$, holding elements

$$\begin{aligned} t_{k,n} &= e^{j\frac{2\pi}{K}(k+k_0)(n+n_0)} = e^{j\frac{1\pi}{K}kn_0} \cdot \underbrace{e^{j\frac{2\pi}{K}kn}}_{\mathrm{DFT}} \cdot e^{j\frac{2\pi}{K}k_0(n+n_0)} \\ &\quad \text{with} \quad k = 0(1)K-1\,, \quad n = 0(1)2K-1 \quad , \end{aligned} \tag{4.41}$$

is demonstrated. One way to implement this in matrix notations is given by

$$\mathbf{T}_{\mathrm{GDFT}} = \mathbf{D}_1 \cdot \mathbf{T} \cdot \mathbf{D}_2 \tag{4.42}$$

whereby $\mathbf{D}_1$ and $\mathbf{D}_2$ are diagonal matrices

$$\mathbf{D}_1 = e^{j\frac{2\pi}{K}kn_0}\mathbf{I}_K \tag{4.43}$$

$$\mathbf{D}_2' = \mathrm{diag}\Big\{e^{j\frac{2\pi}{K}k_0(n+n_0)}\Big\} \in \mathbb{C}^{2K\times 2K}\ ,\ n = 0(1)2K-1 \tag{4.44}$$

and $\mathbf{T} \in \mathbb{C}^{K \times 2K}$ with elements $t_{k,n} = e^{j\frac{2\pi}{K}kn}$. $\mathbf{T}$ can be expressed in terms of a K-point DFT matrix $\mathbf{T}_{\mathrm{DFT}}$,

$$\mathbf{T} = [\mathbf{T}_{\mathrm{DFT}} \ , \ \mathbf{T}_{\mathrm{DFT}}] = \mathbf{T}_{\mathrm{DFT}} \cdot [\mathbf{I}_K \ \mathbf{I}_K] \quad . \tag{4.45}$$

The matrix $\mathbf{D}_2' \in \mathbb{C}^{2K \times 2K}$ in (4.44) can be shown to take the form

$$\mathbf{D}_2' = \begin{bmatrix} \mathbf{D}_2 & \mathbf{0} \\ \mathbf{0} & -\mathbf{D}_2 \end{bmatrix} \quad , \tag{4.46}$$

where $\mathbf{D}_2 \in \mathbb{C}^{K \times K}$ only covers the first K diagonal elements of $\mathbf{D}_2'$. Thus, a factorization of the original GDFT matrix

$$\mathbf{T}_{\mathrm{GDFT}} = \mathbf{D}_1 \mathbf{T}_{\mathrm{DFT}} \mathbf{D}_2 \, [\mathbf{I}_K \ -\mathbf{I}_K] \quad , \tag{4.47}$$

is yielded.

Reduced GDFT Matrix. The above results can be transfered to the reduced GDFT matrix in (4.34) which arose from the omission of $K/2$ subband signals in the case of real valued input signals and can be denoted as

$$\mathbf{T}_{\mathrm{GDFT},r} = \mathbf{D}_{1,r} \cdot \mathbf{T}_{\mathrm{DFT},r} \cdot \mathbf{D}_2 \tag{4.48}$$

with the reduced phase correcting matrix $\mathbf{D}_{1,r} = e^{j\frac{2\pi}{K}kn_0}\mathbf{I}_{K/2}$ and the upper half of a K-point DFT matrix $\mathbf{T}_{\mathrm{DFT},r}$. Savings arise, as the latter may be calculated using standard FFT algorithms [20]. Even though half the solution of this K-point FFT will be discarded, the calculation can present a major reduction in computations over performing matrix multiplications in either (4.34) or (4.48).

4.2.3 Computational Complexity

Applying both polyphase and transform factorization introduced in Secs. 4.2.1 and 4.2.2, an analysis filter bank operation can be expressed by

$$\underline{Y}(z) = \underbrace{\mathbf{D}_{1,r}}_{2K} \cdot \underbrace{\mathbf{T}_{\mathrm{DFT},r}}_{4K \log_2 K} \cdot \underbrace{\mathbf{D}_2}_{2K} \cdot \underbrace{\mathbf{P}(z)}_{L_p} \cdot \underline{X}(z) \quad . \tag{4.49}$$

We now record the necessary real valued multiplications [1] when evaluating (4.49) from right to left for N fullband sampling periods:

Polyphase Network. The scalar products between the polyphase components of the input signal and the M polyphase components of length L_p/M in the matrix $\mathbf{P}(z)$ result in L_p multiplications.

Frequency Offset. The matrix multiplication with $\mathbf{D}_2$ can be mainly managed by book-keeping operations, and K multiplications of the real valued output of the polyphase network with both real and imaginary part of the diagonal elements of $\mathbf{D}_2$, resulting in $2K$ real valued multiplications.

DFT Matrix. If K is a power of two, an FFT requires $4K \log_2 K$ real multiplications for complex data. Unless K is prime, mixed-radix algorithms can be found attaining a similar efficiency than a popular radix-2 FFT [20].

Phase Correction. The multiplication with $\mathbf{D}_{1,r}$ requires $K/2$ complex, i.e. $2K$ real valued multiplies with the diagonal elements.

Therefore, in total the computational complexity per fullband sample results in

$$C_{\text{bank}} = \frac{1}{N}\left(4K \log_2 K + 4K + L_p\right) \tag{4.50}$$

real multiplications for the analysis filter bank operation.

For a synthesis operation, the same number of multiplications has to be computed, if the parahermitian of the efficient factorization in (4.49) is applied:

$$\underline{\hat{X}}(z) = \underbrace{\tilde{\mathbf{P}}(z)}_{L_p} \cdot \underbrace{\mathbf{D}_2^*}_{2K} \cdot \underbrace{\mathbf{T}_{\text{DFT},r}^H}_{4K \log_2 K} \underbrace{\mathbf{D}_1^*}_{2K} \underline{Y}(z) \quad . \tag{4.51}$$

Note, that the multiplication with $\mathbf{D}_2^*$ again only requires $2K$ real multiplications, since the imaginary result does not need to be processed for the input to the polyphase network $\tilde{\mathbf{P}}(z)$.

[1] The multiplication of two complex numbers $x_1 = x_1^{(r)} + jx_1^{(i)}$ and $x_2 = x_2^{(r)} + jx_2^{(i)}$,

$$x_1 \cdot x_2 = x_1^{(r)}x_2^{(r)} - x_1^{(i)}x_2^{(i)} + j(x_1^{(r)}x_2^{(i)} + x_2^{(r)}x_1^{(i)}) \quad ,$$

requires 4 multiplications and two additions. Alternatively by re-shuffling, this can be performed in 3 multiplications and 5 additions in a structure somewhat harder to implement [115]. Therefore, one full complex multiplication will be accounted by 4 real valued multiplications.

4.3 SSB Modulated Real Valued Filter Banks

This section will discuss a method for obtaining alias free, real valued subband signals of uniform bandwidth by single sideband (SSB) modulation. We start off from the Weaver method introduced in Sec. 3.4.3.2, which with the help of an equivalent complex modulation can be factorized into a complex modulated filter bank and a modification term. Including the computationally efficient scheme for implementing GDFT modulated filter banks derived in the previous section, an SSB method with very low computational complexity will be obtained.

4.3.1 SSB by Weaver Method and Modifications

Single sideband modulation was introduced in Chap. 3 for oversampled real valued filter bank techniques. The problem with decimating real valued bandpass signals without spectral overlap in any of the subband signals was solved by modulating the subbands into the baseband prior to decimation. In the Weaver method based on quadrature modulation shown in Figs. 3.17 and 3.18, one branch of the analysis filter bank can be compactly expressed by modulating the frequency band of interest into the baseband, cut it out by a suitable lowpass filter $h[n]$, and finally modulate it up by half of the channel bandwidth. The orthogonality of sine and cosine in the modulation procedure ensures that spectral overlaps in the signals are cancelled at the summation of the normal and quadrature component in Fig. 3.17.

To analyse the Weaver modulation, we employ an equivalent form to the structures shown in Figs. 3.17 and 3.18 using complex notation and modulation, which is illustrated in Fig. 4.7 [27]. For a reason to become apparent in Sec. 4.3.2 in order to compare to complex filter banks and with reference to the comments on page 64, the decimation factor is here denoted as $N/2$. For the analysis of the SSB demodulation applied as kth branch of the analysis filter bank, we can

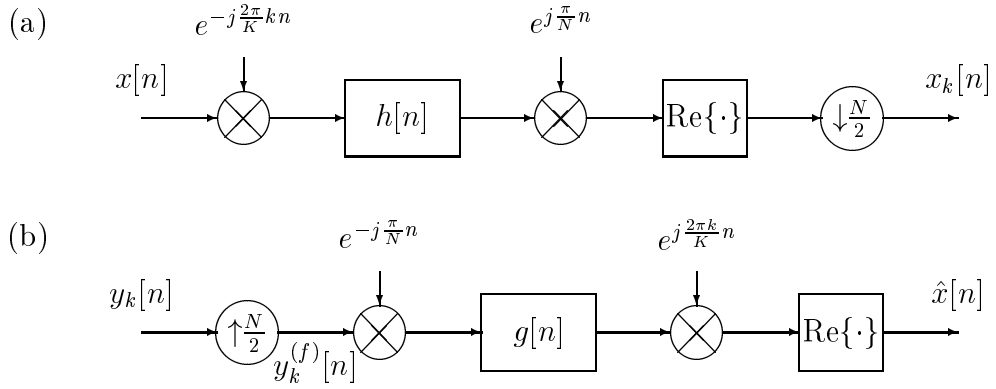

Figure 4.7: Complex quadrature modulation equivalent to the Weaver method for SSB in Figs. 3.17 and 3.18: (a) demodulation and for analysis and (b) modulation for synthesis filter branches.

describe the decimated subband signal at the output in Fig. 4.7(a) as

$$x_k[n] = \mathrm{Re}\Big\{e^{j\frac{\pi}{N}nN/2}\sum_{\nu=0}^{L_p-1} x[nN/2-\nu]\cdot e^{-j\frac{2\pi}{K}k(nN/2-\nu)}\cdot h[\nu]\Big\} \tag{4.52}$$

$$= \mathrm{Re}\Big\{e^{j(\frac{\pi}{N}-\frac{2\pi k}{K})nN/2}\sum_{\nu=0}^{L_p-1} x[nN/2-\nu]\cdot \underbrace{e^{j\frac{2\pi}{K}k\nu}h[\nu]}_{h_k[\nu]}\Big\}. \tag{4.53}$$

Obviously, the quadrature demodulation can be interpreted as filtering by a complex DFT modulated bandpass filter $h_k[n]$, followed by a displacement in frequency by the modulation term $e^{j(\frac{\pi}{N}-\frac{2\pi}{K}k)n}$. It is therefore possible to perform SSB analysis using a DFT filter bank followed by a modification which imposes the frequency shift.

The SSB quadrature modulation shown in Fig. 4.7(b) results in an output $\hat{x}_k[n]$ for the kth branch of the synthesis filter bank, which will form the reconstructed signal $\hat{x}[n]$ when summed up together with the remaining $K-1$ (or $K/2-1$ for real valued input $x[n]$) branch outputs. In terms of the upsampled kth subband signal $y_k^{(f)}[n]$, where the superscript $^{(f)}$ refers to sampling at the fullband rate, the output $\hat{x}_k[n]$ is given by

$$\hat{x}_k[n] = \mathrm{Re}\Big\{e^{j\frac{2\pi}{K}nk}\sum_{\nu=0}^{L_p-1}\Big(y_k^{(f)}[n-\nu]e^{-j\frac{\pi}{N}(n-\nu)}\Big)\,g[\nu]\Big\} \quad . \tag{4.54}$$

By introducing a spurious modulation term $e^{-j\frac{2\pi k}{K}(n-n)}$ into (4.54),

$$\hat{x}_k[n] = \mathrm{Re}\Big\{ \sum_{\nu=0}^{L_p-1} e^{j\frac{2\pi k}{K}n} \cdot e^{-j\frac{2\pi k}{K}(\nu-\nu)} \cdot \Big(y_k^{(f)}[n-\nu] e^{-j\frac{\pi}{N}(n-\nu)} \Big) \, g[\nu] \Big\} \quad (4.55)$$

$$= \mathrm{Re}\Big\{ \sum_{\nu=0}^{L_p-1} \Big(y_k^{(f)}[n-\nu] e^{-j\frac{\pi}{N}(n-\nu)} e^{j\frac{2\pi k}{K}(n-\nu)} \Big) \underbrace{e^{j\frac{2\pi k}{K}\nu} g[\nu]}_{g_k[\nu]} \Big\} \quad , \quad (4.56)$$

the SSB modulation can be separated into a preprocessing of the subband signal by modulation with $e^{-j(\frac{\pi}{N}-\frac{2\pi}{K}k)n}$, thus reversing the frequency displacement introduced in (4.53), and filtering with a modulated filter $g_k[n]$ belonging to a DFT modulated synthesis filter bank.

Depending on the number of subbands K covering $\Omega \in [0; 2\pi]$, according to Fig. 3.16(a) for real valued input a modulated DFT filter bank will produce either one or two real valued subband signals of bandwidth $2\pi/N$: at $k = 0$ for odd K and at $k = 0$ and $k = K/2$ for even K. If these channels are passed unaffected through the modification stages, these subband signals could be decimated by a factor N. Then components of the subband systems will be running at two different sampling rates, N and $N/2$, which can be unpleasant to implement. On the other hand decimating the special subbands $k = 0$ and possibly $k = K/2$ at only a factor of $N/2$ unnecessarily gives away efficiency. This provides the motivation for modifying GDFT filter banks to decompose signals into real valued subbands.

4.3.2 SSB by GDFT Filter Bank Modification

The previous section has derived how the SSB modulation using the Weaver method can be linked to a DFT filter bank with modifications. Here, a GDFT filter bank will be employed for the same purpose, with a structure shown in Fig. 4.8, whereby the analysis filter bank is only decimated by a factor $N/2$. This will leave large spectral gaps, which can be — after appropriately shifting the spectrum by a modification stage — filled with reversed spectral images in the real operation $\mathrm{Re}\{\cdot\}$. Reconstruction of the original fullband signal will require a pre-processing to perform a complex modulation on the subband signals to bring

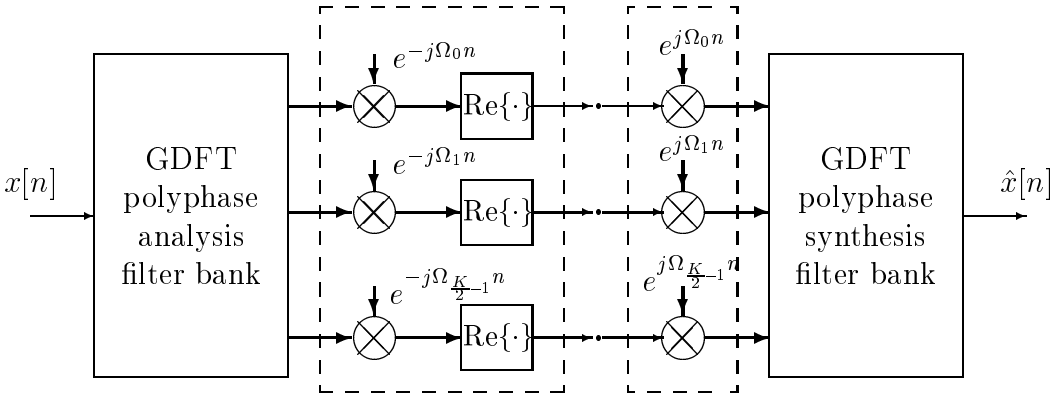

Figure 4.8: Complex valued oversampled GDFT analysis and synthesis filter banks with modifications stages to achieve real valued subband signals.

the correct spectral part into place to be retained by the synthesis filter bank. In the following, the correct modifications of the subband signals will be established.

The kth filter $h_k[n]$ of a GDFT analysis filter bank as described in (4.1) covers a channel of bandwidth $2\pi/K$ with a center angular frequency at

$$\Omega_c = \frac{2\pi(k+k_0)}{K} \quad . \tag{4.57}$$

This also describes the position of the passband characteristic in the PSD of the kth undecimated subband signal, $x_k^{(f)}[n]$. If $x_k^{(f)}[n]$ is decimated by a factor $N/2$, the frequency axis is re-scaled by a factor $N/2$, and $N/2-1$ image spectra are filled in equidistantly between the originals. Although other solutions are possible, it is easiest to locate the original band-position and to perform a complex modulation from $\Omega = \frac{N}{2}\Omega_c$ down to $\Omega = \pi/2$, as indicated in Fig. 4.9. Thus, the modulation frequencies for the analysis filter bank outputs can be chosen as

$$\Omega_k = \left(\frac{2(k+\frac{1}{2})\pi}{K} - \frac{\pi}{N}\right)\frac{N}{2} = \frac{N(k+\frac{1}{2})\pi}{K} - \frac{\pi}{2} \quad . \tag{4.58}$$

to align the original images in the decimated subband signals in the spectral interval $\Omega \in [0;\pi]$. The interval $\Omega = [-\pi;0]$ is initially unoccupied and is filled with a reversed image spectrum, since the real operation $\mathrm{Re}\{\cdot\}$ enforces symmetry to the frequency origin. Fig. 4.10 gives an example of what the PSDs of the subband

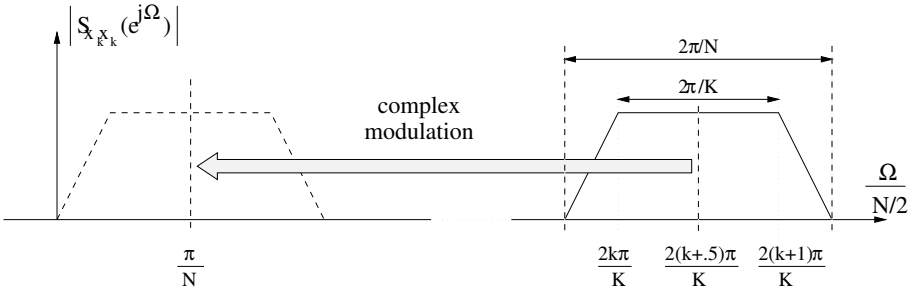

Figure 4.9: Power spectral density of the kth undecimated subband signal to explain the complex modulation procedure to align the passband in the region $\Omega \in [0; \pi]$ analytically.

signals on the analysis side look like prior to and after modulation with (4.58) for white noise excitation. Here, the prototype filter shown in Fig. 4.2 is used for $K/2 = 8$ subbands and decimation by $N/2 = 7$. Clearly, after modification the spectra are aligned in the positive half of the baseband, and real operation will not destroy the signal and preserve narrow spectral gaps between adjacent image spectra similar to Fig. 4.4(b) for complex subband signals.

To describe the reconstruction properties of the modified GDFT filter bank, we first look at the transfer from the kth output $x_k[n]$ of the GDFT analysis filter bank to the kth synthesis filter input signal $y_k[n]$. By representing $x_k[n] = x_k^{(r)}[n] + jx_k^{(i)}[n]$ in terms of its real and imaginary part, indicated by superscripts, the applied modifications according to Fig. 4.8 by the modulation on analysis and synthesis side are given by

$$y_k[n] = \mathrm{Re}\Big\{(x_k^{(r)}[n] + jx_k^{(i)}[n])e^{-j\Omega_k n}\Big\} e^{j\Omega_k n} \tag{4.59}$$

$$= \Big\{x_k^{(r)}[n]\cos(-\Omega_k n) - x_k^{(i)}[n]\sin(-\Omega_k n)\Big\} e^{j\Omega_k n} \quad , \tag{4.60}$$

where Euler's formula $e^{j\phi} = \cos(\phi) + j\sin(\phi)$ has been exploited. Further using the equalities

$$\cos(\phi) = \frac{1}{2}\left(e^{j\phi} + je^{-j\phi}\right) \tag{4.61}$$

$$\sin(\phi) = \frac{1}{2j}\left(e^{j\phi} - je^{-j\phi}\right) \tag{4.62}$$

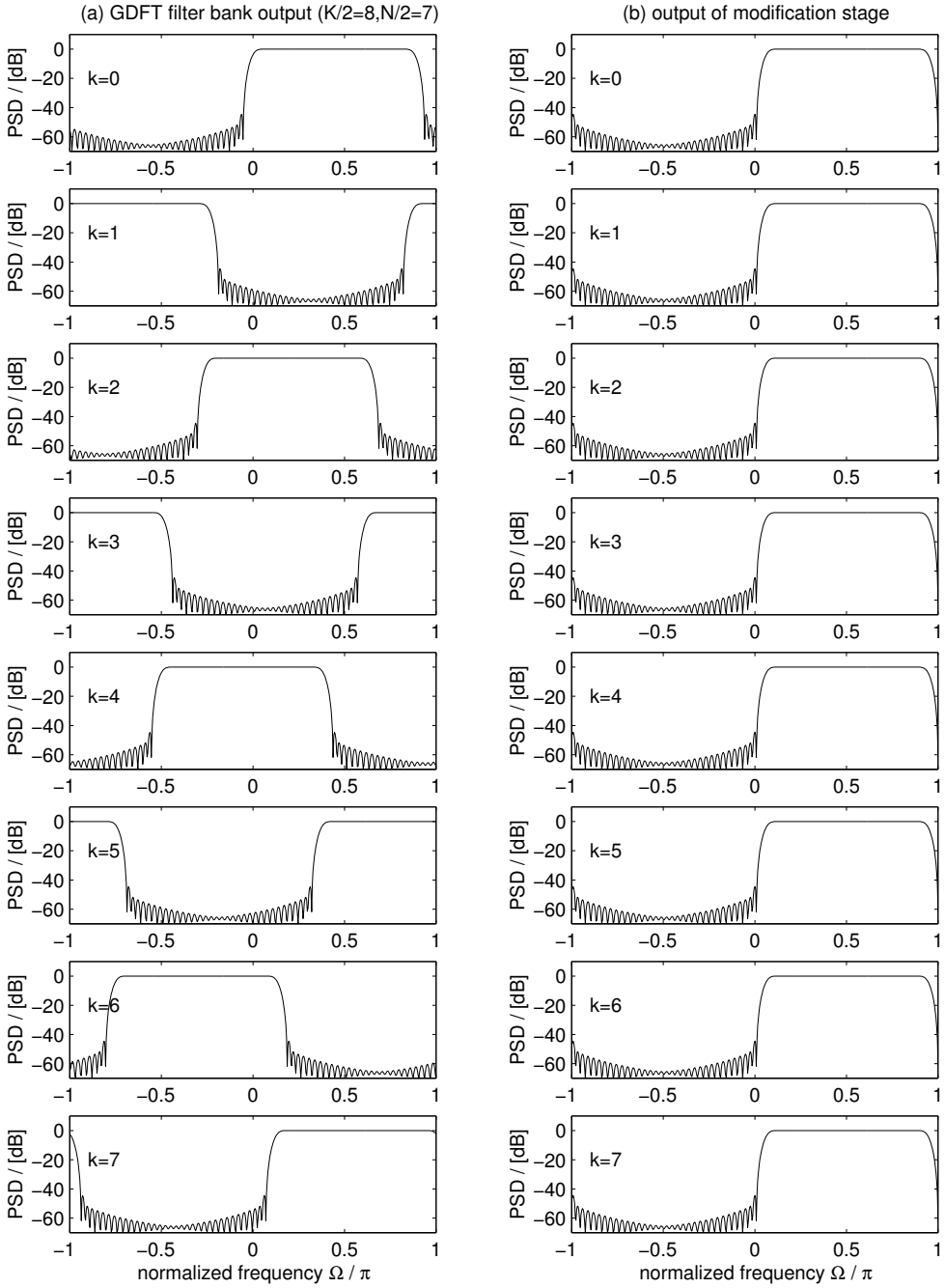

Figure 4.10: Power spectral density of all $K/2$ subband signals in a modified GDFT filter bank with $K/2 = 8$ channels and decimation by $N/2 = 7$ (a) prior to and (b) after modulation for correcting the frequency alignment of the subband spectra to the region $\Omega \in [0; \pi]$.

we proceed to

$$y_k[n] = \frac{1}{2}\left\{x_k^{(r)}[n]\left(1+je^{j2\Omega_k n}\right)+x_k^{(i)}[n]\left(j+e^{j2\Omega_k n}\right)\right\} \quad (4.63)$$

$$= x_k[n]+x_k^*[n]\cdot e^{j(2\Omega_k n+\frac{\pi}{2})} \quad (4.64)$$

where besides the original signal $x_k[n]$ a modulated version has appeared. The modulation frequency $2\Omega_k = 2N(k+1/2)/K\pi - \pi$ can be shown to shift with its first summand onto a spectral repetition of $X(e^{j\Omega})$, and finally by $-\pi$ into a previous unoccupied spectral gap. As for the original signal spectrum shown in Fig. 4.9 the modifications are transparent according to (4.64), the synthesis filters will pass it, while suppressing the added reversed spectra with their stopbands.

Complexity. Obtaining real valued subband signals is connected with some additional costs in performing the filter bank calculations stated for the complex GDFT filter banks in (4.50). The additional overhead for performing the post- and preprocessing of GDFT analysis and synthesis filter bank is given by $K/2$ complex valued multiplications. In case of the analysis bank, only the real output of the modulation has to be computed, yielding K real multiplications. Similarly, the synthesis side multiplies real valued subband samples with complex quantities, yielding for both analysis and synthesis

$$C_{\text{bank}} = \frac{2}{N}\left(4K\log_2 K + 5K + L_p\right) \quad (4.65)$$

multiplications per fullband period. Note, that compared to the cost for complex GDFT banks in (4.50) the computational effort for the SSB is approximately doubled. For real valued input, both filter banks produce $K/2$ subband signals. While however the complex GDFT subband signals can be decimated by N, this factor is halved in the SSB case.

4.4 Complex Vs Real Valued Subband Processing

The original incentive for subband adaptive filtering has been the reduction of computational complexity. While the previous sections were focused on the

derivation and implementation of oversampled filter banks with particular respect to efficiency, no considerations have yet been made on the computational complexity of the overall system, consisting of both subband processing task and calculation of the filter bank operations. Therefore, this section will look into the complexity of processing in subbands, and in particular address which preferences should be made regarding the possibilities of real and complex valued subband processing.

To judge subband processing for real and complex subbands on an equal basis, we assume that the subbands are produced by filter banks derived from the same prototype lowpass filter $p[n]$ with bandwidth $B = 2\pi/K$. This ensures that for both signal decompositions, aliasing in the subbands and reconstruction error are approximately identical, as will be demonstrated in Sec. 4.5. Further, we can find an $N = \lfloor 2\pi/B \rfloor$, where B is the bandwidth covering both passband and transition bands of the prototype filter. Therefore generally the following statements can be made:

1. the decimation rate N for complex subband signals can be twice as high as for real valued signals, which are only allowed to be downsampled by $N/2$;

2. if for convenience integer decimation is employed (although possible [129], fractional sampling is awkward), the complex approach offers twice the number of possibilities of decimation ratios over a finer range to choose.

Point (1) will be exploited to compare the complexity of implemented subband processing in real and complex arithmetic.

Let us assume some processing task is performed on L_a samples in a real valued subband implementation, e.g. by an adaptive filter of length L_a. If the computational complexity of performing the operations associated with this processing is of order $\mathcal{O}(L_a^I)$, the number of multiplications can be written in form of a polynomial in L_a with coefficients c_i^{real}

$$C_{\text{proc}}^{\text{real}}(L_a) \;=\; \sum_{i=0}^{I} c_i^{\text{real}} \cdot L_a^i \;=\; \sum_{i=0}^{I} \;, C_{\text{proc},i}^{\text{real}} \tag{4.66}$$

where $C_{\text{proc},i}^{\text{real}} = c_i^{\text{real}} \cdot L_a^i$. As an example from Chap. 2, the computational complexity of the RLS can is given as $C_{\text{RLS}} = 3L_a^2 + 3L_a + x$. For complex valued

subband processing with identical filter bank quality and performance measures [172], the doubling of the decimation factor results in shorter filters of length $L_a/2$ (or even slightly less if (3.58) is considered) and all processing to be run at only half the rate. However, one complex multiplication usually requires 4 real valued operations. Therefore, assuming that real and complex valued algorithms differ by nothing more than the requirement of respectively real and complex arithmetic, a ratio of computational complexity between processing with real and complex valued subband signals for the ith term in sum (4.66), $C^{\text{real}}_{\text{proc},i}$, can be derived as

$$C^{\text{real}}_{\text{proc},i} \propto L_a^i \quad , \tag{4.67}$$

$$C^{\text{cmplx}}_{\text{proc},i} \propto 4 \cdot \left(\frac{1}{2} \cdot \left(\frac{L_a}{2}\right)^i\right) \quad , \tag{4.68}$$

yielding

$$\frac{C^{\text{cmplx}}_{\text{proc},i}}{C^{\text{real}}_{\text{proc},i}} = \frac{c_i^{\text{cmplx}}}{c_i^{\text{real}}} = \frac{1}{2^{i-1}}. \tag{4.69}$$

This ratio allows an approximation of the complexity ratio for real and complex valued processing, by inserting the term of highest order I into (4.69) [166]. Here however, the exact computational complexity of algorithms can be derived, which with complex arithmetic now compares by [167]

$$C^{\text{cmplx}}_{\text{proc}}(L_a/2) = \sum_{i=0}^{I} c_i^{\text{cmplx}} \cdot \frac{L_a^i}{2} = \sum_{i=0}^{I} 2^{1-i} \cdot c_i^{\text{real}} \cdot L_a^i \tag{4.70}$$

Thus, generally where an algorithm or application exhibits high computational complexity ($I > 1$), a complex valued implementation will be preferred. However, for algorithms of $\mathcal{O}(L_a)$ with a high number of overhead calculations c_0^{real}, a real valued approach can be more efficient if the savings out-weigh the additional cost in the filter bank calculation described in Sec. 4.3.2.

Tab. 4.1 lists the complexities for real valued processing of a number of adaptive filtering algorithms discussed in Chap. 2. The complex implementations of NLMS, RLS, and affine projection (APA) algorithm have been introduced and simply require a 4 times higher load in terms of real valued multiplications [72, 106]. For RLS implementations, complex processing can roughly half the

Algorithm	Computational Complexity	
	$C_{\text{proc}}^{\text{real}}(L_a)$	$C_{\text{proc}}^{\text{cmplx}}(L_a/2)$
Normalized LMS	$3 + 2L_a$	$6 + 2L_a$
Fast APA, order p	$20p + 2L_a$	$40p + 2L_a$
Recurs. Least Squares	$3L_a + 3L_a^2$	$3L_a + 1.5L_a^2$

Table 4.1: Number of real multiplications of different algorithms in dependence of the filter length L_a for real valued implementation.

processing load over real valued calculations, while for LMS-type algorithms, processing is approximately equal in both real or complex subbands. However, for the latter, the lower processing gain for the filter bank calculation would favour an implementation in complex subbands; a more detailed survey of this case will be presented in Chap. 6. For the APA, the load independent of the filter length can be large enough for high projection orders p to prefer a real valued implementation.

4.5 Filter Design

The previous sections have dealt with modulated filter banks, where all filters in analysis and synthesis bank are derived from one single prototype lowpass filter. This section will discuss some properties that these prototype filters have to fulfill. Furthermore we will give two methods of how to obtain appropriate prototype filters. The first one uses an iteration method to construct prototype filters for power-of-2 channel filter banks, the second directly constructs prototype filters for an arbitrary number of bands K.

4.5.1 Requirements

This section discusses two requirements of the filter bank design — good stop-band attenuation for the suppression of aliasing in the subbands, and perfect reconstruction.

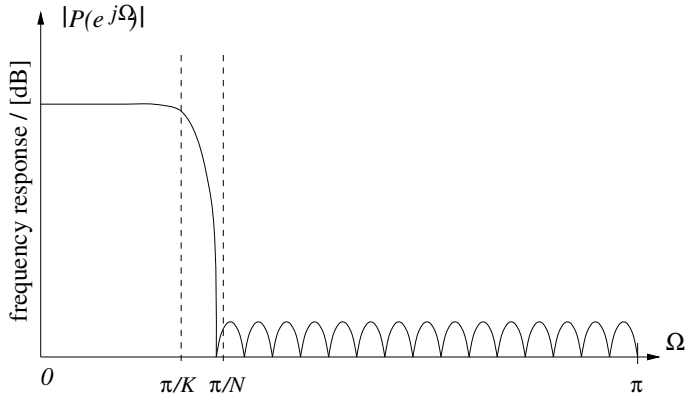

Figure 4.11: Required frequency response of a real valued prototype filter $p[n]$ for a K channel oversampled modulated GDFT filter bank with decimation by N.

4.5.1.1 Filter Bandwidth and Cut-Off

The frequency response of a prototype filter $p[n]$ for a K-channel GDFT bank with decimation by N is shown in Fig. 4.11. Therefore, the cut-off of the real valued prototype filter $p[n]$ is required to be at π/K, with a transition band reaching up to π/N. Every frequency component of an input signal in the interval $[\pi/N; \pi]$ will be aliased into the baseband after filtering and decimation, and cause a distortion of the subband signal, which can be modelled as additive noise, motivating an SNR-like measure for white Gaussian input signals [172]:

$$\mathrm{SAR} = \frac{\int_0^{\pi/N} |P(e^{j\Omega})|^2 d\Omega}{\int_{\pi/N}^{\pi} |P(e^{j\Omega})|^2 d\Omega} \quad , \tag{4.71}$$

where SAR means *signal-to-alias ratio*. The denominator of (4.71) forms a measure of the stopband energy, which a filter design would have to minimize. A formulation in terms of the coefficients of $p[n]$ will be sought in Sec. 4.5.3.

4.5.1.2 Power Complementary Condition

If aliasing is sufficiently suppressed, approximate time-invariance of the input-output behaviour of the filter bank system in Fig. 3.1 is ensured and the near PR condition reduces to the requirement of power complementarity [69, 151],

$$\sum\nolimits_{k=0}^{K-1} H_k^*(z^{-1}) \cdot H_k(z) = \underline{\tilde{H}}(z)\underline{H}(z) \stackrel{!}{=} 1 \quad , \tag{4.72}$$

where $\underline{H}(z) = [H_0(z)H_1(z)\cdots H_{K-1}(z)]^T$ is a vector holding the K analysis filters. Exploiting the modulation of the bandpass filters $H_k(z)$, $\underline{H}(z)$ can be expressed by

$$\underline{H}(z) = \mathbf{T}_{\mathrm{GDFT}} \cdot \underbrace{\mathrm{diag}\{1, z^{-1}, \cdots z^{-2K+1}\}}_{\Lambda_z} \cdot \underline{P}(z) \tag{4.73}$$

where $\mathbf{T}_{\mathrm{GDFT}} \in \mathbb{C}^{K\times 2K}$ is a full GDFT matrix as given in (4.47) and $\underline{P}(z)$ a vector holding $2K$ polyphase components of $P(z)$,

$$\underline{P}(z) = \left[P_0^{(2K)}(z^{2K}) \;,\; P_1^{(2K)}(z^{2K}) \;,\; \cdots \; P_{2K-1}^{(2K)}(z^{2K})\right] \quad . \tag{4.74}$$

For the product on the left hand side of (4.72), one yields

$$\begin{aligned}
\underline{\tilde{H}}(z)\underline{H}(z) &= \underline{\tilde{P}}(z)\tilde{\Lambda}_z \begin{bmatrix} \mathbf{I}_K \\ -\mathbf{I}_K \end{bmatrix} \underbrace{\mathbf{D}_2^* \mathbf{T}_{\mathrm{DFT}}^H \mathbf{D}_1^* \mathbf{D}_1 \mathbf{T}_{\mathrm{DFT}} \mathbf{D}_2}_{K\cdot\mathbf{I}_K} \cdot \\
&\qquad \cdot [\mathbf{I}_K \; -\mathbf{I}_K]\, \Lambda_z \underline{P}(z) \qquad (4.75) \\
&= K\underline{\tilde{P}}(z)\tilde{\Lambda}_z \begin{bmatrix} \mathbf{I}_K & -\mathbf{I}_K \\ -\mathbf{I}_K & \mathbf{I}_K \end{bmatrix} \Lambda_z \underline{P}(z) \stackrel{!}{=} 1 \quad , \qquad (4.76)
\end{aligned}$$

with Λ_z as defined in (4.73. With the definition of a modified prototype filter in (4.38), the requirement of power complementarity condition in (4.72) for the filter bank can now be identified to be equivalent to demanding

$$\sum\nolimits_{k=0}^{K-1} \breve{P}_k(z^{-K}) \cdot \breve{P}_k(z^K) \stackrel{!}{=} \frac{1}{K} \quad , \tag{4.77}$$

where $\breve{P}_k(z)$ are the K polyphase components of the modified prototype filter $P(z)$. By looking at an arbitrary summand k on the left hand side,

$$\left(z^{-k} P_k^{(2K)}(z^{2K}) - z^{-(k+K)} P_{k+K}^{(2K)}(z^{2K})\right) \cdot \left(z^{k} P_k^{(2K)}(z^{-2K}) - z^{(k+K)} P_{k+K}^{(2K)}(z^{-2K})\right), \tag{4.78}$$

it is clear that the auto-terms are non-zero only on a $2K$ grid, while the non-zero components of mixed terms all lie exactly in between. Since this holds for all $k \in \{0; K-1\}$, the requirement of (4.77) can be expressed directly in terms of the K polyphase components of the unmodified prototype filter,

$$\sum\nolimits_{k=0}^{K-1} P_k(z^{-K}) \cdot P_k(z^K) \stackrel{!}{=} \frac{1}{K} \quad . \tag{4.79}$$

This is an important result, since (4.79) is fulfilled if and only if $\tilde{P}(z)P(z)$ is a Kth-band filter [151], also often referred to as Nyquist(K) filter in the communications flavoured literature [44, 83, 88]. In the time domain, the property (4.79) corresponds to a Kth-band filter having zero coefficients at multiples of K apart from the center sample at time $n = 0$,

$$r_{pp}[n] = \tilde{p}[n] * p[n] \quad \text{is a } K\text{th-band filter} \tag{4.80}$$

$$\Longleftrightarrow \qquad r_{pp}[nK] = \delta[n] \quad , \tag{4.81}$$

where $r_{pp}[n]$ is the auto-correlation sequence of $p[n]$. The construction of K-th band filters can be achieved by a variety of methods including constraint optimization using e.g. linear algebraic [151, 142] or windowing techniques [159, 160]. Once the Kth-band filter $r_{pp}[n]$ is designed, a difficulty arises from necessary factorization of $R_{pp}(z) \bullet\!\!-\!\!\circ\, r_{pp}[n]$ to extract analysis and synthesis filters [160, 88]. The design, for example, in [159] fails to provide linear phase filters.

4.5.2 Dyadically Iterated Halfband Filters

It is possible to create — with some restrictions — filters fulfilling the Kth-band property with their auto-correlation function in good approximation from a filter $p^0[n]$ with a halfband auto-correlation sequence, which are widely tabled in literature [27, 31, 45] or can be constructed [99, 44]. In the following, we will sketch an iterative method based on the close connection between filter banks and the discrete wavelet transform [96, 136]. A similar approach is known in the literature as interpolated FIR (IFIR) filters [107, 46].

The idea is to dyadically scale down the impulse response of a filter $p^0[n]$, where $p^0[-n] * p^0[n]$ has halfband property, i.e. stretch it to twice its support on the time axis. This will also scale down the auto-correlation of $p^0[n]$ by a factor of two, and zeros-crossings previously at periodicity 2 for the halfband filter, will now appear spaced at 4 samples, thus fulfilling the definition of a quarter-band filter [170]. Further scaling will finally provide filters $p[n]$ creating Kth-band filters for higher channel numbers.

Dyadic down-scaling can be achieved through expansion by 2 and a suitable

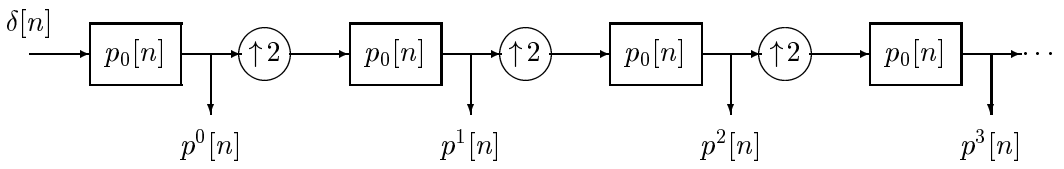

Figure 4.12: Flow graph for dyadic iteration of a prototype filter $p_0[n]$ to yield $p^i[n]$, where $K = 2^{i+1}$, whose auto-correlations satisfy Kth-band conditions, if the auto-correlation of $p_0[n]$ has halfband property.

interpolation, for which here the original filter $p^0[n]$ is employed,

$$\begin{aligned} p^i[n] &= p^{i-1}[\frac{n}{2}] * h[n], \qquad i \in \mathbb{N}/\{0\} \\ &\quad \text{with } p^0[-n] * p^0[n] \quad \text{halfband filter} \quad , \end{aligned} \tag{4.82}$$

which is shown as a flow graph in Fig. 4.12 for the first four iterations. With $i \to \infty$, (4.82) will tend to a continuous scaling function belonging to the discrete wavelet transform implemented by a dyadic, binary tree filter bank created from the lowpass filter $p^0[n]$ and its dual highpass filter [45, 161]. If the iteration (4.82) converges, the filters $p^i[n]$ represent discrete sampled versions of the scaling function. Finally, this connection ensures that scaling as described in the previous paragraph will work.

Example. For the 32-tap filter 32C from [27], measures of power complementarity of dyadically iterated K-channel prototype filters according to (4.82) are presented in Tab. 4.2 and prove the validity of the proposed method. In the frequency domain, scaling an impulse response results in the scaling of the frequency axis, as shown in Fig. 4.13. Expansion of the time domain signal with zeros introduces a highpass image spectrum with center frequency $\Omega_c = \pi$, which is subsequently filtered out by interpolation with the original filter $p^0[n]$, as illustrated by the frequency responses of the filter 32C and its first three iterations in Fig. 4.13(a)–(d).

Besides its advantageous simplicity, the dyadic iteration has several drawbacks. Firstly only filter banks can be constructed which have a power-of-two

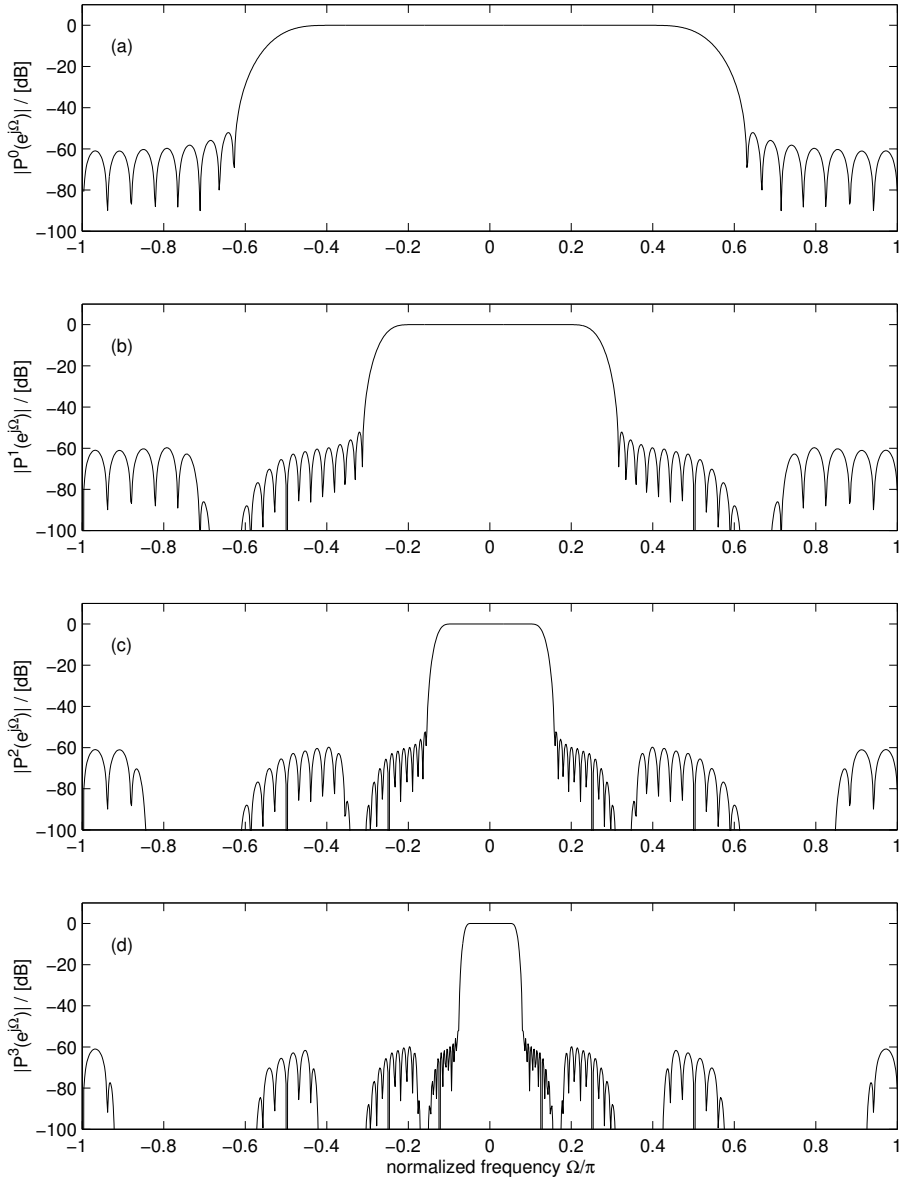

Figure 4.13: (a) Frequency response of original halfband QMF filter 32C [27] and three iteration (b)–(d) yielding filters whos auto-correlation satisfy quarter-band, 1/8th-band, and 1/16th-band filter conditions.

iteration no. i	0	1	2	3	4	5
channel no. K	2	4	8	16	32	64
filter length L_p	32	94	218	466	962	1954
error $10\log_{10} e^2$	-64.96	-64.02	-63.42	-63.10	-63.26	-63.36

Table 4.2: Dyadic iteration of halfband filter 32C [27], with resulting channel number K, prototype filter length L_p, and measure of power complementarity, $e = \|1 - \sum_{k=0}^{K-1} P_k(z^{-K})P_k(z^K)\|_2$, at the ith iteration.

number of channels K. Furthermore, the choice of possible decimation rates is limited, and the stopband attenuation, responsible for aliasing in the subband signals invariably fixed. It is also clear from inspection of Fig. 4.13 that deep gaps in the stopband appear in course of the interpolation, which costs filter length and therefore unnecessary computations and filter bank delay.

4.5.3 Iterative Least Squares Design

This section presents a least-squares design of suitable prototype lowpass filters, which directly minimizes both stopband energy and power complementarity as discussed in Sec. 4.5.1 where both criteria have been expressed in terms of the prototype filter. Here, first measures for stopband energy and power complementarity will be derived in terms of the filter coefficients, which are then used in a least-squares formulation for iterative minimization [163, 164].

4.5.3.1 Stopband Energy

A common method to determine a measure for the stopband energy

$$E_s = \frac{1}{\pi}\int_{\pi/N}^{\pi} |P(e^{j\Omega})|^2 d\Omega \tag{4.83}$$

introduced as a filter design criterion in Sec. 4.5.1.1 is given by the eigenfilter method for linear phase filters [151, 142, 71], whereby the real part of the frequency response is evaluated for a set of discrete frequencies collected in a vector

$\underline{\Omega} = [\Omega_0,\ \Omega_1\ \cdots\ \Omega_{I-1}]^T,\ \Omega_i \in [\pi/N;\pi],\ i = 0(1)I-1$

$$\mathrm{Re}\{P(e^{j\Omega_i})\} = \mathbf{T}_{\mathrm{DCT}} \cdot \mathbf{p} \quad . \tag{4.84}$$

Note that the left hand side represents a vector quantity. The vector $\mathbf{p} \in \mathbb{R}^{L_p \times 1}$ contains the coefficients of the prototype filter,

$$\mathbf{p} = \left[p[0], p[1], \cdots p[L_p - 1]\right]^T, \tag{4.85}$$

while $T_{\mathrm{DCT}} \in \mathbb{R}^{M \times L_p}$ is a DCT transform holding cosine terms at the discrete frequencies Ω_i,

$$\mathbf{T}_{\mathrm{DCT}} = \begin{bmatrix} 1 & \cos(\Omega_0) & \cos(2\Omega_0) & \dots & \cos((L_p-1)\Omega_0) \\ 1 & \cos(\Omega_1) & \cos(2\Omega_1) & \dots & \cos((L_p-1)\Omega_1) \\ \vdots & \vdots & \vdots & \ddots & \vdots \\ 1 & \cos(\Omega_{I-1}) & \cos(2\Omega_{I-1}) & \dots & \cos((L_p-1)\Omega_{I-1}) \end{bmatrix}. \tag{4.86}$$

An approximation of the stopband energy in 4.83 is now given by

$$E_s \approx \frac{1}{\pi}\|\mathbf{T}_{\mathrm{DCT}} \cdot \mathbf{p}\|_2^2 \quad . \tag{4.87}$$

Symmetry and therefore linear phase of the prototype filter $p[n]$ is enforced by introducing a matrix $\mathbf{S}_1^T = \left[\mathbf{I}_{L_p/2}, \mathbf{J}_{L_p/2}\right]$ such that $\mathbf{p}$ is mapped onto a vector $\mathbf{b} \in \mathbb{R}^{L_p/2}$ holding only the first $L_p/2$ coefficients of the prototype,

$$\mathbf{b} = \frac{1}{2}\mathbf{S}_1^T \cdot \mathbf{p} \quad . \tag{4.88}$$

It is easily verified that this mapping can be reversed by $\mathbf{p} = \mathbf{S}_1 \cdot \mathbf{b}$.

4.5.3.2 Power Complementary Condition

In Sec. 4.5.1.2 the near perfect reconstruction condition for the filter bank had been traced back to a power complementary condition of the prototype filter under the assumption that the stopband energy of the filter was sufficiently small. To create an expression in terms of the filter coefficients which can be minimized, the power complementary condition (4.79) needs to be formulated in the time domain.

For a convenient matrix formulation of the time domain operations, a vector $\mathbf{p}_k \in \mathbb{R}^{L_p/K}$ is defined to hold the kth polyphase component of $p[n]$, i.e.

$$\mathbf{p}_k = \big[p[k],\ \ p[K+k],\ \ \cdot\ \ p[rK+k]\big]^T, \quad r = \lfloor \frac{L_p}{K} \rfloor, \tag{4.89}$$

where for convenience L_p is assumed to be an integer multiple of the channel number K. Further, we define a convolutional matrix $\mathbf{P}_k \in \mathbb{R}^{(2Lp/K-1)\times(L_p/K)}$,

$$\mathbf{P}_k = \begin{bmatrix} \mathbf{p}_k & & \mathbf{0} \\ & \mathbf{p}_k & \\ & & \ddots \\ \mathbf{0} & & \mathbf{p}_k \end{bmatrix}. \tag{4.90}$$

Using the definitions (4.89) and (4.90), the power complementary condition (4.79) manifests itself in the time domain as

$$\sum_{k=0}^{K-1} \mathbf{P}_k \cdot \mathbf{J}_K \cdot \mathbf{p}_k \stackrel{!}{=} \underbrace{\begin{bmatrix} \underline{0} \\ 1/K \\ \underline{0} \end{bmatrix}}_{\mathbf{d}} \tag{4.91}$$

where the reverse identity matrix $\mathbf{J}_K$ has been used to convert a convolution into the required correlation operation, and $\mathbf{d}$ defines a delay with suitable zero vectors $\underline{0}$ of length $L_p/K-1$. The sum on the left hand side of (4.91) can be further condensed to matrix notation by defining a matrix $\mathbf{V}$ and an auxiliary vector $\mathbf{v}$,

$$\sum_{k=0}^{K-1} \mathbf{P}_k \cdot \mathbf{J}_K \cdot \mathbf{p}_k = \underbrace{[\mathbf{P}_0\mathbf{J}_K,\ \mathbf{P}_1\mathbf{J}_K,\ \cdots\ \mathbf{P}_{K-1}\mathbf{J}_K,\ ]}_{\mathbf{V}} \cdot \underbrace{\begin{bmatrix} \mathbf{p}_0 \\ \mathbf{p}_1 \\ \vdots \\ \mathbf{p}_{K-1} \end{bmatrix}}_{\mathbf{v}} = \mathbf{V}\mathbf{S}_2 \cdot \mathbf{p}. \tag{4.92}$$

The matrix $\mathbf{S}_2$ is a suitable $L_p \times L_p$ permutation matrix such that $\mathbf{S}_2^T$ performs a mapping from the synchronously ordered prototype coefficients in $\mathbf{p}$ onto the sequence of polyphase vectors in $\mathbf{v} = \mathbf{S}_2^T \cdot \mathbf{p}$. The formulation

$$\mathbf{V}\mathbf{S}_2\mathbf{S}_1 \cdot \mathbf{b} \stackrel{!}{=} \mathbf{d} \tag{4.93}$$

finally defines the power complementary condition including the symmetry constraint for the prototype filter.

4.5.3.3 Least Squares Formulation

To minimize stopband energy in (4.87) and achieve approximate power complementarity as defined by (4.93), a least squares (LS) problem

$$\mathbf{b} = \arg\min_{\mathbf{b}} \left\| \underbrace{\begin{bmatrix} \mathbf{V}(\mathbf{b})\cdot\mathbf{S}_2\cdot\mathbf{S}_1 \\ \gamma\cdot\mathbf{T}_{\mathrm{DCT}}\cdot\mathbf{S}_1 \end{bmatrix}}_{\mathbf{A}} \mathbf{b} - \begin{bmatrix} \mathbf{d} \\ \underline{0} \end{bmatrix} \right\|_2^2 \tag{4.94}$$

has to be solved, where γ allows a weighting between both design criteria. The notation $\mathbf{V}(\mathbf{b})$ is given to indicate the dependency of the system matrix $\mathbf{A} \in \mathbb{R}^{(2L_p/K+I-1)\times L_p/2}$ upon the filter coefficients. Thus, unfortunately (4.94) is not a quadratic problem and may exhibit local minima. However, analysis in [66] suggests for a similarly posed problem that the cost function in $\mathbf{b}$ possesses 3 minima, of which two are symmetric with opposite sign and a third one defines a saddle point in between for $\mathbf{b} = \underline{0}$.

The minimization can be performed iteratively [122, 121, 71], solving at each iteration j

$$\mathbf{b}_j = \arg\min_{\mathbf{b}_j} \left\| \begin{bmatrix} \mathbf{V}(\mathbf{b}_{j-1})\cdot\mathbf{S}_2\cdot\mathbf{S}_1 \\ \gamma\cdot\Lambda_\omega\cdot\mathbf{T}_{\mathrm{DCT}}\cdot\mathbf{S}_1 \end{bmatrix} \mathbf{b}_j - \begin{bmatrix} \mathbf{d} \\ \underline{0} \end{bmatrix} \right\|_2^2, \tag{4.95}$$

where a previous solution $\mathbf{b}_{j-1}$ is substituted to achieve a quadratic approximation of (4.94). A similar approach is reported in [82], where e.g. alternately analysis and synthesis filters are kept constant while the other one is optimized to achieve a solvable quadratic expression.

The resulting quadratic LS problem (4.95) can be easily solved using standard linear algebraic tools [58]. As stopping criterion, the optimization may be regarded as sufficient when the change from $\mathbf{b}_{j-1}$ to $\mathbf{b}_j$ falls below a certain threshold [66].

An additional weighting matrix Λ_ω in (4.95) can help to improve the stopband attenuation towards the band edge. Furthermore, a relaxation can be introduced to solve for an a priori solution $\mathbf{b}'_k$ at iteration step j, from which the a posteriori

Design	K	N	L_p	CPU time	max(j)	RE	SAR
(a)	16	12	192	11s	11	-54dB	56dB
(b)	16	12	240	23s	13	-68dB	70dB
(c)	16	12	384	95s	14	-91dB	92dB
(d)	16	14	448	125s	12	-54dB	57dB

Table 4.3: Characteristics of four different iterative LS designs (a)–(d) for prototype filters shown in Fig. 4.14; the left columns specify the design parameters $\{K, N, L_p\}$, while the right hand columns indicate the convergence speed of the design algorithm and performance measures in terms of reconstruction error (RE) and SAR.

solution is obtained by $\mathbf{b}_j = \alpha \mathbf{b}'_j + (1-\alpha)\mathbf{b}_{j-1}$, for $0 < \alpha \leq 1$, which adds robustness to the convergence of the iterative LS algorithm.

4.5.3.4 Design Examples

Fig. 4.14 shows a couple of prototype filters obtained with the above iterative LS design, with design specifications and resulting measures listed in Tab. 4.3. The number of evaluated frequencies Ω_i for the stopband energy has to be chosen such that the resulting system of equations $\mathbf{A}\mathbf{b}_j = [\mathbf{d} \quad \underline{0}]^T$ is overdetermined. A pseudo-inverse of $\mathbf{A}$ will then yield an optimum $\mathbf{b}_j$ in the least squares sense. Implemented in Matlab [97], the initial coefficients $\mathbf{b}_0$ are calculated by a remez filter design, and for a relaxation $\alpha = 0.5$ the design converges quickly for the discussed LS method. Tab. 4.3 states the number of iterations and CPU time required on a Sparc20 workstation. The performance measure signal-to-alias ratio (SAR) refers to (4.71) while the reconstruction error defines the inaccuracy in (4.93), i.e.

$$\mathrm{RE} = 10 \cdot \log_{10} \|\mathbf{V}\mathbf{S}_2\mathbf{S}_1\mathbf{b} - \mathbf{d}\|_2^2 \quad . \tag{4.96}$$

Compared to the halfband iteration design introduced in the previous section, the LS design yields considerably enhanced results. Comparing the LS design in Tab. 4.3 to the $K = 16$ design in Tab. 4.2, which would allow for decimation

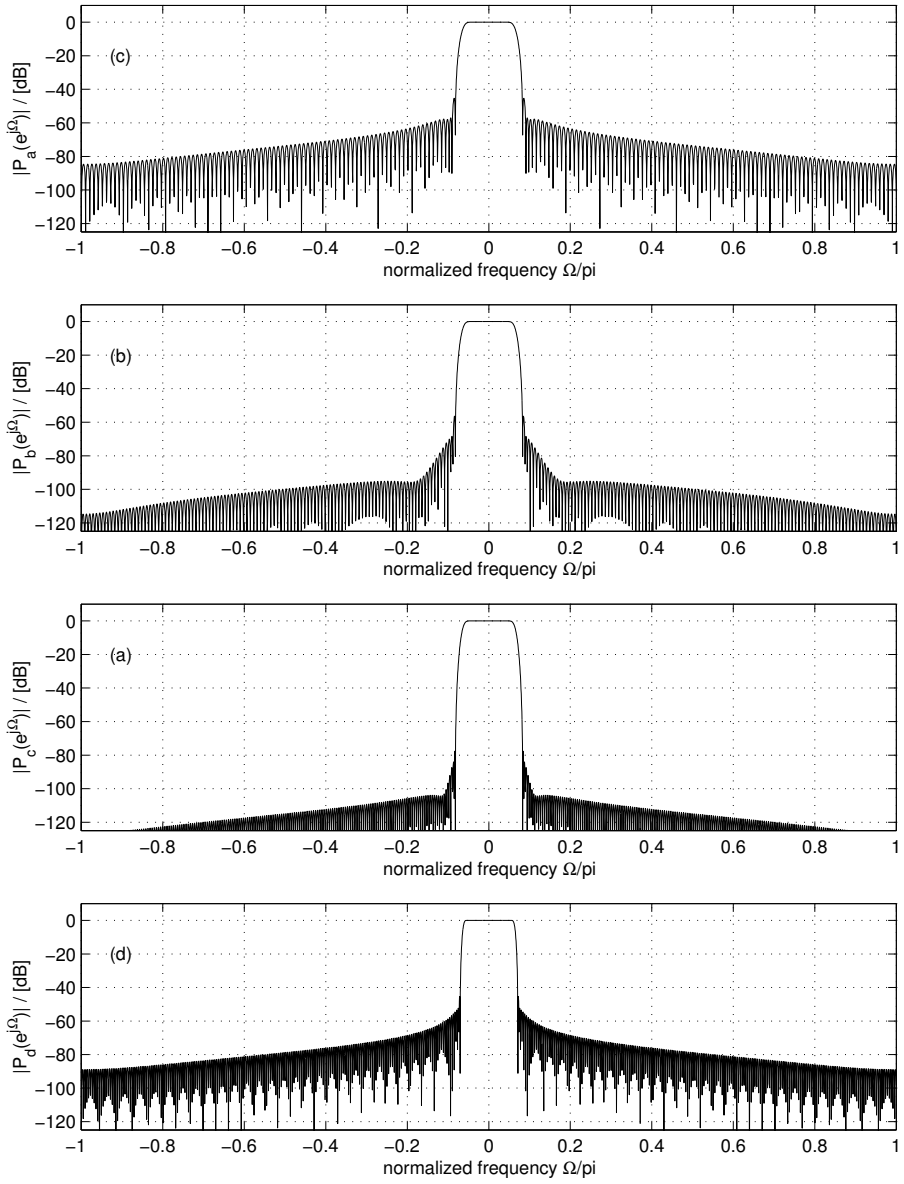

Figure 4.14: Frequency responses of prototype filters constructed using an iterative LS design for $K = 16$ channel filter bank with possible decimation by $N \leq 12$ for (a)–(c) and $N \leq 14$ for (d); performance measures are given in Tab. 4.3.

by $N = 12$ with about 59dB and for $N = 13$ with 52dB SAR, clearly the filter length can approximately be halved at almost identical performance for designs (a) and (b), or reach a sharper transition band and higher possible decimation rate at equal cost and quality measures with design (d), thus allowing for more efficient subband processing.

Bifrequency Transfer Function. Aliasing distortion and imaging introduced by decimators and expanders in multirate systems can be completely described by bifrequency transfer functions [27]. The sampling rate conversion causes — if aliasing is not sufficiently suppressed — the multirate system to be linear periodically time-varying (LPTV) with a period equivalent to the least common multiple of all sampling rate changes occurring within the system. The overall impulse response of such a system, $h[n_1, n_2]$, therefore depends on the time of observation n_2 and the time of excitation n_1 [76]. Based on $h[n_1, n_2]$, the bifrequency transfer function is given by

$$H\left(e^{j\Omega_2}, e^{j\Omega_1}\right) = \frac{1}{2\pi} \sum_{n_1=-\infty}^{+\infty} \sum_{n_2=-\infty}^{+\infty} h[n_2, n_1] \cdot e^{j(\Omega_1 n_1 - \Omega_2 n_2)} \quad , \tag{4.97}$$

which relates a frequency Ω_1 at the input to each frequency Ω_2 at the system output.

Using the measurement method by Reng and Heinle [120, 75], Fig. 4.15 shows the bifrequency transfer function of a GDFT modulated filter bank consisting of analysis and synthesis as shown in Fig. 4.1 with a reduced number of $K/2 = 8$ subbands and decimation by $N = 14$, based on the prototype filter listed in Tab. 4.3 as design (d). The main diagonal in Fig. 4.15 indicates that the signal components are passed without noticeable amplitude distortion, i.e. the overall filter bank is power complementary. The off-diagonals represent the alias level creating a noise floor at about -60 dB below. Note that for an LPTV system, aliasing occurs only along so called Dirac lines [27, 76], i.e. discrete off-diagonals. Further note that the lines for $\Omega_2 \pm \Omega_1 = \pi$ are missing, since for this case the modulated filters fulfill the quadrature mirror filter (QMF) condition, resulting in alias cancellation in the synthesis bank.

Fig. 4.16 shows the measurement of the bifrequency transfer function of an

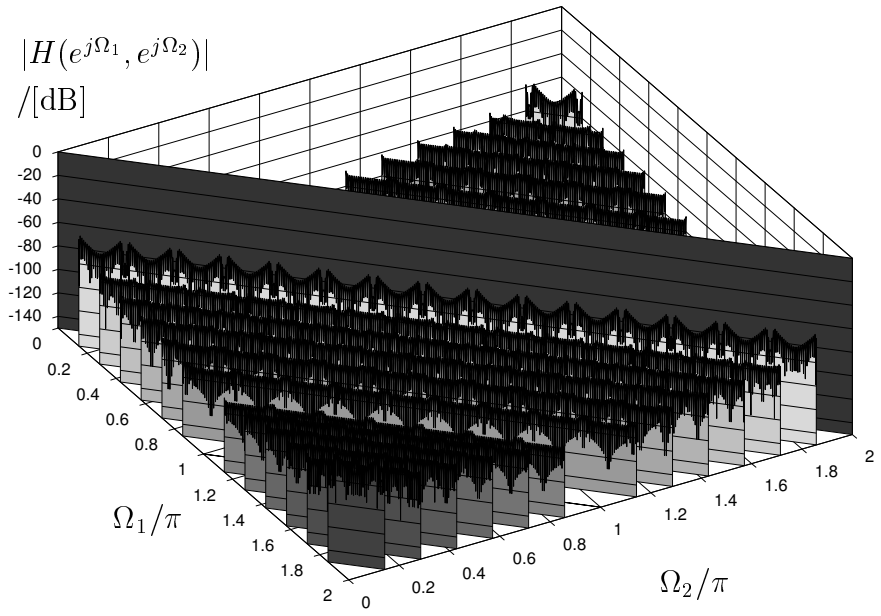

Figure 4.15: Measurement of the bifrequency transfer function for a GDFT filter bank with $K/2 = 8$ complex channels and decimation by $N = 14$, using the prototype filter $p[n]$ shown in Fig. 4.2(a).

SSB modified GDFT modulated filter bank with $K/2 = 8$ real valued subband signals decimated by $N/2 = 7$. This filter bank is derived from the same prototype filter as the GDFT filter bank shown in Fig. 4.15. Since this system is decimated at only half the rate of the previous complex filter bank, aliasing is restricted to $N/2 - 1$ Dirac lines on either side of the main diagonal.

4.6 Concluding Remarks

In this chapter oversampled GDFT filter banks have been introduced. Some particular conditions arising from the offset values for time and frequency in the modulating complex exponential have been highlighted, notably the organization of the passbands of the filter bank filters, and their linear phase property. An efficient implementation of this type of filter bank has been suggested for arbitrary integer decimation $N \leq K$. It is based on a factorization of the polyphase analysis matrix into a real valued polyphase network and a GDFT transform, which can be further factorized for fast implementations using FFT algorithms.

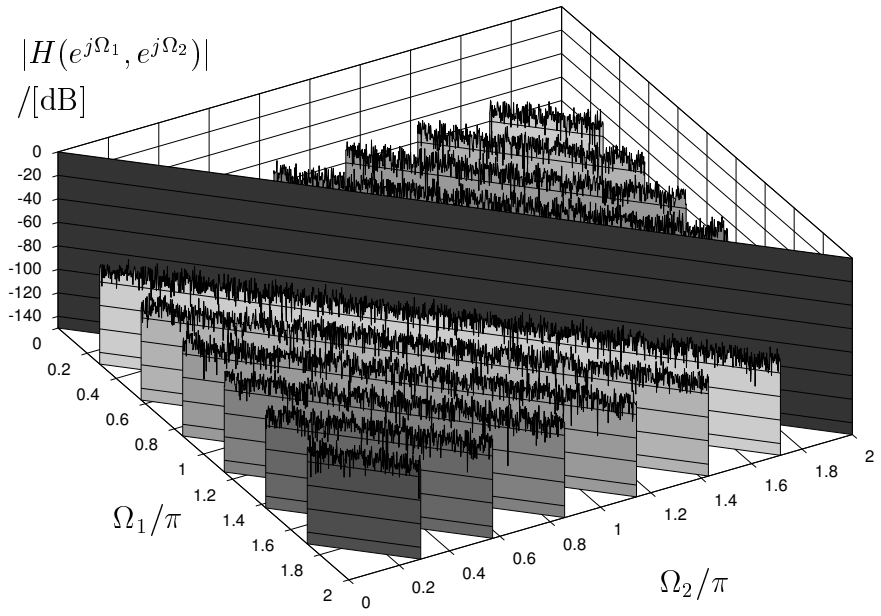

Figure 4.16: Measurement of the bifrequency transfer function for a modified GDFT filter bank to perform an SSB with $K/2 = 8$ real channels and decimation by $N/2 = 7$, using the prototype filter $p[n]$ shown in Fig. 4.2(b).

Modifications have been established for the GDFT filter bank to implement an SSB modulated filter bank with real valued subbands. Again, the factorization of the GDFT filter banks involved allows for a highly efficient implementation. Based on the same prototype and therefore implementing approximately identical performance characteristics, the SSB modified GDFT filter bank produces real valued subbands at twice the rate of a complex GDFT subband implementation.

A comparison between real and complex subband processing has been made, which takes into account both the computational complexity of the filter bank implementation and the subband processing e.g. performed by adaptive filters. This has yielded the initially surprising fact, that complex subband processing is despite its complex arithmetic generally at level with real valued subbands for $\mathcal{O}(L_a)$ algorithms and outperforms for orders $\mathcal{O}(L_a^2)$ algorithms and greater, which is mainly due to the higher possible sampling rate for the complex system. However, exceptions exist e.g. for the APA and potentially other algorithms, for which a real valued implementation may be considered advantageous.

Finally, design methods have been presented which allow to construct prototype lowpass filters for oversampled GDFT filter banks with low aliasing level in the subband signals, based on a dyadic iteration of tabulated filters and by an iterative LS design. In Chap. 5, the performance of subband adaptive systems will be closely linked to the optimization criteria in the latter design algorithm, enabling to create application specific filter banks for subband adaptive systems with predefined performance limits.

Chapter 5

Performance of Subband Adaptive Filter Systems

This chapter discusses the performance and limitations in performance of subband adaptive filtering (SAF) in oversampled subbands. Sec. 5.1 will first introduce and review different general aspects of the performance of SAF systems. In particular, aliasing in the subbands which may limit the MMSE performance will be addressed in Sec. 5.2, and Sec. 5.3 will link inaccuracies in the adapted equivalent fullband model to the employed analysis and synthesis filter banks. Based on the use of GDFT filter banks as introduced in the previous chapter, some properties of the resulting subband adaptive structures are derived in these two sections, which can be directly linked to quality measures of the filter bank design. Finally, Sec. 5.4 will demonstrate the impact of different set-up parameters on the subband adaptive system by simulation and validate the performance measures given in Secs. 5.2 and 5.3.

5.1 General Performance Limiting Influences

First, we will concentrate on general performance limiting influences for subband adaptive filter systems. Sec. 5.1.1 will define different aspects and measures of SAF performance, e.g. final MSE, accuracy of the adapted SAF, and convergence speed. A discussion of how they are affected by different parameters of the set-up

will follow in Sec. 5.1.2.

5.1.1 Performance Criteria

5.1.1.1 Final MSE

The quality of adaptation can be judged from the final achievable mean squared error value, which ideally represents an ensemble average and can therefore be time-varying. For stationary situations the MSE level for $n \to \infty$ gives an indication for the quality of adaptation. Since the final MSE level is an absolute quantity, sometimes it is more interesting to measure by how much an initial, i.e. uncancelled, error level can be reduced through the application of the subband adaptive filter system. This gives rise to the definition of *noise reduction*, which represents an SNR-like measure

$$\text{noise reduction} = 10 \cdot \log_{10} \left(\frac{\mathcal{E}\{d^2[n]\}}{\mathcal{E}\{e^2[n]\} \mid_{n \to \infty}} \right) \quad . \tag{5.1}$$

Note that noise reduction is defined in terms of the fullband desired signal $d[n]$ and the reconstructed fullband error signal $e[n]$. It is also possible to define a noise reduction measure based on the subband desired and error signals, which will be revisited in Sec. 5.2.2. Both measures for fullband and subbands can be directly linked if the employed filter banks perform frame expansions, since a fixed energy relation between subband and fullband signals exists.

5.1.1.2 Modelling Error

Besides measuring the MSE of the error signal, it is also possible to assess the state or quality of adaptation in terms of the final weight values of the subband adaptive filter impulse responses and their distance from the optimal solution. This implies, that either the Wiener Solution for the subband filters is known, or that a reconstruction of the fullband equivalent model to be derived in Sec. 5.3.1 can be compared to the "unknown" system that the SAF set-up is supposed to identify. The latter clearly cannot give any indication for system performance in the case of a band-limited input signal, since the optimally achievable model

is only defined at the excited frequencies, and has an arbitrary since undefined frequency response otherwise [86].

5.1.1.3 Convergence Speed

For most adaptive filter applications, it is desirable to find and reach optimal or almost optimal performance as fast as possible. For algorithms like the LMS discussed in Sec. 2.3, a measure for the convergence speed is given by a time constant associated with its exponential convergence. For more complex set-ups like subband adaptive filtering, where the adaptive algorithm is embedded in a subband architecture, the behaviour is often difficult to condense into a single measure. However, in practical applications, convergence speed can be judged by observing the time required for the error of the SAF system to reach a stationary value, i.e. the final MSE as introduced in Sec. 5.1.1.1.

5.1.1.4 Robustness towards Observation Noise

The presence of observation noise on the desired signal $d[n]$, which is assumed to be uncorrelated with the input signal $x[n]$, has a number of implications on the adaptive system. The MMSE is not equal to zero, and the residual error signal injects noise into the adaptation of the adaptive filter coefficients. This can (for example in the LMS' case) cause inaccuracy of the identified model and an additional variance term in the error signal, which in Sec. 2.3.3.3 was referred to as excess MSE. If the level of observation noise is very high, i.e. the desired signal has low SNR, the adaptive filters may not converge.

Another aspect of robustness is how well the algorithm preserves the observation noise contained in the desired signal. Although labelled noise, in many applications like AEC or noise cancellation the observation noise is a speech signal or similar signal of interest, which is to be recovered. However, many fast converging algorithms like NLMS or APA can show a rather aggressive behaviour towards the observation noise, as for short filter lengths and large step size, a best LS fit of the input signal to the current desired signal value is attempted [130, 140], as indicated in Sec. 2.5.1.2. Thus, often a measure called echo return loss enhancement (ERLE) similar to (5.1) is preferred, whereby the observation

noise $s[n]$ is subtracted from both the desired and error,

$$\text{ERLE} = 10 \cdot \log_{10} \left(\frac{\mathcal{E}\{(d[n] - s[n])^2\}}{\mathcal{E}\{(e[n] - s[n])^2\} \mid_{n \to \infty}} \right) \quad , \tag{5.2}$$

therefore only judging the reduction of the signal of interest and considering any changes made to the observation noise. The name ERLE refers to its original application of assessing the performance of echo cancellers in the presence of near end speech.

The literature provides an amazing number of suggestions how to improve the robustness of adaptive algorithms [171], mostly by introducing a variable step-size parameter $\mu[n]$, which is to be adjusted such that optimal adaptation is secured despite the (temporary) presence of observation noise, e.g. in the form of a near end speaker in AEC. Approaches in [125, 98] steer the step-size based on the estimated correlation between error and input signal. More sophisticated methods in AEC attempt to detect double talk situations where the near end speaker is active and adaptation of the SAF system has to be frozen [77, 17, 16]. However, clearly robustness is a mostly algorithmic related issue, and not specific to subband adaptive systems.

5.1.2 Performance Limitations

Different parameters in the set-up of an SAF system are important in determining its performance. In the following, we will partly review the literature and thereafter collect and discuss facts that have been striven for in Chapters 3 and 4.

5.1.2.1 Model Truncation

The question of how to choose the length of the subband adaptive filters is important in the sense that a too short model will — for the case of white noise excitation — only be able to converge to a truncated response and thus noisy version of what the optimal impulse response should be.

For the critically sampled case, Sec. 3.4.2 presented equations from [53, 54] describing the optimal Wiener solution for the subband adaptive filters in (3.57),

which allowed us to derive the required filter length (3.58) dependent on the order of the unknown system to be identified, and the length of analysis and synthesis filters. The latter cause an increase in filter length which can be justified by the transients introduced by the filter banks. Due to the decimation, these transients are likely to differ in the kth subband between desired and input signal, and hence have to be appropriately modelled by the subband adaptive filters. It is worthwhile to note that the transients caused by the analysis filter bank generally require the subband adaptive filters to operate non-causally, which can be easily pictured by inspecting the example in Fig. 3.10. Therefore, the desired signal usually needs to be delayed for correct adaptation, unless the plant to be identified is known to possess a sufficient delay.

Analysis in one of the pioneering papers by Kellermann [86] and more recently in [175] argues on the basis of (3.54), by assuming ideal analysis filters with a rectangular frequency response and hence infinite support in the time domain. Their results for the optimum subband filters are decaying but infinite solutions.

Based on the analysis in Sec. 3.4.2 and on practical results in [135, 88, 66], it usually appears reasonable for worst case scenarios to choose the length of the adaptive filter, L_a, as

$$L_a = \left\lceil \frac{2L_p + L_s}{N} \right\rceil \quad , \tag{5.3}$$

where L_p and L_s are the lengths of filter bank prototype filter $p[n]$ and the unknown system $s[n]$, respectively, and N the decimation ratio. This formula can be derived analogous to (3.58) assuming a paraunitary relationship between analysis and synthesis filter bank for the oversampled case. Similarly, in worst case scenarios delaying the desired signal by L_p/N samples in the subbands has been shown to be more than sufficient in practice.

If a truncated model should occur, the unknown system can be imagined as a superposition of an identifiable and an unidentifiable part, where the output of the latter contributes to the observation noise in the system, since the correlation it imposes on the desired signal is inaccessible to the SAF structure. This causes an additional term on the MMSE and will create an inaccurate, and in the case of LMS-type algorithms noisy model. However, even if infinitely long subband

adaptive filters were required for optimum performance and adaptation without model truncation [175], other limiting factors to be introduced in Sec. 5.2 will dominate the lower error bound.

5.1.2.2 Spectral Separation and Eigenvalue Spread

Spectral Separation. By dividing the spectrum of the input signal into intervals, filter banks are often viewed as to "whiten" the spectra of the subband signals with respect to the fullband signal. However, instead of whitening we here rather refer to this phenomenon as *spectral separation*, since the filter banks also have an adverse effect on the whiteness of the subband signals by introduceing notches due to non-perfect filter banks and OSRs > 1, as seen in Fig. 4.4. The convergence speed of mainly LMS-type adaptive filters depends on the eigenvalue spread of the input signal as introduced in Sec. 2.3, which can be approximated by the ratio between minimum and maximum value of its PSD as in (2.52). Clearly for a strongly coloured input signal a separation into smaller spectral intervals as performed by the analysis filter bank can help to form more balanced ratios, i.e. a smaller eigenvalue spread, and thus increase the convergence speed. This will be demonstrated in Sec. 5.4.

Eigenvalue Spread. As mentioned before, the increase in convergence speed due to spectral separation can be degraded by the colouring (notches) introduced by the filter banks. As input frequencies in the transition band of analysis filters are considerably attenuated, the input to the adaptive algorithm carries only weak spectral information on this part of the signal and thus indirectly of the unknown system, and the SAFs can adapt these spectral parts only very slowly [101]. With narrower transition bands as required for filter banks operating close to critical decimation, a better overall convergence behaviour of the SAF system seems achievable. On the other hand, broader transition bands that allow only a lower decimation ratio to be implemented will result in a faster update rate of the adaptive algorithm, which again enhances convergence. Sec. 5.4 will discuss the resulting differences in performance.

5.2 Minimum Mean Squared Error Limitations

In Sec. 3.4.1 the problem caused by aliasing in the subbands was introduced. Here, novel limits will be derived for the PSD of the minimum residual error signal due to aliasing in the subbands, and the resulting minimum mean squared error (MMSE). Also, an easy-to-apply measure will be created, that can directly link the stopband attenuation of the prototype filter design in Sec. 4.5 to the noise reduction achievable by an SAF.

5.2.1 Measuring Aliasing

Sec. 4.5 introduced an SNR-type measure for the aliasing in the subbands caused by decimation and non-perfect stopband attenuation of the prototype filter for white Gaussian input. For a further discussion of the adaptation error, we are interested in a power spectral density description of the minimum error of the Wiener solution, to be compared to the adaptively achievable power spectral densities of both the subband and reconstructed fullband final error signals.

While the SAR measure in Sec. 4.5 has ignored colouredness of the input signal to solely judge the quality of the filter bank, now the spectral characteristics of the input signal have to be taken into account. This poses a problem, as the power spectral density of the input signal is a quadratic quantity, and a simple superposition of spectral parts to describe aliasing would give an incomplete solution, lacking the cross-terms in the PSD as spectral de-correlation of the input signal cannot generally be assumed. Therefore, the approach taken here assumes the knowledge of a white iid noise excited source model, $L(e^{j\Omega})$, as shown in Fig. 5.1, which together with the filters $H_k(z)$ of the analysis bank is used to calculate aliasing terms from the systems' spectra, while the excitation noise remains white iid in the decimation stage. With these two steps, finally the power spectral densities due to aliasing can be derived.

5.2.1.1 Method

Sec. 3.1.1 introduced the formulation for the frequency domain effect of decimation. Assume we want to decimate the signal $x[n]$ in Fig. 5.1(a) and would

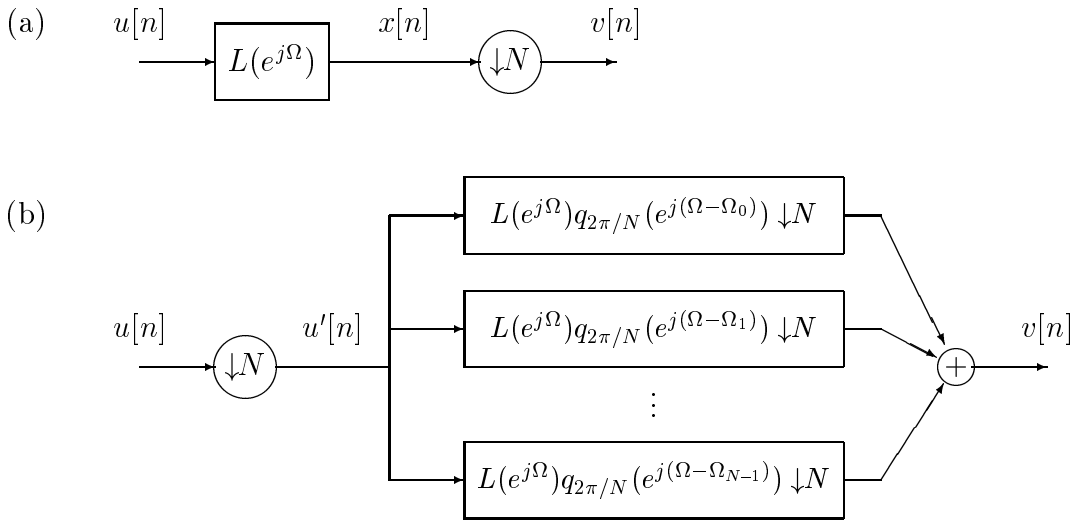

Figure 5.1: The identity of the structures (a) and (b) is exploited to calculate the PSD of a decimated signal $v[n]$ by assuming a source model $L(e^{j\Omega})$ excited by white noise $u[n]$; the $q_{2\pi/\Omega}(e^{j(\Omega-\Omega_n}$ are appropriately positioned rectangular windows of width $2\pi/N$; the notation "$\downarrow N$" indicates decimation of the windowed source model by N.

like to have knowledge about the PSD $S_{vv}(e^{j\Omega})$ of the decimated signal, $v[n]$, it cannot be directly expressed in terms of $S_{xx}(e^{j\Omega})$ since the PSD is a quadratic quantity, and a decimation description analogue to (3.2) would be incomplete since it omits any terms due to spectral correlation in the input signal $x[n]$. The strategy used here is to include a white noise excited source model $L(e^{j\Omega})$ such that

$$S_{xx}(e^{j\Omega}) = |L(e^{j\Omega})|^2 S_{uu}(e^{j\Omega}) \tag{5.4}$$

is fulfilled with an uncorrelated process $u[n]$ of unit variance, i.e. $S_{uu}(e^{j\Omega}) = 1$. This source model is also often termed the innovations filter and its existence is guaranteed if the Paley-Wiener condition is fulfilled, i.e. $x[n]$ is not strictly band-limited or has a line spectrum [112]. In the following, both existence and knowledge of $L(e^{j\Omega})$ are assumed. Thus, it becomes possible to swap the source model $L(e^{j\Omega})$ with the decimator, carefully taking into account the occurring spectral superpositions indicated in (3.2). In the resulting scenario shown in Fig. 5.1(b), the decimation can be directly applied to the white noise process

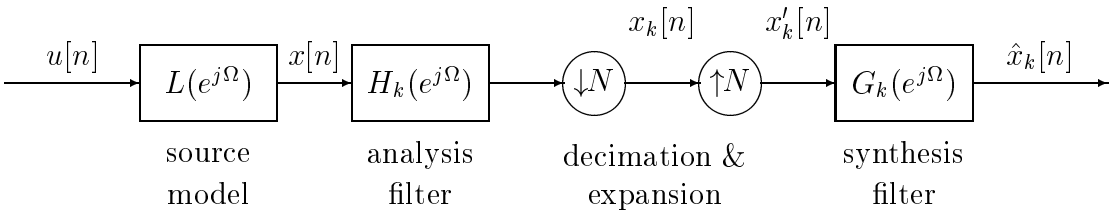

Figure 5.2: Block diagram for analysis of aliasing due to decimation by N in the kth subbands

exciting the source model $L(e^{j\Omega})$. After decimation by N, obviously this noise is still white with identical variance, i.e. $S_{u'u'}(e^{j\Omega}) = 1$.

For the following analysis, for a branch of the analysis / synthesis filter bank the model in Fig. 5.2 is used. There, the kth branch of the analysis filter bank, characterized by the filter $H_k(e^{j\Omega})$, is excited by a signal $x[n]$, which we assume to be a non-deterministic signal arising from a white noise excited source model $L(e^{j\Omega})$ as discussed previously. After decimation and expansion by N, on the synthesis side the signal is filtered by the kth synthesis filter $G_k(e^{j\Omega})$. By definition of our GDFT filter bank, we have $G_k(e^{j\Omega}) = H_k(e^{j\Omega})$ according to (4.18).

5.2.1.2 Power Spectral Density Description for Decimated and Expanded Subbands

Decimation and expansion of a signal by a factor of N causes the original spectrum to be superimposed by $N-1$ shifted copies of itself. Following the thoughts in Sec. 5.2.1.1, we only apply this superposition to a combined system consisting of the source model $L(e^{j\Omega})$ and the kth analysis filter $H_k(e^{j\Omega})$

$$\breve{F}_{x'_k}(j\Omega) = \frac{1}{N}\sum_{n=0}^{N-1} L\left(e^{j(\Omega-\frac{2\pi n}{N})}\right)\cdot H_k\left(e^{j(\Omega-\frac{2\pi n}{N})}\right)\cdot q_{2\pi/N}(\Omega-\Omega_k) \quad , \tag{5.5}$$

where $q_{2\pi/N}(\Omega-\Omega_k)$ is a rectangular frequency domain window,

$$q_{2\pi/N}(\Omega-\Omega_k) = \begin{cases} 1 & \text{for} \quad \Omega \in \left[\Omega_k;\Omega_k+\frac{2\pi}{N}\right] \\ 0 & \text{for} \quad \Omega \notin \left[\Omega_k;\Omega_k+\frac{2\pi}{N}\right] \end{cases} \quad , \tag{5.6}$$

and a frequency offset

$$\Omega_k = \frac{(2k+1)\pi}{K} - \frac{\pi}{N} \tag{5.7}$$

is chosen such that according to Fig. 4.9 the passband defined for the kth analysis filter including its transitions bands is always contained in the term $n = 0$ within the sum (5.5). All other terms $n \in [1; N-1]$ define aliased spectral parts. Note that the superposed filter spectrum $\breve{F}_{x'_k}(j\Omega)$ is only non-zero for a small window defined by (5.6). It is periodized by

$$F_{x'_k}(e^{j\Omega}) = \sum_{i=-\infty}^{\infty} \breve{F}_{x'_k}\left(j\left(\Omega - \frac{2\pi i}{N}\right)\right) \tag{5.8}$$

which represents the sum over all parallel branches in Fig. 5.2(b) with the additional inclusion of the kth analysis filter. Now the PSD of $x'_k[n]$ is given by

$$S_{x'_k x'_k}(e^{j\Omega}) = \left|F_{x'_k}(e^{j\Omega})\right|^2 \cdot S_{u'u'}(e^{j\Omega}) = \left|F_{x'_k}(e^{j\Omega})\right|^2 \quad . \tag{5.9}$$

From this PSD description of $x'[n]$, it is easy to obtain both PSD of decimated subband signal and reconstructed fullband signal. The first arises from rescaling the frequency axis in (5.9), yielding

$$S_{x_k x_k}(e^{j\Omega}) = S_{x'_k x'_k}(e^{j\Omega/N}) = \left|F_{x'_k}(e^{j\Omega/N})\right|^2 \quad . \tag{5.10}$$

For the PSD of the reconstructed fullband signal, the synthesis filters $G_k(e^{j\Omega}) = H_k(e^{j\Omega})$ are included into the transfer function model,

$$F_{\hat{x}}(e^{j\Omega}) = \sum_{k=0}^{K-1} F_{x'_k}(e^{j\Omega}) \cdot H_k(e^{j\Omega}) \quad , \tag{5.11}$$

and the PSD is similarly given by

$$S_{\hat{x}\hat{x}}(e^{j\Omega}) = \left|F_{\hat{x}}(e^{j\Omega})\right|^2 = \left|\sum_{k=0}^{K-1} F_{x'_k}(e^{j\Omega}) \cdot H_k(e^{j\Omega})\right|^2 \quad . \tag{5.12}$$

5.2.1.3 Power Spectral Densities of Minimum Error Terms

The formulations of PSDs for MMSE terms is based on a partitioning of the intermediate spectrum in (5.5) of the transfer from the decimated source model input to the upsampled subband signal $x'_k[n]$ into

$$\breve{F}_{x'_k}(j\Omega) = \breve{F}^{(S)}_{x'_k}(j\Omega) + \breve{F}^{(A)}_{x'_k}(j\Omega) \quad , \tag{5.13}$$

where the superscripts $^{(S)}$ and $^{(A)}$ refer to signal of interest and aliased parts, respectively, defined as

$$\breve{F}^{(S)}_{x'_k}(j\Omega) = \frac{1}{N} F(e^{j\Omega}) H_k(e^{j\Omega}) \cdot q_{2\pi/N}(\Omega - \Omega_k) \quad , \quad \text{and} \tag{5.14}$$

$$\breve{F}^{(A)}_{x'_k}(j\Omega) = \frac{1}{N} \sum_{n=1}^{N-1} F(e^{j(\Omega - \frac{2\pi n}{N})}) H(e^{j(\Omega - \frac{2\pi n}{N})}) \cdot q_{2\pi/N}(\Omega - \Omega_k). \tag{5.15}$$

By periodization analogous to (5.8) formulations for decimated and expanded systems $F^{(S)}_{x'_k}(e^{j\Omega})$ and $F^{(A)}_{x'_k}(e^{j\Omega})$ can be derived from these intermediate spectra. With these two quantities, the PSD of the kth expanded subband signal in (5.9) can be split into four terms,

$$S_{x'_k x'_k}(e^{j\Omega}) = S^{(S)}_{x'_k x'_k}(e^{j\Omega}) + S^{(S,A)}_{x'_k x'_k}(e^{j\Omega}) + S^{(A,S)}_{x'_k x'_k}(e^{j\Omega}) + S^{(A)}_{x'_k x'_k}(e^{j\Omega}), \tag{5.16}$$

where two auto-terms

$$S^{(S)}_{x'_k x'_k}(e^{j\Omega}) = \left| F^{(S)}_{x'_k}(e^{j\Omega}) \right|^2 \quad \text{and} \tag{5.17}$$

$$S^{(A)}_{x'_k x'_k}(e^{j\Omega}) = \left| F^{(A)}_{x'_k}(e^{j\Omega}) \right|^2 \quad , \tag{5.18}$$

and two cross-terms between signal of interest and aliased parts

$$S^{(S,A)}_{x'_k x'_k}(e^{j\Omega}) = F^{(S)}_{x'_k}(e^{j\Omega}) \cdot \left(F^{(A)}_{x'_k}(e^{j\Omega}) \right)^* \quad \text{and} \tag{5.19}$$

$$S^{(A,S)}_{x'_k x'_k}(e^{j\Omega}) = \left(F^{(S)}_{x'_k}(e^{j\Omega}) \right)^* \cdot F^{(A)}_{x'_k}(e^{j\Omega}) = \left(S^{(S,A)}_{x'_k x'_k}(e^{j\Omega}) \right)^* \tag{5.20}$$

define the different contributions from signal of interest and alias signal components to the overall power spectral density.

Assuming that an optimal filter removes all un-aliased signal components, the PSD of the minimum mean square error (MMSE) signal will only consist of the auto-term of aliased signal parts in (5.16),

$$S^{\text{MMSE}}_{x_k x_k}(e^{j\Omega}) = S^{(A)}_{x'_k x'_k}(e^{j\Omega/N}) = \left| F^{(A)}_{x'_k}(e^{j\Omega/N}) \right|^2 \quad , \tag{5.21}$$

which has already been rescaled in terms of its frequency index by a factor of N to correctly reflect the minimum error PSD of the kth decimated subband signal $x_k[n]$. The superscript MMSE indicates that (5.21) gives the PSD of the error signal provided the adaptive filter has achieved optimum adaptation and

the error signal is minimum. The above PSD can be related to the MMSE value by evaluating the inverse Wiener-Khintchine transform [123] for zero time shift,

$$\xi_{\mathrm{MMSE},k} = \frac{1}{2\pi} \int_0^{2\pi} S_{x_k x_k}^{\mathrm{MMSE}}(e^{j\Omega}) d\Omega \quad . \tag{5.22}$$

Similarly, the PSD of the reconstructed minimum error signal is derived from (5.12) by splitting $F_{x'_k}(e^{j\Omega})$ into true and aliased components, and assuming that all true signal parts have been removed by the optimally adjusted adaptive filter. This yields for the PSD

$$S_{\hat{x},\hat{x}}^{\mathrm{MMSE}}(e^{j\Omega}) = \left| \sum_{k=0}^{K-1} F_{\hat{x}_k}^{(A)}(e^{j\Omega}) \right|^2 = \left| \sum_{k=0}^{K-1} F_{x'_k}^{(A)}(e^{j\Omega}) \cdot \tilde{H}_k(e^{j\Omega}) \right|^2 . \tag{5.23}$$

Analogous to the subband case, the minimum mean squared reconstructed error value due to aliasing is given by

$$\xi_{\mathrm{MMSE}} = \frac{1}{2\pi} \int_0^{2\pi} \left| \sum_{k=0}^{K-1} F_{x'_k}^{(A)}(e^{j\Omega}) \cdot \tilde{H}_k(e^{j\Omega}) \right|^2 d\Omega. \tag{5.24}$$

The MMSE value of the fullband reconstructed error signal can also be accessed by exploiting the fixed energy — and therefore power — relation between subbands and fullband given by a tight frame condition in (3.19) such as satisfied by the employed GDFT filter bank when constructed according to Sec. 4.5.

5.2.2 MMSE Approximations

In the following, approximations to estimate the MMSE will be derived, which are more workable than the limits stated in Sec. 5.2.1.3 since they can be calculated directly from the frequency response of the prototype filters. The involved approximations will be justified by considering the two extrema of white noise and narrowband (sinusoidal) input in Sec. 5.2.2.3, and underpined by simulations in Sec. 5.4.

5.2.2.1 Subband MMSE

In a first approximation step, spectral correlation between different signal parts superposed in the decimation stage is neglected. Thus, the PSD of the subband

signals can be directly related to the PSD of the input signal. Instead of calculating the absolute levels of aliasing in the subbands, we can now also create an SNR-like ratio between the signal levels of true signal of interest and aliased signal parts, which is referred to here as signal-to-aliasing ratio (SAR)

$$\mathrm{SAR}_k = \frac{P_k^{(S)}}{P_k^{(A)}} = \frac{\int_{\Omega_{p,k}} |H_k(e^{j\Omega})|^2 S_{xx}(e^{j\Omega}) d\Omega}{\int_{\Omega_{s,k}} |H_k(e^{j\Omega})|^2 S_{xx}(e^{j\Omega}) d\Omega} \quad . \tag{5.25}$$

The quantity $S_{xx}(e^{j\Omega})$ is the PSD of the input signal to a filter bank with filters $H_k(e^{j\Omega})$, and $\Omega_{p,k}$ and $\Omega_{s,k}$ are the passband and stopband frequency intervals of the kth analysis filter $H_k(e^{j\Omega})$. In a second approximation, $S_{xx}(e^{j\Omega})$ if further assumed to be white, i.e. $S_{xx}(e^{j\Omega}) = \sigma_{xx}^2$, yielding

$$\mathrm{SAR}_k = \frac{\int_0^{\pi/N} |P(e^{j\Omega})|^2 d\Omega}{\int_{\pi/N}^{\pi} |P(e^{j\Omega})|^2 d\Omega} \quad , \tag{5.26}$$

which only depends on the characteristics of the prototype filter $p[n]$. This directly corresponds with (4.71) and the design criterion demanding good stopband attenuation in Sec. 4.5.

5.2.2.2 Fullband MMSE

For uniform modulated filter banks implementing tight frames, all subband signals contribute with the same proportion to the reconstructed fullband signal. This fact is exploited by looking for the maximum true signal and aliased signal levels amongst all subbands, which will hence reconstruct to determine the maximum levels of true signal of interest and aliased components in the fullband. The maximum power level for the signal of interest amongst the $K/2$ subbands may be defined as

$$P_{\max}^{(S)} = \max_k \left\{ \frac{1}{2\pi} \int_{\Omega_{p,k}} |H_k(e^{j\Omega})|^2 S_{xx}(e^{j\Omega}) d\Omega \right\}, \tag{5.27}$$

while

$$P_{\max}^{(A)} = \max_k \left\{ \frac{1}{2\pi} \int\limits_{\Omega_{s,k}} |H_k(e^{j\Omega})|^2 S_{xx}(e^{j\Omega}) d\Omega \right\} \tag{5.28}$$

determines the maximum level of aliasing found in the subbands. $\Omega_{p,k}$ and $\Omega_{s,k}$ define the frequency range of passband (p) and stopband (s) of the k analysis filter $H_k(e^{j\Omega})$. Thus, in the reconstructed signal, the SAR is given by

$$\text{SAR} = \frac{P_{\max}^{(S)}}{P_{\max}^{(A)}} \quad . \tag{5.29}$$

For uncorrelated Gaussian input, $S_{xx}(e^{j\Omega}) = \sigma_{xx}^2$, (5.27) now takes the form

$$P_{\max}^{(S)} = \frac{1}{2\pi} \int\limits_{\Omega_{p,k}} |H_k(e^{j\Omega})|^2 \sigma_{xx}^2 d\Omega, \qquad \forall\, k \in \{0; K-1\} \tag{5.30}$$

$$= \frac{\sigma_{xx}^2}{\pi} \int\limits_{0}^{\pi/N} |P(e^{j\Omega})|^2 d\Omega \quad , \tag{5.31}$$

where $p[n] \circ\!\!-\!\!\bullet\, P(e^{j\Omega})$ is the prototype lowpass filter, from which the complex passband filters $H_k(e^{j\Omega})$ emerge by modulation. A similar figure can be established for the aliased contributions, and finally the SAR of the reconstructed fullband signal can be expressed as

$$\text{SAR} = \frac{\int\limits_{0}^{\pi/N} |P(e^{j\Omega})|^2 d\Omega}{\int\limits_{\pi/N}^{\pi} |P(e^{j\Omega})|^2 d\Omega} \tag{5.32}$$

entirely in terms of the prototype filter's characteristics.

5.2.2.3 Considerations for Narrowband Input

The above approximations were assumed to be white noise input signals. In the following we want to look at the opposite extreme by considering narrowband (i.e. sinusoidal input) to demonstrate the validity of the above SAR approximations also for other input signal types. The presented analysis will be based on the

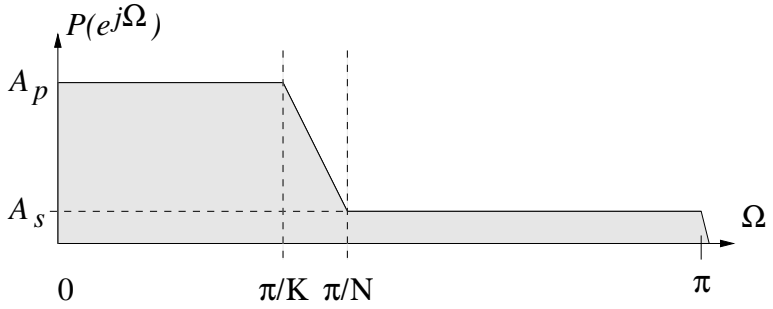

Figure 5.3: Idealized frequency response of prototype filter $P(e^{j\Omega})$ with constant gain A_p and A_s in passband and stopband to analyse SAR for narrowband input.

idealized frequency response of a prototype filter $P(e^{j\Omega})$ in Fig. 5.3 with constant gain in both passband and stopband,

$$P(e^{j\Omega}) = \begin{cases} A_p \quad , & \Omega \in [0;\pi/K] \\ A, \quad A_p > A > A_s \quad , & \Omega \in (\pi/K;\pi/N) \\ A_s \quad , & \Omega \in [\pi/N;\pi] \quad . \end{cases} \tag{5.33}$$

Note that here $P(e^{j\Omega})$ has only been defined on the frequency interval $[0;\pi]$, but is in fact symmetric to $\Omega = 0$ and periodic with 2π.

With a sinusoid of frequency $\Omega_{\sin} \in [0;\pi]$ as the input signal, $X(e^{j\Omega}) = \sum_\nu \delta(\Omega - \Omega_{\sin} + 2\pi\nu)$, for one bandpass filter $H_i(e^{j\Omega})$, $i \in [0;K-1]$ the sinusoid will lie exactly within its passband covering a frequency interval $\Omega_{p,i}$, and the maximum signal level is given by

$$P_{\max}^{(S)} = \frac{1}{2\pi} \int\limits_{\Omega_{p,i}} \left| H_i(e^{j\Omega}) \cdot \delta(\Omega - \Omega_{\sin}) \right|^2 d\Omega \quad , \quad \Omega_{\sin} \in \Omega_{p,i} \tag{5.34}$$

$$= \frac{A_p^2}{2\pi} \int\limits_{\Omega_{p,i}} \delta(\Omega - \Omega_{\sin})\, d\Omega = \frac{A_p^2}{2\pi} \quad . \tag{5.35}$$

Thus, the SAR in the ith subbands tends towards $\mathrm{SAR}_i \to +\infty$. Similarly, for a number of frequency bands, the sinusoidal frequency will lie in the stopband causing an aliased signal energy $P^{(A)} = A_s^2/(2\pi)$. Since no signal of interest is present, for these subbands we have $\mathrm{SAR}_k \to -\infty$. Finally, remaining frequency bands will contain the sinusoid in one of their transition bands and posses infinite SAR.

To evaluate the SAR of the reconstructed signal without knowledge of how many bands exactly will have SAR $\to +\infty$ or $-\infty$, we look at one single analysis filter — without loss of generality we choose $P(e^{j\Omega})$ — and assume that the sinusoidal frequency $\Omega_{\sin}$ is a random variable uniformly distributed on the interval $[0;\pi]$. The probabilities for $\Omega_{\sin}$ to fall into either passband, transition band, or stopband respectively are given by

$$p_p = \mathcal{P}(0 \le \Omega_{\sin} \le \frac{\pi}{K}) = \frac{1}{K} \tag{5.36}$$

$$p_t = \mathcal{P}(\frac{\pi}{K} < \Omega_{\sin} < \frac{\pi}{N}) = \frac{1}{N} - \frac{1}{K} \tag{5.37}$$

$$p_s = \mathcal{P}(\frac{\pi}{N} \le \Omega_{\sin} \le \pi) = \frac{N-1}{N} \quad . \tag{5.38}$$

Omitting the unspecified contribution(s) from any transition bands, the SAR on the synthesis side is approximately given by

$$\text{SAR} \approx \frac{A_p^2 \cdot p_p}{A_s^2 \cdot p_s} = \frac{A_p^2}{A_s^2} \cdot \frac{\frac{1}{K}}{\frac{(N-1)}{N}} = \frac{\int_0^{\pi/K} A_p^2 d\Omega}{\int_{\pi/N}^{\pi} A_p^2 d\Omega} \tag{5.39}$$

$$= \frac{\int_0^{\pi/K} |P(e^{j\Omega})|^2 d\Omega}{\int_{\pi/N}^{\pi} |P(e^{j\Omega})|^2 d\Omega} \approx \frac{\int_0^{\pi/N} |P(e^{j\Omega})|^2 d\Omega}{\int_{\pi/N}^{\pi} |P(e^{j\Omega})|^2 d\Omega} \quad , \tag{5.40}$$

where an ideal frequency response $P(e^{j\Omega})$ as shown in Fig. 5.3 has been assumed and the approximation is based on the negligible contribution of the transition band energy to the whole passband energy. This approximation is very accurate for small oversampling ratio OSR $= K/N$. Thus, the original approximation for white Gaussian input in (5.32) has been reached, and validated for a wider range of input signals.

The main advantages of the approximation with the SAR measure over the MMSE introduced in the previous section lies in the sole dependence on characteristics of the prototype filter. By considering a power ratio between the signal of interest and alias components, all signal dependent quantities dropped using simplifications which seem to be justified, and which will be further justified

by experiments in Sec. 5.4. In the interpretation of the MMSE and SAR, the MMSE defined the absolute lower limit for the adaptation error, while SAR will give the difference in error power between the unadapted state and optimal filter adjustment, i.e. a relative quantity.

5.3 Modelling Accuracy

Apart from the residual error variance, another criterion for the state of adaptation is the Euclidean distance between the optimum weights and the Wiener solution. In the subband adaptive filter case, a distinction has to be made between the Wiener solution for the subband adaptive filter, and the question, how the subband adaptive filter system as a whole can represent the unknown system. While the first question has been addressed in e.g. [53, 54, 66], here we are interested in how the choice of the analysis and synthesis filter banks affects the accuracy of a representation of the unknown system. This is achieved by reconstructing an "equivalent fullband model" from the subband adaptive filter responses, which in the following will be assumed to be optimally adapted.

5.3.1 Equivalent Fullband Model Reconstruction

The reconstruction of an equivalent fullband model will first be performed analytically by a 2-band example using PR or near PR critically decimated filter banks, based on expressions for the optimal subband adaptive filter responses in [53, 54]. In a second part, a general reconstruction method will be based on a modification of the graphical flow graph of the subband adaptive filter system.

5.3.1.1 Analytical Two-Band Example

For the case of critically sampled filter banks with cross-terms as discussed in Sec. 3.4.2.1, the optimal subband responses are given by the filter matrix (3.56),

which for the case of two subband channels can be brought into the form [53, 54]

$$\mathbf{W}(z) = \frac{1}{A}! \begin{bmatrix} H^2(z^{\frac{1}{2}})S(z^{\frac{1}{2}}) - H^2(-z^{\frac{1}{2}})S(-z^{\frac{1}{2}}) & H(z^{\frac{1}{2}})H(-z^{\frac{1}{2}})\left(S(-z^{\frac{1}{2}}) - S(z^{\frac{1}{2}})\right) \\ H(z^{\frac{1}{2}})H(-z^{\frac{1}{2}})\left(S(z^{\frac{1}{2}}) - S(-z^{\frac{1}{2}})\right) & H^2(z^{\frac{1}{2}})S(-z^{\frac{1}{2}}) - H^2(-z^{\frac{1}{2}})S(z^{\frac{1}{2}}) \end{bmatrix} \tag{5.41}$$

where $A = H^2(z) - H^2(-z)$ is approximated in [53, 54] by a delay. Also, for ease of representation, the original analysis and synthesis filters in [54] have been replaced by selecting a QMF filter pair in analysis and synthesis filter bank, and choosing the synthesis filters as reversed copies of the analysis filters,

$$H_0(z) = H(z) \tag{5.42}$$
$$H_1(z) = H_0(-z) = H(-z) \tag{5.43}$$
$$G_0(z) = H_1(-z) = H(z) \tag{5.44}$$
$$G_1(z) = -H_0(-z) = -H(-z) \quad , \tag{5.45}$$

where $H(z)$ is a suitable symmetric prototype lowpass filter.

If the unknown system $S(z)$ is projected into subbands using the analysis filter bank, the formulations

$$S_0(z) = \frac{1}{2}\left\{H_0(z^{\frac{1}{2}})S(z^{\frac{1}{2}}) + H_0(-z^{\frac{1}{2}})S(-z^{\frac{1}{2}})\right\} = \tag{5.46}$$
$$= \frac{1}{2}\left\{H(z^{\frac{1}{2}})S(z^{\frac{1}{2}}) + H(-z^{\frac{1}{2}})S(-z^{\frac{1}{2}})\right\} \tag{5.47}$$
$$S_1(z) = \frac{1}{2}\left\{H_1(z^{\frac{1}{2}})S(z^{\frac{1}{2}}) + H_1(-z^{\frac{1}{2}})S(-z^{\frac{1}{2}})\right\} = \tag{5.48}$$
$$= \frac{1}{2}\left\{H(-z^{\frac{1}{2}})S(z^{\frac{1}{2}}) + H(z^{\frac{1}{2}})S(-z^{\frac{1}{2}})\right\} \tag{5.49}$$

arise. A reconstruction of the subband projections $S_0(z)$ and $S_1(z)$ from the subbands finally yields

$$\hat{S}(z) = S_0(z^2)G_0(z) + S_1(z^2)G_1(z) = \tag{5.50}$$
$$= \frac{1}{2}\left(H^2(z) - H^2(-z)\right) \cdot S(z) \quad , \tag{5.51}$$

where the term $H^2(z) - H^2(-z)$ according to the selection (5.42)–(5.42) obviously can be expressed as

$$H^2(z) - H^2(-z) = H_0(z)G_0(z) + H_1(z)G_1(z) \quad , \tag{5.52}$$

which is a power complementary condition as introduced in Sec. 4.5.1.2 and with PR filter banks will only constitute a delay.

Next, a reconstruction from the subbands is performed by multiplying from the right with the decimated and expanded analysis filters in modulation description, and from the left with the synthesis filter bank,

$$\begin{aligned}
\hat{W}(z) &= [G_0(z)\ \ G_1(z)] \cdot \mathbf{W}(z^2) \cdot \begin{bmatrix} H_0(z) & H_0(-z) \\ H_1(z) & H_1(-z) \end{bmatrix} \cdot \begin{bmatrix} 1 \\ 1 \end{bmatrix} && (5.53) \\
&= \frac{1}{A}\left(H^2(z) - H^2(-z)\right) \cdot (H(z) - H(-z)) \cdot \\
&\qquad \cdot S(z) \cdot (H(z) + H(-z) && (5.54) \\
&= \left(H^2(z) - H^2(-z)\right) \cdot S(z) && (5.55)
\end{aligned}$$

which yields a result identical to (5.51). Thus, the overall impulse response of the subband adaptive system, the equivalent fullband model, is obtained by applying an impulse to the entire subband adaptive filter system consisting of the analysis bank in series with the adapted subband filter impulse responses including the cross-terms and the synthesis bank [170].

5.3.1.2 General Reconstruction Method

We are now interested in the equivalent fullband model of a general subband adaptive system, with particular interest in the oversampled, cross-term free case shown in Fig. 5.4. If optimal adaptation of the subband adaptive filter responses is assumed, the subband error signals will have minimum variance. Since the filter banks under consideration implement tight frames, the minimum condition of the subband error variances also ensures the variance of the reconstructed error will be minimum. Thus, in the optimally adapted case, the synthesis bank can be split to separately reconstruct a fullband desired signal and perform a synthesis operation on the output of the adapted subband filters. When finally subtracting the two fullband signals, the result should remain the same.

The separation of the synthesis is visualized as a block diagram in Fig. 5.5 hinting at the reconstruction procedure [172]: if an impulse is applied to both branches, the desired signal followed by an analysis–synthesis operation, and the lower branch containing the subband adaptive filter system, the two outputs

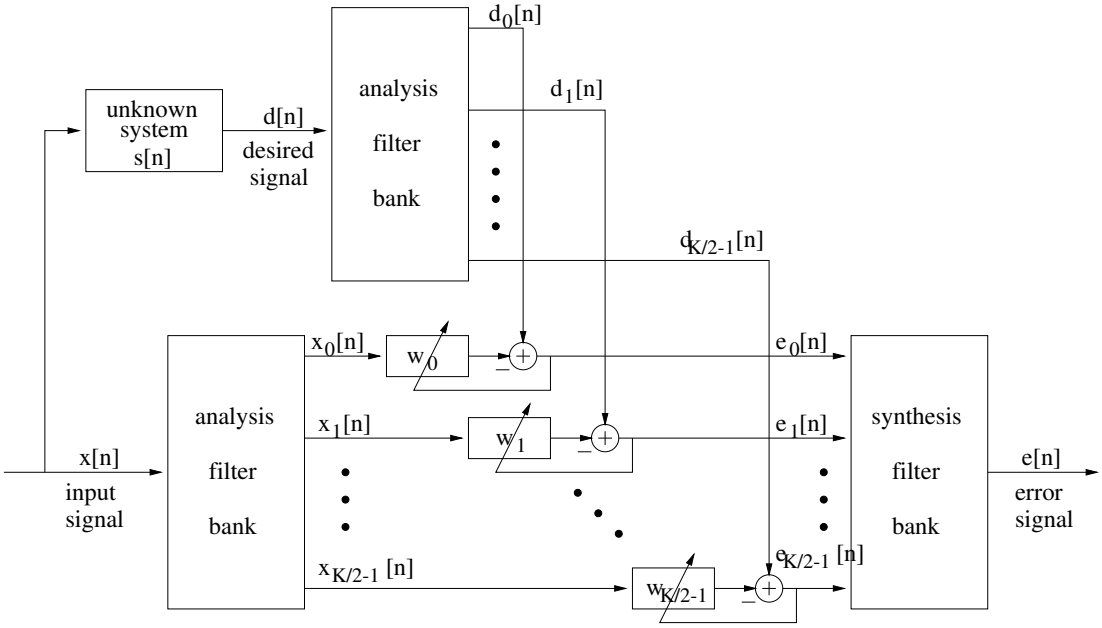

Figure 5.4: Cross-term free subband adaptive filter system in a system identification setup with an unknown system $s[n]$.

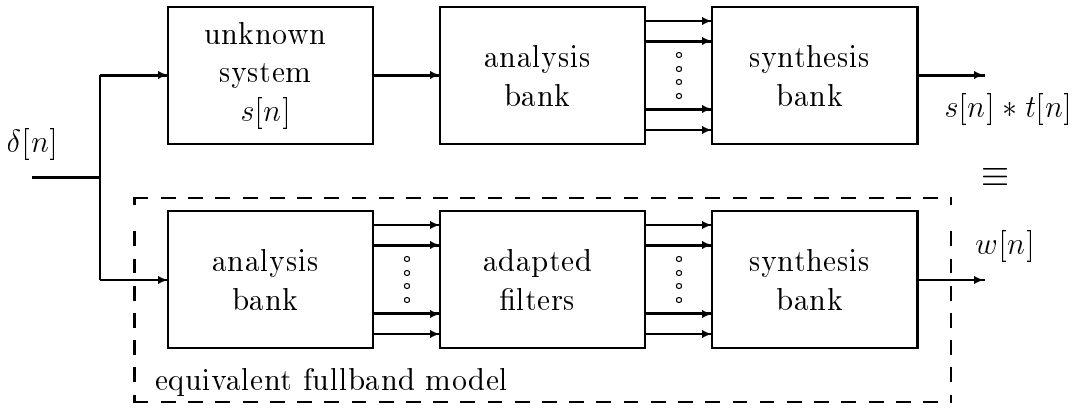

Figure 5.5: Separation of system identification structure for reconstruction of fullband equivalent model.

should be identical under the assumption of perfect adaptation, and the absence of any other inhibiting circumstances like observation noise or truncation effects due to too short adaptive filters.

Therefore, the fullband equivalent model is formed by the response to an impulse applied to serial system of analysis bank, adapted subband filters, and synthesis bank, like in the preceding example for the critically sampled two channel case. The difference from the true system is marked by the response of the combined analysis – synthesis bank, which under ideal condition again should only form a delay.

5.3.2 Maximally Achievable Model Accuracy

The discussed reconstruction of the fullband equivalent model from the subband adaptive filter responses allows interpretations on the maximum accuracy or the minimum error of the subband adaptive filter system with respect to its distance from the ideal overall fullband system to be identified. If we assume perfect adaptation conditions, the resulting equivalent fullband model $w[n]$ will be given by

$$w[n] = s[n] * t[n] \quad , \tag{5.56}$$

where $s[n]$ is the impulse response of the unknown system and $t[n]$ the distortion function of the filter bank. The notation in (5.56) already assumes that the overall filter bank possesses negligible alias distortion, as otherwise $t[n]$ would be periodically time-varying. Thus, if it is taken for granted that the filter bank design as discussed in Sec. 4.5 has provided a filter bank with very low aliasing in the subbands and thus in the reconstructed signal, the overall transfer function of the series of analysis and synthesis bank can be considered to be an LTI system $t[n] \quad \circ\!\!-\!\!\bullet \quad T(z)$, which is often termed distortion function [151] and describes both amplitude and phase distortion of the filter bank systems in Fig. 3.1. This allows us to state the limit for the model accuracy in terms of the reconstruction error (RE)

$$\mathrm{RE} = \| t[n] \; - \; \delta[n - L_p + 1] \|_2 = \| T(z) - z^{-L_p+1} \|_2 \quad , \tag{5.57}$$

where $\|\cdot\|_2$ indicates the l_2 norm. Since $T(z)$ is given by [151]

$$T(z) = \sum_{k=0}^{K-1} H_k(z) \cdot G_k(z) \quad , \tag{5.58}$$

the error measure (5.57) for model accuracy is equivalent to the deviation from power complementarity in Sec. 4.5.1.2. If designing a prototype filter using the iterated LS method of Sec. 4.5.3, the power complementarity requirement is described by (4.93), and can therefore be used to a priori state the model accuracy as

$$\mathrm{RE} = \|\mathbf{V}\mathbf{S}_1\mathbf{S}_2 \cdot \mathbf{b} \; - \; \mathbf{d}\|_2 \quad . \tag{5.59}$$

This also describes the distortion imposed on any signal fed through the SAF system.

The analysis presented here assumed that aliasing is sufficiently suppressed. Is this a reasonable and valid assumption? Sec. 5.2.1 has indicated that the minimum achievable error within the subbands is limited by the SAR, which has been linked to the stopband attenuation of the employed prototype filter. The residual noise again causes an excess MSE, which for example with LMS type algorithms is proportional to the MMSE and prohibits an accurate adjustment of the subband adaptive filters. Therefore, if the error in perfect reconstruction was considerably lower than the SAR, the error limit would still be linked to the subband SAR. It is therefore vital to design the prototype filter such that its stopband energy is *at least* as small as its deviation from perfect reconstruction. With this balance between stopband attenuation and perfect reconstruction, it is justified to swap the requirements of perfect reconstruction (PR) with power complementarity (PC).

5.4 Simulations and Results

Simulations presented within this section will evaluate the influence of various parameters in an SAF system using GDFT filter banks. Furthermore, examples are given to underline the validity of the performance limitations calculated in Secs. 5.2 and 5.3.

	K/N	L_p	RE/[dB]	SAR/[dB]	ρ
$p_1[n]$	32/28	896	-55	57	$2.7 \cdot 10^{-2}$
$p_2[n]$	32/24	960	-114	109	$4.5 \cdot 10^{-4}$
$p_3[n]$	32/20	960	-175	170	$5.6 \cdot 10^{-6}$
$p_4[n]$	32/16	896	-193	180	$8.5 \cdot 10^{-8}$

Table 5.1: Filter design using the iterative LS method of Sec. 4.5.3 for $K/2 = 16$ subbands and various decimation ratios $N = 16(4)28$.

5.4.1 Subband Parameters

This section will evaluate how the choice of the channel number K and the decimation ratio N of the SAF will affect convergence. Sec. 5.4.1.1 investigates the adaptation for a fixed number of subbands and a variable decimation ratio, while in Sec. 5.4.1.2, the impact of the number of subbands will be surveyed by varying K at a fixed oversampling ratio (OSR) K/N.

5.4.1.1 Oversampling Ratio

Filter Banks. Tab. 5.1 lists 4 prototype filters, which are designed for $K/2 = 16$ subbands and a number of different decimation ratios. With these prototype filters, subband adaptive systems operating at different oversampling ratios (OSR)

$$\text{OSR} = \frac{K}{N} \geq 1 \tag{5.60}$$

can be created. For convenience, the lengths of the prototype filters have been chosen such that polyphase implementation of the filter banks can be kept simple with L_p being an integer multiple of $\text{lcm}(K, N)$. Fig. 5.6 shows the resulting frequency responses of the four prototype filters. Note that the 3 dB crossing point $|P_i(e^{j\pi/16})| = \sqrt{1/2}$, $i = 1(1)4$ is given through the required power complementarity of the filters.

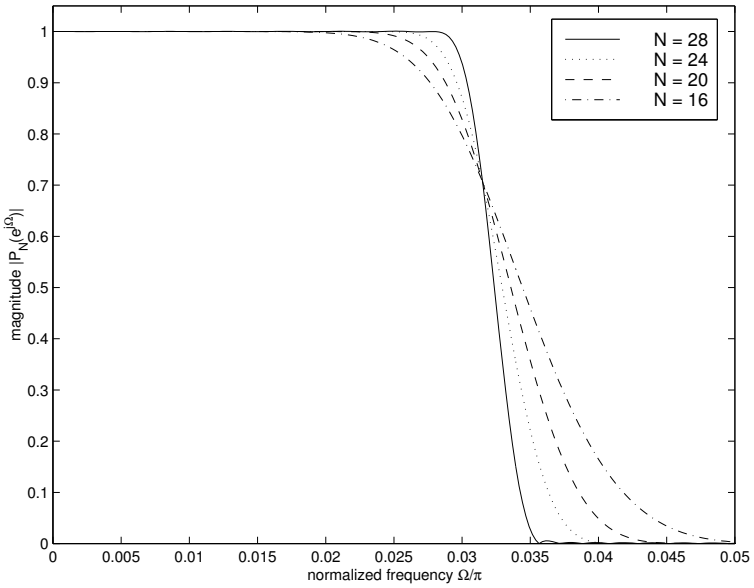

Figure 5.6: Frequency response of prototype filters $p_i[n]$, $i = 1(1)4$, for $K = 32$ and various decimation ratios $N = 16(4)28$, belonging to the prototype design listed in Tab. 5.1.

Eigenvalue Spread. To analytically estimate the eigenvalue spread of the subband signals, the input signal to the analysis filter bank will be assumed to be normally distributed and white. Since all bandpass filters in the filter bank are modulated versions, only a representative subband signal produced by the prototype filter will be evaluated. An approximation of the PSD for the subband signals omitting any spectral correlations between aliased components in the decimation stage similar to the proceeding in Sec. 5.2.2 is given by the squared magnitude of the prototype filter decimated by N,

$$S_{xx}(e^{j\Omega}) \;\approx\; P_l(e^{j\Omega})P_l^*(e^{-j\Omega}) \tag{5.61}$$

$$\bullet\!\!-\!\!\circ$$

$$r_{xx}[n] \;\approx\; p_l[n] * p_l[-n] \quad , \tag{5.62}$$

where $p_l[n]$, $l = 0(1)N-1$, is the lth of N polyphase components of the prototype filter. A result of the approximation is that it does not matter which of the N polyphase components is picked to calculate (5.62). If N is chosen such that no aliasing in the subbands will occur, all N polyphase components will

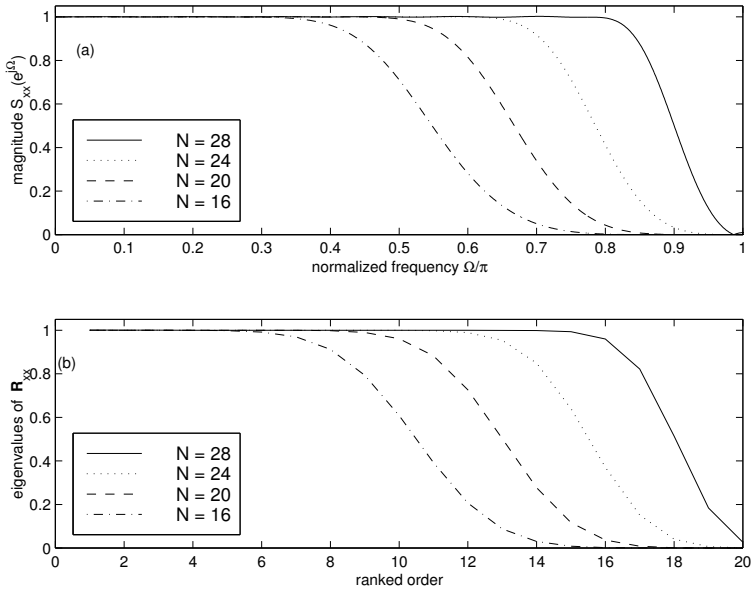

Figure 5.7: (a) subband PSD for filter bank with $K = 32$ and various decimation ratios $N = 16(4)28$; (b) eigenspectra of a 20×20 auto-correlation matrix belonging to the curves in (a).

have an identical magnitude response, but differ in their phase. However, in the auto-correlation operation, any phase information is lost, and thus all N components will yield identical results in (5.62). Fig. 5.7 shows the approximated PSDs of a subband produced by the lowpass prototype filters in Tab. 5.1 decimated by the according factor N, as well as the eigenspectra, which are composed of ordered eigenvalues of a 20×20 [1] auto-correlation matrix $\mathbf{R}_{xx}$ based on the auto-correlation sequence $r_{xx}[n]$ in (5.62), closely corresponding with the subband PSDs.

Simulations. The following simulations consist of the identification of a delay of 1000 taps using an NLMS algorithm with normalized step size $\tilde{\mu} = 0.4$. A simple delay has been shown to be difficult to adapt to, since a delay passes all frequencies equally and the slow convergence at the band-edges will have a main

[1] The dimension of $\mathbf{R}_{xx}$ is likely to influence the eigenvalue spread. Here, it has been selected arbitarily, we are only interested in the relative difference between different subband realizations.

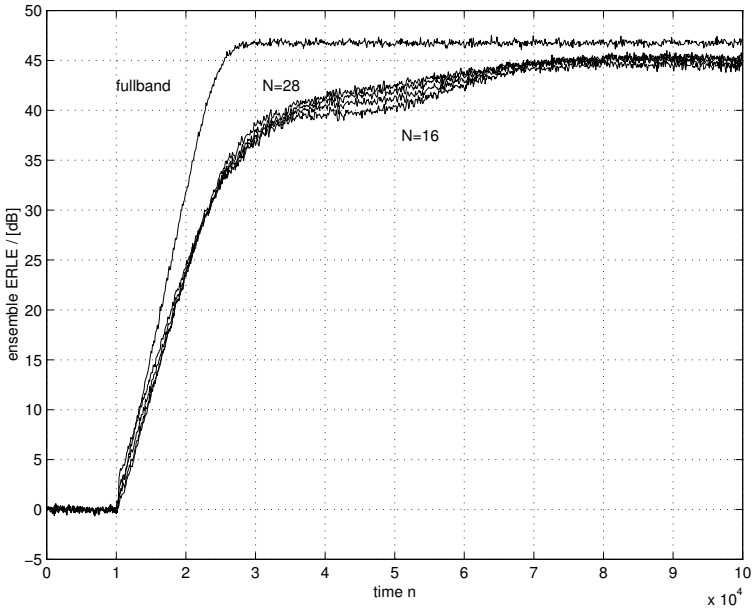

Figure 5.8: ERLE curves for identification of a delay with white input signal in both fullband and $K/2 = 16$ subbands produced by a complex valued GDFT modulated filter banks with different decimation ratios $N = \{16, 20, 24, 28\}$.

influence on the overall adaptation behaviour [101, 88]. To enforce equal conditions on the subband adaptive filters despite the various aliasing levels produced by different filter banks in Tab. 5.1, observation noise at an SNR of 45dB is added to the desired signal.

Simulations for white Gaussian input $x[n]$ are shown in Fig. 5.8 for a complex valued GDFT filter banks with $K/2 = 16$ subbands and decimation ratios N of 28, 24, 20, and 16. For comparison, the convergence curve of a fullband NLMS algorithm for same system specifications has been added. Identical simulations using an SSB modified GDFT filter bank for adaptation in real valued subband signals are shown in Fig. 5.9 for decimation ratios of $N/2 = 14$, 12, 10, and 8. Apparently, for both SAF systems using complex valued GDFT and real valued SSB subband signals, the decimation ratio has no really strong effect on the convergence, and they converge with approximately equal speed at the different OSRs. Compared to the fullband performance, apparently the SAFs exhibit after an initially equally fast adaptation a slower convergence to the final MSE, and

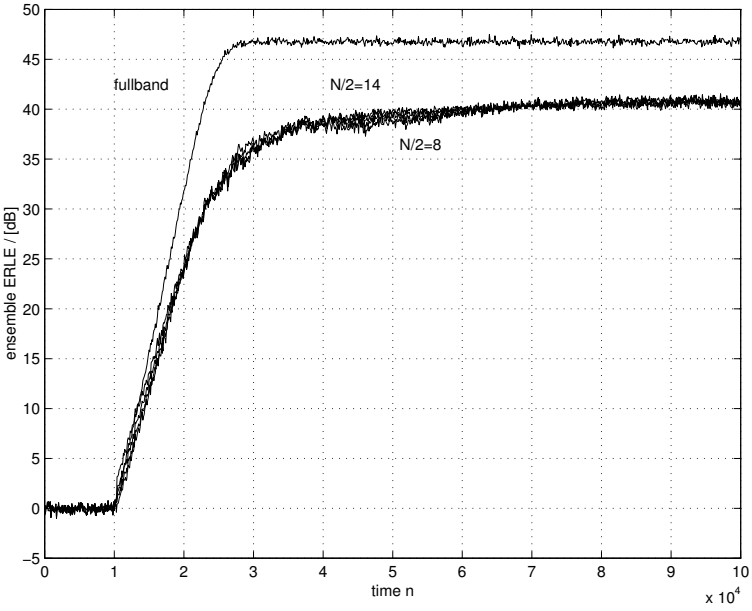

Figure 5.9: ERLE curves for identification of a delay with a white input signal in real valued subbands produced by SSB modified GDFT filter banks for decimation ratios $N/2 = \{8, 10, 12, 14\}$.

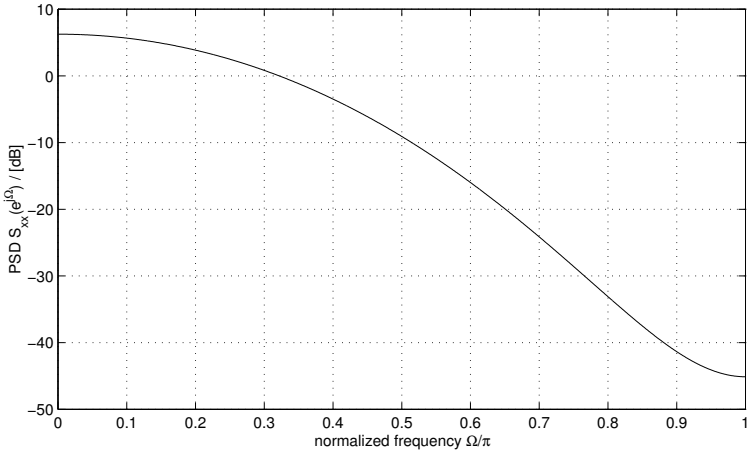

Figure 5.10: PSD of input signal for simulations with coloured noise.

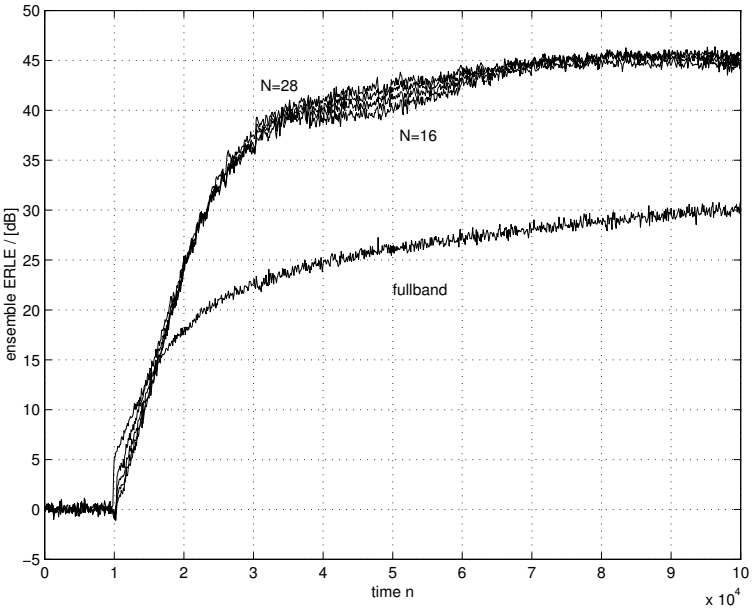

Figure 5.11: ERLE curves for identification of a delay with coloured input signal in both fullband and $K/2 = 16$ subbands produced by a complex valued GDFT modulated filter banks with different decimation ratios $N = \{16, 20, 24, 28\}$.

are still far from being completely adapted after $0.1 \cdot 10^6$ iterations. This is due to the very high eigenvalue spread ρ of the decomposed input signal for the SAFs, which is listed in the last column of Tab. 5.1 for the prototype filters employed for the different OSRs. Also interestingly, the SSB modified GDFT system has a considerably poorer convergence towards the final MSE, since the PSDs of the subband signals posses two notches compared to one in the complex valued subband signals, as can be easily pictured from Fig. 4.10. No explanation has yet been found for the "bumps" of slow convergence appearing in the learning curves with increasing OSR.

The same simulations are repeated using a coloured input signal with a PSD shown in Fig. 5.10. Simulation results for SAF systems using GDFT and SSB modified GDFT filter banks with different oversampling ratios are given in Figs. 5.11 and 5.12. Remarkably, while the fullband NLMS algorithm is now severly slowed down, the convergence characteristics for SAF have hardly changed compared to the white noise excitation in Figs. 5.8 and 5.9, since the spectrum

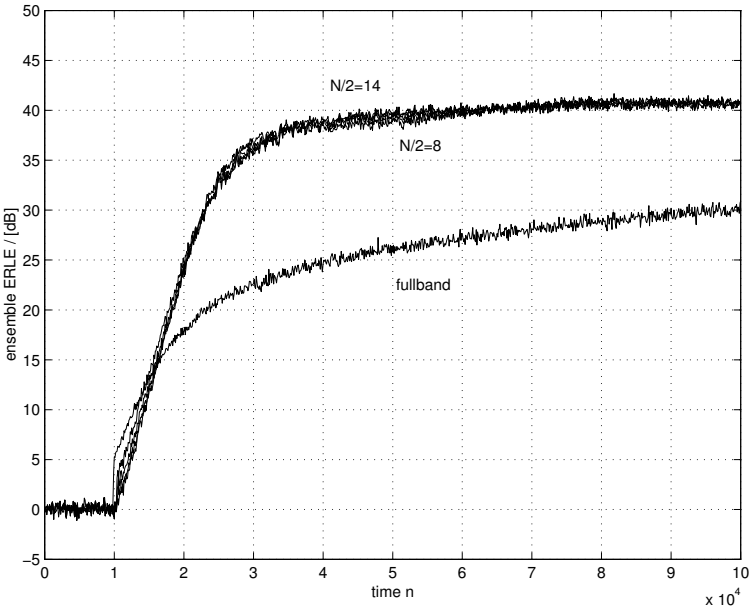

Figure 5.12: ERLE curves for identification of a delay with coloured input signal in real valued subbands produced by SSB modified GDFT filter banks for decimation ratios $N/2 = \{8, 10, 12, 14\}$.

$\Omega = [0; \pi]$ is divided into 16 intervals, thus reducing the relative difference between extrema of the PSD in each band.

Concluding, the subband approach appears reasonably competitive for the white noise excitation case, where it maintains speed through shorter adaptive filters in the subbands, and gives great benefit for adaptation for coloured noise input. The relative insensitivity of the SAF to the OSR suggests that lower filter order at low OSR is traded off against longer filters, higher update rates, and higher eigenvalue spread at higher OSR, with a very slight convergence speed advantage for decimation ratios close to the critical rate. This allows us to choose the OSR of an SAF based on the criterion of computational complexity, as low OSRs will allow for more efficient implementations.

5.4.1.2 Number of Subbands

In the previous section, the decimation ratio was varied for a fixed number of subbands. Now the interest in on how the number of subbands $K/2$ influences

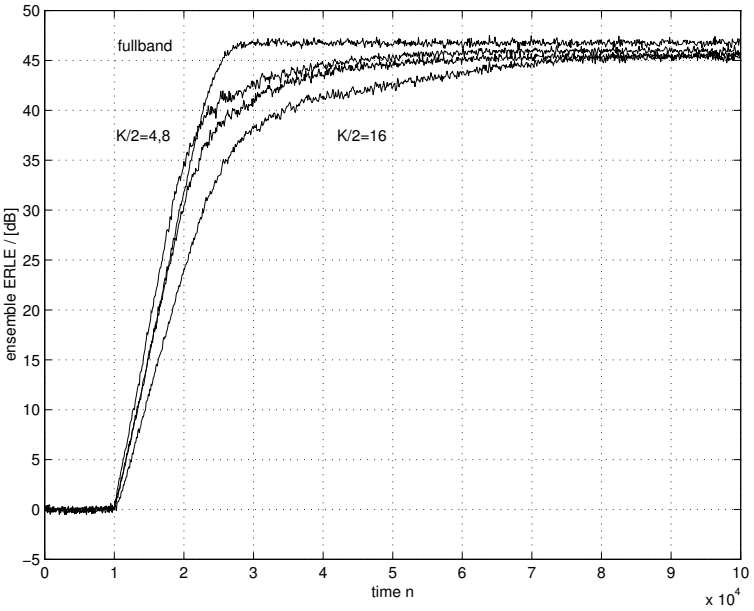

Figure 5.13: ERLE curves for identification of a delay with white input signal in subbands produced by complex valued GDFT filter banks for different number of subbands $K/2 = \{4, 8, 16\}$

convergence, which will be performed at a fixed OSR $K/N = 8/7$ for different values of K. Simulations for the identification of a delay of 1000 samples by SAFs using complex GDFT filter banks are given for white input signal in Fig. 5.13 and for coloured input in Fig. 5.14 with a PSD drawn in Fig. 5.10, in comparison with a fullband adaptive NLMS algorithm.

For the broadband noise simulation in Fig. 5.13, the SAF learning curves migrate towards the fullband behaviour as the number of subbands is lowered. The subbands of the different systems will have similar eigenvalue spread since the OSR is constant, however the reduced adaptive filter length for the higher number of subbands seems not to completely compensate for the slower algorithmic convergence due to the lower update rate. With coloured noise excitation in Fig. 5.14, the SAF systems with $K/2 = 8$ and 16 subbands perform almost identical to the case of white noise excitation in Fig. 5.13, since they seem to provide a sufficient separation of the coloured input spectrum to balance convergence. The opposite appears to be true for the case $K/2 = 4$ which now falls back behind

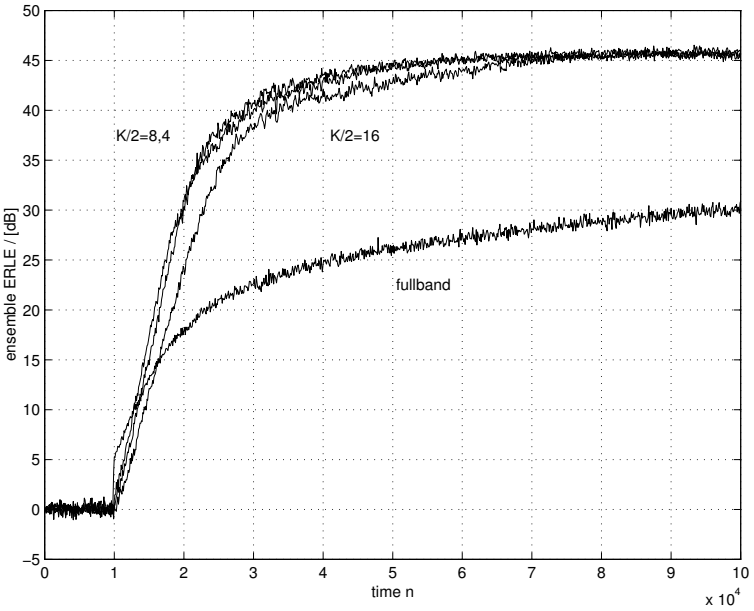

Figure 5.14: ERLE curves for simulation as in Fig. 5.13 for coloured input signal.

$K/2 = 8$ in terms of convergence speed.

In terms of convergence speed, the performance of the SAF system depends on the noise shape of the input signal in the particular application. For the example given in Fig. 5.14, the choice $K/2 = 8$ would be preferred over $K/2 = 4$ or 16. However, besides convergence speed issues, in Chap. 6 the computational complexity of SAF systems will be researched, which will depend to a large extend on the number of subbands.

5.4.2 Performance Limits

5.4.2.1 PSD of Minimum Error Signal

To demonstrate the validity of the PSD description for the minimum error signal as introduced in Sec. 5.2.1.2 based on aliased signal components in the subbands, a system identification example is described in the following. The system is an IIR filter with 5 complex conjugate pole pairs shown in the pole-zero plot in Fig. 5.15. Thus, the system possesses an exponentially decaying impulse response shown in

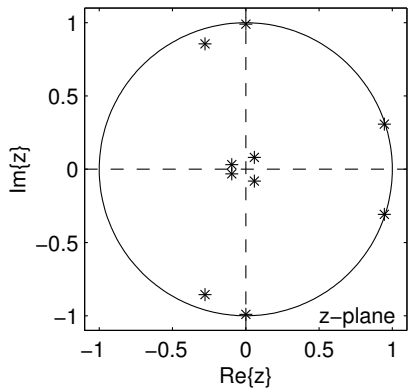

Figure 5.15: Pole-zero plot of the unknown system used for system identification; poles are marked by "$*$".

Fig. 5.16, which slowly drops in power at a rate of approximately 40dB / 1000 samples. This slow decay is due to two pole pairs sitting in close proximity of the unit circle. To exclude other error sources, correct filter lengths for the subband adaptive filter was ensured, and no observation noise was added.

Example 1. For identification, a decomposition into $K/2 = 8$ subbands decimated by $N = 14$ is used to perform subband adaptive filtering using an NLMS algorithm with step size $\tilde{\mu} = 0.8$. Since one of the poles lies exactly at a band edge, the convergence exhibits a very slow mode [101] and only after half a million iterations, the algorithm appears to be almost completely adapted, as the MSE curve in Fig. 5.17 illustrates. A number of PSDs of the error signal have been calculated in Fig. 5.18 over time intervals in which the error was assumed stationary. The solid upper line marks the PSD of the error signal before adaptation is switched on at time $n = 10000$, which also represents the magnitude response of the unknown system, since it is excited by white noise of unit variance. More PSD samples of the measured error signal have been evaluated over a time window of $40 \cdot 10^3$ samples at $n = 0.2 \cdot 10^6$, $n = 0.3 \cdot 10^6$, and $n = 0.5 \cdot 10^6$. Clearly, while the error's energy at the band edges (marked in Fig. 5.18 by dashed vertical lines) is further reduced with each PSD sample, some spectral peaks remain unaffected.

Fig. 5.19 give a comparison between the PSD of the reconstructed fullband error signal of the SAF and a prediction of the residual error PSD based on

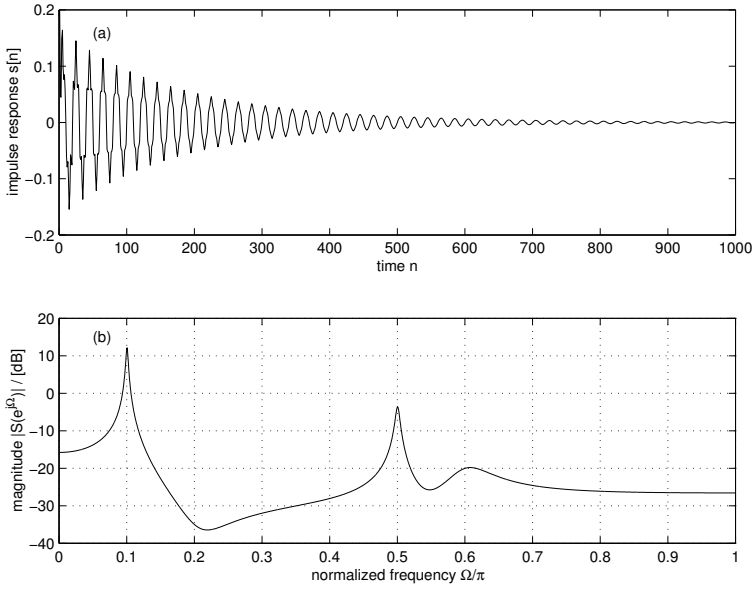

Figure 5.16: (a) Impulse response and (b) magnitude response of the unknown system.

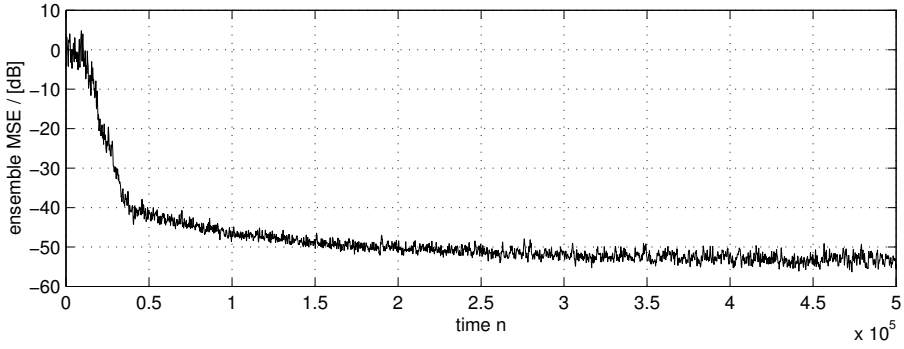

Figure 5.17: Reconstructed fullband MSE of an SAF identifying the unknown system characterized in Figs. 5.15 and 5.16.

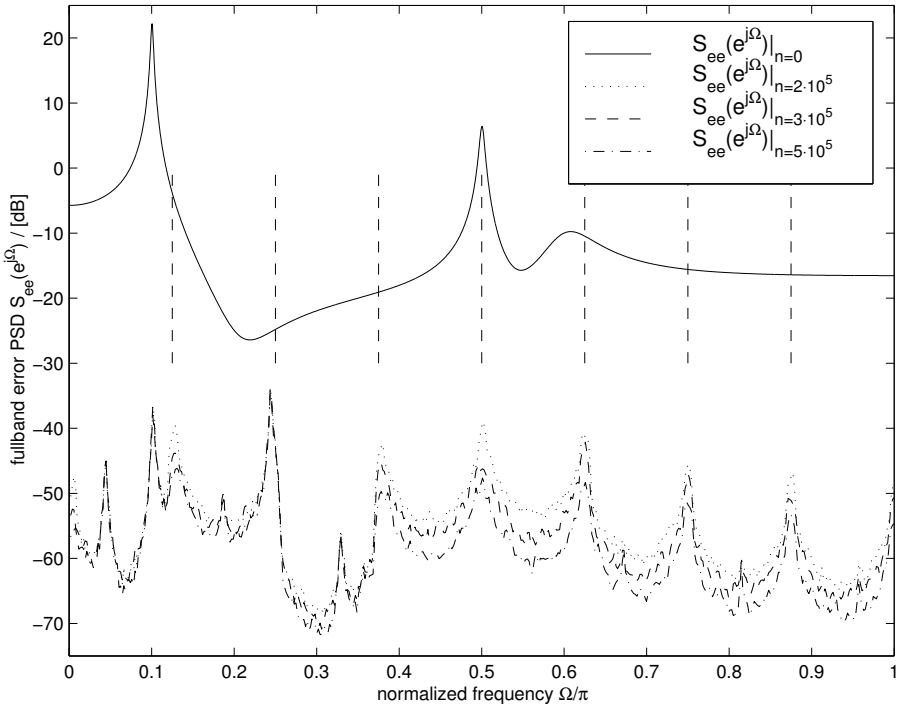

Figure 5.18: PSD of error signal before adaptation is switched on for $n = 10 \cdot 10^3$ (solid), and after $n = 0.2 \cdot 10^6$ (dotted), $n = 0.3 \cdot 10^6$ (dashed), and $n = 0.5 \cdot 10^6$ (dash-dotted) iterations.

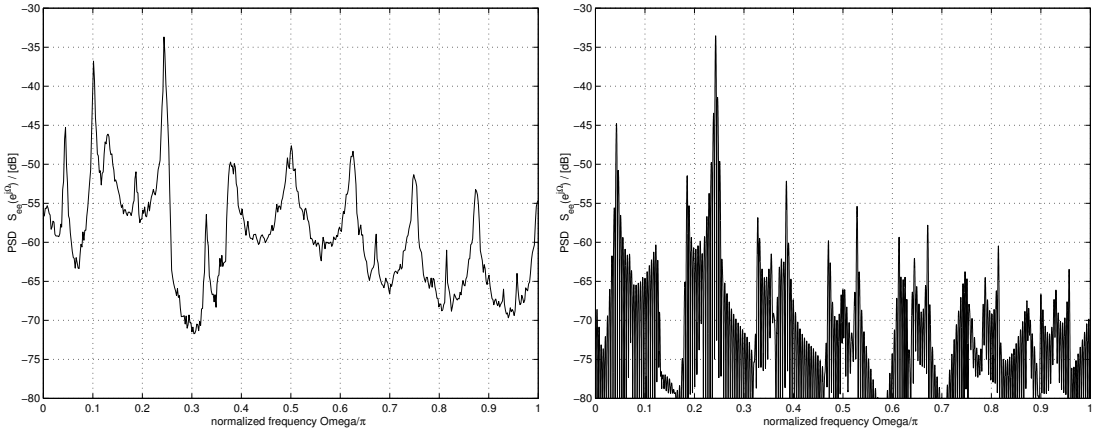

Figure 5.19: (left) PSD of SAF error after $n = 0.5 \cdot 10^6$ iterations; (right) prediction of PSD of residual error signal due to aliasing based on the knowledge of the source model (here the unknown system) and the employed filter banks.

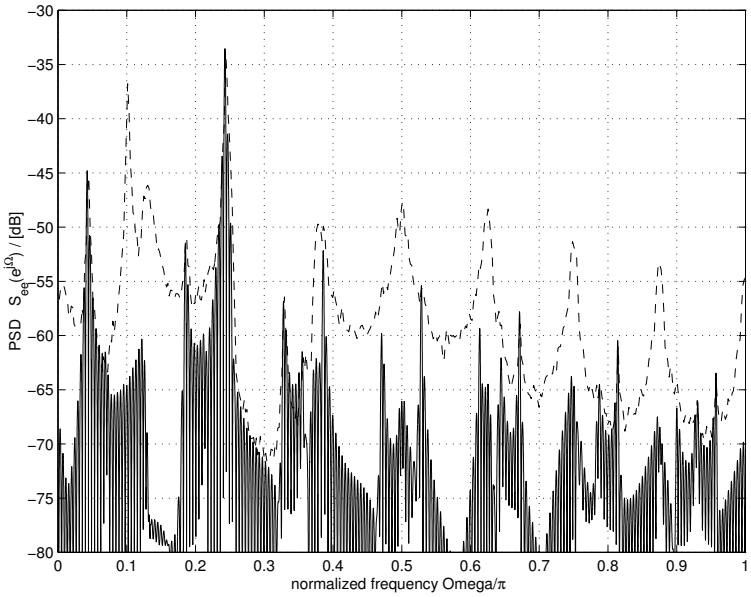

Figure 5.20: Predicted residual error PSD (solid) overlaid with the true error PSD measured after $n = 0.5 \cdot 10^6$ iterations.

aliased components in the subband signals. This prediction has been calculated by approximating the equations presented in Sec. 5.2.1.3 with DFTs of the source model, analysis and synthesis filters. The peaks in this spectrum represent aliased components of the input signal caused by the resonances at $\Omega = 0.1\pi$ and $\Omega = 0.5\pi$. Fig. 5.20 shows both curves overlaid, and it can be appreciated that the measured PSD forms an envelope of the predicted lower error PSD bound over large spectral intervals. Deviations occur at the band edges, and for the frequencies $\Omega = 0.1\pi$ and $\Omega = 0.5\pi$, where the original peaks of the uncancelled error signal resided. This insufficient adaptation of the error can be justified by the slow convergence properties at band edges [101] and by the fact that the error power is dominated by the aliased peak at $\Omega = 0.1\pi + \frac{2\pi}{N} \approx 0.24\pi$, and minimizing the rest of the spectrum will not greatly contribute to a lowering of the MSE.

Example 2. A second example demonstrates the prediction of the residual error PSD for a system identification set-up with coloured input signals as shown in Fig. 5.10. The system to be identified is identical to the one used in the previous example, apart from the strong pole originally at the band-edge $\Omega = 0.5\pi$ now

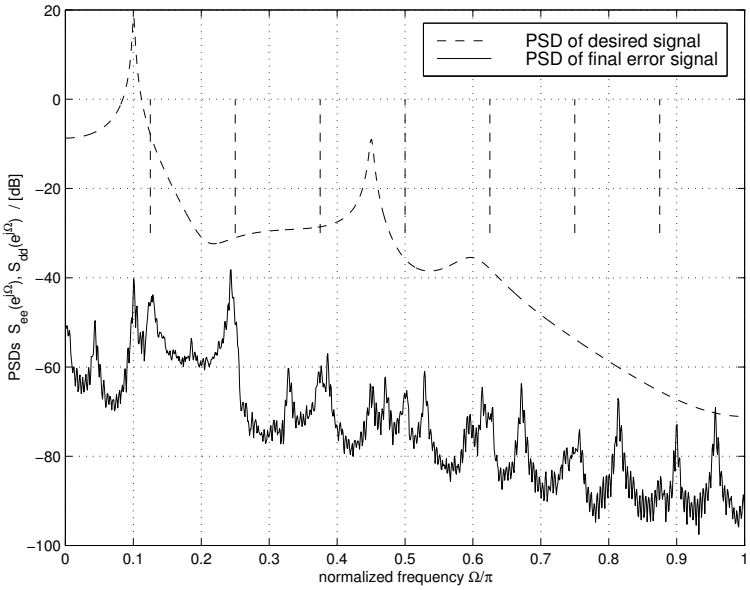

Figure 5.21: PSD of error signal before and after adaptation, using an unknown system with 5 poles and coloured input signal.

sitting at an angle of $\Omega = 0.45\pi$. Again, the SAF set-up uses a modulated GDFT filter bank with $K/2 = 8$ subbands, decimation by $N = 14$, and NLMS algorithms with $\tilde{\mu} = 0.8$ operating in the subbands. Fig. 5.21 shows the measured PSDs of the error signal before and after adaptation ($n = 0.2 \cdot 10^6$). The prediction of the residual error PSD used a source model consisting of the unknown system and the noise shaping filter producing the PSD of the input signal as in Fig. 5.10. The result is overlaid with the measured PSD in Fig. 5.22, and obviously fits very well as a lower bound. As one pole has been moved from the band edge to the center position of the 3rd subband, the adaptation is more accurate after shorter time than in the previous example, and the error signal contains less uncancelled energy at the band edges and the strong original peaks at $\Omega = 0.1\pi$ and $\Omega = 0.45\pi$.

5.4.2.2 Performance Measures

Performance limitations of SAF systems closely related to the filter design parameters of power complementarity and stopband attenuation have been derived in

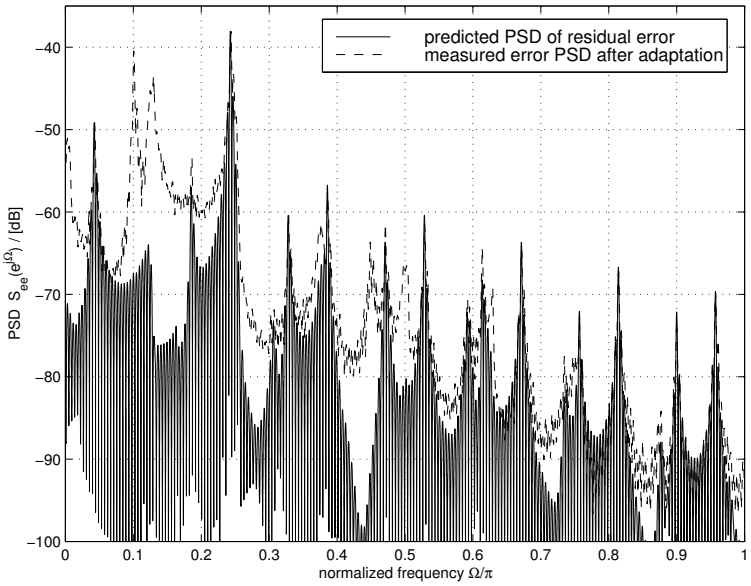

Figure 5.22: Comparison between the predicted PSD of the minimum error and the measured error PSD for coloured input signal.

Secs. 5.2.2 and 5.3.2. To test for validity, a number of prototype filters have been designed using the iterative LS design of Sec. 4.5.3 for the application in SAF systems with $K/2 = 8$ subbands and decimation by $N = 12$, but different weighting γ between the conditions of power complementarity and stopband attenuation. The resulting measures of perfect reconstruction (RE) and signal-to-alias ratio (SAR) according to (4.71) and (4.96) three different γ-designs with a filter length of $L_p = 192$ taps are shown in Tab. 5.2.

The unknown system was set to be a simple delay, and identification with a white Gaussian input signal used an RLS algorithm for adaptation of the SAF with a forgetting factor $\beta = 0.9995$. The RLS was here preferred over LMS-type algorithms to avoid slow convergence due to the coloured nature of the subband signals introduced by the analysis filter bank. Tab. 5.2 displays in its two right columns the noise reduction, i.e. the difference between the variances of the uncancelled and adapted error signal, and the error of the reconstructed equivalent fullband model with respect to the delay to be identified. Apparently for all three designs, both quantities match very closely with the measures derived from the prototype filter, and can therefore be well used for predicting the MMSE

Prototype Design			Simulation Results	
$10\log_{10}(\gamma)$	RE/dB	SAR/dB	$10\log_{10}(\|\|w-s\|\|_2^2)$	$10\log_{10}(\sigma_{dd}^2/\sigma_{ee}^2)$
0	-54.0821	55.6	-54.0153	54.0
30	-34.6191	65.2	-34.6143	66.2
60	-18.0016	77.8	-18.0010	78.5

Table 5.2: Predicted fullband model error and final MSE compared to simulation results (all quantities in [dB]).

performance of the implemented SAF system.

For the more complex simulations presented in Sec. 5.4.2.1, the noise reduction values attained by the SAF systems were measured to be -53.93dB for example 1 as shown in Fig. 5.17, and -56.73dB for example 2, for which the PSDs of uncancelled and cancelled error signal are given in Fig. 5.21. The characteristics of the prototype filter $p[n]$ used for the decomposition into $K/2 = 8$ subbands and decimation by $N = 14$ — contained in Tab. 4.3 as design (d) — exhibit an SAR value -57.01dB calculated according to (4.71). This very closely agrees with the measured noise reduction for the system identification in example 2, which used a very long impulse response as the unknown system and a coloured input signal. For example 1, the discrepancy between the SAR value of the prototype filter and the noise reduction of -53.93dB can be explained by the SAF not being completely adapted after $0.5 \cdot 10^6$ iterations, which is indicated in Fig. 5.18 by the remaining energy in the PSD at the band edges.

5.5 Concluding Remarks

A number of performance characteristics of subband adaptive filter systems have been addressed in this chapter. The main aspects were focused on the convergence behaviour of the SAF set-up, and the performance limitations in the MMSE behaviour.

For the minimum error performance of SAF, the analysis of aliased signal

components has been used to calculate the limits for the power spectral density of the minimum error signal, based on the knowledge of a source model and the characteristics of the analysis and synthesis filter bank. Approximations have been derived for the MMSE in both subbands and fullband, which have been linked to the stopband attenuation of the prototype filter of the filter bank. The equivalent fullband model, i.e. the impulse response of the overall SAF system consisting of analysis filter bank, subband adaptive filters, and synthesis filter bank, has been shown to be limited in its accuracy by the reconstruction error of the employed filter banks.

The calculated or estimated performance limitation on MMSE and fullband equivalent model have been verified by simulation, which agree well with the two design criteria of the prototype filter, stopband attenuation and reconstruction error. Although these measures have specifically addressed GDFT modulated filter banks, similar derivation can be made for other filter bank types. The appeal lies in the fact that these measures provide convenient tools to design filter banks for SAF systems fulfilling pre-specified performance limits [172]. Thus, for applications like acoustic echo control, where the adaptation error is the most important issue, the banks can be designed to be just good (and short) enough to satisfy relaxed constraints on the model error.

Concerning convergence speed, several influencing factors have been addressed, including the filter length of the adaptive filter, the update rate, and the eigenvalue spread of the subband decomposition of the input signal. The effect of varying the oversampling ratio and the number of subbands was highlighted in a number of simulations. Results from these simulations suggest that the OSR has a minor influence on the convergence speed, while the number of subbands is governed by an optimal trade-off between the spectral separation for coloured PSD of the input signal, and the reduced update rate and SAF filter length prevalent with higher channel numbers K for constant OSR. Generally compared to a fullband adaptive solution, the convergence speed slowed down particularly when approaching the MMSE, but was considerably enhanced for coloured input signals.

As lowering the OSR has hardly any influence — and if at all, it appears to

be a positive one — on the convergence speed, but does greatly reduce the computational complexity of the implemented system due to the reduced adaptive filter length and lower update rate of all involved filters, it appears sensible to run the SAF system at the lowest possible rate, i.e. using an oversampling ratio close to one. Since the demand for an efficient implementation also includes the maximum exploitation of computational saving in the filter bank implementation, we finally come back to the GDFT filter banks presented in Chap. 4 when assessing the complexity of the overall SAF system and comparing it to other implementations in the following chapter.

Chapter 6

Variable Tap-Profiles For Subband Adaptive Filters

The subband adaptive filtering approach allows a selection of a different set of algorithmic parameters for each subband. While in the past section this has been exploited to choose different convergence parameters to increase the overall convergence speed, here we will discuss methods to vary the filter lengths of the different adaptive filters in an SAF system. We first introduce the underlying idea and review related work in Sec. 6.1. Sec. 6.2 analyses the potential benefits and also gives an insight and comparison into the computational savings achievable with different subband approaches. Two algorithms for variable filter tap-profile are presented in Sec. 6.3. Finally, Sec. 6.4 discusses some simulations and results.

6.1 Idea and Background

6.1.1 Motivation

For the identification of long impulse responses, such as found in acoustic echo control problems, the achievable model is often a truncated representation due to the computational limitation of the digital signal processor (DSP) on which an adaptive system is implemented. As a solution to reduce the computational complexity, the subband adaptive approach has been discussed in Chap. 3. A method to further enhance the efficient use of computational resources on a DSP

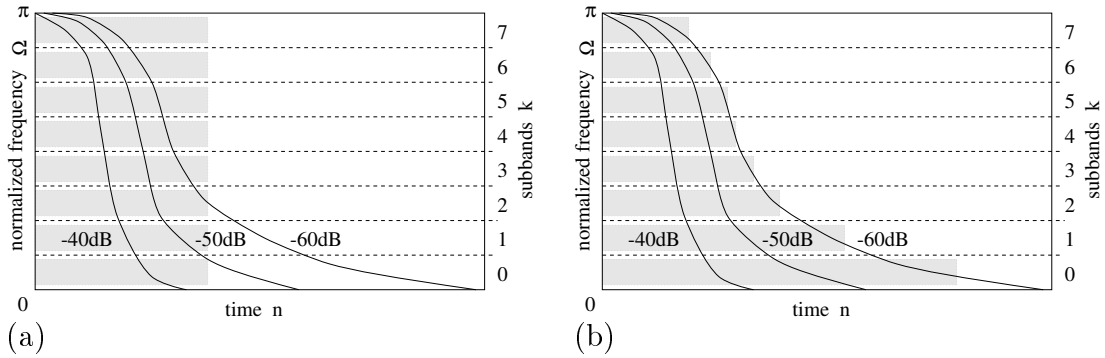

Figure 6.1: (a) uniform and (b) optimized tap-profile for an SAF with $K/2 = 8$ subbands, with decay levels for the power of the unknown system; the under-laid shaded areas represent the equivalent lengths of the subband filters with respect to the fullband.

is by introducing a variable tap-profile subband adaptive system, whereby computational resources can be dynamically allocated to subbands where they are required. If the unknown system to be identified is spectrally unbalanced or the involved signals are coloured, this approach can be advantageous.

Fig. 6.1 shows three decay levels of the spectral power belonging to the spectrogram of some unknown system. In many applications, this decay is spectrally unbalanced, as for example in room acoustics low frequencies generally reverberate longer due to frequency dependent absorption by the walls. If such a spectrally unbalanced system is to be identified by an SAF system, and each subband has an adaptive filter of equal length (as indicated in Fig. 6.1(a)), the resulting fullband model error will be dominated by the subband whose filter length is shortest compared to the unknown system's decay time in that frequency band. As an example, in Fig. 6.1(a)), the band $k = 0$ would be mainly responsible for the magnitude of the final modelling error after adaptation. Fig. 6.1(b) shows an optimization of the tap-profile — i.e. the lengths of the different SAFs — such that with the same overall number of coefficients the SAF system will actually have improved performance, since the remaining truncation errors in the different subbands are approximately equalized.

The optimization of the tap-profile of an SAF system can therefore by viewed as the task to exploit the resources of a DSP with a given computational benchmark to achieve an enhanced overall performance. The author's idea was based

on subband ADPCM, where signals are decomposed and differently quantized in each frequency band. From a fixed pool of bits, each band is allocated a different bit resolution depending on the relative signal energy within that band, thus increasing the signal quality at a fixed bit rate of transmission. Transfered to the SAF problem, more computations and thus longer filters can be dedicated to subbands with a high error power, while coefficients are withdrawn from those with low power. Thus, balancing the different subband errors can help to achieve a minimization of a global (fullband) error, as will be derived in Sec. 6.3.

6.1.2 Approaches and Methods

The idea of tap-profile optimization is not new. Different approaches can be found in the literature and will be discussed in the following, whereby we first look into schemes calculating an approximate optimum profile prior to start running the SAF system. Finally, adaptive solutions will be reviewed.

6.1.2.1 A Priori Optimization

The approach illustrated in Fig. 6.1 is performed in [1], which describes the implementation of a commercial AEC system. Based on the measured energy decay of an impulse in two representative rooms, the filter lengths of the SAFs are set to a pre-specified tap-profile [1, 2]. Work presented in [34] not only takes spectrally unbalanced room impulse responses into account, but also considers the spectral shape of speech and the characteristics of the human ear to derive an LS solution for a fixed optimum tap-profile.

6.1.2.2 Adaptive Schemes

To achieve and maintain approximate optimality of the SAF system during operation in order to track changes and to be able to take set-ups in different environments into account, the tap-profile can be varied adaptively. The original SAF system is then ammended by a second adjustment algorithm as shown in Fig.6.2, which will try to *balance* the subband errors. This idea was first presented in [91] and referred to as automatic tap-assignment. The exchange of coefficients

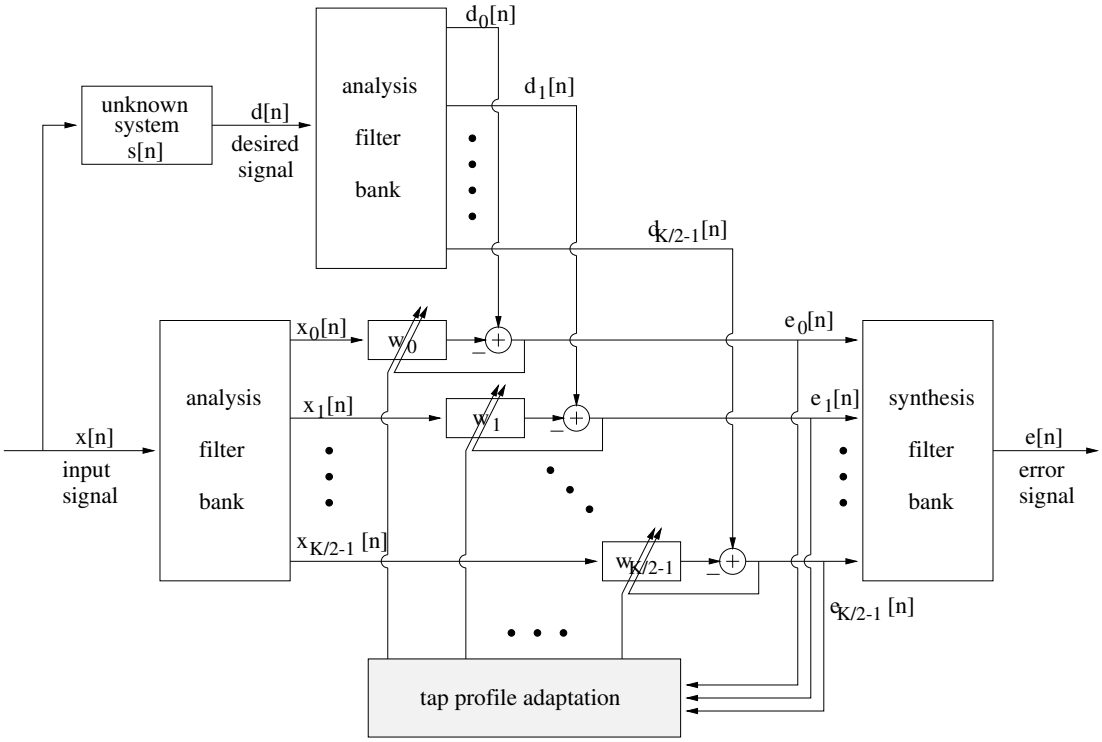

Figure 6.2: Subband adaptive filter system with adaptive adjustment of the tap-profile.

between two filters in undecimated subbands was performed based on a criterion dependent on the subband error signals only. Modifications of this tap-assignment algorithm are presented in [143, 144], which perform a tap-allocation based on a mixed criterion of the input signal and the trailing coefficients of the impulse responses of the SAFs. A general theory on both the methods by [91] and [143, 144] will be developed in Sec 6.3. The work in [158] extends the ideas in [91, 143] by the inclusion of perceptual criteria based on the human ear similar to the a priori optimization by [34].

The benefit of yielding a lower model truncation error with tap-profile adaptation over standard subband or fullband adaptive filtering is demonstrated in [170], which also describes a simplified criterion over [143]. The experimentation uses critically decimated filter banks with cross-terms according to [54], but with a suboptimal filter bank implementation. A generalization of the global error minimization presented in [170] is performed in [162] to include tap-profile adaptation in oversampled non-uniform subbands [71, 69] as depicted in Fig. 3.20. Both approaches in [170] and [162] are somewhat tedious, the first through the necessary inclusion of cross-terms, the latter through various subsampling ratios in different subbands and the resulting subband-dependent computational cost and fullband time-representation of coefficients, which requires inconvenient exchange rates[1] for shifting filter taps between subbands.

6.2 Equivalent Fullband Model Length and Complexity

In the following, we will motivate the variable tap-profile approach by comparing a fullband adaptive filter with a number of different SAF systems based on the critically decimated [54], and the oversampled GDFT and SSB modified GDFT filter banks [167] presented in Chap. 4. First, the resulting complexities based on constant equivalent fullband model length will be evaluated in Sec. 6.2.1. In Sec. 6.2.2, the problem will reversed, and we ask for the fullband model length

[1] in ECU — equal complexity units [162]

based on an implementation with a fixed number of computations, as, for example, given when implementing SAF systems on a DSP.

6.2.1 Complexity Based on Constant Equivalent Fullband Model Length

Although generally any adaptive filtering algorithm can be employed, for the following analysis and examples, the complexity of the NLMS algorithm will be used. The linear order of complexity creates an interesting case since real and complex subband processing costs are approximately the same, as derived in Sec. 4.4.

6.2.1.1 Computational Cost

For a general SAF system as depicted in Fig. 6.2, the computational cost consists of three filter bank operations and the filtering and update procedures in the subbands. Concerning the subband adaptive filters, we want to look at two extrema for the tap-profile:

- *uniform tap-profile*, where all subband filters have equal length[2];
- *concentrated tap-profile*, where all computations are dedicated to one single subband.

Let us first consider the uniform case. A practical relation between the length of the equivalent fullband model $L_a^{(f)}$ and the length of the SAF length L_a has been derived in Sec. 5.3.1, where the superscript $^{(f)}$ refers to the fullband sampling rate. Therefore, the length of the subband adaptive filters can be calculated according to (5.3) as

$$L_a = \frac{L_a^{(f)} + 2L_p}{N} \quad , \tag{6.1}$$

which accounts for the transients in the subband domain caused by the filter banks. Including the filter bank operation, the total computational costs for SAF

[2]The restriction to uniform filter banks ensures that the fullband time representation of each filter is equal. For similar considerations for SAF in non-uniform subbands with a number of different decimation ratios, please see [162].

systems with real input can be stated for oversampled GDFT modulated complex filter banks as

$$C_{\text{tot}}^{\text{GDFT}} = \frac{1}{N}\left\{3\cdot(4K\log_2 K + 4K + L_p) + 4\frac{K}{2}\left(2\frac{L_a^{(f)}+2L_p}{N}+3\right)\right\} \tag{6.2}$$

real multiplication per fullband period, where the filter bank cost is given by (4.50), $K/2$ is the number of subbands decimated by N, and L_p the length of the prototype filter. For an SAF employing SSB modified GDFT filter banks, whose computational complexity is given by (4.65), processing in real valued subbands amounts to a total cost of

$$C_{\text{tot}}^{\text{SSB}} = \frac{2}{N}\left\{3\cdot(4K\log_2 K + 5K + L_p) + \frac{K}{2}\left(2\frac{L_a^{(f)}+2L_p}{N/2}+3\right)\right\} \tag{6.3}$$

real valued multiplications.

For comparison, the total computational cost for an NLMS subband adaptive filter operating in critically decimated subbands produced by DCT modulated filter banks, which requires using the structure suggested in [53, 54], is given by

$$C_{\text{tot}}^{\text{DCT}} = \frac{2}{K}\Bigg\{3\cdot(\underbrace{4K\log_2 K + 4K + L_p}_{C_{\text{bank}}}) + \underbrace{\frac{K}{2}\left(2\frac{L_a^{(f)}+2L_p}{K/2}+3\right)}_{\text{adaptive main terms}} + \\ + \underbrace{(K-2)\left(\frac{2}{3}\frac{L_a^{(f)}+2L_p}{K/2}+3\right)}_{\text{adaptive cross terms}} + \underbrace{(K-2)\left(\frac{2L_p-1}{K/2}\right)}_{\text{fixed cross terms}}\Bigg\}. \tag{6.4}$$

This assumes that cosine modulated filter banks have been used, and have been calculated using an efficient polyphase structure almost identical to the one for oversampled SSB modified GDFT filter banks discussed in Chap. 4. It is easy to realize that the additional modulation for the SSB modification is not required, since the subband spectra are already aligned. The subband dependent phase shift $\pm\pi/4$ can be incorporated into the phase correcting matrix $\mathbf{D}_1$ in (4.43). Thus only a real operation is performed (at no cost) on the output of a GDFT filter bank with decimation by $K/2$. The cost for the SAF consists of three contributions in (6.4): the adaptive main terms in each of the $K/2$ subbands, and $K-2$ cross-terms, which can be split into a fixed and an adaptive part as

discussed in Sec. 3.4.2.1 (Fig. 3.14). The adaptive cross-terms are set to one third of the length of the main adaptive subband filters[3], as hinted in [54]

To obtain the total cost for a concentrated tap-profile, i.e. SAF is only performed within one single subband, the factor $K/2$ in the adaptive terms of (6.2)–(6.4) is omitted.

6.2.1.2 Example and Comparison

Fig. 6.3 shows the total cost $C_{\text{tot}}^{\text{GDFT}}$ derived in (6.2) for an SAF system using oversampled GDFT filter banks relative to the cost of a fullband implementation of the NLMS, yielding $C^{(f)} = 2L_a^{(f)} + 3$. For four different lengths of the fullband equivalent model $L_a^{(f)}$, the graphs indicate the cost ratio as a function of the number of subbands, $K/2$, of the specific subband implementation with a constant OSR $= 8/7 \approx 1.14$. As a rule of thumb, the length L_p of the prototype filter was set to $L_p(K) = 16 \cdot K$, a realistic value for real-time AEC applications [137], which yields an approximately constant filter quality for variable K and constant OSR when using the iterative LS design introduced in Sec. 4.5.3.

The cost ratios plotted in Fig. 6.3 illustrate how the computational savings initially rise with the number of subbands $K/2$, until for large $K/2$ most of the computations are used for the required filter bank operations, and the cost reduction levels out and would even recede for very large numbers of subbands. For a flexible tap-profile as indicated in Fig. 6.1, the pair of curves for uniform and concentrated tap distribution form the margins in between which the true cost reduction with a variable tap-profile will lie. As an example, using an implementation with $K/2 = 32$ subbands, the computational cost is reduced to 5% (10%) of the fullband implementation for the given response lengths of 16000(2000) taps, assuming a uniform tap-profile. For a concentrated tap-profile, this cost ratio would be down to 1%(7%) of the cost for a fullband implementation.

For an SAF system employing SSB modified oversampled GDFT filter banks for real valued subband processing, Fig. 6.4 shows cost curves according to (6.3) for identical conditions to the previous complex subband processing example in

[3]Experiments in [88] show that system identification problems, where the unknown systems have poles at band-edges, 1/3 of the adaptive main term's length is not sufficient. Thus, for a high performance system, the cost may be higher than shown here.

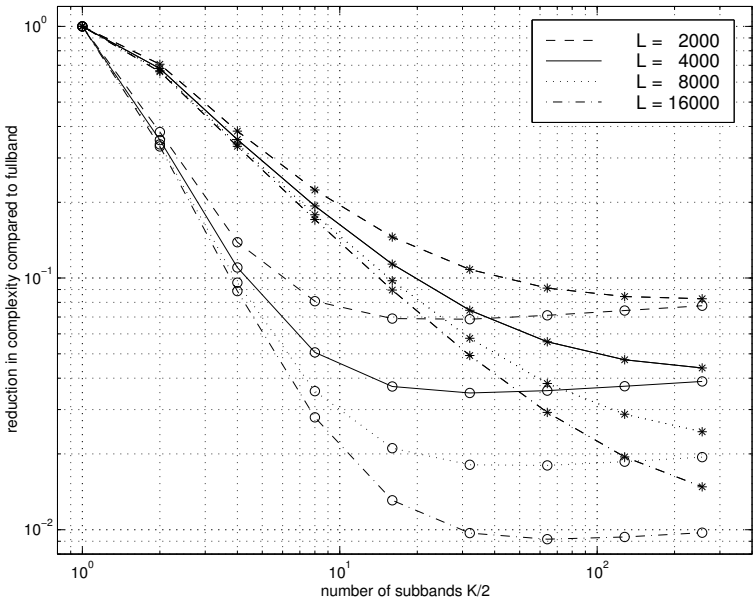

Figure 6.3: Relative cost $C_{\text{tot}}^{\text{GDFT}}/C^{(f)}$ as a function of the number of subbands $K/2$ for various given lengths $L_a^{(f)}$ of the equivalent fullband model and uniform ($*$) and concentrated ($\circ$) tap-profiles.

Fig. 6.3. As discussed in Sec. 4.4, the cost for the actual subband processing is identical, however the filter bank operation requires approximately twice the number of multiplications. Therefore, the curves behave similarly to Fig. 6.3 whenever the cost for filter bank operations is small relative to the computational cost of the subband processing, i.e. for small channel numbers $K/2$ and very long response lengths $L_a^{(f)}$. Otherwise, SAF systems using GDFT filter banks and complex arithmetic are clearly advantageous.

Fig. 6.5 displays the cost ratios achievable when critically sampled filter banks are used, yielding the computational complexity derived in (6.4). Compared to the previous SSB example, the higher decimation ratio of $K/2$ clearly cannot compensate for the cost introduced by the required cross-terms, and the cost performance is generally worse than for the SSB case in Fig. 6.4, and far behind the cost reduction achieved for the GDFT case in Fig. 6.3.

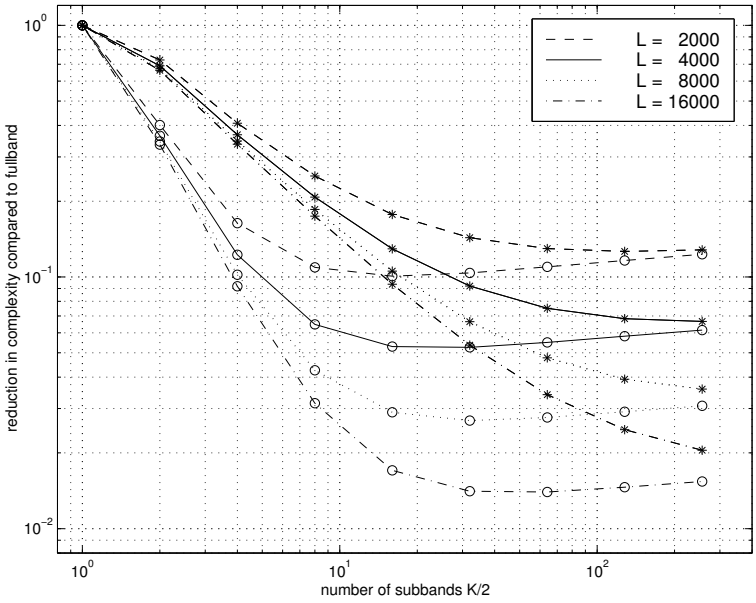

Figure 6.4: Relative cost $C_{\text{tot}}^{\text{SSB}}/C^{(f)}$ as a function of the number of subbands $K/2$ for various given lengths $L_a^{(f)}$ of the equivalent fullband model and uniform ($*$) and concentrated ($\circ$) tap-profiles.

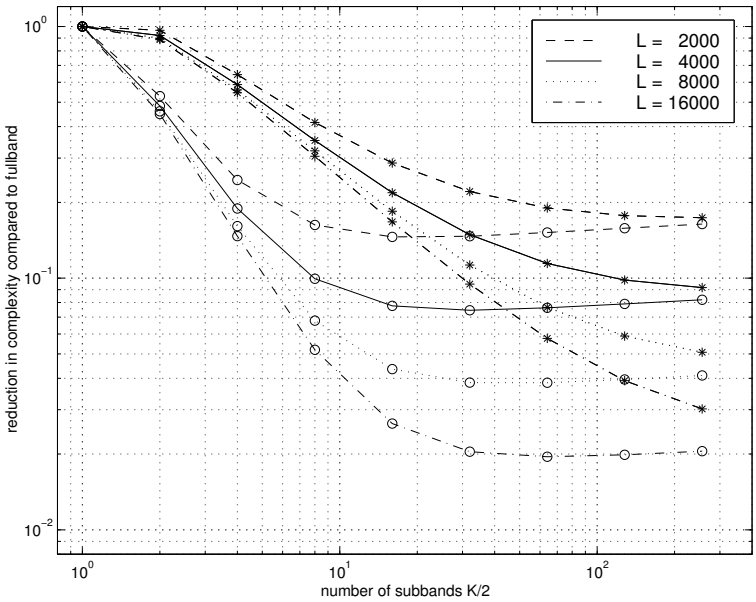

Figure 6.5: Relative cost $C_{\text{tot}}^{\text{DCT}}/C^{(f)}$ as a function of the number of subbands $K/2$ for various given lengths $L_a^{(f)}$ of the equivalent fullband model and uniform ($*$) and concentrated ($\circ$) tap-profiles.

6.2.2 Equivalent Fullband Model Length Based on Constant Complexity

An interesting case arises when (6.2) – (6.4) are solved for the equivalent fullband model length $L_a^{(f)}$ in dependency of the overall computational cost. Thus, for a fixed number of computations, which are for example given by the benchmark performance of a specific DSP chip, it is possible to predict which model length the overall SAF system is capable to provide for different subband implementations (oversampled GDFT, oversampled SSB modified GDFT, and critically sampled cosine modulated filter bank) and a variable number of subbands $K/2$.

For SAF systems with complex subbands produced by GDFT filter banks, the fullband equivalent model length in dependency of the available number of computations C_{tot} can be derived from (6.2) by rearrangement. In Fig. 6.6, these equivalent fullband lengths are depicted relative to the length of an NLMS implementation in the fullband with $L = (C_{\text{tot}} - 3)/2$. As in Sec. 6.2.1, it is distinguished between the two cases of "uniform" and "concentrated" tap-profile. Thus, for a given benchmark performance C_{tot} and a variable tap-profile, the true increase in the fullband model length will lie between these two marginal cases indicated in Fig. 6.6.

Fig. 6.7 shows the same curves for a real valued SAF system using SSB modified GDFT filter banks. Clearly noticeable, the groups of curves are wider spread and the increase in model length for low benchmarks C_{tot} is not as good compared to Fig. 6.6. This is again due to the doubled cost of the filter bank operation, which has a stronger influence if the complexity for the subband processing is rather low.

The relative increase in model length for a real valued SAF system based on critically decimated cosine modulated subbands is illustrated in Fig. 6.8. Due to the number of computations required for the cross-terms, the resulting gain in filter length is not only further spread for the different given computational complexities C_{tot}, but also drops for a high number of subbands $K/2$. The explanation is that the filter bank operations become so costly for high $K/2$, that there is hardly any computational power left to perform the subband processing. A similar behaviour could be demonstrated for the curves depicted in in Fig. 6.6

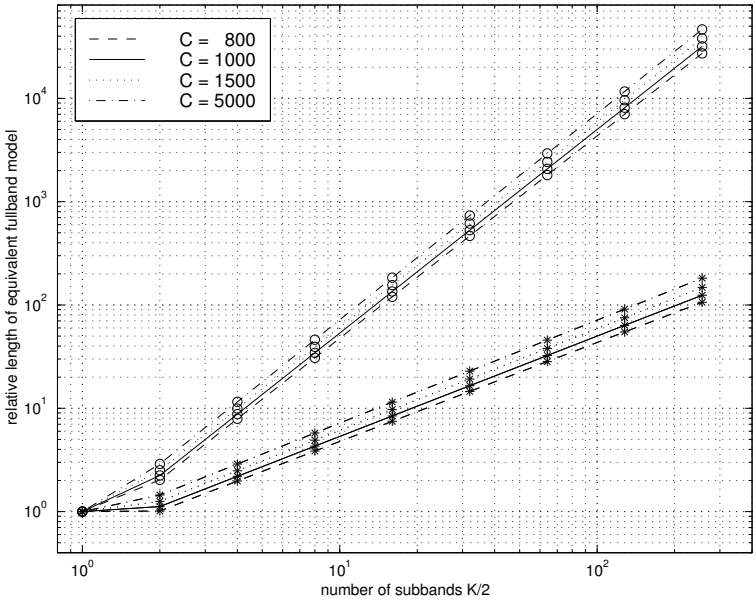

Figure 6.6: Relative equivalent fullband model length $L_a^{(f)}/L$ of an SAF system with GDFT modulated filter banks as a function of the given total complexity C_{tot} and the number of subbands $K/2$ for $(*)$ and concentrated $(\circ)$ tap-profiles.

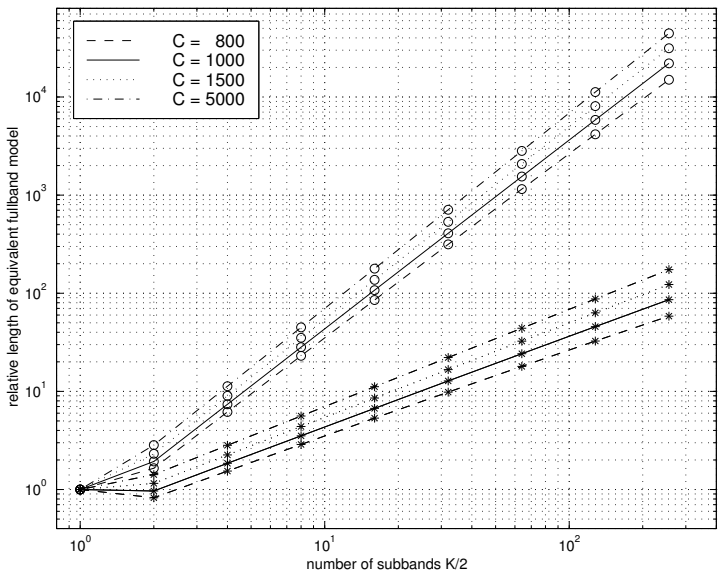

Figure 6.7: Relative equivalent fullband model length $L_a^{(f)}/L$ of an SAF system with SSB modified GDFT modulated filter banks as a function of the given total complexity C_{tot} and the number of subbands $K/2$ for $(*)$ and concentrated $(\circ)$ tap-profiles.

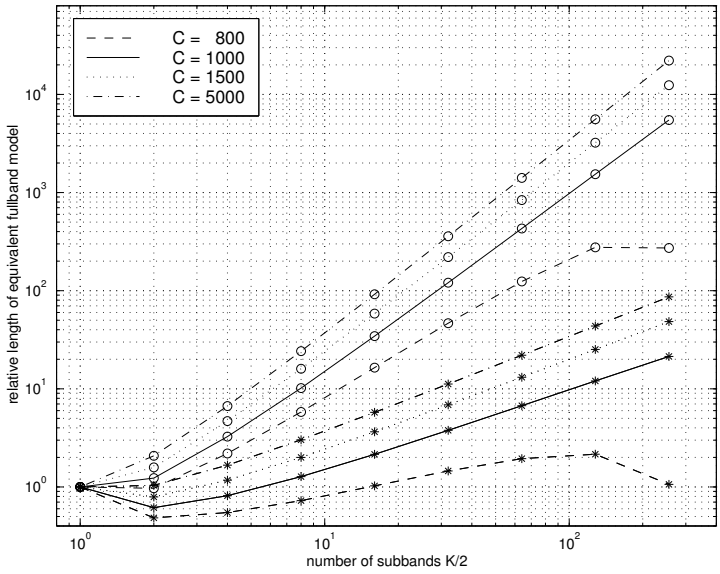

Figure 6.8: Relative equivalent fullband model length $L_a^{(f)}/L$ of an SAF system with critically sampled cosine modulated filter banks as a function of the given total complexity C_{tot} and the number of subbands $K/2$ for $(*)$ and concentrated $(\circ)$ tap-profiles.

and in Fig. 6.7, if only the $K/2$ was selected to be high enough.

The examples given here used an NLMS algorithm, which exhibits an order of complexity that is linear in the adaptive filter's length. For other algorithms as introduced in Chap. 2, similar curves can be determined by inserting the appropriate complexity as discussed in Sec. 4.4 into (6.2) – (6.4). This enables us to judge the efficiency of a certain filter bank operation in combination with the desired algorithm and thus helps to derive the required numbers of subbands for an SAF system to be acceptable for a specific application.

6.3 Tap-Profile Adaptation

Motivated by the likely increase in efficiency when adopting non-uniform SAF lengths, we now look into schemes of how to determine the optimum tap-profile below. For adaptive methods, we proceed with a description for a tap re-distribution mechanism, which can be driven by a selection of criteria briefly introduced.

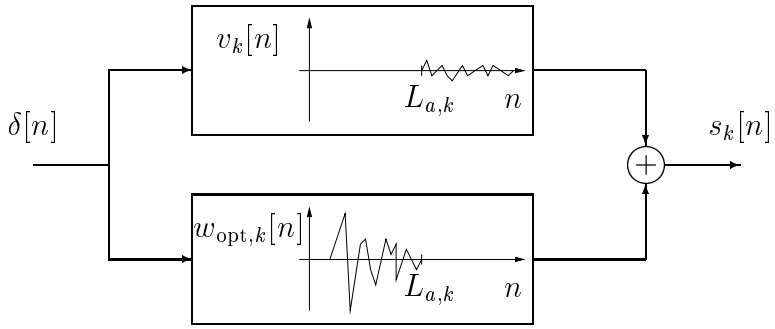

Figure 6.9: Separation of the optimum filter $w_{\mathrm{opt,k}}[n]$ into an identifiable part, $w[n]$, and an unidentifiable component, $v_k[n]$ due to model truncation at $n = L_{a,k}$.

6.3.1 Optimum Tap-Profile

6.3.1.1 Minimum Subband MSE

The minimum mean squared error (MSE) in the kth subband is given by

$$\mathcal{E}\left\{\left|e_k[n]\right|^2\right\} = \mathcal{E}\left\{\left(d_k[n] - y_k[n]\right)\left(d_k[n] - y_k[n]\right)^H\right\} \tag{6.5}$$

with signals defined as in Fig. 6.2. In particular, the desired signal $d_k[n]$ can be expressed in terms of a system $s_k[n]$ representing the unconstrained (in terms of filter length) Wiener solution for the subband adaptive filter, and an observation noise term $z_k[n]$ including true observation noise and artifacts like aliased signal components,

$$d_k[n] = \mathbf{s}_k^H \mathbf{x}_{k,n} + z_k[n] \quad . \tag{6.6}$$

The output of a filter of length $L_{a,k}$ which is optimal in the MSE sense is given by

$$y_k[n] = \mathbf{w}_{\mathrm{opt},k}^H \mathbf{x}_{k,n} \quad . \tag{6.7}$$

By defining the mismatch between the unconstraint optimum solution, $\mathbf{s}_k[n]$, and the constraint optimum solution, $\mathbf{w}_{\mathrm{opt},k}$, as $\mathbf{v}_k = \mathbf{s}_k - \mathbf{w}_{\mathrm{opt},k}$ as illustrated in Fig. 6.9, the minimum MSE (MMSE) in the kth band, $\xi_{\mathrm{MMSE},k}$, is denoted as

$$\xi_{\mathrm{MMSE},k} = \mathcal{E}\left\{\left|e_k[n]\right|^2\right\}\Big|_{\min} \tag{6.8}$$

$$= \mathcal{E}\left\{\left(\mathbf{v}_k^H \mathbf{x}_{k,n} + z_k[n]\right)\left(\mathbf{v}_k^H \mathbf{x}_{k,n} + z_k[n]\right)^H\right\} \quad . \tag{6.9}$$

Under the assumption that the observation noise $z_k[n]$ has zero mean and is uncorrelated with the input signal $x_k[n]$, and both $z_k[n]$ and $x_k[n]$ are wide sense stationary, the subband MMSE yields

$$\xi_{\mathrm{MMSE},k} = \mathcal{E}\left\{\mathbf{v}_k^H \mathbf{x}_{k,n} \mathbf{x}_{k,n}^H \mathbf{v}_k\right\} + \mathcal{E}\{z_k[n] z_k^*[n]\} \tag{6.10}$$

$$= \mathbf{v}_k^H \mathcal{E}\left\{\mathbf{x}_{k,n} \mathbf{x}_{k,n}^H\right\} \mathbf{v}_k + \sigma_{z_k z_k}^2 \quad . \tag{6.11}$$

Let us further assume that the analysis filter bank is ideal and performs a sufficiently fine decomposition such that the input signal in the kth subband, $x_k[n]$, is approximately decorrelated. Therefore the auto-correlation matrix $\mathbf{R}$ of the kth subband input signal can be approximated as

$$\mathbf{R}_{x_k x_k} = \mathcal{E}\left\{\mathbf{x}_{k,n} \mathbf{x}_{k,n}^H\right\} \approx \sigma_{x_k x_k}^2 \cdot \mathbf{I} \quad . \tag{6.12}$$

Using this assumption, the MMSE in (6.11) can be written as

$$\xi_{\mathrm{MMSE},k} = \sigma_{x_k x_k}^2 \mathbf{v}_k^H \mathbf{v}_k + \sigma_{z_k z_k}^2 \quad . \tag{6.13}$$

If the mismatch vector $\mathbf{v}_k$ is expanded,

$$\xi_{\mathrm{MMSE},k} = \sigma_{x_k x_k}^2 \cdot \sum_{n=L_{a,k}}^{\infty} \left|s_k[n]\right|^2 + \sigma_{z_k z_k}^2 \quad , \tag{6.14}$$

it becomes clear that the approximated MMSE depends on the energy of the residual impulse response of the unknown system after model truncation, weighted by the variance of the input signal and biased by the noise variance $\sigma_{z_k z_k}^2$.

6.3.1.2 Minimization of Global MSE

Considering that the filter banks employed in an SAF system, as for example shown in Fig. 6.2, implement tight frame decompositions, (3.19) guarantees a fixed energy transfer between the fullband and the different subband signals of the decomposition. If we further assume that the SAFs operate in steady-state, the frame equation can be written for the error signals as

$$\sum_{n=N_1}^{N_2} e^2[n] = \frac{1}{A} \cdot \sum_{k=0}^{K-1} \sum_{n=N_1/N}^{N_2/N} e_k[n] e_k^*[n] \tag{6.15}$$

$$= \frac{2}{A} \cdot \sum_{k=0}^{K/2-1} \sum_{n=N_1/N}^{N_2/N} e_k[n] e_k^*[n] \quad , \tag{6.16}$$

where the samples in fullband and subbands have been evaluated over a fullband interval of sufficient length N_2-N_1, which in the subbands is accordingly shorter by the decimation factor N. The constant A is the frame bound of the tight frame and is equal to the oversampling ratio, $A = \mathrm{OSR} = K/N$. By taking expectations $\mathcal{E}\{\cdot\}$ of both sides, we yield

$$\sum_{n=N_1}^{N_2} \mathcal{E}\left\{e^2[n]\right\} \;=\; \frac{2N}{K} \cdot \sum_{k=0}^{K/2-1} \sum_{n=N_1/N}^{N_2/N} \mathcal{E}\left\{\left|e_k[n]\right|^2\right\} \quad . \tag{6.17}$$

Assuming steady-state behaviour of the adaptive filters and ergodicity of the involved signals, the expectation values can be regarded as constants over time. Therefore, the sums over n can be simplified, and finally an expression for the fullband MSE has been reached:

$$\mathcal{E}\left\{e^2[n]\right\} = \frac{2}{K} \cdot \sum_{k=0}^{K/2-1} \mathcal{E}\left\{\left|e_k[n]\right|^2\right\} \quad . \tag{6.18}$$

Although this result may seem rather obvious in the uniform case, its modification for non-uniform subband signals [69] is interesting, as it introduces fixed weightings for the different subband contributions to the variance of the reconstructed error signal [162].

Minimizing the global MSE obviously leads to the problem of appropriately minimizing the $K/2$ subband MSEs. Since the task is to vary the tap-profile while the overall complexity of the SAF system remains constant, this minimization can be formulated as a constraint optimization problem:
Minimize the subband MSEs

$$\min_{\mathbf{w}_k} \left\{\mathcal{E}\left\{\left|e_k[n]\right|^2\right\}\right\} \qquad \forall k \in \{0, K/2-1\} \tag{6.19}$$

subject to the constraints

$$\mathcal{E}\left\{\left|e_i[n]\right|^2\right\} \;\stackrel{!}{=}\; \mathcal{E}\left\{\left|e_j[n]\right|^2\right\} \qquad \forall i,j \in \{0, K/2-1\}, \tag{6.20}$$

$$\sum_{K=0}^{K/2-1} L_{a,k} \;\stackrel{!}{=}\; const. \tag{6.21}$$

For a fixed solution, this constraint optimization problem could be solved using standard optimization techniques, e.g. Lagrange [18].

Here, we are looking for an adaptive solution over the global MSE by controlling the filter lengths. Thus, if the subband errors converge to the subband MMSEs, and we can adjust the tap profile such that these errors are all of the same size, the global error will converge to its minimum. However, this decision may be unwillingly, e.g. in the presence of observation noise due to (6.14), or willingly biased, e.g. by introducing a weighting in (6.18) to account for psychoacoustic considerations [34, 158].

6.3.2 Tap-Distribution Mechanism

For adapting the tap profile of subband adaptive filters, Ma *et al.* [91] and Sugiyama *et al.* [143] provide two approaches. Both have in common to modify the tap profile every Q samples, such that every filter is shortened by ΔL taps and the pool of $\Delta L \cdot K/2$ freed taps is then redistributed by

$$L_{a,k}[n/Q+1] \;=\; L_{a,k}[n/Q] \;-\; \Delta L \;+\; \frac{\Delta L \cdot K}{2} \cdot \frac{(c_k[n/Q])^p}{\sum_{k=0}^{K/2-1}(c_k[n/Q])^p} \qquad (6.22)$$

according to an appropriate criterion $c_k[n/Q]$, which reflects a measure of how well the adapted filter in the kth subband performs. Two such measures will be introduced in Sec. 6.3.3. The criterion $c_k[n/Q]$ in (6.22) is normalized using a p-norm such that the sum over all $K/2$ criteria yields unity, and hence the total number of taps is preserved. However, this only presents a possibility; in the literature as well as within the experimentation in Sec. 6.4, only the case $p = 1$ has been surveyed.

The algorithms in [91, 143] use complex additional exchange rules to avoid fractional values in (6.22) while preserving the overall number of coefficients to be constant for all times n. The approach employed here keeps a fractional record for the tap-profile, which by normalization can be easily stabilized against the accumulation of rounding errors. Finally the tap-profile employed during the next Q subband sampling periods is a round-off version of this fractional record.

A vital assumption for (6.22) to converge is that the ideal subband impulse response is decaying. This ensures that the subband error variance is inversely proportional to the length $L_{a,k}$ of the SAFs. As the unknown systems may involve a delay (e.g. in acoustic room impulse responses due to the transport delay

between loudspeaker and microphone) or the desired signal is delayed to enable adaptation, it has to be made sure that a minimum number of taps remain in each SAF to match and model at least that delay.

For critically sampled SAF systems based on DCT-IV modulated filter banks, the tap-profile of both the main and cross-terms could be adapted [170]. Concerning the cross-terms however, a required minimum number of coefficients in each band usually allows only few changes and therefore does not give much benefit.

6.3.3 Distribution Criteria

How can we estimate how well the adaptive filter in the kth subband performs with respect to the other $K/2$ subbands? In the following, we will look at two criteria based on the subband MMSE in (6.14), that will allow a formulation of an adaptive tap exchange between subbands in Sec. 6.3.2. However, we will also see that the previously introduced global optimization is open to interpretations.

6.3.3.1 Error-based Performance Measure.

The first approach to a criterion is based on a direct estimate of the subband MSEs. First introduced in [91], the measure c_k is an estimate of the error power or variance, $\hat{\sigma}^2_{e_k e_k}$ over the last R subband samples,

$$c_k[n/Q] \;=\; \hat{\sigma}^2_{e_k e_k} = \frac{1}{R}\sum_{r=0}^{P-1} e_k[n-r]\cdot e_k^*[n-r] \quad . \tag{6.23}$$

To obtain a reasonable estimate, firstly the interval R has to be sufficiently large. Secondly, ideally this measurement should only take place at times when the adaptive filters have already reached their steady-state operation, i.e. ideally $R < Q$.

Problems arise in the presence of coloured observation noise. Since the observation noise power $\sigma^2_{z_k z_k}$ in (6.14) is not influenced by the filter length, a tap-distribution algorithm using this criterion would dedicate most of the taps to subbands with a high observation noise, although the source for the error level is not model truncation. This is an ideal example for a situation in which this tap-adaptation criterion would fail to provide an unbiased solution [135, 170].

6.3.3.2 Reduced Criterion

Eqn. (6.14) has been exploited to create a criterion similar to [143], whereby the power of the last S taps of an adaptive filter is taken to estimate the truncation error, weighted by a measurement of the input signal power over a window of R samples,

$$c_k[n/Q] \;=\; \underbrace{\frac{1}{R}\sum_{r=0}^{R-1} x_k(n-r)x_k^*(n-r)}_{\text{estimate of signal power}} \cdot \underbrace{\frac{1}{S}\sum_{s=0}^{S-1} w_k\left[L_{a,k}[n]-s\right] w_k^*\left[L_{a,k}[n]-s\right]}_{\text{estimate of truncation error}}. \tag{6.24}$$

Although clearly the influence of observation noise has been suppressed, this criterion introduces a twofold bias in the MSE estimate for (6.14). Firstly, bands with shorter decay will be favoured since their last S untruncated coefficients will be more powerful than those of a longer decay, if decays are approximately exponential. Secondly, a colouring of input signal power will somewhat deviate the result from what has previously been assumed as "optimum" for the identification of an unknown system. The motivation for a variable tap-profile has originally been to balance the filter lengths of the SAFs according to the decay of the unknown system in different frequency bands. If the specific application is less targeted on the identification of an unknown system, but the cancellation of some unwanted signal, as e.g. the far end speaker's echo in AEC, then minimization of (6.24) across all SAFs will be "optimum" in the sense of a minimum variance of the fullband reconstructed error signal, not necessarily a "best-fit" for the unknown system as indicated in Fig. 6.1.

Compared to the error-based criterion (6.23), the reduced criterion can be computed with a minimum overhead over the regular update procedure of the SAFs. While the criterion in Sec. 6.3.3.1 requires to keep track of R past values of the error signal (which otherwise does not need to be memorized), the evaluation of (6.24) only performs an estimate of the input power, which is similarly required in the normalization step of the NLMS algorithms. Finally, the weights $\mathbf{w}_k$ are readily accessible for the approximation of the truncation error. While the criterion in [143] is a computationally intensive average of the right hand side of (6.24) over the last P iterations, the approach presented above only

introduces a very low additional computational overhead of $(S+3)/NR$ multiplications and $K/(2NR)$ divisions per fullband sampling period for a complex subband implementation.

6.4 Simulations

This section will give some examples and insight into the benefit and behaviour of variable tap-profiles for SAF systems. First, a system identification problem will be discussed, whereby for a realistic result, a fixed computational benchmark is used to demonstrate the efficiency of subband adaptive filtering, and how a variable tap-profile can further enhance its performance. A brief comparison of the two tap-assignment criteria presented in Sec. 6.3.3 will conclude this section.

6.4.1 Performance at Given Benchmark

To obtain a realistic benchmark figure, we assume a Motorola DSP56002 processor [105], capable of 20 million multiply accumulate (MAC) operations per second. Supposing that about 50% of the instruction cycles are required for overheads like data transfer with ADC/DAC devices, interrupt handling, and indexing, at a sampling rate of 16kHz there will be approximately $C_{\text{tot}} = 1250$ MACs available per sampling period.

Re-arranging equations (6.2) – (6.4), the total number of available filter coefficients in the SAFs, L_{tot}, can be determined for SAF systems based on oversampled GDFT, oversampled SSB modified GDFT, and critically sampled DCT-IV modulated filter banks. The according value for each SAF system type are stated in Tab. 6.1. For the DCT-IV modulation based SAF system, only the total number of coefficients in the main terms is given.

The unknown system $S(z)$ to be identified by the different adaptive architectures is an all-pole model

$$S(z) = A \cdot \sum_{i=0}^{I-1} \frac{1}{1 - 2\rho_i \cos(\theta_i) z^{-1} + \rho_i^2 z^{-2}} \tag{6.25}$$

where for this specific case the 5 poles described in Tab. 6.2 have been selected.

The gain factor A was chosen such that the impulse response $s[n] \circ\!\!-\!\!\bullet\, S(z)$

method	tap-profile	L_{tot}	$L_a^{(f)}$	$10\log_{10}(\sigma_{dd}^2/\sigma_{ee}^2)$	$10\log_{10}\|\|s-w\|\|_2^2$
fullband	—	624	624	-3.11 dB	2.20 dB
DCT-IV	uniform	1285	1200	-2.28 dB	0.39 dB
	adaptive	1285	2400	6.57 dB	-5.42 dB
SSB	uniform	3187	2900	15.75 dB	-11.76 dB
	adaptive	3187	6600	48.96 dB	-48.80 dB
GDFT	uniform	1887	3400	21.21 dB	-12.43 dB
	adaptive	1887	6150	48.73 dB	-47.83 dB

Table 6.1: Comparison of fullband and SAF systems for system identification of long impulse response at a fixed computational benchmark in terms of noise reduction and model error.

i	0	1	2	3	4
θ_i/π	0.1	0.45	0.48	0.6	0.9
ρ_i	0.9987	0.999	0.85	0.9	0.8

Table 6.2: Angles θ and radii ρ of poles of unknown system $S(z)$.

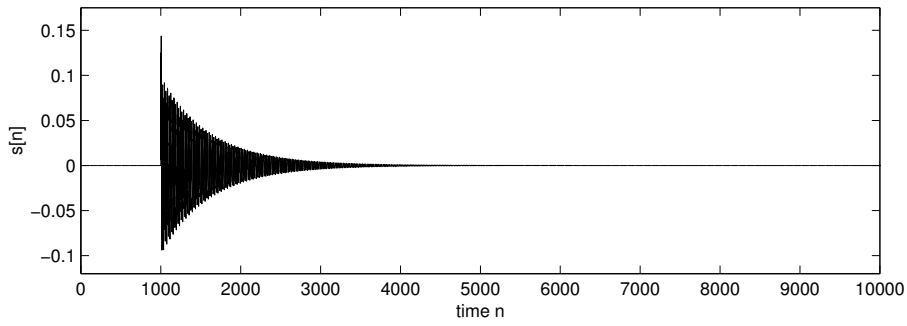

Figure 6.10: Impulse response $s[n]$ of the unknown system.

(shown in Fig. 6.10) satisfies $\|s[n]\|_2 = 1$, i.e. possesses unit energy. For the different SAF systems, the unknown system was given an additional delay of 1000 taps to avoid non-causality of the subband responses to be identified. No delay was set for the system identification using the fullband NLMS adaptive filter. For all simulations, the normalized step size of the NLMS was set to $\tilde{\mu} = 0.9$.

Critically Sampled SAF System. The simulation results for adaptive system identification in critically sampled DCT-IV modulated subbands is shown in Fig. 6.11. The prototype filter used here is an iterated halfband design listed in Tab. 4.2 for $K = 16$. The learning curves in Fig. 6.11(a) are given for the two cases of fixed uniform and adaptive tap-profile using the error criterion in (6.23). For both cases, the resulting fullband equivalent model length $L_a^{(f)}$ is supplied in Tab. 6.1. Clearly for uniform tap-distribution, this model length is not long enough to allow the SAF system to properly adapt, since the observation noise level caused by the truncation is too high. For a similar reason, the fullband identification completely fails. With a variable tap-profile, the algorithm manages to reduce the error variance by a small amount, since the tap-profile is adapted to a more suitable form for this problem, as indicated in Fig. 6.11(c). The PSD of the final MSE in Fig. 6.11(b) clearly shows how the error spectrum is further reduced with an adaptive profile in the two bands $k = 0$ and $k = 3$ dominating the overall error. Note that band edges are marked by vertical dashed lines.

Real Valued Oversampled SAF System. Fig. 6.12 presents the SAF system identification results using SSB modified GDFT filter banks with $K/2 = 8$ subbands and decimation by $N/2 = 7$, and the prototype design of Tab. 4.3(d). In general, the results are far superior to the DCT case in Fig. 6.11, since the cross-terms required in the DCT based SAF systems are as costly as the complete filter bank operation, and not enough calculations remain to allow sufficient SAF lengths. As in the SSB modified GDFT based system no cross-terms are required, the system can dedicate a much higher number of computations to adaptive filtering.

Note in particular how in the SSB case the error PSD in Fig. 6.12(b) is balanced when the tap-profile adaptation is introduced. While the error spectrum

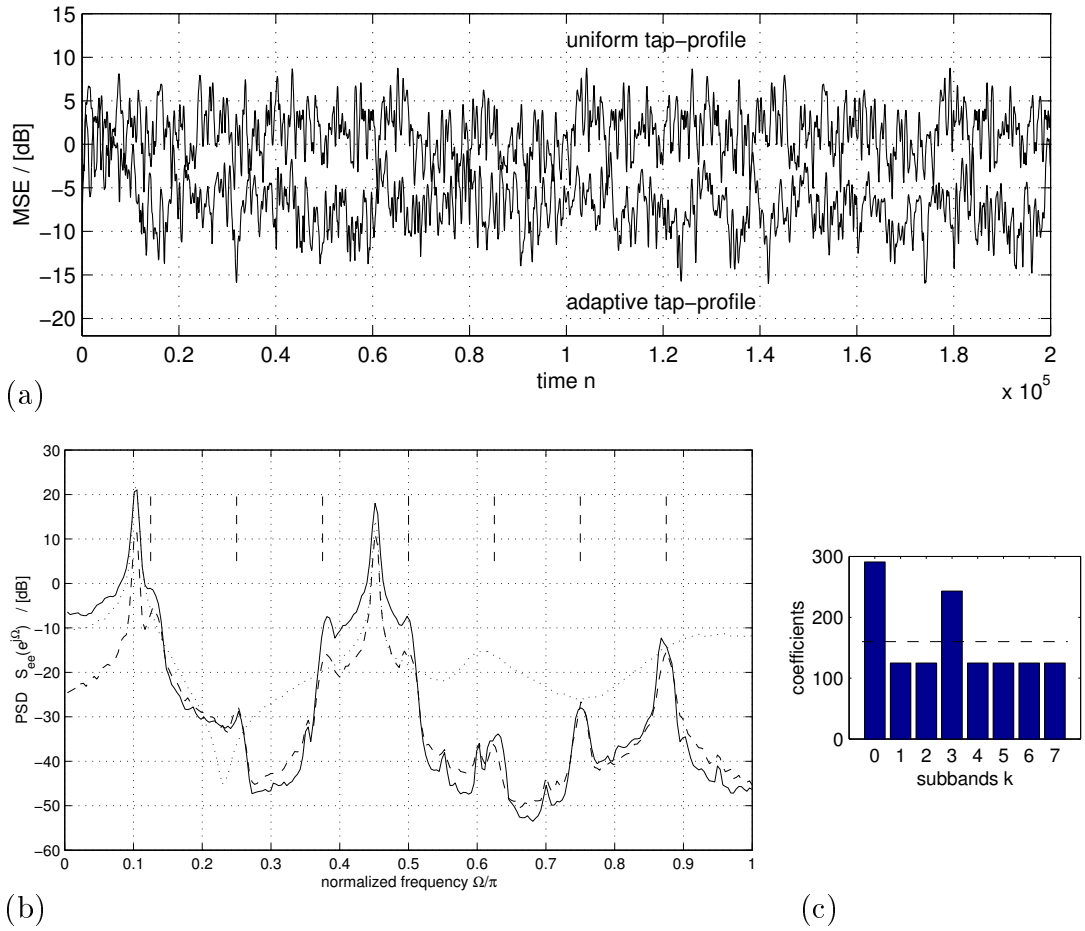

Figure 6.11: $K/2 = 8$ subband SAF system with critically sampled DCT-IV modulated filter banks: (a) locally averaged squared reconstructed fullband error; (b) PSD of desired signal (dotted) and of final error for uniform (solid) and adaptive (dashed) tap-profile; (c) uniform (straight line) and adapted (bar plot) tap-profile.

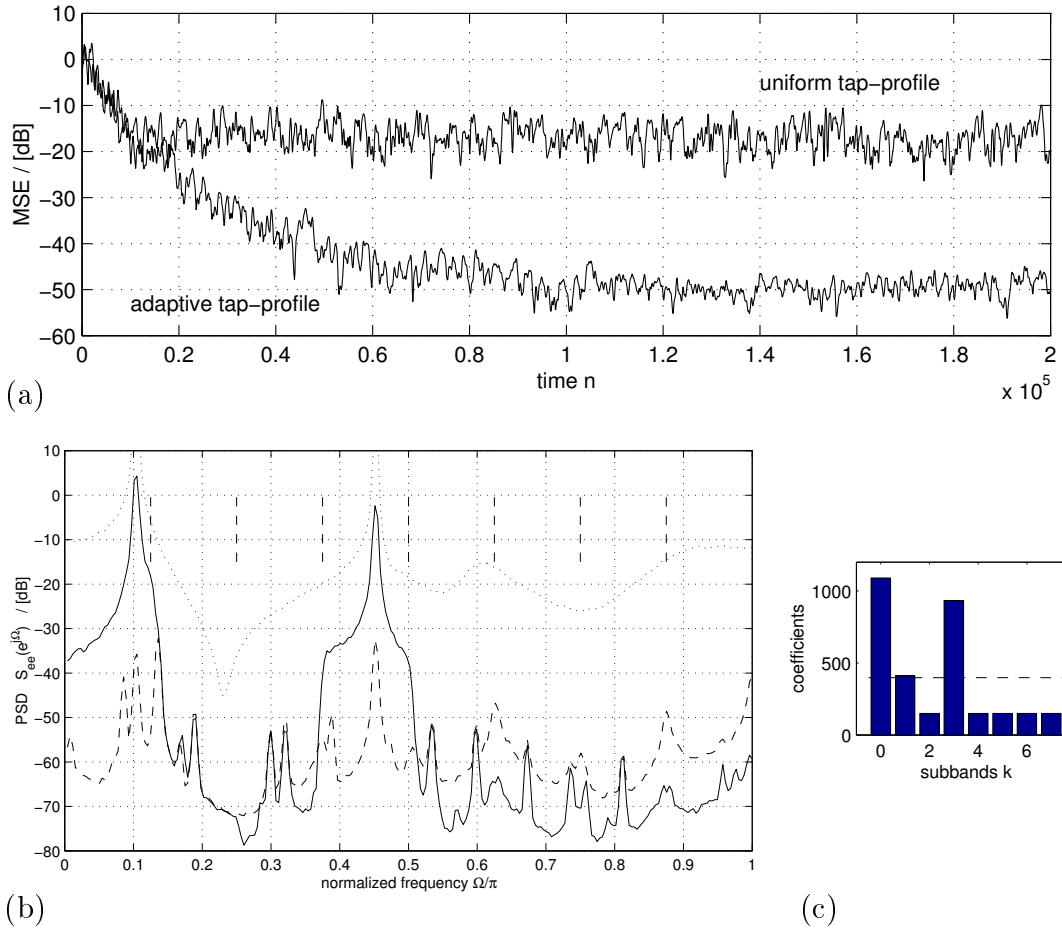

Figure 6.12: $K/2 = 8$ subband SAF system with oversampled SSB modified GDFT filter banks: (a) locally averaged squared reconstructed fullband error; (b) PSD of desired signal (dotted) and of final error for uniform (solid) and adaptive (dashed) tap-profile; (c) uniform (straight line) and adapted (bar plot) tap-profile.

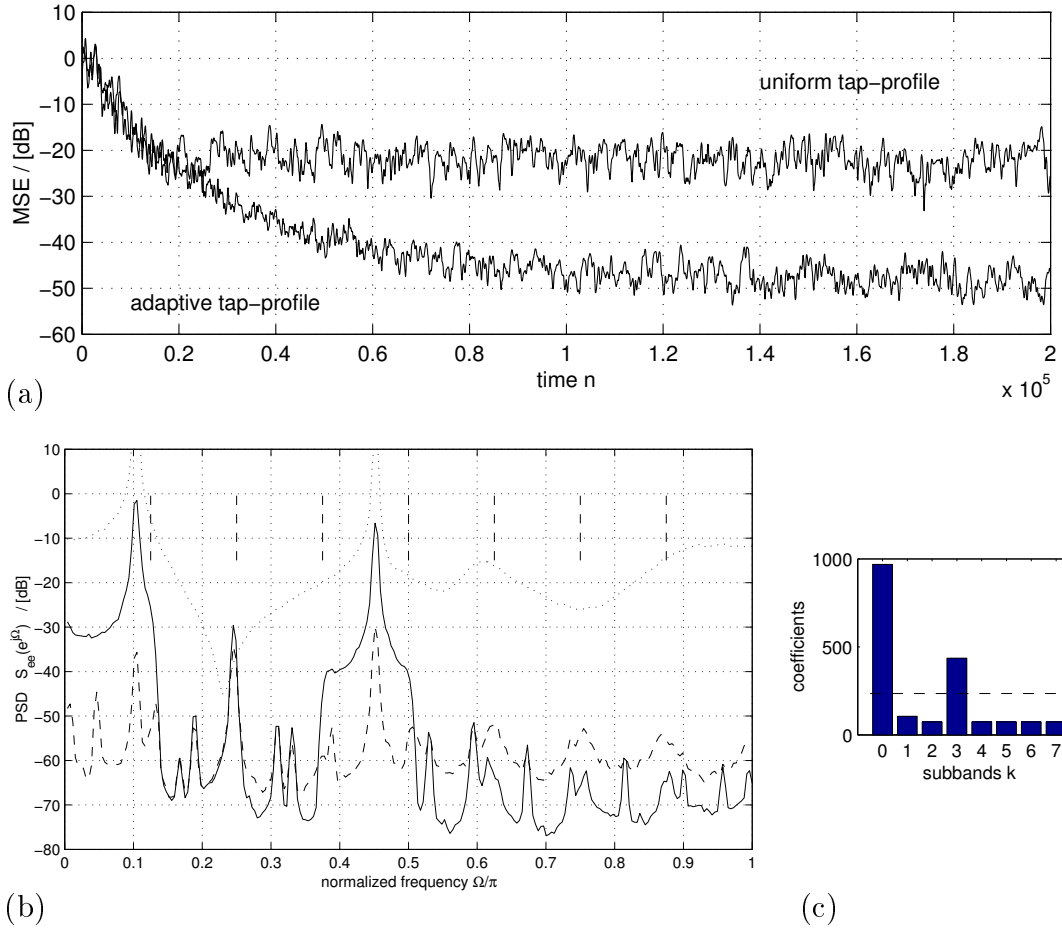

Figure 6.13: $K/2 = 8$ subband SAF system with oversampled GDFT filter banks: (a) locally averaged squared reconstructed fullband error; (b) PSD of desired signal (dotted) and of final error for uniform (solid) and adaptive (dashed) tap-profile; (c) uniform (straight line) and adapted (bar plot) tap-profile.

is slightly increased in unimportant bands due to the withdrawal of coefficients there, the error in the dominating bands can be more effectively suppressed, thus yielding a considerably enhanced noise reduction and a better accuracy for the identified fullband equivalent model, for which measures are stated in Tab. 6.1.

Complex Valued Oversampled SAF System. Results for a complex valued SAF system using a GDFT modulated filter bank, which are based on the same prototype as the SSB modified GDFT bank system discussed above, are given in Fig. 6.13. Although the overall number of coefficients is smaller than in the SSB case, the GDFT system is running at only half the sampling rate, and therefore

manages to achieve a better performance than the SSB for a uniform tap-profile. Again, the introduction of a variable tap-profile allows the balancing of the various subband errors as indicated in Fig. 6.13(b) and hence further reduces the fullband final MSE.

Truncation Error. To demonstrate that the main hindrance in the adaptation of the above SAF systems was in fact the model truncation due to the very long impulse response $s[n]$ of the unknown system, the errors of the equivalent reconstructed fullband model, $w[n]$, are plotted in Fig. 6.14. The fullband models have been calculated from the adapted subband responses (for the critically sampled system including the cross-terms) according to Sec. 5.3.1. Shown are the results for the three different SAF systems, each for uniform and adaptive tap-profile. The approximate lengths of the reconstructed fullband models $L_a^{(f)}$ are listed in Tab. 6.1. It is easy to appreciate that truncation is the main source of error, as no observation noise has been injected, and the SAR values for the prototypes are approximately 57 dB for all filter banks used. Since the truncation contributes to the MMSE, also the identifiable part of the impulse response will be noise corrupted due to the excess MSE yielded when using LMS-type algorithms.

6.4.2 Bias of Tap-Profile Adaptation

To give an example of the tap assignment algorithms' behaviour, we try to identify a slowly decaying system similar to previous examples, with a frequency response as shown in Fig. 6.15(a), using both the error based and reduced criterion discussed in Sec. 6.3.3. For identification, we employ an NLMS subband adaptive system operating in 8 critically decimated subbands, which are produced by DCT-IV modulated filter banks based on the prototype lowpass filter from Tab. 4.2 for $K = 16$. Factorized cross-terms have been included according to [53, 54] and Fig. 3.4.2.1, where the lengths of the adaptive cross-terms are set to one third of the initial uniform SAF length of the main terms.

Fig. 6.15(b) and (c) show the learning curves of the tap-profile evolving over time for a white noise (unit variance) excited system identification set-up with no added observation noise. Numbers at the right margin of each figure indicate the

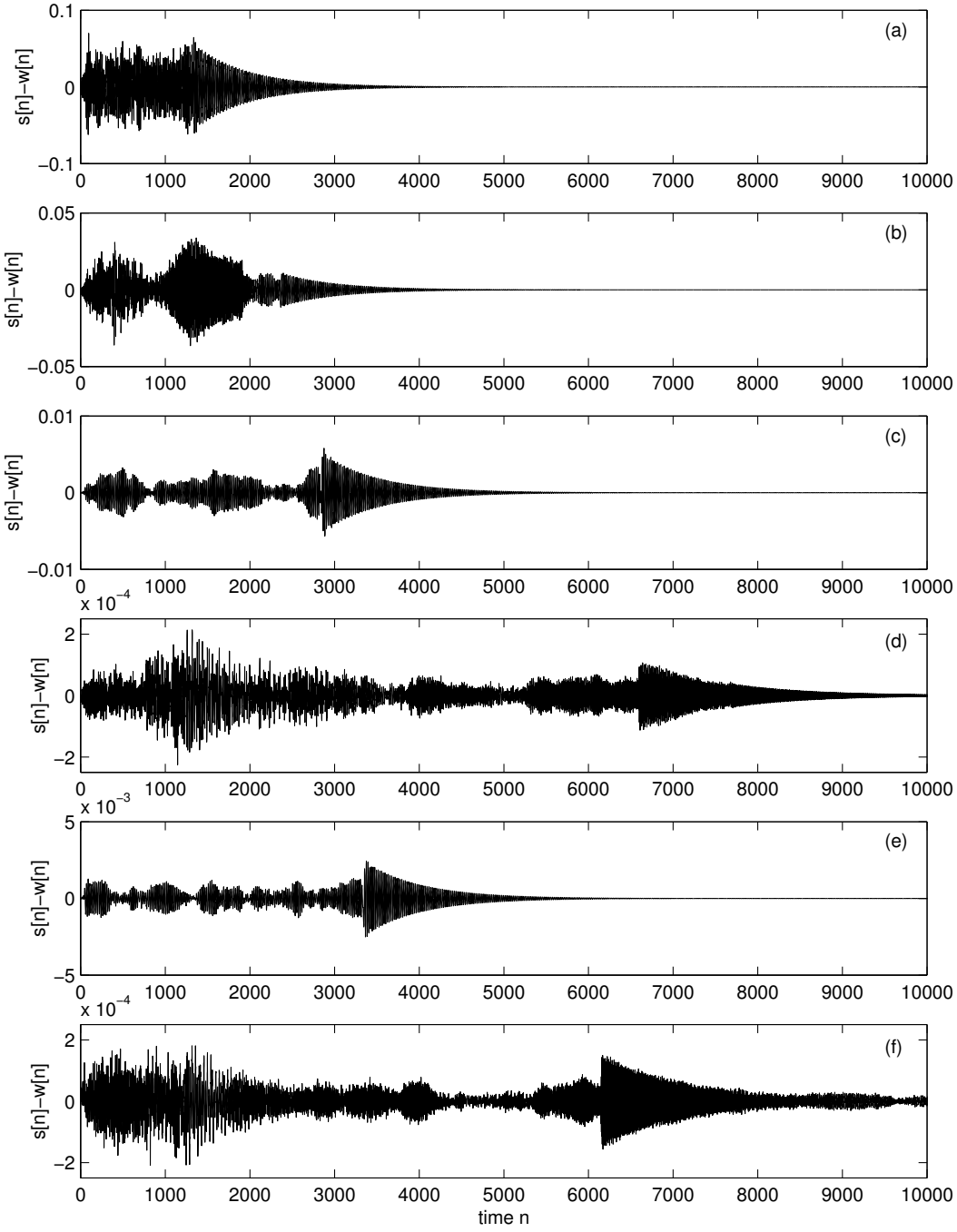

Figure 6.14: Error in the equivalent reconstructed fullband model: critically sampled SAF system with (a) uniform and (b) adaptive tap-profile; oversampled real valued SAF system with (c) uniform and (d) adaptive tap-profile; (e) oversampled complex valued SAF system with (e) uniform and (f) adaptive tap-profile.

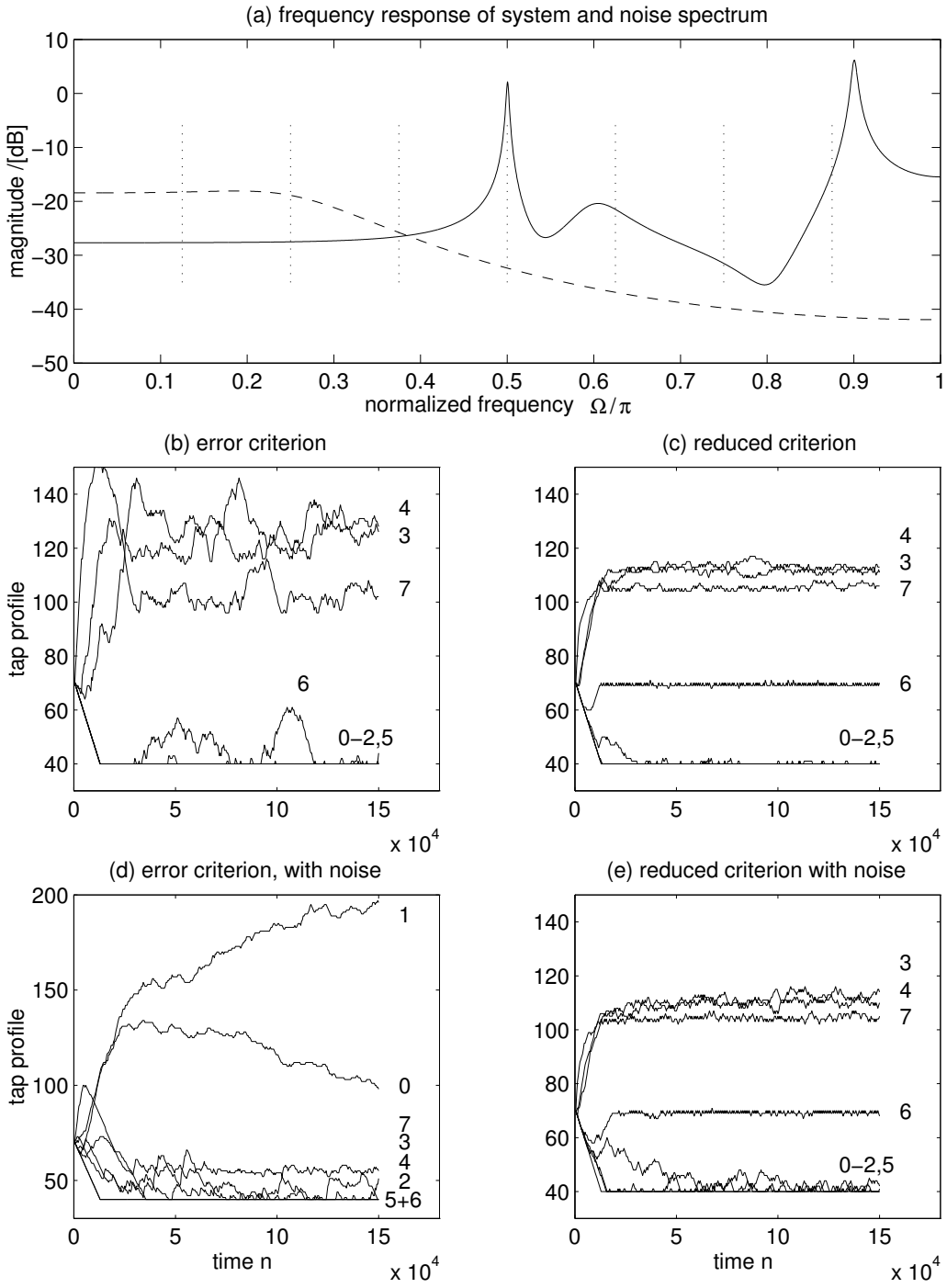

Figure 6.15: (a) Frequency response of unknown system to be identified (solid) and the PSD of the observation noise (dashed); band edges are plotted as vertical dotted lines; tap-profile trajectories for noiseless (b,c) and noisy (d,e) case for error and reduced criterion based tap distribution algorithms (taken from [170]).

criterion	error (6.23)	reduced (6.24)
noise free	50.7 dB	43.5 dB
noisy	15.0 dB	17.4 dB

Table 6.3: Noise reduction measures, $10\log_{10}(\sigma_{dd}^2/\sigma_{ee}^2)$, for the noise-free and noisy (SNR -18.5 dB) system identification examples given in Fig. 6.15 using adaptive tap-distribution based on two different criteria.

subband number k for each line, corresponding successively to the 8 frequency intervals specified in Fig. 6.15(a) by vertical dashed lines. Obviously, the noise free simulation behaves as expected, and with either criterion most taps are dedicated to the subbands for $k = 7$ containing one strong pole of the unknown system, and to $k = 3$ and 4, which share a strong pole sitting at the band edge $\Omega = \pi/2$.

The same system identification simulations are repeated with coloured observation noise added at -18 dB SNR to the desired signal; the PSD of the noise is plotted in Fig. 6.15(a) as a dashed line. The resulting trajectories of the 8 SAF lengths are depicted in Fig. 6.15(e) and (f). While the assignment behaviour of the reduced criterion of (6.24) is hardly influenced, the error based criterion [91] is completely biased by the observation noise. For the latter case, the tap distribution algorithm dedicates most adaptive filter coefficients to the bands $k = 0$ and 1, where the observation noise is spectrally strongest, although an increase in filter length cannot help to further reduce the error power.

The final reduction in error power achieved by the four different system identification simulations described above is given in Tab. 6.3. From these values, it becomes obvious that for the noise free case, the error based criterion outperforms the reduced criterion, which is likely to yield a bias as discussed in Sec. 6.3.3.2. With observation noise added, the reduced criterion however performs more robustly as seen in Fig. 6.15(f) and yields a higher noise reduction than the strongly biased error criterion.

6.5 Concluding Remarks

This chapter has been concerned with the efficient use of system resources by exploiting spectral properties of the unknown system or the input signal. In such an environment of spectrally unbalanced signals, the largest subband error dominates the accuracy and performance of the overall SAF system. This has motivated the idea of adopting a non-uniform tap-profile which is able to balance truncation errors occurring e.g. due to the spectrally different decay of the unknown system to be identified. A number of approaches found in the literature for both fixed and adaptive adjustment of the tap-profile have been reviewed.

Two extrema for distributing computations over the subbands have been analysed. The first extreme case is a uniform tap-profile, where each subband has the same time representation, which for uniform subband decompositions is equivalent for the SAFs to posses identical filter lengths and same number of computations per subband. The other extremum is formed by a concentrated tap-profile, where all computations are dedicated to one single subband. These extrema defined the performance margins for variable tap-profiles.

For the NLMS algorithm, the total cost of an SAF system based on different subband decompositions (oversampled GDFT, oversampled SSB modified GDFT, and critically sampled DCT-IV modulated filter banks) has been derived. Based on this, the performance margins have been calculated for two scenarios, where (i) the cost reduction for a fixed time representation of the SAF system and (ii) the time representation at fixed cost (e.g. given by the benchmark performance of a DSP) are of interest. For required cost reduction or increase in time representation, it is therefore possible to select an SAF system suitable for a particular application, specified by its parameters (filter bank type, number of subbands, decimation rate).

For an adaptive adjustment of the tap-profile, we have adopted a tap-distribution mechanism driven by a criterion for the performances of the different SAFs in the system. We have based our derivation for a suitable SAF performance measure on the minimization of the global error, which creates a background theory for distribution criteria reported in the literature. This has yielded a subband error based criterion, and a reduced criterion suppressing the bias introduced

by coloured observation noise. Their properties when employed to adjust the tap-profile of SAF systems have been demonstrated and verified by simulation.

The benefit of the subband approach and a possible further enhancement by tap-profile adaptation for adaptive filtering has been demonstrated in a series of examples, where a fixed computational benchmark was given for the identification of a very long impulse response. As a side effect, this has also highlighted the superior properties of oversampled subband approaches in terms of computational system complexity over the critically sampled case.

Chapter 7

Conclusions

7.1 Résumé

Motivated by the identification of long impulse responses, this thesis has discussed and compared subband adaptive filter structures based on complex and real valued oversampled modulated filter banks, their components, implementations, limitations, and design.

Adaptive Filter Algorithms. Adaptive filtering has been reviewed, with a focus on popular algorithms such as LMS, RLS, and affine projection. Some insight has been given into the derivation of these algorithms and their similarities, with the main emphasis on their computational complexity, and their convergence and tracking properties. In particular, the convergence speed of LMS-type algorithms was strongly affected by coloured input signals. Regarding the computational complexity, the only difference between real and complex valued implementations for the presented algorithms was the use of complex arithmetic, which in terms of real valued multiplications is simply an increase by a factor of four.

Background and Review of Adaptive Filtering in Subbands. Moving towards subband implementations, first basic multirate operations were introduced. The reason for reducing the sampling rate was based on two facts. Firstly, for band-limited signals the sampling rate could be lowered in accordance with the bandpass sampling theorem, where differences arose for the decimation of real

valued and complex valued signals. While for analytic or complex bandpass signals, decimation of a signal based on its bandwidth is unproblematic, for real valued signals bandpass sampling is bound by strict rules. Secondly, another legitimation for decimation was given based on orthonormal decompositions of a signal into a number of decimated subbands, which was extended to redundant decompositions representing frame expansions. This naturally led to filter banks implementing such signal expansions.

To analyse filter banks, we introduced two analysis methods: modulation description and polyphase representation. From the latter, efficient implementations of filter banks and the conditions for perfect reconstruction were derived. The modulation description approach was used to analyse subband adaptive filter (SAF) systems based on critically decimated perfect reconstruct (PR) filter banks, which resulted in the requirement of cross-terms at least between adjacent subbands due to aliasing. An example illustrating the corresponding time domain effect of "information leakage" was given.

To avoid cross-terms in the SAF structure, a number of different approaches were reviewed, including critically sampled systems based on non-PR filter banks with spectral loss or other distortions, and oversampled approaches. The latter covered complex valued and real valued filter banks. For real valued oversampled filter banks, two strategies where discussed to circumvent problems encountered with bandpass sampling: filter banks with non-uniform bandwidths and band-positions of the frequency bands, and a single-sideband modulation approach, whereby subbands are modulated into the baseband prior to decimation.

GDFT Filter Banks. Aiming for near PR filter banks only, we investigated a certain type of complex valued modulated filter bank based on a generalized DFT (GDFT) modulation. The generalization of the DFT modulation consisted of the inclusion of offsets in time and frequency indices to obtain a linear phase property and an odd-stacked positioning of the analysis filters' passbands. For real valued input signals, this allowed us to retain only half the number of complex valued subbands, based on redundancy considerations. For the synthesis filter bank, an

infinite number of solutions existed in the oversampled case. Here, the minimum-norm solution, i.e. the parahermitian or left pseudo-inverse of the analysis bank has been chosen. Backed by frame theory, this selection bore useful numerical properties such as improved robustness towards noise in the subband domain and a fixed energy relation between fullband and subbands, and practical advantages, as the synthesis prototype filter is identical to the one for the analysis bank.

Regarding implementation, starting from the polyphase representation for general non-integer oversampling, we derived a factorization into a real valued polyphase network, that only depended on the polyphase components of the prototype filter, and followed by a GDFT transform applying a complex rotation to the outputs of the polyphase network. This transform could be further factorized, such that it mainly reduced to the computation of a DFT, which could be realized by an FFT for fast evaluation. Thus, a highly efficient implementation was obtained.

The presented GDFT filter bank has been modified such that an SSB modulated real valued filter bank was implemented, circumventing the Weaver method. Due to the low complexity of the GDFT implementation, we thus obtained a fast Weaver-like SSB decomposition. For the same number of subbands, this filter bank required about twice the number of computations of the standard GDFT filter bank, and produced real valued subband samples at twice the rate.

To judge the overall computational complexity of implemented SAF systems, a comparison for the cost ratio between real and complex valued processing has been derived. While for example for linear algorithmic orders of subband processing (like LMS), both methods were shown to be equally costly, the complex implementation turned out to be more efficient by about a factor of two for a quadratic order of complexity (e.g. RLS).

Two methods have been introduced to obtain suitable prototype filters for GDFT and SSB modified GDFT filter banks. The first would construct prototype filters for filter banks with higher channel numbers (restricted to powers of two) by appropriate scaling of a halfband filter, which was accomplished by iterative expansion and interpolation. Secondly, criteria for perfect reconstruction and low aliasing level in the subband signals were derived in terms of the prototype

filter which enabled a fast converging iterative least squares optimization. A weighting between the two criteria allowed us to trade power complementarity against stopband attenuation.

Subband Adaptive Filter Performance. Novel limits for the power spectral density (PSD) of the error signal at the Wiener solution have been derived, based on the aliasing created in the filter banks, and a knowledge of the source models of the decomposed signals. This allowed us to state the minimum mean squared error (MMSE), which has approximated by an easy-to-apply measure (SAR — signal-to-aliasing ratio) describing the lower limit for the MSE solely based on the prototype filter of the filter bank. The equivalent fullband model of the overall SAF system has been derived from the adapted weights of the SAFs, and has been shown to be limited in its accuracy by the distortion function (i.e. the deviation from power complementarity) of the filter bank. Thus, the two main limits of final error performance could be directly linked to the design of the prototype filter.

A number of simulations were performed to verify the derived limits, for which the results matched remarkably well with the predicted quantities. Further experiments aimed to evaluate the convergence speed showed that SAF systems using an NLMS algorithm were almost insensitive to coloured input signals. While for white noise excitation, fullband algorithms gave a clear, but narrow advantage, for coloured input signals subband approaches considerably outperformed the fullband algorithm. Remarkably, the oversampling ratio was shown to have none or only little influence on the convergence speed of SAF systems. For the number of subbands, it turned out that, with regard to convergence speed, an optimum existed, given by a trade-off between the spectral separation of the coloured input signal, the spectral notches introduced by the analysis filters, and the different update rates and subband adaptive filter lengths.

Tap-Profile Adaptation. Finally, we have discussed the possibility of variable tap-profiles for subband adaptive filters. This enabled the application of more filter coefficients to subbands where they are required to identify an otherwise truncated model. Based on a global error minimization approach two

different distribution criteria were derived, of which the first attempted a direct minimization of the error. A second, reduced criterion for unbiased performance in the presence of coloured observation noise was introduced which presented a simplified algorithm compared to a similar method in the literature.

The performance of SAF systems with variable tap-profile was illustrated by noise-free and noisy simulations, which gave an account of the sensitivity and bias of the discussed algorithms. For system identification experiments with a spectrally balanced unknown system with a long impulse response, the benefit of variable tap-profile approach was clearly demonstrated. Also comparison for the efficiency of different SAF systems was performed, which was exercised using the NLMS algorithms as an example. This gave a clear indication of the advantage of oversampled SAF systems with low OSR over critically decimated systems with cross-terms.

7.2 Core Results

The main aim throughout this thesis was to achieve an efficient implementation for adaptive filter systems, for which we have chosen the subband approach. Therefore, the clear task was to find methods to ensure that both the subband decomposition and processing algorithms were as computationally efficient as possible.

Since subband processing is most efficient at low OSR, thus avoiding cross-terms but still operating close to the critical rate, this has to be accommodated by the filter banks. This has been enabled by deriving a highly efficient polyphase implementation of a complex valued modulated GDFT filter bank with a judicious selection of properties for non-integer OSRs. A real valued filter bank using an SSB modified GDFT bank allowed a highly efficient implementation of subband decompositions for real valued subband processing. The choice whether to perform real or complex subband processing is specific to the particular adaptive algorithm to be used, and can be answered based on its computational complexity. The high performance advantage of complex valued systems has been surprising in this context.

Final convergence limits for subband adaptive filters and the accuracy of the achievable equivalent fullband model based on aliasing and other distortions introduced by the employed filter banks were explicitly derived, and agreed very well with simulation results. Both an approximation of the MMSE and the model accuracy were linked to conditions on the prototype filter of the filter bank, which are directly related to criteria in the prototype filter design. Together with a presented iterative least-squares design algorithm, it is therefore possible to construct filter banks for SAF applications with pre-defined performance limits. The appeal is that for applications like acoustic echo cancellation, where the adaptation error is the most important issue, the filter banks can be designed to be just good (and short) enough to satisfy relaxed constraints on the model error.

7.3 Outlook

This thesis concludes with suggestion for further work, either to improve and elaborate, or to transfer some of the presented ideas to other applications.

7.3.1 Extensions

In Chap. 6, the tap-distribution mechanism was introduced implicitly using the p-norm for normalization of the criterion used, although only $p = 1$ was employed. In fact, different values for p could be tried, which would yield possibly interesting cases of convergence. For the case $p > 1$, it is expected that the band with the largest error will be assigned coefficients more quickly, while for $0 < p < 1$, the tap withdrawal from bands with smallest error would be enforced.

Although the subband approach has been shown to improve convergence in the presence of coloured input, a number of other methods could be evaluated for their additional benefit in particular to combat slow convergence at band-edges [101] e.g. as encountered in Fig.5.18. Fast converging algorithmic approaches include transform-domain adaptive filtering [128, 5], where the filter input is preprocessed by a sliding unitary transform. This approximately decorrelates the input values in the tap-delay line of the filter. A complete decorrelation is given by the Karhunen-Loeve transform [72], but other transforms like DFT or DCT can

already provide a considerable whitening [4]. An evaluation of a transform of the length of the adaptive filter is required to be calculated at every sampling period. Although elegant methods exist to reduce complexities of some of the transforms to linear order in the filter length [6], it appears promising for inclusion into the subband approach, since the computational load would be considerably lower than for a fullband transform-domain implementation.
A second approach to increase convergence speed at the band-edges is given by a selection of filter banks such that the analysis filters are wider than the synthesis filters [32, 79, 40, 106]. Thus, the SAFs are supplied with enough signal energy at the band-edges, while superfluous slow converging modes are filtered out on the synthesis side. Particularly, it should be interesting to survey which conditions have to be fulfilled by the filter banks to guarantee the PR property, and develop an appropriate prototype design.

Finally, the iterative least-squares design presented in Chap. 4 exhibited an uneven stopband attenuation. To yield a flatter stopband response as obtained with minimax filter designs, a re-weighting during the iterative design steps could be attempted.

7.3.2 Related Applications

A dual application to filter banks for subband decompositions are transmultiplexers as shown in Fig. 7.1, which stack several users for transmission over one line [154]. There, a synthesis filter bank performs the multiplexing of data at the sender, while an analysis bank acting as demultiplexer retrieves the users on the receiving side. An oversampled approach (or rather undersampled with respect to the filter banks) could lead to an increased robustness against channel interference.

Since fast implementations of the Gabor expansion have so far only been reported for integer oversampling ratios [104, 47, 11], the fast polyphase implementation of the GDFT filter bank presented in Chap. 4 can be transfered and applied.

Wavelet-based applications like detection [171, 80] or noise reduction [168, 169] suffer from the phase-sensitivity of the orthogonal DWT and therefore currently

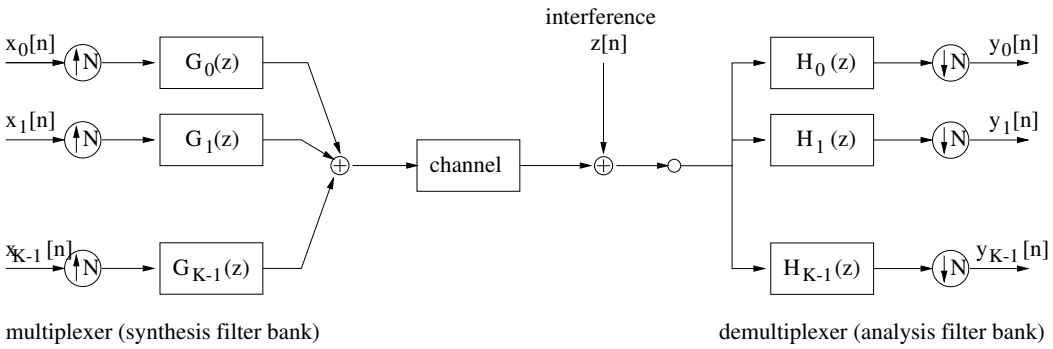

Figure 7.1: Transmission of K users over one channel by a transmultiplexer using filter banks; note that $N \geq K$.

require "translation-invariant" DWT transforms implemented by undecimated filter banks [25]. Although oversampled Gabor expansions are not "translation-invariant" in the true sense, signal energy is guaranteed to be found within a specific subband independent of the fullband signal's phase, if the expansion produces a low level of subband aliasing. Hence, oversampled Gabor transforms appear as a useful alternative to wavelet techniques [41], while a low OSR can maintain a low level of additional computational complexity.

Apart from the system identification / noise cancellation set-up targeted within this thesis, other applications like adaptive equalization [116] or line enhancement are possible [177]. For adaptive equalization (or inverse system identification [174]), very long impulse responses can occur when the channel to be inverted is considerably distorting. Also coloured channel output may motivate an SAF system to be applied. Although the delay of the filter banks inhibits direct use for delay sensitive applications like active noise control (ANC [36, 139]), a possibility is given by so called delay-less structures [102, 38, 109] where adaptation is performed in the subband domain but filtering is done in the fullband. In each decimated period the updated subband weights are transformed back into the time domain. This calculation is based on frequency domain methods and assumes a uniform tap-profile. For a general case, applying the reconstruction method in Sec. 5.3.1 could be employed.

Bibliography

[1] P. Abbott. Acoustic Echo Cancelling in Video Telephony and Conferencing on a Single DSP. In *Proceedings of DSP UK II*, volume 2, London, December 1994.

[2] P. Abbott. *Personal Communication.* Signals and Software, Ltd, Harrow, England, April 1996.

[3] F. Amano and H. Perez. "A New Subband Echo Canceler Structure". In *Proc. IEEE International Conference on Acoustics, Speech, and Signal Processing*, volume 5, pages 3585–3588, Toronto, Canada, May 1991.

[4] F. Beaufays. "Orthogonalizing Adaptive Algorithms: RLS, DFT/LMS, and DCT/LMS". In B. Widrow and E. Walach, editors, *Adaptive Inverse Control.* Prentice Hall, Englewood Cliffs, NJ, 1995.

[5] F. Beaufays. "Transform-Domain Adaptive Filters — An Analytical Approach". *IEEE Transactions on Signal Processing*, Vol.43(No.2):pp.422–431, February 1995.

[6] F. Beaufays. *"Two-Layer Linear Structures for Fast Adaptive Filtering"*. PhD thesis, Systems Laboratory, Department of Electrical Engineering, Stanford University, June 1995.

[7] M. G. Bellanger. *Adaptive Digital Filters and Signal Analysis.* Marcel Dekker Inc., New York, 1987.

[8] N. J. Bershad and P. L. Feintuch. "Analysis of the Frequency Domain Adaptive Filter". *Proceedings of the IEEE*, Vol.67(No.12):pp.1658–1659, Dec. 1979.

[9] N. J. Bershad and O. M. Macchi. "Comparison of RLS and LMS Algorithms for Tracking A Chirped Signal". In *Proc. IEEE International Conference on Acoustics, Speech, and Signal Processing*, volume 2, pages 896–899, Glasgow, Scotland, May 1989.

[10] N. J. Bershad and O. M. Macchi. "Adaptive Recovery of a Chirped Sinusoid in Noise, Part 1: Performance of the RLS Algorithm". *IEEE Transaction on Signal Processing*, Vol.39(No.3):pp.583–594, March 1991.

[11] H. Bölcskei and F. Hlawatsch. "Oversampled Filter Banks: Optimal Noise Shaping, Design Freedom, and Noise Analysis". In *Proc. IEEE International Conference on Acoustics, Speech, and Signal Processing*, volume IV, pages 2453–2456, Munich, Germany, April 1997.

[12] H. Bölcskei and F. Hlawatsch. "Oversampled Modulated Filter Banks". In H. G. Feichtinger and T. Strohmer, editors, *Gabor Analysis and Algorithms — Theory and Applications*, chapter 9. Birkhäuser, 1997.

[13] H. Bölcskei, F. Hlawatsch, and H. G. Feichtinger. "On the Equivalence of DFT Filter Banks and the Gabor Expansion". In *SPIE Proc. – Wavelet Applications in Signal and Image Processing III*, volume 2569, pages 128–139, San Diego, CA, 1995.

[14] H. Bölcskei, F. Hlawatsch, and H. G. Feichtinger. "Oversampled FIR and IIR Filter Banks and Weyl-Heisenberg Frames". In *Proc. IEEE International Conference on Acoustics, Speech, and Signal Processing*, volume III, pages 1351–1354, Atlanta, GA, May 1996.

[15] K. Brandenburg and T. Sporer. "NMR and Masking Flag: Evaluation of Quality Using Perceptual Criteria". In *Proc. International Conference of the Audio Engineering Society*, pages 169–179, Portland, Oregon, 1992.

[16] C. Breining. "Applying a Neural Network for Stepsize Control in Echo Cancellation". In *Proc. International Workshop on Acoustic Echo and Noise Control*, pages 41–44, Imperial College, London, September 1997.

[17] C. Breining and P. Dreiseitel. "Zustandsabhängige Steuerung einer Freisprecheinrichtung mit Geräuschreduktion". In *Proc. 9. Aachener Kolloquium Signaltheorie*, Aachen, Germany, 1997.

[18] I. Bronstein and K. Semendjajew. *Taschenbuch der Mathematik.* Verlag Harri Deutsch, Thun und Frankfurt/Main, 23rd edition, 1987.

[19] M. Budde. Adaptive Filtering in Subbands Using Critical Decimated and Oversampled Filter Banks. Technical report, Signal Processing Division, University of Strathclyde, Glasgow, U.K., July 1996.

[20] C. S. Burrus and T. W. Parks. *DFT/FFT and Convolution Algorithms: Theory and Implementation.* Wiley, NJ, 1985.

[21] P. L. Chu. "Weaver SSB Subband Acoustic Echo Canceller". In *IEEE Workshop on Applications of Signal Processing to Audio and Acoustics*, 1993.

[22] A. Cichocki and R. Unbehauen. *Neural Networks for Optimization and Signal Processing.* John Wiley & Sons Ltd., Chichester, 1993.

[23] G. A. Clark, S. K. Mitra, and S. R. Parker. "Block Implementation of Adaptive Digital Filters". *IEEE Transactions on Circuits and Systems — II: Analog and Digital Signal Processing*, Vol. CAS-28(No.6):pp.584–592, June 1981.

[24] G. A. Clark, S. R. Parker, and S. K. Mitra. "A Unified Approach to Time- and Frequency-Domain Realization of FIR Adaptive Digital Filters". *IEEE Transactions on Acoustics, Speech, and Signal Processing*, Vol. ASSP-31(No.5):pp.1073–1083, Oct. 1983.

[25] R. R. Coifman and D. L. Donoho. "Translation-Invariant De-Noising". In A. Antoniadis, editor, *Wavelets and Statistics.* Springer Verlag, 1995.

[26] A. J. Coulson. "A Generalization of Nonuniform Bandpass Sampling". *IEEE Transactions on Signal Processing*, Vol.43(No.3):pp.694–704, March 1995.

[27] R. E. Crochiere and L. R. Rabiner. *Multirate Digital Signal Processing*. Prentice Hall, Englewood Cliffs, NJ, 1983.

[28] Z. Cvetković and M. Vetterli. "Overcomplete Expansions and Robustness". In *Proc. IEEE International Symposium on Time-Frequency and Time-Scale Analysis*, pages 325–328, Paris, June 1996.

[29] Z. Cvetković and M. Vetterli. "Oversampled Filter Banks". *IEEE Transactions on Signal Processing*, Vol.46(No.5):pp.1245–1255, May 1998.

[30] Z. Cvetković and M. Vetterli. "Tight Weyl-Heisenberg Frames in $l^2(\mathbb{Z})$". *IEEE Transactions on Signal Processing*, Vol.46(No.5):pp.1256–1259, May 1998.

[31] I. Daubechies. *Ten Lectures on Wavelets*. SIAM, Philadelphia, 1992.

[32] P. L. de León II and D. M. Etter. "Experimental Results with Increased Bandwidth Analysis Filters in Oversampled Subband Acoustic Echo Cancelers". *IEEE Signal Processing Letters*, Vol.2(No.1):pp.1–3, January 1995.

[33] P. L. de León II and D. M. Etter. "Experimental Results of Subband Acoustic Echo Cancelers under Sperically Invariant Random Processors". In *Proc. IEEE International Conference on Acoustics, Speech, and Signal Processing*, volume 2, pages 961–964, Atlanta, GA, May 1996.

[34] E. Diethorn. "Perceptually Optimum Adaptive Filter Tap Profiles for Subband Acoustic Echo Cancellers". In *Proc. International Conference on Signal Processing and Technology*, pages 290–293, Boston, MA, 1995.

[35] G. P. M. Egelmeers. *Real Time Realization Concepts of Large Adaptive Filters*. PhD thesis, Technical University Eindhoven, 1995.

[36] S. Elliott and P. Nelson. *Active Control of Sound*. Academic Press, London, 1992.

[37] S. Elliott and P. Nelson. "Active Noise Control". *IEEE Signal Processing Magazine*, Vol.10(No.4):pp. 12 –35, October 1993.

[38] P. Eneroth and T. Gänsler. "A Modified Open-Loop Delayless Subband Adaptive Echo Canceller". In *Proc. International Workshop on Acoustic Echo and Noise Control*, pages 156–159, Imperial College, London, September 1997.

[39] P. Estermann. *Adaptive Filter im Frequenzbereich: Analyse und Entwurfsstrategie*. PhD thesis, Eidgenössische Technische Hochschule Zürich, 1996.

[40] B. Farhang-Boroujeny and Z. Wang. "Adaptive Filtering in Subbands: Design Issues and Experimental Results for Acoustic Echo Cancellation". *Signal Processing*, Vol.61(No.3):pp.213–223, 1997.

[41] H. G. Feichtinger and T. Strohmer, editors. *Gabor Analysis and Algorithms — Theory and Applications*. Birkhäuser, Boston, MA, October 1997.

[42] E. R. Ferrara. "Frequency-Domain Adaptive Filtering". In C. F. N. Cowan and P. M. Grant, editors, *Adaptive Filters*, chapter 6, pages 145–179. Prentice Hall, Englewood Cliffs, NJ, 1985.

[43] W. Fischer and I. Lieb. *Funktionentheorie*. Vieweg Verlag, Braunschweig, Germany, 1983.

[44] N. J. Fliege. "Half-Band Bandpass Filters and Filter Banks with Almost Perfect Reconstruction". *IEEE Transactions on Acoustics, Speech, and Signal Processing*, Vol.35(No.1):pp.59–66, January 1987.

[45] N. J. Fliege. *Multiraten-Signalverarbeitung*. B.G.Teubner, Stuttgart, 1993.

[46] N. J. Fliege. *Multirate Digital Signal Processing: Multirate Systems, Filter Banks, Wavelets*. John Wiley & Sons, Chichester, 1994.

[47] B. Friedlander and A. Zeira. "Oversampled Gabor Representation for Transient Signals". *IEEE Transactions on Signal Processing*, Vol.43(No.9):pp.2088–2094, Sept. 1995.

[48] I. Furukawa. "A Design of Canceller of Broad Band Acoustic Echo". In *Int. Teleconference Symposium*, pages 1/8–8/8, Tokyo, 1984.

[49] T. Furukawa, H. Kubota, and S. Tsujii. "The Orthogonal Projection Algorithm for Block Adaptive Signal Processing". In *Proc. IEEE International Conference on Acoustics, Speech, and Signal Processing*, volume II, pages 1059–1062, Glasgow, Scotland, UK, May 1989.

[50] S. L. Gay and R. J. Mammone. "Fast Converging Subband Acoustic Echo Cancellation Using Rap on the WE DSP16A". In *Proc. IEEE International Conference on Acoustics, Speech, and Signal Processing*, volume 2, pages 1141–1144, Albuquerque, NM, April 1990.

[51] S. L. Gay and S. Tavathia. "The Fast Affine Projection Algorithm". In *Proc. IEEE International Conference on Acoustics, Speech, and Signal Processing*, volume V, pages 3023–3026, Detroit, Michigan, 1995.

[52] A. Gilloire. "Experiments with Subband Acoustic Echo Cancelers for Teleconferencing". In *Proc. IEEE International Conference on Acoustics, Speech, and Signal Processing*, pages 2141–2144, Dallas, April 1987.

[53] A. Gilloire and M. Vetterli. "Adaptive Filtering in Subbands". In *Proc. IEEE International Conference on Acoustics, Speech, and Signal Processing*, pages 1572–1575, New York, April 1988.

[54] A. Gilloire and M. Vetterli. "Adaptive Filtering in Subbands with Critical Sampling: Analysis, Experiments and Applications to Acoustic Echo Cancelation". *IEEE Transactions on Signal Processing*, Vol.SP-40(No.8):pp.1862–1875, Aug. 1992.

[55] B. Girod. "What's Wrong With Mean Squared Error?". In A. Watson, editor, *Visual Factors of Electronic Image Communications*. MIT Press, 1993.

[56] B. Girod, F. Hartung, and U. Horn. "Subband Image Coding". In M. J. T. Smith and A. N. Akansu, editors, *Subband and Wavelet Transforms: Design and Applications*, chapter 7. Kluwer Academic Publishers, Boston, October 1995.

[57] B. Girod, R. Rabenstein, and A. Stenger. *Einführung in die Systemtheorie*. B. G. Teubner Verlag, Stuttgart, 1997.

[58] G. H. Golub and C. F. Van Loan. *Matrix Computations*. Johns Hopkins University Press, Baltimore, Maryland, 3rd edition, 1996.

[59] S. Gudvangen and S. J. Flockton. "Comparison of Pole-Zero and All-Zero Modeling of Acoustic Transfer Functions". *IEE Electronics Letters*, Vol.28(No.21):pp.1976–1978, 1992.

[60] S. Gudvangen and S. J. Flockton. "Modeling of Acoustic Transfer-Functions for Echo-Cancelers". *IEE-Proc Vision Image and Signal Processing*, Vol.142(No.1):pp.47–51, 1995.

[61] E. Häensler. "The Hands-Free Telephone Problem: an Annoted Bibliography". *Signal Processing*, Vol.27(No.3):pp.259–271, June 1992.

[62] E. Hänsler. "The Hands-Free Telephone Problem: an Annoted Bibliography Update". *Annales des Télécommunications*, Vol.49(No.7-8):pp.360–367, Juli/August 1994.

[63] E. Hänsler. "The Hands-Free Telephone Problem: A Second Annotated Bibliography Update". In *Proc. International Workshop on Acoustic Echo and Noise Control*, Røros, Norway, 1995.

[64] E. Hänsler. "From Algorithms to Systems — It's a Rocky Road". In *Proc. International Workshop on Acoustic Echo and Noise Control*, pages K1–K4, London, September 1997.

[65] J. E. Hart, P. A. Naylor, and O. Tanrikulu. "Polyphase All-Pass IIR Structures for Subband Acoustic Echo Cancellation". In *Proc. EUROSPEECH*, pages 1813–1816, Berlin, Germany, Sept. 1993.

[66] M. Harteneck. *Real Valued Filter Banks for Subband Adaptive Filtering*. PhD thesis, Signal Processing Division, University of Strathclyde, 1998.

[67] M. Harteneck, J. Paez-Borallo, and R. W. Stewart. "A Filterbank Design for Oversampled Filter Banks without Aliasing in the Subbands". In *2nd*

IEEE UK Symposium on Applications of Time-Frequency and Time-Scale Methods, Coventry, UK, August 1997.

[68] M. Harteneck, J. Paez-Borallo, and R. W. Stewart. "An Oversampled Subband Adaptive Filter Without Cross Adaptive Filters". In *International Workshop on Acoustic Echo and Noise Control*, pages 136–139, London, UK, September 1997.

[69] M. Harteneck, J. M. Páez-Borrallo, and R. W. Stewart. "An Oversampled Subband Adaptive Filter Without Cross Adaptive Filters". *Signal Processing*, Vol.64(No.1):pp.93–101, January 1998.

[70] M. Harteneck and R. W. Stewart. "An Oversampled Subband Adaptive Filter Without Cross Adaptive Filters". In *Asilomar Conference on Signals, Systems, and Computers*, Monterey, CA, November 1997.

[71] M. Harteneck and R. W. Stewart. "Filterbank Design for Oversampled Filter Banks Without Aliasing in the Subbands". *IEE Electronics Letters*, Vol.38(No.18):pp.1538–1539, August 1997.

[72] S. Haykin. *Adaptive Filter Theory*. Prentice Hall, Englewood Cliffs, 2nd edition, 1991.

[73] S. Haykin. *Adaptive Filter Theory*. Prentice Hall, Englewood Cliffs, 3rd edition, 1996.

[74] F. Heinle, R. Rabenstein, and A. Stenger. "A Measurement Method for the Linear and Nonlinear Properties of Electro-Acoustic Transmission Systems". *Signal Processing*, Vol.64(No.1):pp.49–60, January 1998.

[75] F. A. Heinle. "A New Approach to the Compensation of Aliasing in Transform and Subband Coders". In *Proc. IEEE International Conference on Acoustics, Speech, and Signal Processing*, pages 2457–2460, Munich, Germany, April 1997.

[76] F. A. Heinle and H. W. Schüßler. "An Enhanced Method for Measuring the Performance of Multirate Systems". In *Proc. International Conference on Digital Signal Processing*, pages 182–187, Limassol, Cyprus, June 1995.

[77] P. Heitkämper. "An Adaptation Control for Acoustic Echo Cancellers". *IEEE Signal Processing Letters*, Vol.4(No.6):pp.170–172, June 1997.

[78] G. T. Herman. *Image Reconstruction From Projections: The Fundamentals of Computerized Tomography.* Academic Press, New York, 1980.

[79] Y. Higa, H. Ochi, and S. Kinjo. "A Subband Adaptive Filter with a Variable Analysis Filter Bank". In *Proc. IEEE International Conference on Acoustics, Speech, and Signal Processing*, volume 2, pages 1727–1730, Atlanta, GA, May 1996.

[80] U. Hoppe, U. Eysholdt, and S. Weiß. "A Sequential Detection Method for Late Auditory Evoked Potentials". In *International Conference of the IEEE Engineering in Medicine and Biology Society*, Amsterdam, The Netherlands, November 1996.

[81] H. P. Hsu. "Sampling". In J. Gibson, editor, *The Mobile Communications Handbook*, chapter 2, pages 13–22. CRC Press, Boca Raton, Florida, 1996.

[82] V. K. Jain and R. E. Crochiere. "A Novel Approach to the Design of Analysis/Synthesis Filter Banks". In *Proc. IEEE International Conference on Acoustics, Speech, and Signal Processing*, 1983.

[83] K. D. Kammeyer. *Nachrichtenübertragung.* (Serie Informationstechnik). B.G.Teubner, Stuttgart, 1992.

[84] W. Kellermann. "Kompensation akustischer Echos in Frequenzteilbändern". In *Aachener Kolloquium*, pages 322–325, Aachen, Germany, 1984.

[85] W. Kellermann. "Kompensation akustischer Echos in Frequenzteilbändern". *Frequenz*, Vol.39(No.7/8):pp.209–215, July 1985.

[86] W. Kellermann. "Analysis and Design of Multirate Systems for Cancellation of Acoustical Echoes". In *Proc. IEEE International Conference on*

Acoustics, Speech, and Signal Processing, volume 5, pages 2570–2573, New York, 1988.

[87] H. Kiya, H. Yamazaki, and K. Ashihara. "An Oversampling Subband Adaptive Digital Filter with Rational Decimation Ratios". *Electronics and Communication in Japan, Part 3*, Vol.78(No.1):pp.89–97, January 1995.

[88] L. Lampe. Adaptive filtering in oversampled subbands. Studienarbeit, University of Strathclyde, Glasgow, UK, August 1997.

[89] D. Linebarger, B. Raghothaman, D. Begušić, and R. DeGroat. "Low Rank Transform Domain Adaptive Filtering". In *Asilomar Conference on Signals, Systems, and Computers*, volume 1, pages 123–127, Pacific Grove, CA, November 1997.

[90] Q.-G. Liu and B. Champagne. "Simple Design of Filter Banks for Subband Adaptive Filtering". In *Proc. International Workshop on Acoustic Echo and Noise Control*, pages 132–135, Imperial College, London, September 1997.

[91] Z. Ma, K. Nakayama, and A. Sugiyama. "Automatic Tap Assignment in Sub-Band Adaptive Filter". *IEICE Transactions on Communications*, Vol.E76-B(No.7):pp.751–754, July 1993.

[92] O. M. Macchi. "A General Methodology for Comparison of Adaptive Filtering Algorithms in a Nonstationary Context". In *European Signal Processing Conference*, volume 1, pages 189–192, Barcelona, Spain, September 1990.

[93] O. M. Macchi. *Adaptive Processing: The LMS Approach with Applications in Transmission*. Wiley, New York, 1995.

[94] O. M. Macchi and N. J. Bershad. "Adaptive Recovery of a Chirped Sinusoid in Noise, Part 2: Performance of the LMS Algorithm". *IEEE Transaction on Signal Processing*, Vol.39(No.3):pp.595–602, March 1991.

[95] S. Makino, J. Noebauer, Y. Haneda, and A. Nakagawa. "SSB Subband Echo Canceller Using Low-Order Projection Algorithm". In *Proc. IEEE International Conference on Acoustics, Speech, and Signal Processing*, volume 2, pages 945–948, Atlanta, GA, May 1996.

[96] S. G. Mallat. "A Theory for Multiresolution Signal Decomposition: The Wavelet Representation". *IEEE Transactions on Pattern Analysis and Machine Intelligence*, Vol.11(No.7):pp.674–692, July 1989.

[97] The MathWorks, Inc., Natick, MA. *Matlab 5.0*, December 1996.

[98] K. Mayyas and T. Aboulnasr. "A Robust Variable Step Size LMS-Type Algorithm: Analysis and Simulations". In *Proc. IEEE International Conference on Acoustics, Speech, and Signal Processing*, pages 1408–1411, 1995.

[99] F. Mintzer. "On half-band, third-band and Nth band FIR filters and their design". *IEEE Transactions on Acoustics, Speech, and Signal Processing*, Vol.ASSP-30(No.10):pp.734–738, October 1982.

[100] M. Montazeri and P. Duhamel. "A Set of Algorithms Linking NLMS and Block RLS Algorithms". *IEEE Transactions on Signal Processing*, Vol.43(No.2):pp.444–453, Feb. 1995.

[101] D. R. Morgan. "Slow Asymptotic Convergence of LMS Acoustic Echo Cancellers". *IEEE Transactions on Speech and Audio Processing*, Vol.2(No.3):pp.126–136, March 1995.

[102] D. R. Morgan and J. C. Thi. "A Delayless Subband Adaptive Filter Architecture". *IEEE Transactions on Signal Processing*, Vol.43(No.8):pp.1819–1830, August 1995.

[103] J. M. Morris and Y. H. Lu. "Discrete Gabor Expansion of Disrete-Time Signals in $l_2(\mathbb{Z})$ Via Frame-Theory". *Signal Processing*, Vol.40(No.2-3):pp.155–181, 1994.

[104] J. M. Morris and H. Xie. "Fast Algorithms for Generalized Discrete Gabor Expansion". *Signal Processing*, Vol.39(No.3):pp.317–331, 1994.

[105] Motorola Inc. *"DSP56002 Digital Signal Processor User's manual"*, 1993.

[106] A. Nakagawa, Y. Haneda, and S. Makino. "Subband Acoustic Echo Canceller Using Two Different Analysis Filters and 8th Order Projection Algorithm". In *Proc. International Workshop on Acoustic Echo and Noise Control*, pages 140–143, Imperial College, London, September 1997.

[107] Y. Neuvo, D. Cheng-Yu, and S. K. Mitra. "Interpolated Finite Impulse Response Filters". *IEEE Transactions on Acoustics, Speech, and Signal Processing*, Vol.32(No.6):pp.563–570, June 1984.

[108] C. L. Nikias and M. Shao. *Signal Procseeing with Alpha-Stable Distributions and Applications*. John Wiley & Sons, 1995.

[109] K. Nishikawa and H. Kiya. "Conditions for convergence of a delayless subband adaptive filter and its efficient implementation". *IEEE Transactions on Signal Processing*, Vol.46(No.4):pp.1158–1167, April 1998.

[110] B. Nitsch. "The Partitioned Exact Frequency Domain Block NLMS Algorithm". In *Proc. International Workshop on Acoustic Echo and Noise Control*, pages 45–48, Imperial College, London, Sept. 1997.

[111] K. Ozeki and T. Umeda. "An Adaptive Filtering Algorithm Using an Orthogonal Projection to an Affine Subspace and Its Properties". *Electronics and Communications in Japan*, Vol.67-A(No.5):pp.19–27, February 1984.

[112] A. Papoulis. *Probability, Random Variables, and Stochastic Processes*. McGraw-Hill, New York, 3rd edition, 1991.

[113] S.-C. Pei and M.-H. Yeh. "An Introduction to Discrete Finite Frames — Methods for Describing Vector Behavior for Signal Representation". *IEEE Signal Processing Magazine*, Vol.14(No.6):pp.84–96, November 1997.

[114] L. Pelkowitz. "Frequency Domain Analysis of Wrap-Around Error in Fast Convolution Algorithms". *IEEE Transactions on Acoustics, Speech, and Signal Processing*, Vol. ASSP-29(No.3):pp.413–422, June 1981.

[115] W. H. Press, S. A. Teukolsky, W. T. Vetterling, and B. P. Flannery. *Numerical Recipes in C.* Cambridge University Press, Cambridge, 2. edition, 1992.

[116] J. G. Proakis. "Channel Equalization". In J. D. Gibson, editor, *The Mobile Communications Handbook*, chapter 6, pages 56–80. CRC Press / IEEE Press, 1996.

[117] R. Rabenstein. Private communications, October 1997.

[118] P. Regalia and A. Liavas. "Performance Assessments of FIR versus IIR Models in Acoustic Echo Cancellation". In *Proc. International Workshop on Acoustic Echo and Noise Control*, pages 5–8, Imperial College, London, UK, September 1997.

[119] R. L. Reng. "Polyphase and Modulation Descriptions of Multirate Systems — A Systematic Approach". In *Proc. International Conference on Digital Signal Processing*, pages 212–217, Limassol, Cyprus, June 1995.

[120] R. L. Reng and H. W. Schüßler. "Measurement of Aliasing Distortion and Quantization Noise in Multirate Systems". In *Proc. IEEE International Symposium on Circuits and Systems*, pages 2328–2331, SanDiego, CA, 1992.

[121] M. Rossi, J.-Y. Zhang, and W. Steenaart. "A New Algorithm for Designing Prototype Filters for M-Band Pseudo QMF Banks". In *European Signal Processing Conference*, volume II, pages 1195–1198, Trieste, September 1996.

[122] M. Rossi, J.-Y. Zhang, and W. Steenaart. "Iterative Least Squares Design of Perfect Reconstruction QMF Banks". In *Proc. Canadian Conference on Electrical and Computer Engineering*, May 1996.

[123] H. Schlitt. *Systemtheorie für stochastische Prozesse.* Springer Verlag, Berlin, 1992.

[124] M. Schönle, N. J. Fliege, and U. Zölzer. "Parametric Approximation of Room Impulse Responses by Multirate Systems". In *Proc. IEEE International Conference on Acoustics, Speech, and Signal Processing*, volume I, pages 153–156, Minneapolis, May 1993.

[125] T. J. Shan and T. Kailath. "Adaptive Algorithms with an Automatic Gain Control Feature". *IEEE Transactions on Circuits and Systems*, Vol.CAS-35(No.1):pp.120–127, January 1988.

[126] C. E. Shannon. "A Mathematical Theory of Communications (Part I)". *Bell Syst. Technic. Journal*, Vol.27:pp.379–423, 1948.

[127] C. E. Shannon. "A Mathematical Theory of Communications (Part II)". *Bell Syst. Technic. Journal*, Vol.27:pp.623–656, 1948.

[128] J. J. Shynk. "Frequency-Domain and Multirate Adaptive Filtering". *IEEE Signal Processing Magazine*, Vol.9:pp.14–37, Jan. 1992.

[129] D. T. M. Slock. "Fractionally-Spaced Subband and Multiresolution Adaptive Filters". In *IEEE International Conference on Acoustics, Speech and Signal Processing*, volume 5, pages 3693–3696, 1991.

[130] D. T. M. Slock. "On the Convergence Behaviour of the LMS and the Normalized LMS Algorithms". *IEEE Transactions on Signal Processing*, Vol.41(No.9):pp.2811–2825, September 1993.

[131] M. J. T. Smith and T. P. Barnwell III. "A New Filter Banks Theory for Time-Frequency Representations". *IEEE Transactions on Acoustics, Speech, and Signal Processing*, Vol.35(No.3):pp.314–327, March 1987.

[132] V. Solo and X. Kong. *Adaptive Signal Processing Algorithms — Stability and Performance*. Prentice Hall, Englewood Cliffs, NJ, 1995.

[133] V. Somayazulu, S. Mitra, and J. Shynk. "Adaptive Line Enhancement Using Multirate Techniques". In *Proc. IEEE International Conference on Acoustics, Speech, and Signal Processing*, volume 2, pages 928–931, Glasgow, Scotland, UK, May 1989.

[134] M. M. Sondhi and W. Kellermann. "Adaptive Echo Cancellation for Speech Signals". In S. Furui and M. M. Sondhi, editors, *Advances in Speech Signal Processing*, chapter 11, pages 327–356. Marcel Dekker, New York, 1989?

[135] U. Sörgel. Adaptive Filtering in Subbands Using Critical Sampling and Tap Assignement. Technical report, Signal Processing Division, University of Strathclyde, Glasgow, U.K., April 1996.

[136] P. Steffen, P. N. Heller, R. A. Gopinath, and C. S. Burrus. "Theory of Regular M-Band Wavelet Bases". *IEEE Transactions on Signal Processing*, Vol. SP-41(No.12):pp.3497–3511, 1993.

[137] A. Stenger. Private communications, August 1997.

[138] A. Stenger and R. Rabenstein. "An Acoustic Echo Canceller with Compensation of Nonlinearities". In *European Signal Processing Conference*, Rodos, Greece, September 1998.

[139] R. W. Stewart, R. J. Duncan, and S. Weiss. "Multichannel Adaptive Active Noise Cancellation Using the DSP56001". In *Proc. IEEE International Conference on Acoustics, Speech, and Signal Processing*, volume 1, pages 185–188, Minneapolis, May 1993.

[140] R. W. Stewart, S. Weiss, and D. H. Crawford. "Convergence Behaviour of LMS-Type Algorithms for Adaptive Noise Control in Noisy Doppler Environments". In *International Symposium on Methods and Models in Automation and Robotics*, volume I, pages 69–76, Miedzyzdroje, Poland, September 1996.

[141] G. Strang. *Linear Algebra and Its Applications*. Academic Press, New York, 2nd edition, 1980.

[142] G. Strang and T. Nguyen. *Wavelets and Filter Banks*. Wellesley–Cambridge Press, Wellesley, MA, 1996.

[143] A. Sugiyama and A. Hirano. "A Subband Adaptive Filtering Algorithm with Adaptive Intersubband Tap-Assignment". *IEICE Transactions on*

Fundamentals of Electronics, Communications, and Computer Science, Vol.E77-A(No.9):pp.1432–1438, October 1994.

[144] A. Sugiyama and F. Landais. "A New Adaptive Intersubband Tap-Assignment Algorithm for Subband Adaptive Filters". In *Proc. IEEE International Conference on Acoustics, Speech, and Signal Processing*, volume V, pages 3051–3054, Detroit, Michigan, 1995.

[145] M. Takana, Y. Kaneda, S. Makino, and J. Kojima. "A Fast Projection Algorithm for Adaptive Filtering". *IEICE Transactions on Fundamentals of Electronics, Communications, and Computer Sciences*, Vol.E87-A(No.10):pp.1355–1361, October 1995.

[146] O. Tanrikulu, B. Baykal, and A. G. Constantinides. "The Fast Affine Projection Algorithm". In *Proc. IEEE International Conference on Acoustics, Speech, and Signal Processing*, volume V, pages 3023–3026, Detroit, Michigan, 1995.

[147] O. Tanrikulu, B. Baykal, A. G. Constantinides, and J. Chambers. "Residual Signal in Sub-Band Acoustic Echo Cancellers". In *European Signal Processing Conference*, volume 1, pages 21–24, Trieste, Italy, September 1996.

[148] O. Tanrikulu, B. Baykal, A. G. Constantinides, and J. Chambers. "Residual Echo Signal in Critically Sampled Subband Acoustic Echo Cancellers Based on IIR and FIR Filter Banks". *IEEE Transactions on Signal Processing*, Vol.45(No.4):pp.901–912, 1997.

[149] R. Unbehauen. *Systemtheorie*. R.Oldenbourg Verlag, München, Wien, 5. edition, 1990.

[150] P. P. Vaidyanathan. "Multirate Digital Filters, Filter Banks, Polyphase Networks, and Applications: A Tutorial". *Proceedings of the IEEE*, Vol.78(No.1):pp.56–93, January 1990.

[151] P. P. Vaidyanathan. *Multirate Systems and Filter Banks*. Prentice Hall, Englewood Cliffs, 1993.

[152] P. Vary. "On the Design of Digital Filter Banks Based on a Modified Principle of Polyphase". *Archiv Elektrische Übertragung*, Vol.33:pp.293–300, 1979.

[153] R. G. Vaughan, N. L. Scott, and D. R. White. "The Theory of Bandpass Sampling". *IEEE Transactions on Signal Processing*, Vol.39(No.9):pp.1973–1984, September 1991.

[154] M. Vetterli. "Perfect Transmultiplexers". In *Proc. IEEE International Conference on Acoustics, Speech, and Signal Processing*, volume V, pages 2567–2570, Tokyo, Japan, April 1986.

[155] M. Vetterli. "A Theory of Multirate Filter Banks". *IEEE Transactions on Acoustics, Speech, and Signal Processing*, Vol.35(No.3):pp.356–372, March 1987.

[156] M. Vetterli and Z. Cvetković. "Oversampled FIR FIlter Banks and Frames in $l^2(\mathbb{Z})$". In *Proc. IEEE International Conference on Acoustics, Speech, and Signal Processing*, volume 2, pages 1530–1533, Atlanta, GA, May 1996.

[157] M. Vetterli and C. Herley. "Wavelets and Filter Banks: Theory and Design". *IEEE Transactions on Signal Processing*, Vol.40(No.9):pp:2207–2232, September 1992.

[158] M. Vukadinovic and T. Aboulnasr. "A Study of Adaptive Intersubband Tap Assignment Algorithms from a Psychoacoustic Point of View". In *Proc. IEEE International Symposium on Circuits and Systems*, volume 2, pages 65–68, Atlanta, May 1996.

[159] G. Wackersreuther. "Some New Aspects of Filters for Filter Banks". *IEEE Transactions on Acoustics, Speech, and Signal Processing*, Vol. ASSP-34(No.10):pp.1182–1200, October 1986.

[160] G. Wackersreuther. *Ein Beitrag zum Entwurf digitaler Filter Bänke*. PhD thesis, Insitut für Nachrichtentechnik, Universität Erlangen-Nürnberg, 1987.

[161] S. Weiß. Rekonstruktion Akustisch Evozierter Potentiale. Technical report, Univ.-HNO-Klinik Erlangen / Lehrstuhl für Technische Elektronik, Universität Erlangen-Nürnberg, Germany, Dec. 1994.

[162] S. Weiß, M. Harteneck, and R. W. Stewart. "Adaptive System Identification with Tap-Assignment in Oversampled and Critically Sampled Subbands". In *Proc. International Workshop on Acoustic Echo and Noise Control*, pages 148–151, Imperial College, London, September 1997.

[163] S. Weiß, M. Harteneck, and R. W. Stewart. "Efficient Design and Implementation of an Oversampled GDFT Modulated Filter Bank for Subband Processing". In *Digest IEE Colloquium on Digital Filters: an Enabling Technology*, pages 12/1–12/8, London, April 1998.

[164] S. Weiß, M. Harteneck, and R. W. Stewart. "On Implementation and Design of Filter Banks for Subband Adaptive Systems". In *IEEE Workshop on Signal Processing Systems (SiPS'98)*, Cambridge, MA, October 1998.

[165] S. Weiß and U. Hoppe. "Recognition and Reconstruction of Late Auditory Evoked Potentials Using Wavelet Analysis". In *Proc. IEEE International Symposium on Time-Frequency and Time-Scale Analysis*, pages 473–476, Paris, June 1996.

[166] S. Weiß, L. Lampe, and R. W. Stewart. "Efficient Subband Adaptive Filtering with Oversampled GDFT Filter Banks". In *Digest IEE Colloquium on Adaptive Signal Processing for Mobile Communication Systems*, pages 4.1–4.9, London, England, October 1997.

[167] S. Weiß, L. Lampe, and R. W. Stewart. "Efficient Implementations of Complex and Real Valued Filter Banks for Comparative Subband Processing with an Application to Adaptive Filtering.". In *Proc. International Symposium on Communication Systems and Digital Signal Processing*, pages 32–35, Sheffield, UK, April 1998.

[168] S. Weiß, R. M. Leahy, J. C. Mosher, and R. W. Stewart. "Ensemble Denoising of Spatio-Temporal EEG and MEG Data". In *Proc. 2nd IEEE UK*

Symposium on Applications of Time-Frequency and Time-Scale Methods, pages 33–36, University of Warwick, England, August 1997.

[169] S. Weiß, R. M. Leahy, J. C. Mosher, and R. W. Stewart. "An Ensemble De-Noising Method for Spatio-Temporal EEG and MEG Data". *Applied Signal Processing*, 1998. (Invited paper, to appear).

[170] S. Weiß, U. Sörgel, and R. W. Stewart. "Computationally Efficient Adaptive System Identification in Subbands with Intersubband Tap Assignment for Undermodelled Problems". In *Asilomar Conference on Signals, Systems, and Computers*, pages 818–822, Monterey,CA, November 1996.

[171] S. Weiß, R. W. Stewart, and D. Crawford. Adaptive Noise Suppression Techniques for Emergency Roadside Telephones — Part II: Simulations on Real Data. Technical report, Signal Processing Division, University of Strathclyde, Glasgow, Scotland, January 1996.

[172] S. Weiß, R. W. Stewart, A. Stenger, and R. Rabenstein. "Performance Limitations of Subband Adaptive Filters". In *European Signal Processing Conference*, Rodos, Greece, September 1998.

[173] B. Widrow, J. McCool, and M. Ball. "The Complex LMS Algorithm". *Proceedings of the IEEE*, Vol.63:pp.719–720, August 1975.

[174] B. Widrow and S. Stearns. *Adaptive Signal Processing*. Prentice Hall, Englewood Cliffs, New York, 1985.

[175] R. J. Wilson, P. A. Naylor, and D. Brookes. "Performance Limitations of Subband Acoustic Echo Controllers". In *Proc. International Workshop on Acoustic Echo and Noise Control*, pages 176–179, Imperial College, London, UK, September 1997.

[176] Y. Yamada, H. Ochi, and H. Kiya. "A Subband Adaptive Filter Allowing Maximally Decimation". *IEEE Journal on Selected Areas in Communications*, Vol.12(No.9):pp.1548–1552, September 1994.

[177] G. Y. Yang, N. I. Cho, and S. U. Lee. "On the performance analysis and applications of the subband adaptive digital filter". *Signal Processing*, Vol.41(No.3):pp.295–307, February 1995.

[178] H. Yasukawa. "Performance Degradation of a Subband Adaptive Digital Filter with Critical Sampling". *IEICE Transactions on Fundamentals of Electronics, Communications, and Computer Science*, Vol.E77A(No.9):pp.1497–1501, September 1994.

[179] H. Yasukawa, I. Furukawa, and Y. Ishiyama. "Characteristics of Acoustic Echo Cancellers Using Sub-Band Sampling and Decorrelation Methods". *IEE Electronics Letters*, Vol.24:pp.1039–1040, 1988.

[180] H. Yasukawa and S. Shimada. "An Acoustic Echo Canceller Using Subband Sampling and Decorrelation Methods". *IEEE Transactions on Signal Processing*, Vol.41(No.2):pp.926–930, February 1993.

[181] H. Yasukawa, S. Shimada, and I. Furukawa. "Acoustic Echo Canceller with High Speech Quality". In *Proc. IEEE International Conference on Acoustics, Speech, and Signal Processing*, volume IV, pages 2125–2128, Dallas, April 1987.